UPMC SORBONNE UNIVERSITÉS

Laboratoire Kastler Brossel
Physique quantique et applications

THÈSE DE DOCTORAT
DE L'UNIVERSITÉ PIERRE ET MARIE CURIE

Spécialité : Physique

École doctorale : "Physique en Île-de-France"

réalisée

au Laboratoire Kastler-Brossel

présentée par

Gabriel DUFOUR

pour obtenir le grade de

DOCTEUR DE L'UNIVERSITÉ PIERRE ET MARIE CURIE

Sujet de la thèse :

Réflexion quantique sur le potentiel de Casimir-Polder

—

Quantum reflection from the Casimir-Polder potential

soutenue le 20 novembre 2015

devant le jury composé de

M	Andreas Buchleitner	Rapporteur
M	David Guéry-Odelin	Rapporteur
M^{me}	Marie-Christine Angonin	Examinatrice
M	Olivier Dulieu	Examinateur
M	Valery Nesvizhevsky	Examinateur
M^{me}	Astrid Lambrecht	Directrice de thèse

À la mémoire de mes grands-pères,
Jean Dufour et Michel Durin

Quand j'ai poussé la porte du Laboratoire Kastler Brossel en novembre 2011, je revenais d'un mois de voyage à vélo sur les routes et chemins d'Italie. Astrid Lambrecht et Serge Reynaud m'ont convaincu de me lancer dans une nouvelle aventure, avec son lot d'ascensions ardues, de petites victoires, de problèmes techniques et de découvertes grisantes. Astrid et Serge m'ont accompagné sans relâche au cours du stage et de la thèse qui ont suivi. Je les remercie chaleureusement pour leur gentillesse et leur patience, leurs mots d'encouragement et les nombreuses discussions passionnantes que nous avons eues.

Marie-Pascale Gorza, Romain Guérout, Manuel Donaire et Axel Maury ont été mes compagnons de route au sein de l'équipe "fluctuations quantiques et relativité". Leurs conversations stimulantes et animées ont égayé bien des austères journées de travail. J'ai aussi partagé de très bons moments avec mes collègues et amis du laboratoire et d'au delà, que ce soit dans les courants d'air de la cantine, sous le soleil des arènes ou dans l'ambiance chaleureuse d'une cafétéria. En plus de cette atmosphère amicale, j'ai bénéficié au Laboratoire Kastler Brossel et à l'Université Pierre et Marie Curie de conditions de travail exceptionnelles, je voudrais en remercier les équipes techniques et administratives.

J'ai eu la chance de participer à la collaboration GBAR, un projet ambitieux qui rassemble des chercheurs de tous les horizons géographiques et scientifiques, de Tokyo à Swansea et de la physique des accélérateurs à celle des particules ultrafroides. J'ai hâte que cette belle expérience voie le jour et livre ses premiers résultats. J'ai notamment collaboré étroitement avec Alexei Voronin et Valery Nesvizhevsky que je remercie vivement pour leurs idées fructueuses et leur enthousiasme communicatif. Merci aussi à Valery pour son accueil à l'Institut Laue-Langevin et l'inoubliable visite du réacteur.

Valery me fait également l'honneur de participer à mon jury de thèse, aux côtés de Marie-Christine Angonin, Olivier Dulieu, David Guéry-Odelin et Andreas Buchleitner que je remercie sincèrement de l'intérêt dont ils témoignent ainsi pour mon travail. Je suis particulièrement reconnaissant envers David Guéry-Odelin et Andreas Buchleitner qui ont accepté d'être rapporteurs de ma thèse et je me réjouis d'aller travailler à Freiburg avec Andreas l'année prochaine.

Un grand merci enfin à ma famille et à mes amis, qui m'ont encouragé, questionné, accompagné, consolé, soutenu et supporté, de près ou de loin, tout au long de ce périple.

Gabriel Dufour

Contents

Notation

General

- $\vec{r} = x\vec{e}_x + y\vec{e}_y + z\vec{e}_z$ is a position vector written in the usual Cartesian basis.
- We often single out one direction and denote z or ζ the corresponding coordinate.
- The time variable is denoted t or τ.
- $f(x)$ denotes a function of the variable x and $f'(x) = \dfrac{\mathrm{d}f}{\mathrm{d}x}(x)$ is its derivative; a partial derivative with respect to x is denoted $\dfrac{\partial}{\partial x}$.
- The Schwarzian derivative $\{f, x\}$ is defined by

$$\{f, x\} = \frac{f'''(x)}{f'(x)} - \frac{3}{2}\left(\frac{f''(x)}{f'(x)}\right)^2 \ .$$

- The Wronskian of two functions $f(x)$ and $g(x)$ is

$$\mathcal{W}(f, g) = f(x)g'(x) - f'(x)g(x) \ .$$

- Stars and daggers denote complex and hermitian conjugation, respectively.

Constants

- Reduced Plank constant $\hbar \approx 1.05457 \times 10^{-34}$ J.s
- Speed of light $c \approx 2.99792458 \times 10^{8}$ m.s^{-1}
- Vacuum permittivity $\varepsilon_0 \approx 8.85419 \times 10^{-12}$ F.m^{-1}
- Boltzmann constant $k_B \approx 1.38065 \times 10^{-23}$ J.K^{-1}
- Fine structure constant $\alpha \approx 1/137.036$
- Mass of the hydrogen atom $m_{\mathrm{H}} \approx 1.67353 \times 10^{-27}$ kg

Units

All equations are written in the International System of units but numerical values are sometimes expressed in more convenient units. The energies involved in quantum reflection processes are of the order of the nanoelectronvolt:

$$\text{neV} \approx 1.60217646 \times 10^{-28}\ \text{J}$$

Atomic units (a.u.) are well adapted to express scattering lengths and Casimir-Polder potentials, the atomic length and energy units are respectively

- Bohr radius $\quad a_0 \approx 5.29177 \times 10^{-11}\ \text{m}$
- Hartree $\quad E_h \approx 4.35974 \times 10^{-18}\ \text{J}$

Quantum effects in a gravitational field involve the following scales:

- Length $\quad z_g = \left(\dfrac{\hbar^2}{2m^2\overline{g}}\right)^{1/3} \approx 5.87 \times 10^{-6}\ \text{m}$
- Energy $\quad E_g = \left(\dfrac{\hbar^2 m\overline{g}^2}{2}\right)^{1/3} \approx 9.64 \times 10^{-32}\ \text{J} \approx 6.02 \times 10^{-4}\ \text{neV}$
- Momentum $\quad p_g = (2\hbar m^2\overline{g})^{1/3} \approx 1.80 \times 10^{-29}\ \text{kg.m.s}^{-1}$
- Time $\quad t_g = \left(\dfrac{2\hbar}{m\overline{g}^2}\right)^{1/3} \approx 1.09 \times 10^{-3}\ \text{s}$

where the numerical values are given assuming that m is the mass of the hydrogen atom and $\overline{g} = g$.

Acronyms and symbols

- WKB Wentzel, Kramers and Brillouin semiclassical approximation
- GBAR Gravitational Behavior of Antihydrogen at Rest
- H hydrogen atom $\quad \overline{\text{H}}$ antihydrogen atom
- p proton $\quad \overline{\text{p}}$ antiproton
- e^- electron $\quad \text{e}^+$ positron
- Ps positronium

Special functions

We follow the definitions and notations of the NIST Handbook of Mathematical Functions [1]:

- $\mathrm{Ai}(x)$, $\mathrm{Bi}(x)$ Airy functions
- $Ai(-a_n) = 0$ zeros of the Airy function
- $F(a, b, c; x)$ Gauss hypergeometric function
- $H_n^{(1,2)}(x)$ Hankel functions
- $L_n(x)$ Laguerre polynomials
- $M(a, b, x)$, $U(a, b, x)$ Kummer confluent hypergeometric functions

Introduction

In 1924, de Broglie made the groundbreaking hypothesis that every microscopic particle of momentum p is associated with a wave of wavelength

$$\lambda_{\mathrm{dB}} = \frac{h}{p} \ , \tag{1}$$

where $h = 2\pi\hbar$ is Planck's constant [2]. Two years later, Schrödinger published his celebrated equation

$$-\frac{\hbar^2}{2m}\frac{\mathrm{d}^2\psi}{\mathrm{d}z^2}(z) + V(z)\psi(z) = E\psi(z) \ , \tag{2}$$

which accurately predicted the energy levels of the hydrogen atom by treating the electron as a wave [3]. Ninety years later, the wave-like behavior of quantum matter still captivates physicists. It is responsible for many surprising features of quantum mechanics such as interference, tunneling or the Heisenberg uncertainty principle. In this thesis we will focus on another spectacular manifestation of this wave-like behavior: *quantum reflection*, the reflection of a matter wave on a potential which would not reflect a classical particle.

The initial motivation for this work came from a seemingly unrelated problem: how does antimatter gravitate? Since Dirac's remarkable prediction in 1928 [4] and Anderson's observation of the positron in 1932 [5], antimatter has remained a topic of great interest for physicists. Its apparent scarcity in our universe has led them to search for a hidden asymmetry between particles and their charge conjugates. Our current understanding of the Standard Model fails to account for such a disparity. Gravity, which does not fit in the framework of the Standard Model, is therefore a natural suspect. The GBAR project (Gravitational Behavior of Antihydrogen at Rest) is one of the ongoing endeavors to determine the gravitational pull of the Earth on the simplest of antimatter atoms, antihydrogen. This ambitious experiment will produce, trap and cool antihydrogen before dropping it in the Earth's gravity field, in a modern day reenactment of Galileo's legendary leaning tower experiment.

Part of the present work will be devoted to the free fall of a matter wave in a gravitational potential. However, in the last instants of the anti-atom's fall, another intriguing force comes into play, the Casimir-Polder interaction between the atom and the detection plate. Casimir forces are a manifestation of the irreducible fluctuations

of the quantized electromagnetic field. As such, they constitute macroscopic evidence for the predictions of quantum field theory. While a matter wave is reflected on the gravitational potential much like a classical particle reverses its direction upon reaching the apex of its trajectory, the behavior of a matter wave scattering off the Casimir-Polder potential is very different from that of a classical particle. The Casimir-Polder force is attractive, so that one would expect an incoming atom to be accelerated towards the surface and eventually hit it. On the contrary, we will show that the atom has a significant probability to be reflected away from the surface.

The study of quantum reflection from the Casimir-Polder potential will be the main object of this thesis. We will also touch upon some of the fascinating topics that are connected to this study: the gravitational behavior of antimatter, the free fall of a quantum wavepacket, vacuum fluctuations and Casimir forces.

The GBAR experiment

The recognition that the motion of objects in a gravitational field is independent of their mass and composition was central to the birth of modern science in the 17^{th} century. The universality of free fall or *weak equivalence principle* is a cornerstone of Einstein's General Relativity and it "continues to be a focus of intense theoretical and experimental investigation" [6]. Today, the fact that all bodies undergo the same acceleration g at a given point on the surface of the Earth is verified with ever increasing precision both for macroscopic test masses [7] and atoms [8, 9]. But even as we celebrate the hundredth birthday of Einstein's theory, the mysteries surrounding dark matter and energy remind us that our knowledge of gravitational forces is still incomplete. Our ignorance of how gravity and other interactions are articulated at a fundamental level leaves some room for alternative proposals which include violations of the weak equivalence principle.

In particular, the possibility of an asymmetry in the gravitational behavior of matter and antimatter has been raised [10–14]. Although theoretical arguments and experimental observations have been put forward against "antigravity" [15–17], a direct, model-independent test of the universality of free fall for antimatter is still lacking. A direct measurement of the acceleration $\overline{g}$ of an antimatter particle in the Earth's gravity field is a longtime objective of physicists. Early experiments with charged antiparticles were thwarted by the preponderance of electromagnetic forces over gravity [18]. Current experimental endeavors are thus concentrating on neutral particles, especially the antihydrogen atom. The antihydrogen atom ($\overline{\text{H}}$) is the bound state of an antiproton ($\bar{\text{p}}$) and a positron (e^+); it was first produced at high energies in CERN in 1995 [19]. Since then, much progress has been made towards lower temperatures and longer lifetimes in several experiments based around CERN's Antiproton Decelerator [20, 21]. In particular, the ALPHA experiment was able to put the following bound on the gravitational acceleration $\overline{g}$ of antihydrogen [22]:

$$-65g \leq \overline{g} \leq +110g \ . \tag{3}$$

At CERN, the new deceleration ring ELENA [23] will provide cooler antiprotons

to a new generation of antimatter experiments. AEGIS aims to measure the deflection of a beam of antihydrogen atoms using a Moiré deflectometer [24]. There is also a proposal to build an interferometric gravimeter in the ALPHA experiment [25]. Finally, the GBAR experiment will consist in cooling antihydrogen to the ground state of a harmonic trap before releasing it in the Earth's gravity field and timing its free fall [26, 27]. The specificity of GBAR is that it will produce the antihydrogen ion $\overline{\mathrm{H}}^+$, two positrons orbiting an antiproton, in order to take advantage of ion trapping and cooling techniques [28]. Once the ion is cold, a laser will be used to photodetach the excess positron, letting the neutral antihydrogen atom fall freely towards a detection plate.

The $\overline{\mathrm{H}}^+$ ion will be produced by the successive reaction of an antiproton with two positroniums (the bound state of electron and positron):

$$\bar{\mathrm{p}} + \mathrm{Ps} \rightarrow \overline{\mathrm{H}} + \mathrm{e}^- \ ,$$
$$\overline{\mathrm{H}} + \mathrm{Ps} \rightarrow \overline{\mathrm{H}}^+ + \mathrm{e}^- \ .$$

Producing these reactants and bringing them together in the right conditions will constitute an impressive experimental feat.

Antiprotons are produced by collisions of 26 GeV protons with a target and cooled down to approximately 100 keV by the AD and ELENA rings. They must then be slowed down electrostatically to approximately 1 keV before reaching the reaction chamber. Meanwhile, positronium is formed by implanting positrons in a porous silica sample. The positron captures an electron and the resulting positronium diffuses in the network of nanometric pores until it is expelled back into the vacuum with a well defined energy [29]. The positrons themselves are obtained in the collision of 10 MeV electrons from a linear accelerator (LINAC) with a target. They must then be moderated, accumulated in a Penning trap and sympathetically cooled by a cloud of electrons before being sent on the porous silica sample. The positronium will be excited by laser to a higher energy state in order to maximize the cross-section of the reactions [30].

At the output of the reaction chamber, the $\overline{\mathrm{H}}^+$ ions are separated from the neutral $\overline{\mathrm{H}}$ and the negatively charged $\bar{\mathrm{p}}$ and collide with a Coulomb crystal of laser-cooled Be^+ and HD^+ ions. Their energy is efficiently transfered to the ions of the crystal thanks to the small mass ratios between these three species. One $\overline{\mathrm{H}}^+$-Be^+ pair is then transfered to a Paul trap. Raman sideband cooling is performed on the beryllium ion, which has the effect of sympathetically cooling the antihydrogen ion to the ground state of the harmonic trap [31].

A laser pulse is then used to photodetach the extra positron, defining the starting time of the free fall of the neutral antihydrogen atom. The fall ends by the annihilation of the anti-atom on a detection plate some 10 cm below. The annihilation products (pions and gamma photons) are detected by Micromegas detectors [32] and scintillation counters placed outside the vacuum vessel. The acceleration $\overline{g}$ of antihydrogen is deduced from the free fall time. A 1% precision on $\overline{g}$ is expected after a few months of operation, which has to be compared with the existing bound (3).

Quantum mechanics in a gravitational field

One must keep in mind that the falling antihydrogen atom in the GBAR experiment is not a classical point particle but a quantum matter wave. The fact that the falling wavefunction is extended, and that it expands, means that even if the initial quantum state of the dropped particle is perfectly defined, the time at which the particle reaches the detector is randomly distributed. This is a consequence of the quantum uncertainty on the initial position and momentum of the particle, which are bound by Heisenberg's uncertainty principle. We will compute the arrival time distributions associated with given initial states and discuss the consequences for the precision of the GBAR experiment.

More generally, the absence of notions such as point particle or trajectory complicates the formulation of the weak equivalence principle in quantum mechanics. Another difficulty arises from the fact that the wavefunction explicitly depends on mass, which is not a surprise since mass enters the Schrödinger equation as a parameter, even in the absence of gravity [33–36]. The transformation of the Schrödinger equation under a change of frame provides a possible way out of this problem [37–41]. Indeed, the Schrödinger equation in a uniform gravity field can be obtained from the free equation by changing to an accelerated frame. Conversely, a particle falling in a uniform gravity field appears as a free particle to an observer falling alongside it.

Such theoretical discussions have gone hand in hand with the development experiments. The effect of gravity on quantum systems was first observed in the Colella-Overhauser-Werner experiment [42]. A phase shift was measured between the arms of a neutron interferometer when the device was tilted in the Earth's gravity field. Later on, atomic interferometers were able to measure the local gravitational acceleration with unprecedented precision [43]. Today, dual species/isotope interferometers [8, 9, 44] test the weak equivalence principle at the level of a few parts in 10^7, still well below the performance of torsion balances (one in 10^{13} [7]), but progressing rapidly [45].

Other experiments have observed the bounces of atoms on a liquid helium film [46] or an evanescent light field [47–49]. These *quantum bouncers* are trapped in a potential well formed by the surface on the one hand and gravity on the other hand. The quantum bound states in such a well have been described theoretically [50–52], but because the gravitational force is very weak at atomic scales, extremely cold particles are needed to resolve them experimentally.

These *gravitationally bound states* have first been observed with ultracold neutrons at the Institut Laue-Langevin [53–55]. The neutrons were sent through a waveguide consisting of a reflective bottom surface and an absorbing top surface. As the distance between these two surfaces was reduced, transmission through the device decreased by steps, corresponding to one less bound state fitting inside the waveguide. Gravitationally bound states are a promising tool for metrology, as their energy levels depend on the local gravitational acceleration and could bear the signature of unknown short-range forces. Spectroscopy of these levels can be performed with varying electromagnetic fields or vibrations of the bottom mirror [56–59].

Casimir forces

Coming back to the GBAR experiment, its validity rests on the assumption that no force other than gravity affects the freely falling antihydrogen atom, or at least that any extra force can be accurately accounted for in the result analysis. There will in fact be such a force: the electromagnetic interaction between the atom and detection plate.

Electrically neutral objects have long been known to interact through van der Waals forces. The existence of such interactions was postulated by van der Walls in his 1873 PhD thesis in order to justify his famous equation of state [60]. In 1930, London showed that even particles which do not have a permanent dipole moment interact through the instantaneous dipole which results from quantum fluctuations of the electron cloud. The electrostatic coupling of such instantaneous dipoles leads to the *London dispersion force* [61].

After the war, Verwey and Overbeek found that London's theory failed to explain their experiments with colloidal suspensions [62]. Their results were incompatible with an interaction energy between particles scaling with the distance r as r^{-6}, as predicted by London. Overbeek suggested that the finite time it takes for electromagnetic fields to propagate from one particle to the other should be taken into account. In a short note [63] Casimir and Polder explained that taking this retardation effect into account indeed yielded an energy scaling as r^{-7} at large distances, a result compatible with experiments.

Two years later, Casimir and Polder published a complete quantum electrodynamics calculation of the retarded interaction in the atom-plane and atom-atom configurations [64]. They computed the perturbation of the electromagnetic modes in a box caused by the presence of an atom close to a surface, compared to an atom far from all surfaces. This 2^{nd} order perturbation theory calculation was presented as a preliminary before the 4^{th} order calculation of the atom-atom interaction which followed.

The conceptual breakthrough of Casimir was the interpretation of these forces as the result of a variation of the electromagnetic field's zero-point energy when boundary conditions are modified [65]. He then proceeded to treat the emblematic case of two parallel mirrors in vacuum which experience an attractive force [66]

$$F = -\frac{\hbar c \pi^2 A}{240 L^4} \ , \tag{4}$$

where L the distance between the plates and A their area. Zero-point energy could thus have observable consequences in the macroscopic world and, as Casimir put it, "an experimental confirmation seems not unfeasible and might be of a certain interest" [66].

Actually, it took almost 50 years before a conclusive experimental confirmation of the Casimir force was achieved by Lamoreaux's group in 1997 [67]. The experiment was performed with a sphere and a plane separated by a few microns. Mohideen and collaborators published results for smaller separations the next year [68]. More precise results were obtained by Decca and collaborators by monitoring the shift in frequency of a microelectromechanical resonator brought close to a sphere [69].

On the theoretical side, a great variety of approaches and interpretations were brought forward to describe the phenomenon [70]. Following Casimir's idea, the force

can be seen as a radiation pressure associated with the (thermal and quantum) fluctuations of the electromagnetic field [71]. Alternatively, it can be derived as the interaction of fluctuating dipoles and currents in matter [72, 73].

A notable development of the theory was accomplished by Lifshitz and his colleagues, who included the dielectric properties of the mirrors and the effect of temperature in the calculation of the force [74, 75]. Lifshitz's formula for the Casimir force can be interpreted as a multiple scattering expansion involving the reflection coefficients on the dielectric mirrors. This idea has led to the *scattering approach* to Casimir forces, where the interacting objects are simply described by their scattering properties [76–79]. Two scatterers can be seen as forming a "cavity", and the difference of radiation pressure on the inside and outside of the "cavity" results in a force.

This method is extremely versatile since the force between arbitrary objects can be calculated as long as their scattering properties are known. In the words of Feinberg and Sucher [80], "[the Casimir] interaction may be expressed in terms of measurable quantities that describe the interaction of the individual systems with real photons." Another advantage of the scattering approach is that it does not rely on a regularization scheme. Convergence is ensured by the physical conditions obeyed by the optical response of the scatterers, in particular their transparency at high-frequencies. The interplay of geometry, material properties, temperature and non-equilibrium effects has been successfully investigated within this approach [81]. In this thesis, we will focus on the Casimir-Polder interaction between an atom and a plane surface, which is relevant to GBAR and many other cold atom experiments.

The atom-surface Casimir-Polder interaction has been investigated in a variety of experiments [82]: deflection of atomic or molecular beams flying by a surface or diffracted by a grating, spectroscopy of confined atoms and study of the dynamics of Bose-Einstein condensates near a surface for example. Atoms were also sent to sample the long-range attractive Casimir-Polder potential before being reflected by the short-range repulsive potential of an evanescent wave [83–85] or magnetic mirror [86]. However, the addition of such a repulsive barrier is not absolutely necessary to observe reflection of atoms from a surface. Indeed, scattering of the atomic matter wave on the attractive Casimir-Polder potential itself leads to reflection at low energies, an example of quantum reflection.

The impact of the Casimir-Polder interaction on the GBAR experiment lies not so much in a modification of the free fall time – which is well below the experimental resolution – as in this quantum reflection. The reflected atoms will not be detected at the expected time, leading to a loss in statistics. Moreover, higher energy atoms are less affected by quantum reflection and are thus more likely to be detected. Accurately modeling quantum reflection is therefore necessary to correct this bias.

Quantum reflection

In classical mechanics, there is a clear distinction between regions that are accessible to a particle, where the potential energy is lower than the total energy, and those that are not. Upon reaching the point where energy and potential are equal, a classical particle

necessarily turns back. The wave-like nature of quantum matter blurs these boundaries. A quantum wavefunction can penetrate classically forbidden regions, leading to the famous tunneling effect. Moreover, a quantum wavepacket can reverse its direction of propagation in the absence of a classical turning point. This last phenomenon is commonly known as quantum reflection.

The name "quantum reflection" emphasizes the contrast between the classical and quantum dynamics. In fact, this phenomenon is a general feature of wave propagation in inhomogeneous media [87]: atmospheric and oceanic waves for example, or electromagnetic waves in dielectrics and transmission lines. Roughly speaking, quantum reflection occurs in regions where the wavelength varies rapidly. One of the goals of the present work will be to refine this assertion.

The fact that attractive atom-surface interactions can lead to reflection has been predicted since the early days of quantum mechanics [88, 89]. The role of the attractive van der Waals potential in low-energy atom-surface scattering was emphasized by several authors in the 1970s [90–92] and the importance of including the effect of retardation was recognized at the turn of the century [84, 93].

Observation of the phenomenon has only been achieved relatively recently, because very low temperatures are required to reach sufficiently large wavelengths. The first experiments where carried out in the 1980s with helium and hydrogen atoms scattering off a liquid helium surface [46, 94, 95]. It took several more years before reflection from solid surfaces was observed, first with beams of atoms incident on a surface at grazing incidence [96, 97] and later with Bose-Einstein condensates launched towards the surface at normal incidence [98]. Since, a number of experiments have been carried out with rough or nanostructured surfaces [99–106].

The theory of quantum reflection has tight connections with the Wentzel-Kramers-Brillouin (WKB) semiclassical approximation [107]. In fact, quantum reflection can be seen as a deviation of the exact solutions of the Schrödinger equation from the WKB approximation [108]. For slight departures from the semiclassical approximation, writing the equations in terms of the classical action allows to estimate the small quantum reflection probability [109–112]. This change of coordinate is an example of Liouville transformation, a mathematical tool that we will develop to shed a new light on quantum reflection.

Atom-atom and atom-surface interactions above and below threshold were successfully analyzed in terms of the breakdown of the semiclassical approximation [113–120]. In particular, the quantum reflection probability goes to unity in the "quantum" regime where the energy tends to zero. Material walls could thus be used to trap ultracold atoms [121–123]. Quantum reflection has notably been suggested as a means of trapping and manipulating antihydrogen [124–128], as we will discuss in more detail in this thesis.

Outline of the thesis

The first chapter of this thesis is devoted to the theoretical study of quantum reflection. Quantum reflection is interpreted as a deviation from the semiclassical WKB approximation. This interpretation is made clear by the introduction of Liouville transformations of the Schrödinger equation.

In the next chapter, we apply these results to the case of atoms scattered by the Casimir-Polder potential near a surface. We use the scattering approach to evaluate the Casimir-Polder potential between a hydrogen or antihydrogen atom and various mirrors. We then describe methods to solve the Schrödinger equation in this potential, in particular by taking advantage of Liouville transformations. The results of these calculations and their implications for GBAR are discussed, as well as the role of the boundary condition on the surface.

Chapter III deals with the free fall of quantum wavepackets. We solve the Schrödinger equation for a particle in a gravitational field by considering a free particle in an accelerated frame. The Wigner function formalism is introduced to discuss the links between quantum and classical motion in a linear potential. Based on these results, we calculate the effect of quantum uncertainty on the arrival time in a free fall experiment.

The final chapter aims at making a synthesis of quantum reflection on the one hand and gravitation on the other. We consider atoms that are held in the gravity field above a surface by quantum reflection from the Casimir-Polder potential. We argue that these quantum bouncers are promising tools for antimatter gravity experiments.

Various mathematical results and a discussion of the analogy between quantum reflection and the time-dependent harmonic oscillator are collected in the appendices. Many of the topics covered in this thesis have been the object of publications, listed at the end of this work.

Chapter I
Quantum reflection

This first chapter introduces the phenomenon of quantum reflection and presents the notions and tools that will allow us to understand it and calculate reflection probabilities. We will start by recalling a few results from classical mechanics before introducing the quantum equations. An exactly solvable model of scattering on a potential step will provide a first example of quantum reflection. Afterwards, we will present quantum reflection as a departure from the semiclassical WKB approximation, which we discuss in detail. Based on these ideas, we will define the scattering matrix which gathers the reflection and transmission amplitudes. We will then describe Liouville transformations of the Schrödinger equation, which have the remarkable property of preserving these scattering amplitudes. We will discuss some specific transformations that are relevant to quantum reflection problems. Finally we will show how these transformations bring new insights on high and low energy scattering.

I.1 Classical and quantum mechanics in one dimension

I.1.a Classical mechanics in one dimension

Before addressing the problem of quantum reflection, we give a brief reminder of classical Hamiltonian dynamics in one spatial dimension. Not only will this serve as a reference to understand what is "quantum" in quantum reflection, but it will also allow us to introduce concepts that will prove useful in the semiclassical theory.

Hereafter z is the spatial coordinate and p the conjugate momentum. Classical trajectories $z_{\rm cl}(\tau), p_{\rm cl}(\tau)$ in phase space are those which extremize the action functional

$$S[z(\tau),p(\tau)] \equiv \int_0^t \left[p(\tau)\frac{\mathrm{d}z}{\mathrm{d}\tau}(\tau) - H(z(\tau),p(\tau))\right]\mathrm{d}\tau \ , \tag{I.1}$$

subject to boundary conditions at the initial ($\tau = 0$) and/or final ($\tau = t$) time. Here,

$$H(z,p) \equiv \frac{p^2}{2m} + V(z) \tag{I.2}$$

is the system's Hamiltonian, m is the particle's mass and $V(z)$ the potential. It follows from the Euler-Lagrange equations that the classical trajectories obey Hamilton's equations:

$$\frac{\mathrm{d}z_{\mathrm{cl}}}{\mathrm{d}\tau}(\tau) = \frac{p_{\mathrm{cl}}(\tau)}{m} \ , \qquad \frac{\mathrm{d}p_{\mathrm{cl}}}{\mathrm{d}\tau}(\tau) = -\frac{\mathrm{d}V}{\mathrm{d}z}(z_{\mathrm{cl}}(\tau)) \ . \tag{I.3}$$

We define Hamilton's principal function $S_{\mathrm{cl}}(z,t)$ as the action associated with a classical trajectory $z_{\mathrm{cl}}(\tau)$ which starts at a reference point z_0 at time $\tau = 0$ and ends in z at time $\tau = t$:

$$S_{\mathrm{cl}}(z,t) \equiv S[z_{\mathrm{cl}}(\tau), p_{\mathrm{cl}}(\tau)] = \int_0^t \left[p_{\mathrm{cl}}(\tau)\frac{\mathrm{d}z_{\mathrm{cl}}}{\mathrm{d}\tau}(\tau) - H(z_{\mathrm{cl}}(\tau), p_{\mathrm{cl}}(\tau)) \right] \mathrm{d}\tau \ , \tag{I.4}$$

$$z_{\mathrm{cl}}(0) = z_0 \ , \qquad z_{\mathrm{cl}}(t) = z \ . \tag{I.5}$$

This function obeys the Hamilton-Jacobi equation

$$\frac{\partial S_{\mathrm{cl}}}{\partial t}(z,t) + \frac{1}{2m}\left(\frac{\partial S_{\mathrm{cl}}}{\partial z}(z,t)\right)^2 + V(z) = 0 \ . \tag{I.6}$$

Since the Hamiltonian is constant along a classical trajectory, equal to the energy E, we can rewrite Hamilton's principal function[1]

$$S_{\mathrm{cl}}(z,t) = \int_0^t p_{\mathrm{cl}}(\tau)\frac{\mathrm{d}z_{\mathrm{cl}}}{\mathrm{d}\tau}(\tau)\ \mathrm{d}\tau - Et \ . \tag{I.7}$$

Moreover, we can express the momentum as a function of the position:

$$p_{\mathrm{cl}}(\tau) = \pm\sqrt{2m(E - V(z_{\mathrm{cl}}(\tau)))} \ , \tag{I.8}$$

where the sign depends on the direction of motion. In particular, the momentum cancels and changes sign at points where $V(z) = E$, which are thus known as *classical turning points*. At these points, and only at these points, the particle is reflected. Classical turning points therefore separate regions where $V(z) \leq E$, which are accessible to a classical particle, from those where $V(z) > E$, which are *classically forbidden* and where the classical momentum is undefined. For a trajectory that has no turning point, we can change variables from τ to $\zeta = z_{\mathrm{cl}}(\tau)$ in the integral of equation (I.7) and obtain

$$S_{\mathrm{cl}}(z,t) = \int_{z_0}^{z} \sqrt{2m(E - V(\zeta))}\ \mathrm{d}\zeta - Et \ . \tag{I.9}$$

Finally we use a Legendre transformation to change variables from t to E and arrive at Hamilton's characteristic function:

$$\Sigma_{\mathrm{cl}} \equiv S_{\mathrm{cl}} + Et \ , \qquad \Sigma_{\mathrm{cl}}(z,E) = \int_{z_0}^{z} \sqrt{2m(E - V(\zeta))}\ \mathrm{d}\zeta \ . \tag{I.10}$$

Hamilton's characteristic function obeys a time-independent Hamilton-Jacobi equation:

$$\frac{1}{2m}\left(\frac{\partial \Sigma_{\mathrm{cl}}}{\partial z}(z,E)\right)^2 + V(z) - E = 0 \tag{I.11}$$

and it plays a central role in semiclassical theory (see section I.2.a).

[1] The dependence of E on z_0, z and t is implicit here.

I.1.b Schrödinger equation in one dimension

We now turn to the (non-relativistic) motion of a spinless quantum particle of mass m in one dimension. It is described by a wavefunction $\psi(z,t)$ obeying the Schrödinger equation

$$i\hbar\frac{\partial\psi}{\partial t}(z,t) = -\frac{\hbar^2}{2m}\frac{\partial^2\psi}{\partial z^2}(z,t) + V(z)\psi(z,t) \ . \tag{I.12}$$

Stationary solutions are found by introducing the ansatz

$$\psi(z,t) \equiv \psi_E(z)\exp(-iEt/\hbar) \ , \tag{I.13}$$

which yields the time-independent Schrödinger equation

$$-\frac{\hbar^2}{2m}\frac{\mathrm{d}^2\psi_E}{\mathrm{d}z^2}(z) + V(z)\psi_E(z) = E\psi_E(z) \ . \tag{I.14}$$

When there is no risk of confusion, we drop the index E and use the compact notation

$$\psi''(z) + F(z)\psi(z) = 0 \ , \qquad F(z) \equiv \frac{2m}{\hbar^2}(E - V(z)) \ . \tag{I.15}$$

Here and in the following, primes denote the derivative of a function with respect to its argument. When $F(z)$ is positive, it is equal to the square of the classical momentum (I.8) and determines the associated de Broglie wavelength and wavevector as

$$\lambda_{\mathrm{dB}}(z) \equiv \frac{2\pi}{\sqrt{F(z)}} \ , \qquad k_{\mathrm{dB}}(z) \equiv \sqrt{F(z)} = \frac{2\pi}{\lambda_{\mathrm{dB}}} \ , \qquad F(z) > 0 \ . \tag{I.16}$$

As we have observed in the introduction, equation (I.15) appears in many physical problems, notably wave propagation in inhomogeneous media. The results obtained here in the context of quantum mechanics can be applied to these related problems. Moreover, if z is seen as a time coordinate and ψ as a position, the Schrödinger equation (I.15) is also the classical equation of motion of a harmonic oscillator with a time-dependent spring constant. This provides a connection to the subject of classical and quantum parametric oscillators, which we will discuss in appendix D.

The polar representation of the wavefunction

It is instructive to write the wavefunction in polar form:

$$\psi(z,t) \equiv \sqrt{\rho(z,t)}\exp\left(i\theta(z,t)\right) \ . \tag{I.17}$$

Here $\rho(z,t) = |\psi(z,t)|^2$ is the probability density associated with the wavefunction and $\theta(z,t)$ is a real phase. Injecting the above expression into equation (I.12) and separating

the real and imaginary parts we obtain a pair of coupled equations[2]:

$$\frac{\partial \rho}{\partial t} + \frac{\partial}{\partial z}\left(\frac{\hbar \rho}{m}\frac{\partial \theta}{\partial z}\right) = 0 \ , \tag{I.18}$$

$$\hbar \frac{\partial \theta}{\partial t} + \frac{\hbar^2}{2m}\left(\frac{\partial \theta}{\partial z}\right)^2 + V - \frac{\hbar^2}{2m}\frac{1}{\sqrt{\rho}}\frac{\partial^2 \sqrt{\rho}}{\partial z^2} = 0 \ . \tag{I.19}$$

We can rewrite the first equation as a continuity equation:

$$\frac{\partial \rho}{\partial t}(z,t) + \frac{\partial j}{\partial z}(z,t) = 0 \ , \tag{I.20}$$

where

$$j(z,t) \equiv \frac{\hbar}{2im}\left(\psi^* \frac{\partial \psi}{\partial z} - \psi \frac{\partial \psi^*}{\partial z}\right) = \frac{\hbar \rho}{m}\frac{\partial \theta}{\partial z} \tag{I.21}$$

is the probability density current. The second equation is similar to the Hamilton-Jacobi equation (I.6) for the action $\hbar\theta(z,t)$, but it differs from it by a term of order $\hbar^2$.

The time-independent versions of equations (I.19) are obtained by taking

$$\rho(z,t) \equiv \rho(z) \ , \qquad\qquad \theta(z,t) \equiv \phi(z) - \frac{Et}{\hbar} \ , \tag{I.22}$$

which yields

$$\frac{\mathrm{d}}{\mathrm{d}z}\left(\frac{\hbar \rho}{m}\frac{\mathrm{d}\phi}{\mathrm{d}z}\right) = 0 \ , \tag{I.23}$$

$$\frac{\hbar^2}{2m}\left(\frac{\mathrm{d}\phi}{\mathrm{d}z}\right)^2 + V - E - \frac{\hbar^2}{2m}\frac{1}{\sqrt{\rho}}\frac{\mathrm{d}^2 \sqrt{\rho}}{\mathrm{d}z^2} = 0 \ . \tag{I.24}$$

The continuity equation now states that the current is uniform:

$$j(z,t) = j = \frac{\hbar \rho}{m}\phi'(z) \ . \tag{I.25}$$

This allows us to express the probability density in terms of the derivative of the phase $\phi(z)$:

$$\rho(z) = \frac{mj}{\hbar \phi'(z)} \ . \tag{I.26}$$

The wavefunction can thus be expressed in terms of the phase only:

$$\psi(z) = \sqrt{\frac{mj}{\hbar \phi'(z)}}\exp(i\phi(z)) = \frac{\mathcal{N}}{\sqrt{|\phi'(z)|}}\exp(i\phi(z)) \ . \tag{I.27}$$

[2]To lighten the notation, the functions' variables are omitted when there is no risk of confusion.

In the following, we will often set the constant $\mathcal{N} \equiv \sqrt{\hbar^{-1} m|j|}$ equal to 1 for the sake of simplicity.

We obtain a closed equation for the phase by replacing (I.26) in (I.24):

$$\phi'(z)^2 - F(z) + \frac{1}{2}\{\phi, z\} = 0 \ . \tag{I.28}$$

This equation is reminiscent of the classical time-independent Hamilton-Jacobi equation (I.11), except for an extra term involving the *Schwarzian derivative* $\{\phi, z\}$ of ϕ with respect to z. In general, the Schwarzian derivative of a function $f(x)$ that is differentiable three times is defined by any of the following equalities:

$$\{f, x\} \equiv \frac{f'''(x)}{f'(x)} - \frac{3}{2}\left(\frac{f''(x)}{f'(x)}\right)^2 \tag{I.29}$$

$$= \frac{\mathrm{d}}{\mathrm{d}x}\left(\frac{f''(x)}{f'(x)}\right) - \frac{1}{2}\left(\frac{f''(x)}{f'(x)}\right)^2 \tag{I.30}$$

$$= \frac{\mathrm{d}^2}{\mathrm{d}x^2}\ln(f'(x)) - \frac{1}{2}\left(\frac{\mathrm{d}}{\mathrm{d}x}\ln(f'(x))\right)^2 \tag{I.31}$$

$$= -2\sqrt{f'(x)}\frac{\mathrm{d}^2}{\mathrm{d}x^2}\left(\frac{1}{\sqrt{f'(x)}}\right) \tag{I.32}$$

$$= \lim_{y\to x} 6\frac{\partial^2}{\partial x \partial y}\ln\left(\frac{f(x)-f(y)}{x-y}\right) \ . \tag{I.33}$$

We will discuss this differential operator in more detail in the course of this work. Let us simply mention an important property here: the Schwarzian derivative of a function $f(x)$ is zero if and only if $f(x)$ is a linear fractional transformation[3]:

$$\{f, x\} = 0 \quad \Leftrightarrow \quad f(x) = \frac{ax+b}{cx+d} \ . \tag{I.34}$$

Finally, note that if ϕ is a solution of (I.28), so is $-\phi$, which corresponds to an opposite current. The real solutions of the Schrödinger equation (I.15) cannot be cast into the polar form (I.17) but they are simply obtained by summing or subtracting the wavefunctions associated with ϕ and $-\phi$.

The Wronskian

A central object in the theory of second order differential equations is the Wronskian:

$$\mathcal{W}(\psi_1, \psi_2) \equiv \psi_1(z)\psi_2'(z) - \psi_1'(z)\psi_2(z) \ . \tag{I.35}$$

If ψ_1 and ψ_2 are two solutions of the Schrödinger equation (I.15), we see by taking a derivative with respect to z that the Wronskian is a constant:

$$\frac{\mathrm{d}}{\mathrm{d}z}\mathcal{W}(\psi_1, \psi_2) = \psi_1(z)\psi_2''(z) - \psi_1''(z)\psi_2(z) = 0 \ . \tag{I.36}$$

[3]Fractional linear transformations are also known as homographies or Möbius transformations.

Therefore the Wronskian is a bilinear skew-symmetric form on the space of solutions:

$$\mathcal{W}(\psi_1, \lambda\psi_2 + \psi_3) = \lambda\mathcal{W}(\psi_1, \psi_2) + \mathcal{W}(\psi_1, \psi_3) \ , \tag{I.37}$$
$$\mathcal{W}(\psi_1, \psi_2) = -\mathcal{W}(\psi_2, \psi_1) \ . \tag{I.38}$$

If the two solutions are linearly dependent, their Wronskian vanishes. The converse is true in non-pathological cases.

The Wronskian can therefore be used to retrieve the coefficients of a solution of the Schrödinger equation written as a linear combination of basis solutions:

$$\psi(z) = A\psi_1(z) + B\psi_2(z) \ , \qquad \mathcal{W}(\psi_1, \psi_2) \neq 0 \ , \tag{I.39}$$
$$A = \frac{\mathcal{W}(\psi, \psi_2)}{\mathcal{W}(\psi_1, \psi_2)} \ , \qquad B = -\frac{\mathcal{W}(\psi, \psi_1)}{\mathcal{W}(\psi_1, \psi_2)} \ . \tag{I.40}$$

The probability density current associated with a wavefunction $\psi(z)$ can be expressed as a Wronskian: when ψ is a solution of (I.15), so is its complex conjugate ψ^* and

$$j = \frac{\hbar}{2im}\mathcal{W}(\psi^*, \psi) \ . \tag{I.41}$$

More generally, many physical quantities can be expressed as Wronskians. In particular we show in appendix A that this is the case of the elements of the scattering and transfer matrices.

I.1.c Transmission and reflection on a step

To introduce the concept of quantum reflection, we briefly examine a well-known example of scattering on a potential step

$$V(z) = \frac{U}{1 + \exp(-z/L)} \ . \tag{I.42}$$

We suppose that the energy E is positive and above the step: $E > \max(0, U)$, so that there is no classical turning point. The situation is represented in figure I.1: the wavevector $k_{\mathrm{dB}}(z)$ changes on a length scale L from $k_L \equiv \hbar^{-1}\sqrt{2mE}$ on the left side of the step to $k_R \equiv \hbar^{-1}\sqrt{2m(E-U)}$ on the right. In this case a classical particle arriving from the left with velocity $v_L = \hbar k_L/m$ leaves on the right with a velocity $v_R = \hbar k_R/m$ which is smaller than v_L if the step is repulsive ($U > 0$) or larger if it is attractive ($U < 0$) but is always positive.

As shown in [129], a solution of the Schrödinger equation (I.14) with the potential (I.42) can be expressed with the help of the hypergeometric function [1]:

$$\psi(z) = \frac{e^{ik_R z}}{\sqrt{k_R}} F\left(i(k_L - k_R)L, -i(k_L + k_R)L; 1 - 2ik_R L; -e^{-z/L}\right) \ . \tag{I.43}$$

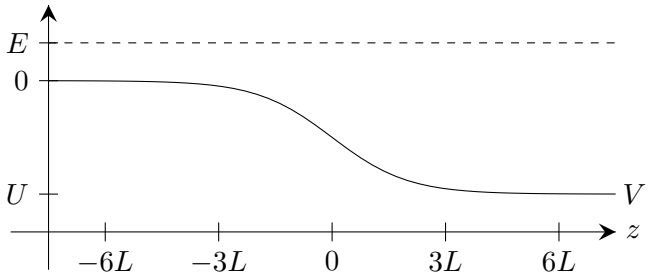

Figure I.1: The step potential (I.42) which causes quantum reflection.

Since the hypergeometric function goes to 1 as z goes to positive infinity, this solution matches a rightward propagating wave with wavevector k_R on the right of the step:

$$\psi(z) \underset{z\to\infty}{\simeq} \frac{e^{ik_R z}}{\sqrt{k_R}} \ . \tag{I.44}$$

On the left side of the step, the wavefunction tends to a sum of counterpropagating waves

$$\psi(z) \underset{z\to-\infty}{\simeq} A\frac{e^{ik_L z}}{\sqrt{k_L}} + B\frac{e^{ik_L z}}{\sqrt{k_L}} \ , \tag{I.45}$$

$$A = \sqrt{\frac{k_L}{k_R}}\frac{\Gamma(-2ik_L L)\Gamma(1-2ik_R L)}{\Gamma(-i(k_L+k_R)L)\Gamma(1-i(k_L+k_R)L)} \ , \tag{I.46}$$

$$B = \sqrt{\frac{k_L}{k_R}}\frac{\Gamma(2ik_L L)\Gamma(1-2ik_R L)}{\Gamma(i(k_L-k_R)L)\Gamma(1+i(k_L-k_R)L)} \ . \tag{I.47}$$

Note that we have chosen the normalization of the waves such that the current is independent of k_L and k_R.

This wavefunction describes the stationary process in which a wave arrives from the left (first term in (I.45)) and is partly reflected on the step (second term in (I.45)), and partly transmitted (equation (I.44)). We define the reflection (resp. transmission) coefficient as the amplitude of the reflected (resp. transmitted) wave divided by that of the incoming wave:

$$r \equiv \frac{B}{A} = \frac{\Gamma(2ik_L L)\Gamma(-i(k_L+k_R)L)\Gamma(1-i(k_L+k_R)L)}{\Gamma(i(k_L-k_R)L)\Gamma(1+i(k_L-k_R)L)\Gamma(-2ik_L L)} \ , \tag{I.48}$$

$$t \equiv \frac{1}{A} = \sqrt{\frac{k_R}{k_L}}\frac{\Gamma(-i(k_L+k_R)L)\Gamma(1-i(k_L+k_R)L)}{\Gamma(-2ik_L L)\Gamma(1-2ik_R L)} \ . \tag{I.49}$$

The square moduli of these amplitudes sum to 1, and can be interpreted as proba-

bilities of reflection or transmission:

$$|r|^2 \equiv R = \frac{\sinh(\pi(k_R - k_L)L)^2}{\sinh(\pi(k_R + k_L)L)^2} \,, \tag{I.50}$$

$$|t|^2 = 1 - R = \frac{\sinh(2\pi k_R L)\sinh(2\pi k_L L)}{\sinh(\pi(k_R + k_L)L)^2} \,. \tag{I.51}$$

The dependence of the reflection probability R on the ratio k_R/k_L which describes the size of the step and on the product $k_L L$ which quantifies its smoothness is shown in figure I.2.

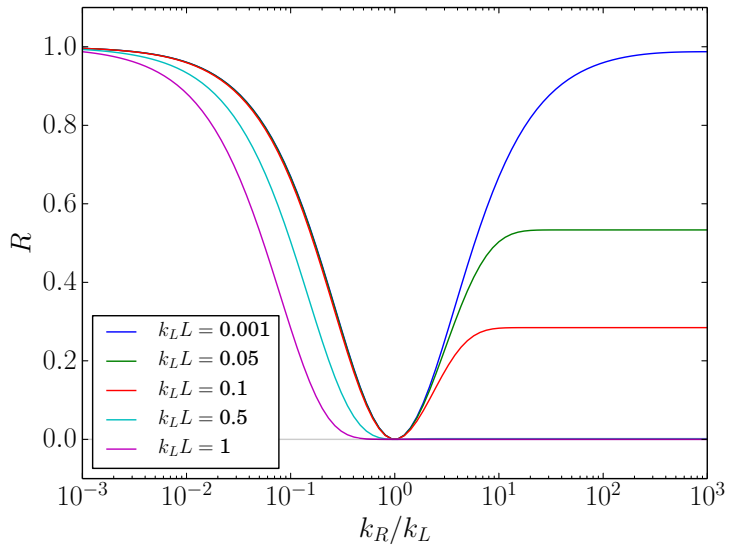

Figure I.2: Reflection probability on a series of steps of varying smoothness $k_L L = 0.001, 0.05, 0.1, 0.5$ and 1 as a function of their repulsive ($k_R/k_L < 1$) or attractive ($k_R/k_L > 1$) character.

At this point we can make several observations:

- Reflection occurs whether the step is attractive ($U < 0$, $k_R > k_L$) or repulsive ($U > 0$, $k_R < k_L$), whereas classically we expect no reflection in either case.
- The reflection probability is zero only for a flat potential ($U = 0$, $k_R/k_L = 1$). It increases when the step height increases, that is when the ratio k_R/k_L moves away from 1.
- The reflection probability is larger for steeper steps (smaller values of L). In the limit $L \to 0$ we recover the well-known result [130]

$$r = \frac{k_L - k_R}{k_L + k_R} \,, \qquad\qquad t = \frac{2\sqrt{k_L k_R}}{k_L + k_R} \,. \tag{I.52}$$

In this limit the reflection probability is invariant under the exchange of k_L and k_R.

Quantum reflection thus appears as a non-adiabatic process which occurs when the potential varies rapidly on the scale of the de Broglie wavelength $\lambda_{\mathrm{dB}} = 2\pi/k_{\mathrm{dB}}$. That being said, the dependence of the reflection probability on the parameters of the problem is rather subtle. For example, figure I.2 shows that in the case where $k_L L = 1$, R barely increases when the step becomes infinitely high ($U \to -\infty, k_R/k_L \to \infty$). In the next section, we will give a rigorous description of quantum reflection as a deviation of the exact quantum dynamics from the semiclassical approximation and we will derive a better criterion to identify situations which give rise to quantum reflection.

I.2 Quantum reflection and the WKB approximation

I.2.a The WKB approximation

We have seen in the example of the previous section that quantum wavefunctions behave in non-classical ways. However, one could argue that we are comparing notions which are not comparable: the behavior of a point particle and that of a wave. To put our definition of quantum reflection on a firmer footing, we need a classical theory for matter waves.

In the previous section, we have defined incident and reflected waves, which was possible only far from the step, where the motion of a quantum wavepacket mimics that of a classical particle: the wavepacket does not split and its center propagates along a classical trajectory. At the step, this picture breaks down and quantum reflection occurs. The objectives of this section are to find a semiclassical description in which the direction of propagation is defined unambiguously and to identify the regions where this description is valid.

The Wentzel-Kramers-Brillouin (WKB) approximation is one of the best known semiclassical approximations to the Schrödinger equation (I.15). This approximation scheme can in fact be traced back to the works of Liouville on the heat equation [131] and Green on waves in canals [132]. It has been introduced in the context of quantum mechanics by Wentzel [133], Kramers [134] and Brillouin [135], who complemented it by connection formulas allowing to relate wavefunctions in classically allowed and forbidden areas (we discuss this issue in more detail in section I.3.e). The contribution of Jeffreys [136] to the mathematical theory is sometimes acknowledged by appending his initial to the name[4].

In the following, unless otherwise mentioned, we place ourselves in a classically allowed region, where $F(z) > 0$.

A first derivation

The most common derivation of the WKB approximation uses an expansion in powers of the reduced Planck constant $\hbar$ (see [110, 133] for example), which emphasizes its

[4]Historical notes on the development of the WKB approximation can be found in [137, 138]

semiclassical nature. Here we first give a related derivation which exploits the similarity between the equation obeyed by the phase of the wavefunction (I.19) and the classical Hamilton-Jacobi equation (I.6). Neglecting the term of order $\hbar^2$ in the quantum equation amounts to neglecting the Schwarzian derivative in the time-independent equation (I.28):

$$\phi'(z)^2 - F(z) = \phi'(z)^2 - k_{\rm dB}(z)^2 \simeq 0 \ . \tag{I.53}$$

In this approximation the phase is a primitive of the de Broglie wavevector:

$$\phi(z) \simeq \pm\phi_{\rm dB}(z) \ , \qquad \phi_{\rm dB}(z) \equiv \int_{z_0}^{z} k_{\rm dB}(\zeta)\ {\rm d}\zeta \ . \tag{I.54}$$

We call this primitive the WKB phase and leave its dependence on the energy E and the reference point z_0 implicit. By comparison with (I.10), we see that it is equal to Hamilton's characteristic function divided by $\hbar$:

$$\phi_{\rm dB}(z) = \frac{1}{\hbar}\Sigma_{\rm cl}(z,E) \ . \tag{I.55}$$

Therefore, within the WKB approximation, a basis of solutions of the Schrödinger equation is

$$\psi^{\pm}_{\rm WKB}(z) \equiv \frac{1}{\sqrt{\phi'_{\rm dB}(z)}}\exp(\pm i\phi_{\rm dB}(z)) = \frac{1}{\sqrt{k_{\rm dB}(z)}}\exp(\pm i\phi_{\rm dB}(z)) \ . \tag{I.56}$$

A second derivation

Another derivation, by Bremmer [108], emphasizes the relationship of the WKB approximation with quantum reflection. We sketch his derivation in the following. To this aim we consider an arbitrary potential $V(z)$ and place ourselves in a classically allowed region ($E > V(z)$) which we divide into N segments with endpoints

$$z_0 < ... < z_{j-1} < z_j < z_{j+1} < ... < z_N \ . \tag{I.57}$$

We now consider an approximation of the potential by a piecewise constant function which takes the value $V(z_j)$ when $z_{j-1} < z < z_j$. The associated wavevector is $k_j \equiv k_{\rm dB}(z_j) = \hbar^{-1}\sqrt{2m(E-V(z_j))}$. This is sketched in figure I.3.

In this staircase potential, we can write the wavefunction on each segment as the sum of a leftward and a rightward traveling component:

$$\psi(z) = \psi^+(z) + \psi^-(z) \ , \qquad \psi^{\pm}(z) \propto \exp(\pm ik_j z) \ , \qquad z_{j-1} \le z < z_j \ . \tag{I.58}$$

Matching the wavefunction and its derivative on both sides[5] of z_j, we find that

$$\begin{pmatrix} \psi^+(z_j^+) \\ \psi^-(z_j^+) \end{pmatrix} = \frac{1}{2k_{j+1}} \begin{pmatrix} k_{j+1}+k_j & k_{j+1}-k_j \\ k_{j+1}-k_j & k_{j+1}+k_j \end{pmatrix} \begin{pmatrix} \psi^+(z_j^-) \\ \psi^-(z_j^-) \end{pmatrix} \ . \tag{I.59}$$

[5] We denote z_j^- and z_j^+ the points immediately to the left and right of z_j, respectively.

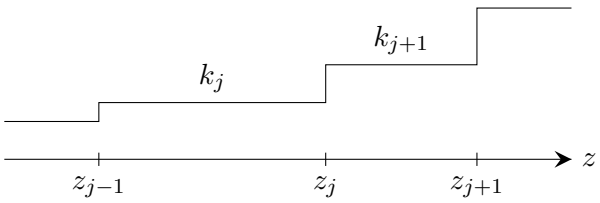

Figure I.3: In Bremmer's derivation of the WKB approximation, the exact potential is approximated by a piecewise constant function. Neglecting reflections at the steps leads to the WKB wavefunction.

In regions where the potential is constant, each wave simply picks up a phase, so that

$$\begin{pmatrix} \psi^+(z_{j+1}^-) \\ \psi^-(z_{j+1}^-) \end{pmatrix} = \begin{pmatrix} e^{ik_{j+1}(z_{j+1}-z_j)} & 0 \\ 0 & e^{-ik_{j+1}(z_{j+1}-z_j)} \end{pmatrix} \begin{pmatrix} \psi^+(z_j^+) \\ \psi^-(z_j^+) \end{pmatrix} . \tag{I.60}$$

We can now form the ratio $\dfrac{\psi^\pm(z_{j+1}^-) - \psi^\pm(z_j^-)}{z_{j+1} - z_j}$ and take the limit of an infinite number of segments the length of which go to zero. We obtain a pair of coupled differential equations for $\psi^\pm(z)$:

$$\psi'^\pm(z) = \left(\pm i k_{\rm dB}(z) - \frac{k'_{\rm dB}(z)}{2k_{\rm dB}(z)} \right) \psi^\pm(z) + \frac{k'_{\rm dB}(z)}{2k_{\rm dB}(z)} \psi^\mp(z) . \tag{I.61}$$

For the moment, we have only reformulated the Schrödinger equation, and one easily checks that if (I.61) is satisfied then $\psi = \psi^+ + \psi^-$ is an exact solution of the Schrödinger equation. The WKB approximation consists in neglecting reflections on all the steps of the staircase potential. This amounts to neglecting non diagonal terms in the matrix which couples rightward and leftward traveling waves in (I.59). The resulting differential equations are then decoupled:

$$\psi'^\pm_{\rm WKB}(z) = \left(\pm i k_{\rm dB}(z) - \frac{k'_{\rm dB}(z)}{2k_{\rm dB}(z)} \right) \psi^\pm_{\rm WKB}(z) \tag{I.62}$$

and we can integrate them under the form of equation (I.56). With this derivation we see that the WKB approximation will be satisfied in regions where $|k'_{\rm dB}(z)/2k_{\rm dB}(z)| \ll k_{\rm dB}(z)$, that is $|\lambda'_{\rm dB}(z)| \ll 4\pi$. This is a sufficient, but not a necessary condition, as we will see later on.

Motion of WKB wavepackets

We now should check that in a region of space and in an energy range where the WKB approximation is valid, the solutions of the Schrödinger equation indeed behave classically. To do so, we form a wavepacket of solutions that are well approximated by rightward traveling WKB waves:

$$\psi(z,t) = \int w(E)\, \psi_E(z)\, \exp(-iEt/\hbar)\, {\rm d}E , \qquad \psi_E(z) \simeq \psi^+_{\rm WKB}(z) . \tag{I.63}$$

Here $w(E)$ is a real-valued weighting function peaked around a central value E_0.

The center of the wavepacket at time t is the position z such that the phase is stationary with respect to E around E_0:

$$\frac{\partial}{\partial E}\left(\phi_{\rm dB}(z) - Et/\hbar\right)\Big|_{E_0} = 0 \ , \quad \text{that is} \quad \frac{\partial}{\partial E}\left(W(z,E) - Et\right)\Big|_{E_0} = 0 \ , \tag{I.64}$$

which yields

$$\int_{z_0}^{z} \frac{m\ \mathrm{d}\zeta}{\sqrt{2m(E_0 - V(\zeta))}} = t \ . \tag{I.65}$$

Let $z_{\rm cl}(\tau)$ be the classical trajectory starting in z_0 with energy E_0 and moving towards the right, it obeys

$$\frac{\mathrm{d}z_{\rm cl}}{\mathrm{d}\tau}(\tau) = \frac{p_{\rm cl}(\tau)}{m} = \frac{\sqrt{2m(E_0 - V(z_{\rm cl}(\tau)))}}{m} \ . \tag{I.66}$$

Using the change of variables $\zeta = z_{\rm cl}(\tau)$ we show that $z_{\rm cl}(t)$ is the solution of (I.65):

$$\int_{z_0}^{z_{\rm cl}(t)} \frac{m\ \mathrm{d}\zeta}{\sqrt{2m(E_0 - V(\zeta))}} = \int_0^t \frac{\mathrm{d}z_{\rm cl}}{\mathrm{d}\tau}(\tau) \frac{m\ \mathrm{d}\tau}{\sqrt{2m(E_0 - V(z_{\rm cl}(\tau)))}} = \int_0^t \mathrm{d}\tau = t \ . \tag{I.67}$$

We conclude that in regions where the WKB approximation is applicable, wavepackets follow the classical trajectory corresponding to their central energy. This justifies the use of WKB wavefunctions as a reference for classical behavior.

I.2.b The badlands function

It is interesting to note that although the WKB wavefunctions (I.56) are not exact solutions of the original Schrödinger equation (I.15), they are exact solutions of a modified Schrödinger equation:

$$\psi''^{\pm}_{\rm WKB}(z) + F(z)(1 + Q(z))\psi^{\pm}_{\rm WKB}(z) \ , \tag{I.68}$$

where the function $Q(z)$ can be written in a variety of ways:

$$\begin{aligned}
Q(z) &\equiv \frac{1}{2F(z)}\{\phi_{\rm dB}, z\} && \text{(I.69)}\\
&= \frac{1}{2}\frac{k''_{\rm dB}(z)}{k_{\rm dB}(z)^3} - \frac{3}{4}\frac{k'_{\rm dB}(z)^2}{k_{\rm dB}(z)^4} && \text{(I.70)}\\
&= \frac{F''(z)}{4F(z)^2} - \frac{5F'(z)^2}{16F(z)^3} && \text{(I.71)}\\
&= \frac{\hbar^2}{2m}\frac{4(V(z)-E)V''(z) - 5V'(z)^2}{16(E - V(z))^3} && \text{(I.72)}\\
&= -\frac{1}{4\pi^2}\left(\sqrt{\lambda_{\rm dB}(z)}\right)^3 \frac{\mathrm{d}^2}{\mathrm{d}z^2}\sqrt{\lambda_{\rm dB}(z)} \ . && \text{(I.73)}
\end{aligned}$$

In regions where $Q(z)$ is small compared to one, the exact and WKB wavefunctions obey essentially the same equation, therefore exact solutions can be written as linear combinations of WKB waves. This is obviously the case in regions of constant potential, but $Q(z)$ can also become negligible in regions where $F(z) = E - V(z)$ is very large, even if $V(z)$ varies rapidly. In these regions the direction of propagation of matter waves can be defined unambiguously, so that no quantum reflection can occur.

It follows that quantum reflection can happen only in regions where $Q(z)$ has significant values. These regions are typically associated to small values of $F(z)$ and/or fast variations of the potential. We expect the WKB approximation to break down in these regions, which are known as the *badlands*.

To illustrate the link between the *badlands function* $Q(z)$ and quantum reflection, we return to the example of the potential step given in section I.1.c. Figure I.4 displays the energy and potential for various choices of parameters, along with the corresponding badlands function. The badlands function features a bump accompanied by a smaller dip and it vanishes away from the step. In the top panel, the potential is kept fixed while the energy is varied and lower energies are seen to be associated with a larger magnitude of the badlands function. The middle panel shows the effect of varying the steepness of the step, with steeper steps corresponding to larger, more localized badlands peaks. Finally, in the bottom panel the step height U is varied. Although higher steps lead to slightly taller badlands peaks, the effect is not very pronounced.

Qualitatively, the height of the badlands peak is well correlated with the probability of quantum reflection (see figure I.2 and the values of R given in the captions of figure I.4). However, at this point we have not established a quantitative link between the badlands function and quantum reflection. For the moment the role of the badlands function is discussed by comparing two different problems associated with equations (I.15) and (I.68). In section I.3.d we will give a more satisfactory interpretation of the badlands function, based only on the physical equation (I.15). Until we provide this firmer footing, the badlands function can only be seen as a clue as to how much quantum reflection can be expected and where it occurs.

I.2.c Coupled WKB waves

We have seen in the previous section that the WKB waves are constructed in such a way that their direction of propagation is well defined. Therefore quantum reflection can be seen as a departure of the exact solution of the Schrödinger equation from its WKB approximation. In particular, it is instructive to write an exact solution to the Schrödinger equation as a linear combination of WKB waves with space-dependent coefficients $a_+(z)$ and $a_-(z)$:

$$\psi(z) \equiv a_+(z)\psi^+_{\mathrm{WKB}}(z) + a_-(z)\psi^-_{\mathrm{WKB}}(z) \ . \tag{I.74}$$

The idea is that $a_\pm$ should be constant in regions where the WKB approximation is accurate but may vary elsewhere, allowing for the conversion of an incident wave into a reflected one. Moreover, we expect any fast variations of the wavefunction to be absorbed in the WKB basis functions, so that the coefficients $a_\pm$ vary slowly.

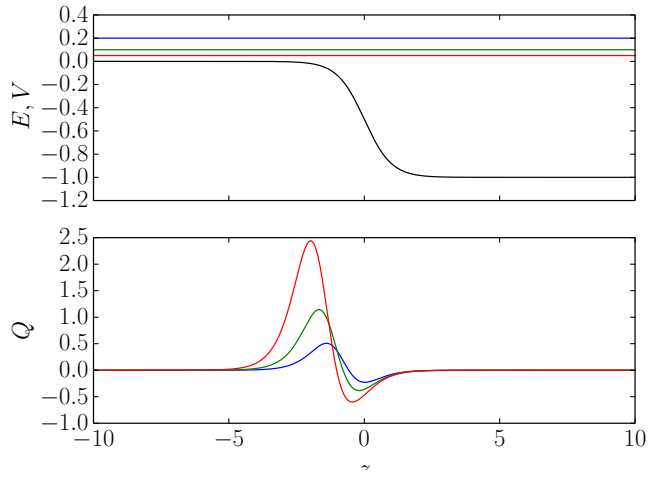

(a) $U = -1$, $L = 0.5$ and $E = 0.2$ (blue), 0.1 (green) and 0.05 (red). The corresponding reflection probabilities for a wave impinging from the left are respectively $R = 4.6$, 11.4 and 21.6%.

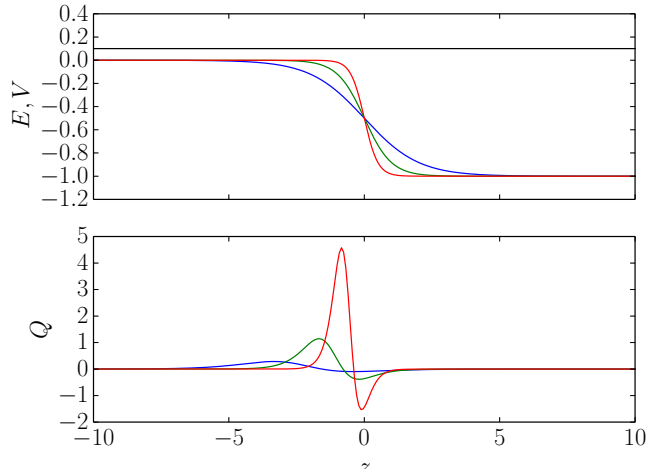

(b) $U = -1$, $E = 0.1$ and $L = 1$ (blue), 0.5 (green) and 0.25 (red). The corresponding reflection probabilities for a wave impinging from the left are respectively $R = 1.8$, 11.4 and 22.2%.

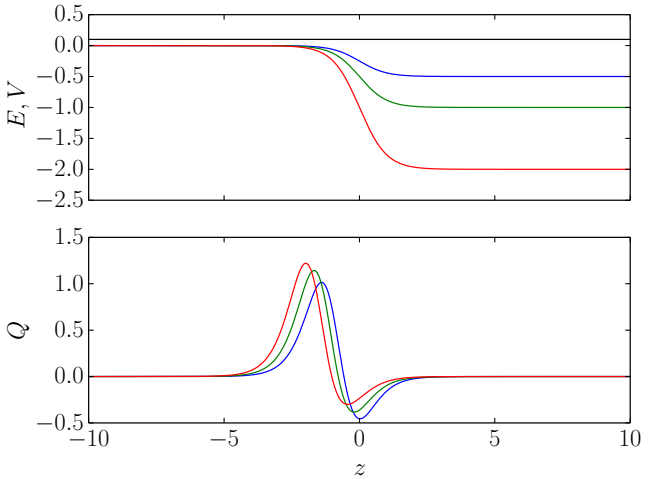

(c) $E = 0.1$, $L = 0.5$ and $U = -0.5$ (blue), -1 (green) and -2 (red). The corresponding reflection probabilities for a wave impinging from the left are respectively $R = 8.5$, 11.4 and 13.0%.

Figure I.4: Potential step (I.42) and badlands function $Q(z)$ for various choices of the energy E (top panel), step width L (middle panel) and step height U (bottom panel). The units used in these plots are such that $\hbar^2/2m = 1$.

Equation (I.74) must be complemented by another condition in order to define $a_\pm(z)$ unambiguously and several choices have been made in the literature. One option is to identify $a_\pm\psi^\pm_{\rm WKB}$ with the right and left moving parts of the wavefunction $\psi^\pm$ introduced in (I.58). Then equations (I.61) yield the following coupled equations for $a_\pm$:

$$a'_\pm(z) = \frac{k'_{\rm dB}(z)}{2k_{\rm dB}(z)} a_\mp(z)\exp(\mp 2i\phi_{\rm dB}(z)) \ . \tag{I.75}$$

This equation is derived in particular by Berry and Mount [110]. This choice leads to the following expression for the derivative of ψ:

$$\psi'(z) = ik_{\rm dB}(z)a_+(z)\psi^+_{\rm WKB}(z) - ik_{\rm dB}(z)a_-(z)\psi^-_{\rm WKB}(z) \ . \tag{I.76}$$

In his 1935 article [139], Kemble recommends a slightly different choice, requiring the derivative of the wavefunction to be given by

$$\psi'(z) = a_+(z)\psi'^+_{\rm WKB}(z) + a_-(z)\psi'^-_{\rm WKB}(z) \ . \tag{I.77}$$

In this case the coefficients $a_\pm$ can be expressed as Wronskians of ψ with the WKB functions:

$$a_\pm(z) = \frac{\mathcal{W}(\psi^\mp_{\rm WKB},\psi)}{\mathcal{W}(\psi^\mp_{\rm WKB},\psi^\pm_{\rm WKB})} = \pm\frac{1}{2i}\mathcal{W}(\psi^\mp_{\rm WKB},\psi) \ . \tag{I.78}$$

This choice is more in line with the method of extracting coefficients of a linear combination using the Wronskian (see equation (I.40)), except that in this case the basis functions are not exact solutions of the equation. Taking the derivative of this Wronskian, and using equations (I.15) and (I.68) obeyed by ψ and $\psi^\pm_{\rm WKB}$ respectively we find

$$\begin{aligned} a'_\pm(z) &= \pm\frac{k_{\rm dB}(z)^2}{2i}Q(z)\psi^\mp_{\rm WKB}(z)\psi(z) \\ &= \pm\frac{k_{\rm dB}(z)}{2i}Q(z)\left(a_\pm(z) + a_\mp(z)\exp\left(\mp 2i\phi_{\rm dB}(z)\right)\right) \ . \end{aligned} \tag{I.79}$$

This procedure can be generalized to any basis of complex conjugate wavefunctions. For any smooth increasing function $\varphi(z)$ we can write

$$\psi(z) = a_+(z)\frac{\exp(i\varphi(z))}{\sqrt{\varphi'(z)}} + a_-(z)\frac{\exp(-i\varphi(z))}{\sqrt{\varphi'(z)}} \ , \tag{I.80}$$

$$a_\pm(z) = \frac{\pm 1}{2i}\mathcal{W}\left(\frac{\exp(\mp i\varphi(z))}{\sqrt{\varphi'(z)}},\psi\right) \ . \tag{I.81}$$

Taking a derivative, we obtain the following coupled equations:

$$a'_\pm(z) = \frac{\pm 1}{2i}\left(\varphi'(z)^2 - F(z) + \frac{1}{2}\{\varphi,z\}\right)\frac{\exp(\mp i\varphi(z))}{\sqrt{\varphi'(z)}}\psi(z) \tag{I.82}$$

$$= \frac{\pm 1}{2i\varphi'(z)}\left(\varphi'(z)^2 - F(z) + \frac{1}{2}\{\varphi,z\}\right)\left(a_\pm(z) + a_\mp(z)\exp(\mp 2i\varphi(z))\right) \ . \tag{I.83}$$

Note however that, in general, the basis functions $\exp(\pm i\varphi(z))/\sqrt{\varphi'(z)}$ cannot be associated to a specific direction of propagation, unlike the particular case of WKB wavefunctions $\varphi(z) = \phi_{\rm dB}(z)$ where we recover the result (I.79).

In all above cases, the current j associated to the wavefunction $\psi(z)$ is proportional to the difference of squared moduli of a_+ and a_-, which is therefore a constant:

$$j = \frac{\hbar}{m}\left(|a_+(z)|^2 - |a_-(z)|^2\right) \ . \tag{I.84}$$

I.2.d Scattering matrix

We suppose now that the coefficients $a_\pm(z)$ have finite limits on both sides of a given *interaction region*. Let L and R denote the left and right sides of that region as represented in figure I.5. We may write these limits in the following ways:

$$a_+^L \equiv a_+^{\rm in} \equiv \lim_{z\to L} a_+(z) \ , \qquad a_+^R \equiv a_+^{\rm out} \equiv \lim_{z\to R} a_+(z) \ , \tag{I.85}$$

$$a_-^L \equiv a_-^{\rm out} \equiv \lim_{z\to L} a_-(z) \ , \qquad a_-^R \equiv a_-^{\rm in} \equiv \lim_{z\to R} a_-(z) \ . \tag{I.86}$$

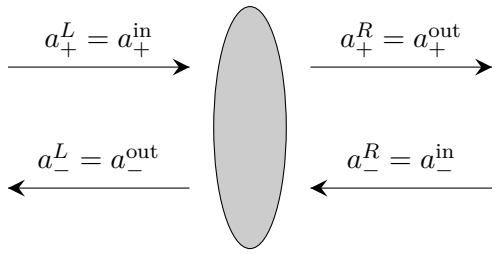

Figure I.5: Diagram showing the amplitudes of leftward and rightward traveling waves on both sides of the scattering region (depicted by the gray ellipse).

We can give a global description of the processes occurring within the interaction region by specifying only the relations between the input and output coefficients with the help of a scattering matrix $\mathcal{S}$:

$$\begin{pmatrix} a_+^{\rm out} \\ a_-^{\rm out} \end{pmatrix} \equiv \mathcal{S} \begin{pmatrix} a_+^{\rm in} \\ a_-^{\rm in} \end{pmatrix} \ , \qquad \mathcal{S} \equiv \begin{pmatrix} \bar{t} & r \\ \bar{r} & t \end{pmatrix} \ . \tag{I.87}$$

In the case where the basis functions are WKB waves, the direction of propagation is well defined on both sides of the interaction region and the elements of the scattering matrix are reflection and transmission coefficients. For example the solution corresponding to an incident wave arriving from the right which is reflected and transmitted by a

localized potential has the following asymptotic behavior:

$$\psi(z) \underset{z\to R}{\simeq} \psi^{-}_{\mathrm{WKB}}(z) + r\ \psi^{+}_{\mathrm{WKB}}(z)\ , \tag{I.88}$$

$$\psi(z) \underset{z\to L}{\simeq} t\ \psi^{-}_{\mathrm{WKB}}(z)\ . \tag{I.89}$$

We can calculate the current j in each of these limits and use the fact that it is a constant to prove that

$$|r|^2 + |t|^2 = 1\ , \tag{I.90}$$

which expresses the conservation of probability during the scattering process, $R \equiv |r|^2$ being the reflection probability and $|t|^2 = 1 - R$ the transmission probability. More generally, the scattering matrix is unitary:

$$\mathcal{S}\mathcal{S}^\dagger = \mathcal{S}^\dagger\mathcal{S} = \mathcal{I}\ . \tag{I.91}$$

A proof of that property and more details on the scattering matrix and the associated transfer matrix can be found in appendix A.

I.3 Liouville transformations of the Schrödinger equation

I.3.a Liouville transformations

In this section we consider transformations which preserve the form of the Schrödinger equation:

$$\psi''(z) + F(z)\psi(z) = 0\ , \tag{I.92}$$

with $F(z)$ an arbitrary real function. Such equations are a particular case of Sturm-Liouville equations [140], the transformation properties of which are detailed in appendix A.

The Liouville transformation [138] is a coordinate change associated with a rescaling of the wave-function. The coordinate change maps the physical $z-$domain into a $\tilde{z}-$domain with $\tilde{z}(z)$ a smooth monotonous function ($\tilde{z}'(z) > 0$). The rescaled wave-function $\tilde{\psi}(\tilde{z})$ is

$$\tilde{\psi}(\tilde{z}) \equiv \sqrt{\tilde{z}'(z)}\psi(z) \tag{I.93}$$

and it also obeys a Schrödinger equation

$$\tilde{\psi}''(\tilde{z}) + \tilde{F}(\tilde{z})\tilde{\psi}(\tilde{z}) = 0\ , \tag{I.94}$$

with a transformed function

$$\tilde{F}(\tilde{z}) = \frac{F(z) - \frac{1}{2}\{\tilde{z}, z\}}{\tilde{z}'(z)^2}\ . \tag{I.95}$$

The curly braces denote the Schwarzian derivative (I.29) of the coordinate transformation $\tilde{z}(z)$.

This transformation was introduced by Liouville in 1837 [131] to derive the approximation to the solutions of the heat equation that would later be known as the WKB approximation. Subsequently, Liouville transformations were mostly used in the same spirit, as a starting point for various approximation schemes. In particular, the transformation is sometimes associated to the names of Miller and Good who developed the comparison equation approximation as a generalization of WKB [141–143], and which we will discuss further in sections I.3.d and I.3.e. Many authors have since proposed variations on the comparison equation approximation [144–148].

The Liouville transformation can also be employed to obtain exact mathematical results, for example to relate various exactly solvable Schrödinger equations [149, 150] or to place bounds on the transmission probability [151]. It is also akin to the Duru-Kleinert transformation of path integrals [152, 153].

Our use of Liouville transformations differs from all these previous works because it is neither used to perform an approximation, nor to obtain analytical results. Our goal here is to perform exact calculations for realistic potentials, precisely in regimes where the comparison equation approximation is not valid [154, 155].

The composition of two Liouville transformations $z \to \tilde{z}$ and $\tilde{z} \to \check{z}$ is again a Liouville transformation $z \to \check{z}$, and the group properties of this composition law is ensured by the Cayley identity for Schwarzian derivatives:

$$\{\check{z}, z\} = \big(\tilde{z}'(z)\big)^2 \, \{\check{z}, \tilde{z}\} + \{\tilde{z}, z\} \ . \tag{I.96}$$

When this identity is applied to inverse transformations ($\check{z} = z$), the following relation is obtained:

$$0 = \big(\tilde{z}'(z)\big)^2 \, \{z, \tilde{z}\} + \{\tilde{z}, z\} \ , \tag{I.97}$$

so that the transformation (I.95) can also be written

$$\tilde{F}(\tilde{z}) = z'(\tilde{z})^2 F(z) + \tfrac{1}{2}\{z, \tilde{z}\} \ . \tag{I.98}$$

The Liouville transformation relates Schrödinger equations with functions $\tilde{F}(\tilde{z})$ and $F(z)$ that can be radically different. However the corresponding physical systems share a number of properties. Indeed many physical quantities can be expressed in terms of Wronskians (I.35) and the Liouville transformations have the remarkable property of preserving these Wronskians:

$$\mathcal{W}(\psi_1, \psi_2) = \tilde{\mathcal{W}}(\tilde{\psi}_1, \tilde{\psi}_2) \ . \tag{I.99}$$

As shown in (I.41), the probability density current j can be written in terms of a Wronskian. It is therefore invariant under Liouville transformations: $j = \tilde{j}$. More generally, we show in appendix A that all scattering amplitudes can be written as Wronskians of particular solutions of the Schrödinger equation. Therefore the Liouville transformation preserves all the scattering properties of a problem.

The equation (I.28) obeyed by the phase of the wavefunction transforms particularly naturally under Liouville transformations. Indeed we can use Cayley's identity to rewrite it more compactly

$$\phi'(z)^2 - F(z) + \frac{1}{2}\{\phi, z\} = \frac{1}{2}\{\exp(2i\phi), z\} - F(z) = 0 \ . \tag{I.100}$$

The Liouville transformation then simply consists in a change of variable in the Schwarzian derivative:

$$\frac{1}{2}\{\exp(2i\tilde{\phi}), \tilde{z}\} - \tilde{F}(\tilde{z}) = 0 \ , \tag{I.101}$$

where the phase transforms as a scalar: $\tilde{\phi}(\tilde{z}) \equiv \phi(z)$. In contrast, the density ρ is not preserved by the transformation, as one deduces from (I.93) that

$$\frac{\mathrm{d}z}{\rho(z)} = \frac{\mathrm{d}\tilde{z}}{\tilde{\rho}(\tilde{z})} \ . \tag{I.102}$$

We have seen in section I.2.c the usefulness of decompositions of the form

$$\psi(z) = a_+(z)\frac{\exp(i\varphi(z))}{\sqrt{\varphi'(z)}} + a_-(z)\frac{\exp(-i\varphi(z))}{\sqrt{\varphi'(z)}} \ , \tag{I.103}$$

$$a_\pm(z) = \frac{\pm 1}{2i}\mathcal{W}\left(\frac{\exp(\mp i\varphi(z))}{\sqrt{\varphi'(z)}}, \psi\right) \ . \tag{I.104}$$

As a consequence of the simple transformation properties of wavefunctions in polar form, this decomposition also transforms very naturally to

$$\tilde{\psi}(\tilde{z}) = \tilde{a}_+(\tilde{z})\frac{\exp(i\tilde{\varphi}(\tilde{z}))}{\sqrt{\tilde{\varphi}'(\tilde{z})}} + \tilde{a}_-(\tilde{z})\frac{\exp(-i\tilde{\varphi}(\tilde{z}))}{\sqrt{\tilde{\varphi}'(\tilde{z})}} \ , \qquad \tilde{\varphi}(\tilde{z}) = \varphi(z) \ , \tag{I.105}$$

$$\tilde{a}_\pm(\tilde{z}) = \frac{\pm 1}{2i}\tilde{\mathcal{W}}\left(\frac{\exp(\mp i\tilde{\varphi}(\tilde{z}))}{\sqrt{\tilde{\varphi}'(\tilde{z})}}, \tilde{\psi}(\tilde{z})\right) = a_\pm(z) \ , \tag{I.106}$$

$$\tilde{a}'_\pm(\tilde{z}) = \frac{\pm 1}{2i}\left(\tilde{\varphi}'^2 - \tilde{F}(\tilde{z}) + \frac{1}{2}\{\tilde{\varphi}, \tilde{z}\}\right)\frac{\exp(\mp i\tilde{\varphi}(\tilde{z}))}{\sqrt{\tilde{\varphi}'(\tilde{z})}}\tilde{\psi}(\tilde{z}) \ . \tag{I.107}$$

The invariance of the $a_\pm$ coefficients under the transformation is another manifestation of the preservation of the scattering amplitudes by Liouville transformations.

We now consider several specific choices of coordinate changes $\tilde{z}(z)$, some of which will be useful to treat quantum reflection problems.

I.3.b Trivial coordinates

Before we start, note that it is vain to look for Liouville transformations that map the original equation onto a trivial one, with $\tilde{F}(\tilde{z}) = 0$ or 1. Indeed, as could be expected, the problem of finding the corresponding coordinate change is equivalent to solving the

original equation. However, working this out allows us to make the connection with a noteworthy property of the Schwarzian derivative.

First, note that if we set $\tilde{F} = 1$ in (I.95), then $\tilde{z}$ obeys the equation (I.28) for the phase ϕ of the wavefunction, so that $\tilde{z} = \phi$. If we instead try to set $\tilde{F} = 0$, then (I.101) becomes

$$\{\exp\left(2i\tilde{\phi}\right), \tilde{z}\} = 0 \ , \tag{I.108}$$

which is solved by (see equation (I.34))

$$\exp\left(2i\tilde{\phi}\right) = \frac{a\tilde{z}+b}{c\tilde{z}+d} \ . \tag{I.109}$$

Solving for $\tilde{z}$, we find that it is the ratio of two solutions of the original equation (I.92):

$$\tilde{z}(z) = \frac{\psi_1(z)}{\psi_2(z)} \ , \tag{I.110}$$

$$\psi_1(z) = d\frac{e^{i\phi}}{\sqrt{\phi'(z)}} - b\frac{e^{-i\phi}}{\sqrt{\phi'(z)}} \ , \qquad \psi_2(z) = -c\frac{e^{i\phi}}{\sqrt{\phi'(z)}} + a\frac{e^{-i\phi}}{\sqrt{\phi'(z)}} \ . \tag{I.111}$$

Application of equation (I.95) then yields a well known result for Schwarzian derivatives: if ψ_1 and ψ_2 are independent solutions of the Schrödinger equation (I.92), then

$$\left\{\frac{\psi_1}{\psi_2}, z\right\} = 2F(z) \ . \tag{I.112}$$

I.3.c Dimensionless coordinate

Putting the Schrödinger equation in non-dimensional form can be seen as a (very basic) Liouville transformation. If $\kappa \equiv \hbar^{-1}\sqrt{2mE}$ is the wavevector in the absence of a potential, we can define the dimensionless coordinate $\tilde{z} \equiv \kappa z$ and the transformed equation is:

$$\tilde{\psi}''(\tilde{z}) + (1 - v(\tilde{z}))\tilde{\psi}(\tilde{z}) = 0 \ , \tag{I.113}$$

with $v(\tilde{z}) \equiv V(z)/E$ the dimensionless potential function and $\tilde{\psi}(\tilde{z}) = \sqrt{\kappa}\psi(z)$ the transformed wavefunction. In this case the Schwarzian derivative vanishes so that no extra potential term appears. Despite its simplicity, this transformation is a reminder that all of the scattering properties of the Schrödinger equation depend only on the function $v(\tilde{z}) = V(\tilde{z}/\kappa)/E$.

I.3.d WKB coordinate

In the absence of classical turning points ($F > 0$), a particularly interesting Liouville transformation is obtained by defining a coordinate proportional to the WKB phase[6]:

$$\boldsymbol{z}(z) \equiv \frac{\phi_{\mathrm{dB}}(z)}{\varkappa} \ . \tag{I.114}$$

[6]For the time being the proportionality constant $\varkappa$ is left unspecified.

Hereafter we use boldfaces to denote quantities related to this coordinate choice. In particular, we have

$$\boldsymbol{\psi}(\boldsymbol{z}) = \sqrt{\frac{k_{\mathrm{dB}}(z)}{\varkappa}}\psi(z) \ , \qquad \boldsymbol{F}(\boldsymbol{z}) = \varkappa^2\left(1 - Q(z)\right) \ . \tag{I.115}$$

$\boldsymbol{F}(\boldsymbol{z})$ can be rewritten in terms of an "energy" and a "potential" (compare with equation (I.15)):

$$\boldsymbol{F}(\boldsymbol{z}) \equiv \boldsymbol{E} - \boldsymbol{V}(\boldsymbol{z}) \ , \qquad \boldsymbol{E} = \varkappa^2 \ , \qquad \boldsymbol{V}(\boldsymbol{z}) = \varkappa^2 Q(z) \ . \tag{I.116}$$

Therefore, with this coordinate choice, the original equation is mapped onto an equation describing scattering on a potential proportional to the badlands function $Q(z)$ (see equation (I.69)). This new potential depends on both the original potential and energy while the new energy depends only on the choice of $\varkappa$.

With this formulation, the role of the badlands function as a criterion of validity of the WKB approximation becomes obvious: in regions where the badlands function is negligible, the transformed equation has solutions $\boldsymbol{\psi}(\boldsymbol{z}) = \exp(\pm i\varkappa\boldsymbol{z})$, which correspond to the WKB wavefunctions in the original coordinate:

$$\psi(z) = \frac{1}{\sqrt{\boldsymbol{z}'(z)}}\boldsymbol{\psi}(\boldsymbol{z}(z)) = \sqrt{\frac{\varkappa}{k_{\mathrm{dB}}(z)}}\exp(\pm i\phi_{\mathrm{dB}}(z)) \propto \psi^{\pm}_{\mathrm{WKB}}(z) \ . \tag{I.117}$$

Another way of seeing this is to express the coupled equations describing the exchange between two waves in the WKB coordinate: if we set $\tilde{z} = \tilde{\varphi} = \phi_{\mathrm{dB}} = \boldsymbol{z}$ ($\varkappa = 1$) in (I.107), we find that

$$\boldsymbol{\psi}(\boldsymbol{z}) = \boldsymbol{a}_+(\boldsymbol{z})\exp(i\boldsymbol{z}) + \boldsymbol{a}_-(\boldsymbol{z})\exp(-i\boldsymbol{z}) \ , \tag{I.118}$$

$$\boldsymbol{a}'_\pm(\boldsymbol{z}) = \frac{\pm 1}{2i}Q(\boldsymbol{z})\exp(\mp i\boldsymbol{z})\boldsymbol{\psi}(\boldsymbol{z}) \tag{I.119}$$

$$= \frac{\pm 1}{2i}Q(\boldsymbol{z})\left(\boldsymbol{a}_\pm(\boldsymbol{z}) + \boldsymbol{a}_\mp(\boldsymbol{z})\exp(\mp 2i\boldsymbol{z})\right) \ . \tag{I.120}$$

The coefficients $\boldsymbol{a}_\pm = a_\pm$ are therefore constant in the regions where $Q(z) \simeq 0$, so that the WKB approximation is valid there.

The WKB approximation thus consists in neglecting the badlands function in equation (I.115) in order to make it trivial to solve. This method is generalized by the comparison equation approximation [110, 141, 143]. The idea behind this approximation is to choose a coordinate change $\tilde{z}(z)$ such that

- $|\{\tilde{z}, z\}| \ll |2F(z)|$, so that the Schwarzian derivative can be neglected in the Liouville-transformed Schrödinger equation (I.94):

$$\tilde{\psi}''(\tilde{z}) + \tilde{G}(\tilde{z})\tilde{\psi}(\tilde{z}) \simeq 0 \ , \tag{I.121}$$

$$\tilde{G}(\tilde{z}) \equiv \frac{F(z)}{\tilde{z}'(z)^2} \simeq \tilde{F}(\tilde{z}) \qquad \text{if} \qquad |\{\tilde{z}, z\}| \ll |2F(z)| \ , \tag{I.122}$$

- the "comparison" equation (I.121) obtained by neglecting the Schwarzian derivative is exactly solvable.

In the case of the WKB approximation, $\tilde{G}(\tilde{z})$ is a constant. In the next section we will introduce the Langer approximation, where $\tilde{G}(\tilde{z})$ is a linear function.

Note that the definition of $\tilde{G}$ imposes $\tilde{G}(\tilde{z})$ and $F(z)$ always have the same sign, so that the original and comparison equations have the same turning point structure. For example the WKB approximation is suitable for problems without a classical turning point while the Langer approximation can be used in problems with one turning point.

Although the comparison equation approximation can be very powerful, it remains an approximation. We stress that, in this work, we make no such approximation as we don't discard any term in the Liouville-transformed Schrödinger equation (I.94). Moreover, the turning point structure of the transformed scattering problem can be qualitatively different from the original. In particular, it can have classical turning points whereas the original problem had none. In fact, the shape of the new potential is generally a peak. Indeed, provided that $\sqrt{\lambda_{\mathrm{dB}}}\frac{\mathrm{d}}{\mathrm{d}z}\sqrt{\lambda_{\mathrm{dB}}}$ vanishes on both sides of the domain, the integral of $\boldsymbol{V}(\boldsymbol{z})$ is always positive. To see this, we change variables from $\boldsymbol{z}$ to z in the integral and perform an integration by parts:

$$\int \boldsymbol{V}(\boldsymbol{z})\mathrm{d}\boldsymbol{z} = \varkappa \int Q(z) k_{\mathrm{dB}}(z)\mathrm{d}z \tag{I.123}$$

$$= -\frac{\varkappa}{2\pi}\int \sqrt{\lambda_{\mathrm{dB}}}\frac{\mathrm{d}^2}{\mathrm{d}z^2}\sqrt{\lambda_{\mathrm{dB}}}\ \mathrm{d}z \tag{I.124}$$

$$= \frac{\varkappa}{2\pi}\int \left(\frac{\mathrm{d}}{\mathrm{d}z}\sqrt{\lambda_{\mathrm{dB}}}\right)^2 \mathrm{d}z > 0\ . \tag{I.125}$$

The aim of the comparison equation approximation is to approximate the original equation by a simpler equation which is as similar to it as possible. Here, in contrast, we will be particularly interested in cases where the original and Liouville-transformed equations correspond to fundamentally different problems in a semiclassical picture.

I.3.e Langer coordinate

Until now, we have considered quantum reflection in the absence of classical turning points, that is also in the absence of classical reflection. In fact, the WKB approximation breaks down at classical turning points: the wavefunctions (I.56) diverge at the turning point since the wavevector k_{dB} vanishes. Nevertheless, one can extend the definition (I.16) of the wavevector to the classically forbidden regions ($F(z) < 0$):

$$k_{\mathrm{dB}}(z) \equiv \frac{i}{\hbar}\sqrt{2m(V(z)-E)}\ , \qquad V(z) > E \tag{I.126}$$

and define exponentially growing or decaying WKB waves in analogy with (I.56):

$$\psi^{\pm}_{\mathrm{WKB}} = \frac{1}{\sqrt{|k_{\mathrm{dB}}|}}\exp\left(\pm\int_{z_0}^{z}|k_{\mathrm{dB}}(\zeta)|\ \mathrm{d}\zeta\right)\ . \tag{I.127}$$

Here, z_0 is a reference point within the classically forbidden region. Connecting the WKB solutions on both sides of a turning point has been an important challenge in the development of the semiclassical approximation. Actually, the names of Wentzel, Kramers and Brillouin are associated with the approximation because they contributed to solve this "connection problem" [133–135].

However, the WKB phase $\phi_{\mathrm{dB}}(z)$ is then no longer a real and strictly increasing function, so that it does not qualify as a coordinate for a Liouville transformation. Moreover, although it can be defined in classically forbidden regions, the badlands function $Q(z)$ diverges at classical turning points. In these conditions, the results of the previous section cannot be applied.

To find a suitable coordinate for a problem with a turning point, we follow the idea of Langer who proposed an alternative solution to the connection problem by means of a specific Liouville transformation which is regular around classical turning points [156, 157]. To simplify, we suppose in the following that $F(z)$ has only one zero z_t and that $F'(z_t) \neq 0$. Thus $F(z)$ is approximately linear in the vicinity of the turning point:

$$F(z) \underset{z\to z_t}{\simeq} F'(z_t)(z - z_t) \ . \tag{I.128}$$

Langer's idea was to use a comparison equation (I.121) which mimics this linear behavior:

$$\tilde{\psi}''(\tilde{z}) + \tilde{G}(\tilde{z})\tilde{\psi}(\tilde{z}) \simeq 0 \ , \tag{I.129}$$

$$\tilde{G}(\tilde{z}) \equiv \frac{F(z)}{\tilde{z}'(z)^2} \equiv \alpha^3(\tilde{z} - \tilde{z}_t) \ , \tag{I.130}$$

where α^3 is a constant[7] of the same sign as $F'(z_t)$ and $\tilde{z}_t = \tilde{z}(z_t)$. Using again boldfaces for all quantities related to this particular choice of coordinate, the Langer coordinate is therefore defined by

$$\boldsymbol{z}'(z) \equiv \sqrt{\frac{F(z)}{\alpha^3(\boldsymbol{z} - \boldsymbol{z}_t)}} \ , \qquad \text{for} \qquad z \neq z_t \ , \tag{I.131}$$

$$\boldsymbol{z}'(z_t) \equiv \frac{F'(z_t)^{1/3}}{\alpha} \ , \qquad \boldsymbol{z}(z_t) \equiv \boldsymbol{z}_t \ . \tag{I.132}$$

This integrates to

$$\boldsymbol{z}(z) = \boldsymbol{z}_t + \frac{\operatorname{sgn}\left(F(z)\right)}{\alpha} \left| \frac{3}{2} \int_{z_t}^{z} \sqrt{|F(\zeta)|}\, \mathrm{d}\zeta \right|^{2/3} \ , \tag{I.133}$$

which is approximately linear around $\boldsymbol{z}_t$. The exact transformed function $\boldsymbol{F}$ is

$$\boldsymbol{F}(\boldsymbol{z}) = \alpha^3(\boldsymbol{z} - \boldsymbol{z}_t) - \frac{1}{2\boldsymbol{z}'(z)}\{\boldsymbol{z}, z\} = \alpha^3(\boldsymbol{z} - \boldsymbol{z}_t) + \frac{1}{2}\{z, \boldsymbol{z}\} \ . \tag{I.134}$$

[7] The cube is introduced here to simplify upcoming equations.

Explicitly evaluating $\boldsymbol{F}$ yields

$$\boldsymbol{F}(\boldsymbol{z}) = \alpha^3(\boldsymbol{z} - \boldsymbol{z}_t) - \frac{5}{16(\boldsymbol{z} - \boldsymbol{z}_t)^2} - \alpha^3(\boldsymbol{z} - \boldsymbol{z}_t)Q(z) \ , \tag{I.135}$$

where $Q(z)$ is the badlands function defined in (I.69). Note that the two last terms in (I.135) diverge individually at the turning point but their sum cancels out there.

In regions where the Schwarzian derivative $\{z, \boldsymbol{z}\}$ is negligible, and in particular near the turning point, the Schrödinger equation tends towards the Airy equation:

$$\boldsymbol{\psi}''(\boldsymbol{z}) + \alpha^3(\boldsymbol{z} - \boldsymbol{z}_t)\boldsymbol{\psi}(\boldsymbol{z}) \simeq 0 \ , \tag{I.136}$$

which is solved by the Airy functions (we discuss these special functions in more detail in section III.3 and appendix C):

$$\boldsymbol{\psi}(\boldsymbol{z}) \simeq A\,\mathrm{Ai}(\alpha(\boldsymbol{z}_t - \boldsymbol{z})) + B\,\mathrm{Bi}(\alpha(\boldsymbol{z}_t - \boldsymbol{z})) \ . \tag{I.137}$$

Langer's comparison equation approximation assumes that this is true everywhere whereas, in our exact treatment, the Schrödinger equation can depart from the Airy equation.

I.3.f Extension to higher dimensions

It is natural to try to extend the Liouville transformation to the Schrödinger equation in higher dimensions. Unfortunately, the success of the Liouville transformation is linked to the particular form of the one dimensional Schrödinger equation (I.92) and it does not extend well to partial differential equations. If the equation is separable, then it is equivalent to several one dimensional equations which one can transform independently. The general case is less simple [158, 159].

In 2D one can take advantage of conformal invariance to write transformations that preserve the shape of the Schrödinger equation

$$\left[\frac{\partial^2}{\partial x^2} + \frac{\partial^2}{\partial y^2} + F(x, y)\right] \psi(x, y) = 0 \ . \tag{I.138}$$

To do so, we rewrite the equation in terms of the complex variables $z = x + iy$ and $z^* = x - iy$:

$$\left[\frac{\partial^2}{\partial z \partial z^*} + F(z, z^*)\right] \psi(z, z^*) = 0 \ . \tag{I.139}$$

If $f(z)$ is an analytic function in the complex plane we can perform the following change of variables $z \to \tilde{z} = f(z)$ and $z^* \to \tilde{z}^* = f(z^*) = f(z)^*$:

$$\left[\frac{\partial^2}{\partial \tilde{z} \partial \tilde{z}^*} + \tilde{F}(\tilde{z}, \tilde{z}^*)\right] \tilde{\psi}(\tilde{z}, \tilde{z}^*) = 0 \ , \tag{I.140}$$

with

$$\tilde{\psi}(\tilde{z}, \tilde{z}^*) = \psi(z, z^*) \qquad \text{and} \qquad \tilde{F}(\tilde{z}, \tilde{z}^*) = |f'(z)|^{-2} F(z, z^*) \ . \tag{I.141}$$

If $\tilde{x}(x,y)$ and $\tilde{y}(x,y)$ are the real and imaginary parts of $\tilde{z}$,

$$\left[\frac{\partial^2}{\partial\tilde{x}^2}+\frac{\partial^2}{\partial\tilde{y}^2}+\tilde{F}(\tilde{x},\tilde{y})\right]\tilde{\psi}(\tilde{x},\tilde{y})=0\ . \tag{I.142}$$

Note that while in 1D any smooth strictly increasing function is a valid coordinate change, in 2D we have the additional requirement

$$\tilde{z}(z)=\tilde{x}(x,y)+i\tilde{y}(x,y)=f(x+iy)\ , \tag{I.143}$$

with f an analytic function, which means $\tilde{x}$ and $\tilde{y}$ must satisfy the Cauchy-Riemann equations:

$$\frac{\partial\tilde{x}}{\partial x}=\frac{\partial\tilde{y}}{\partial y}\qquad\text{and}\qquad\frac{\partial\tilde{y}}{\partial x}=-\frac{\partial\tilde{x}}{\partial y}\ . \tag{I.144}$$

In 3D, there seems to be no simple way of changing coordinates while preserving the shape of the equation

$$\left[\frac{\partial^2}{\partial x^2}+\frac{\partial^2}{\partial y^2}+\frac{\partial^2}{\partial z^2}+F(x,y,z)\right]\psi(x,y,z)=0\ . \tag{I.145}$$

One possibility is to focus on one direction and perform Fourier transforms to eliminate the derivatives in the transverse directions. This results in one equation for each transverse mode:

$$\left[\frac{\partial^2}{\partial z^2}-k_x^2-k_y^2\right]\Psi(k_x,k_y,z)$$
$$=-\iint\frac{\mathrm{d}k_x'}{2\pi}\frac{\mathrm{d}k_y'}{2\pi}\mathcal{F}(k_x-k_x',k_y-k_y',z)\Psi(k_x',k_y',z)\ , \tag{I.146}$$

$$\Psi(k_x,k_y,z)\equiv\iint\mathrm{d}x\,\mathrm{d}y\ \psi(x,y,z)e^{-ik_xx-ik_yy}\ , \tag{I.147}$$

$$\mathcal{F}(k_x,k_y,z)\equiv\iint\mathrm{d}x\,\mathrm{d}y\ F(x,y,z)e^{-ik_xx-ik_yy}\ . \tag{I.148}$$

We can now perform a Liouville transform $z\to\tilde{z}(z)$:

$$\tilde{\Psi}(k_x,k_y,\tilde{z})\equiv\sqrt{\tilde{z}'(z)}\Psi(k_x,k_y,z)\ , \tag{I.149}$$

$$\left[\frac{\partial^2}{\partial\tilde{z}^2}-\frac{k_x^2+k_y^2-\frac{1}{2}\{\tilde{z},z\}}{\tilde{z}'(z)^2}\right]\tilde{\Psi}(k_x,k_y,\tilde{z})$$
$$=-\iint\frac{\mathrm{d}k_x'}{2\pi}\frac{\mathrm{d}k_y'}{2\pi}\frac{\mathcal{F}(k_x-k_x',k_y-k_y',\tilde{z})}{\tilde{z}'(z)^2}\tilde{\Psi}(k_x',k_y',\tilde{z})\ . \tag{I.150}$$

Note that we have proceeded implicitly in the same manner with the time-dependent Schrödinger equation (I.12), which is also not amenable to Liouville transformation. Indeed, we have used a Fourier transform to obtain the time-independent equation (I.15). However, since we did not consider time-dependent potentials, the convolution product which appears here was reduced to an ordinary product.

I.4 Semiclassical and quantum regimes

Performing a Liouville transformation to the WKB coordinate emphasizes the role of the badlands function $Q(z)$ as an indicator of deviations from the semiclassical approximation. We are thus led to define two regimes based on the relative strengths of the two terms in $\boldsymbol{F} = \boldsymbol{E} - \boldsymbol{V} = \varkappa^2(1-Q)$:

- the semiclassical regime if $Q(z) \ll 1$ everywhere,
- the quantum regime if there is a region where $Q(z) \gg 1$.

In the semiclassical regime, one might want to go beyond the WKB approximation which neglects any reflection. Instead of boldly taking $\boldsymbol{V} = 0$, one can treat it as a perturbation in order to evaluate "semiclassically weak" reflection. Approximate expressions for the reflection coefficient have been obtained in this way by several authors [109–112, 160]. This is useful in particular if the original potential $V(z)$ is singular and cannot be treated perturbatively, even at high energy. In contrast the transformed potential $\boldsymbol{V}$ typically vanishes when the energy is sufficiently high.

We illustrate the spirit of these approximations by an example. Starting from the coupled equations (I.119), one can derive the following equation for the ratio $\boldsymbol{a}_+/\boldsymbol{a}_-$:

$$\frac{\mathrm{d}}{\mathrm{d}\boldsymbol{z}}\frac{\boldsymbol{a}_+}{\boldsymbol{a}_-} = \frac{1}{2i}Q(\boldsymbol{z})e^{-2i\boldsymbol{z}}\left(1+\frac{\boldsymbol{a}_+}{\boldsymbol{a}_-}e^{2i\boldsymbol{z}}\right)^2 . \tag{I.151}$$

If we consider the solution obeying an absorbing boundary condition on the left: $\boldsymbol{a}_+(-\infty) = 0$ and $\boldsymbol{a}_-(-\infty) = 1$, then

$$\frac{\boldsymbol{a}_+(\boldsymbol{z})}{\boldsymbol{a}_-(\boldsymbol{z})} = \frac{1}{2i}\int_{-\infty}^{z} Q(\boldsymbol{\zeta})e^{-2i\boldsymbol{\zeta}}\left(1+\frac{\boldsymbol{a}_+(\boldsymbol{\zeta})}{\boldsymbol{a}_-(\boldsymbol{\zeta})}e^{2i\boldsymbol{\zeta}}\right)^2 \mathrm{d}\boldsymbol{\zeta} . \tag{I.152}$$

Since the badlands function has small values in this regime, $\boldsymbol{a}_+/\boldsymbol{a}_-$ is expected to remain small as well. Therefore (I.152) can be used as the basis of a recursive scheme, where at first order the reflection coefficient is given by

$$r = \lim_{z\to\infty}\frac{\boldsymbol{a}_+}{\boldsymbol{a}_-} \underset{Q\ll 1}{\simeq} \frac{1}{2i}\int_{-\infty}^{\infty} Q(\boldsymbol{\zeta})e^{-2i\boldsymbol{\zeta}}\mathrm{d}\boldsymbol{\zeta} . \tag{I.153}$$

We recognize this as the first order Born approximation [130] for the transformed scattering problem (I.115).

We now consider the quantum limit, meaning that there is a region where $Q(z) \gg 1$. In this region, we neglect the energy $\boldsymbol{E} = \varkappa^2$ in the Liouville-transformed Schrödinger equation (I.68):

$$\boldsymbol{\psi}''(\boldsymbol{z}) - \boldsymbol{V}(\boldsymbol{z})\boldsymbol{\psi}(\boldsymbol{z}) \simeq 0 , \qquad \boldsymbol{V}(\boldsymbol{z}) = \varkappa^2 Q(z) = -\frac{1}{2}\{z,\boldsymbol{z}\} . \tag{I.154}$$

Transforming back to the physical coordinate z, we find that $F(z) \simeq 0$. Indeed, our approximation has taken us to the trivial frame mentioned in I.3.b. Therefore, large

values of the badlands function signal regions over which the function $F(z)$ can safely be neglected, and where the wavefunction is thus approximately linear:

$$\psi(z) \underset{Q\gg 1}{\simeq} C\left(1-\frac{z}{a}\right) , \tag{I.155}$$

where C and a are complex constants.

This property should be put in relation with the universality of scattering near the threshold $E = 0$, first noted by Wigner [161]. In particular, it is well-known that the interaction between ultracold particles can be replaced by an effective contact potential which depends on a single parameter, the *scattering length* [129]. For example, this result is used to model interacting Bose-Einstein condensates with the Gross-Pitaevskii equation [162, 163].

In fact, this property applies also to particle-surface collisions, which will be the focus of the next chapter. Indeed, a particle interacting with a plane mirror or two particles interacting through a spherically symmetric potential are both described by a one dimensional Schrödinger equation of the form (I.14) defined on the half-line $z > 0$.

If the wavevector $\kappa \equiv \hbar^{-1}\sqrt{2mE}$ is small enough, the associated wavelength $2\pi/\kappa$ is much larger than the range ℓ of the potential. We can then define two overlapping regions, as shown in figure I.6:

- an inner region such that $z \ll \kappa^{-1}$, where the *energy* is too small to affect the wavefunction,
- an outer region such that $z \gg \ell$, where the *potential* is too small to affect the wavefunction, so that we can write:

$$\psi(z) \underset{z\gg\ell}{\simeq} \frac{\mathcal{N}}{\sqrt{\kappa}}\left(e^{-i\kappa z}+re^{i\kappa z}\right) . \tag{I.156}$$

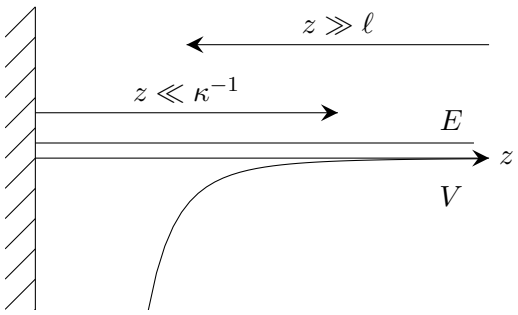

Figure I.6: Diagram showing the overlapping regions where the wavefunction is unaffected by the potential ($z \gg \ell$) or by the energy ($z \ll \kappa^{-1}$) provided $\kappa\ell \ll 1$.

It follows that in the overlap between these two regions, $F(z)$ can be neglected altogether so that the wavefunction (I.156) can be linearized:

$$\psi(z) \underset{\ell \ll z \ll \kappa^{-1}}{\simeq} \mathcal{N} i\sqrt{\kappa}(r-1)z + \mathcal{N}\frac{r+1}{\sqrt{\kappa}} = C\left(1 - \frac{z}{a}\right) , \tag{I.157}$$

$$\text{with} \qquad C = \mathcal{N}\frac{r+1}{\sqrt{\kappa}} , \qquad a = \frac{i}{\kappa}\frac{r+1}{r-1} . \tag{I.158}$$

More rigorously, the region over which $F(z)$ can safely be neglected is given by the criterion $Q(z) \gg 1$ which we have derived above.

Matching (I.157) with the wavefunction in the inner region fixes the value of a, the scattering length, which is therefore independent of the energy. Solving for the reflection coefficient r we find that it has the following energy dependence:

$$r \simeq \frac{\kappa a + i}{\kappa a - i} \simeq -\exp\left(-2i\kappa a\right) , \qquad \kappa\ell \ll 1 , \tag{I.159}$$

where the second expression is equal to the first up to order $(\kappa a)^2$.

The net current towards $z = 0$ is proportional to $1-|r|^2$. If the collision is elastic, the incoming and reflected waves are balanced so that $|r|^2 = 1$ and the scattering length a is real. This is generally the case for inter-atomic collisions. However, in the general case, inelastic processes can occur when the particle-particle or particle-surface separation is small, for example the formation of a reaction product [164] or absorption by the surface [124]. In that case, a is a complex number and its real part determines the scattering phase shift while its imaginary part is a measure of inelasticity :

$$\arg(r) \underset{\kappa\ell \ll 1}{\simeq} -2\kappa\,\mathrm{Re}(a) , \tag{I.160}$$

$$|r|^2 \underset{\kappa\ell \ll 1}{\simeq} \exp\left(-4\kappa b\right) < 1 , \qquad b \equiv -\,\mathrm{Im}(a) > 0 . \tag{I.161}$$

Conclusion

We have shown that WKB waves propagate classically, without reflection. Exact solutions of the Schrödinger equation can be expressed as a sum of counterpropagating WKB waves with varying amplitudes. Exchange between these two waves – that is to say quantum reflection – takes place in regions where the WKB approximation breaks down and that are signaled by the badlands function.

We have introduced Liouville transformations of the Schrödinger equation, which consist in a change of coordinate associated with a rescaling of the wavefunction. These transformations have the remarkable property of leaving the scattering amplitudes unchanged, even if the potential landscape is deeply modified.

In problems without a classical turning point, using the WKB phase as coordinate maps the original equation onto an equivalent equation where the badlands function plays the role of a potential. This transformation makes the significance of the badlands function to quantum reflection clear. In particular, semiclassical and quantum regimes

of scattering can be defined based on how the badlands function compares to 1. We have also defined the Langer coordinate, which is adapted to problems with a classical turning point, and discussed the similarities and differences between our approach and the comparison equation approximation.

In the next chapter, we apply these results to the specific case of quantum reflection on the Casimir-Polder potential.

Chapter II

Reflection from the Casimir-Polder potential

A ground state atom approaching a material surface experiences the attraction of the Casimir-Polder force. The latter varies more and more rapidly, as the potential diverges with an inverse power-law near the surface. Upon reaching this potential "cliff", a classical particle would inevitably fall towards the surface. A matter wave, on the other hand, undergoes quantum reflection. The aim of this chapter is to provide an evaluation of the reflection probability of ground state hydrogen or antihydrogen on a variety of mirrors.

To do so, we will start by expressing the Casimir-Polder potential in terms of the electromagnetic scattering properties of both atom and mirror. This approach will allow us to take into account the material properties of the mirrors, which will be shown to affect the potential and, consequently, quantum reflection. In particular, we will consider mirrors which couple weakly to the electromagnetic field, such as thin slabs, graphene sheets and porous media and show that such mirrors lead to a larger quantum reflection probability [165, 166].

Solving the Schrödinger equation with the Casimir-Polder potential will allow us to evaluate the quantum reflection probability. Rather than solving the equation by brute force, we will expose two methods which take advantage of the link between quantum reflection and the WKB approximation presented in chapter I. We will especially focus on the method of Liouville transformation to the WKB coordinate, as we believe it to be the best suited both for numerical calculations and physical interpretation [154, 155]. It will notably allow us to explain why mirrors which least reflect the electromagnetic field best reflect atoms. More generally, we will show that the quantum reflection probability can be accurately predicted over a wide range of energies and for a great variety of mirrors with the help of a one-parameter model.

Finally, we will discuss the role of the boundary condition on the surface, which models all the physico-chemical processes which may occur there. For antimatter experiments like GBAR, annihilation of the anti-atom upon reaching the surface enforces a simple, absorbing boundary condition. We will show that for matter atoms the situation

can be more involved.

II.1 Casimir-Polder interaction between an atom and a plane

In this section we give the expression of the Casimir interaction energy between two arbitrary objects in the scattering approach, before specializing to the case of an atom in front of a plane.

II.1.a Casimir free energy for two objects in vacuum

We consider two objects at rest in vacuum, separated by a distance L and at thermal equilibrium at temperature T. The interaction of each object with the electromagnetic field is described by a reflection operator $\mathcal{R}$ which gives the field $\vec{\mathcal{E}}_{\text{refl}}$ reflected by the object for a given incident field $\vec{\mathcal{E}}_{\text{in}}$:

$$\vec{\mathcal{E}}_{\text{refl}} = \mathcal{R}\vec{\mathcal{E}}_{\text{in}} \ . \tag{II.1}$$

Since the objects are at rest, this scattering process preserves frequency. Therefore, in the following, it is understood that all fields have a harmonic time dependence $\exp(-i\omega t)$. The proximity of the objects induces a shift in the free energy of the electromagnetic field compared with the situation where they are infinitely far apart. The average force F on the objects derives from this energy difference, which is known as the Casimir free energy $\mathcal{F}_{\text{Cas}}$:

$$F = -\frac{\partial \mathcal{F}_{\text{Cas}}}{\partial L} \ . \tag{II.2}$$

In the scattering approach to Casimir forces, the Casimir free energy $\mathcal{F}_{\text{Cas}}$ has the following expression [167]:

$$\mathcal{F}_{\text{Cas}} = -\hbar \int_0^\infty \frac{\mathrm{d}\omega}{2\pi} N(\omega)\Delta(\omega) \ . \tag{II.3}$$

The first term in the integral is the mean number of photons in a mode of frequency ω at temperature T, given by Plank's law, including the zero-point contribution:

$$N(\omega) = \frac{1}{e^{\hbar\omega/k_B T} - 1} + \frac{1}{2} = \frac{1}{2}\coth\left(\frac{\hbar\omega}{2k_B T}\right) \ , \tag{II.4}$$

The second term is a phase shift acquired by the field during successive reflections on the two objects:

$$\Delta(\omega) = -i\,\mathrm{Tr}\log\left[\left(\mathcal{I} - \mathcal{R}_1\mathcal{T}_{12}\mathcal{R}_2\mathcal{T}_{21}\right)\left(\mathcal{I} - \mathcal{R}_1^*\mathcal{T}_{12}^*\mathcal{R}_2^*\mathcal{T}_{21}^*\right)^{-1}\right] \ . \tag{II.5}$$

The trace represents a summation over all modes of frequency ω. In particular, both propagating and evanescent modes contribute to the Casimir free-energy [76, 167]. $\mathcal{I}$ is the identity operator. The operators $\mathcal{T}_{ij}$ perform translations between the two objects,

so that the product $\mathcal{R}_1\mathcal{T}_{12}\mathcal{R}_2\mathcal{T}_{21}$ represents a round trip of the field between the two objects. When expanding the logarithm, the total phase shift is seen as a sum over the number of such round trips.

For real materials, the reflection matrices obey several physical properties [76, 168]:

- They are transparent at high frequencies, as the motion of electrons cannot follow the oscillations of the field. This provides a physical cut-off to the integration, so that no further regularization scheme is needed.
- They are causal, since the reflected field cannot precede the incoming field. This ensures that the reflection matrices are analytic in the upper half of the complex frequency plane.

These mathematical properties allow us to deform the integration contour into the upper half of the complex frequency plane [169]. It follows that $\mathcal{F}_{\text{Cas}}$ can be expressed as a sum over the poles of the hyperbolic cotangent function $\omega_n = i\xi_n$, where the ξ_n are the Matsubara frequencies:

$$\mathcal{F}_{\text{Cas}} = k_B T {\sum_n}' \operatorname{Tr}\log\left(\mathcal{I} - \mathcal{R}_1\mathcal{T}_{12}\mathcal{R}_2\mathcal{T}_{21}\right) \ , \tag{II.6}$$

$$\xi_n \equiv n\frac{2\pi k_B T}{\hbar} \ , \qquad n \in \mathbb{N} \ , \tag{II.7}$$

where the prime indicates that the term $n = 0$ should carry a weight $\frac{1}{2}$. This expression is more amenable to numerical computation, with oscillating terms converted into decaying exponentials.

Provided the distance L is much smaller than the thermal wavelength $\lambda_T = \hbar c/k_B T$, the sum converges towards a Riemann integral:

$$\mathcal{F}_{\text{Cas}} \underset{L\ll\lambda_T}{\simeq} \hbar\int_0^\infty \frac{\mathrm{d}\xi}{2\pi}\operatorname{Tr}\log\left(\mathcal{I} - \mathcal{R}_1\mathcal{T}_{12}\mathcal{R}_2\mathcal{T}_{21}\right) \ . \tag{II.8}$$

At $T = 300$ K, the thermal wavelength is on the order of 8 μm and it is larger for lower temperatures. Since the typical length scales involved in quantum reflection are on the order of 10-100 nm, we will use the zero-temperature expression (II.8) in the remaining calculations.

In the following, we specialize to the interaction between an atom and a material plane and we start by evaluating the reflection operators of the atom and plane, as well as the translation operators between the two.

II.1.b Scattering on a plane and an atom

We consider an atom located at $\vec{r}_{\text{at}} = (0, 0, z_{\text{at}})$, above a plane interface of equation $z = 0$, as represented in figure II.1. The two are coupled by propagating and evanescent fields. We will perform the scattering calculation for propagating waves only and assume that the result can be analytically continued to the evanescent sector [76, 167].

Given the geometry of the problem, the modes of the electromagnetic field at frequency ω will be expressed in a plane wave basis:

$$\vec{\mathcal{E}}_{\vec{k}_\perp,p,\pm}(\vec{r}) = E_0 \exp(i\vec{k}_\pm \cdot \vec{r})\vec{\epsilon}_{\vec{k}_\perp,p,\pm} \ . \tag{II.9}$$

These modes are labeled by the projection $\vec{k}_\perp$ of the wavevector in the xy plane, the polarization p and the direction of propagation. The wavevector of the upward (respectively downward) propagating electromagnetic wave is $\vec{k}_\pm = \vec{k}_\perp \pm k_z \vec{e}_z$, with k_z fixed by the dispersion relation (in vacuum):

$$k_\pm^2 = k_\perp^2 + k_z^2 = (\omega/c)^2 \tag{II.10}$$

$$k_z = \begin{cases} \sqrt{(\omega/c)^2 - k_\perp^2} & \text{if } (\omega/c)^2 > k_\perp^2 \\ i\sqrt{k_\perp^2 - (\omega/c)^2} & \text{if } (\omega/c)^2 < k_\perp^2 \end{cases} \tag{II.11}$$

In the first case, $k_z \in \mathbb{R}_+$ and the wave is propagating whereas the second case corresponds to evanescent waves ($k_z \in i\mathbb{R}_+$). We place ourselves in the former case, where the transverse electric (TE) and transverse magnetic (TM) polarizations are defined by

$$\vec{\epsilon}_{\vec{k}_\perp,\mathrm{TE},+} \equiv \vec{\epsilon}_{\vec{k}_\perp,\mathrm{TE},-} \equiv \frac{\vec{e}_z \wedge \vec{k}_\perp}{||\vec{k}_\perp||} \ , \qquad \vec{\epsilon}_{\vec{k}_\perp,\mathrm{TM},\pm} \equiv \frac{\vec{\epsilon}_{\vec{k}_\perp,\mathrm{TE},\pm} \wedge \vec{k}_\pm}{||\vec{k}_\pm||} \ . \tag{II.12}$$

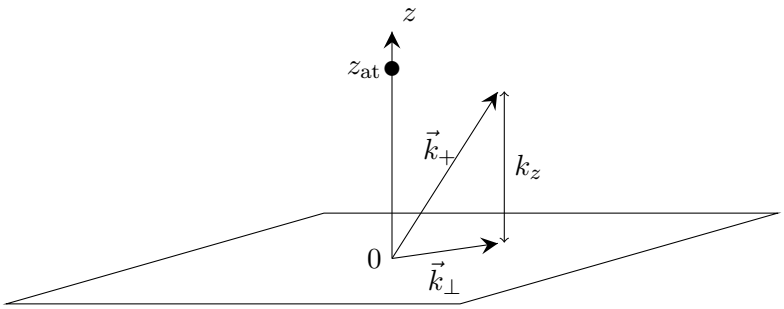

Figure II.1: Atom above a plane surface and decomposition of an upward wavevector $\vec{k}_+$ along its transverse and longitudinal components.

We can now set out to evaluate the matrix elements of the reflection and translation operators in this basis. The translation operators are diagonal:

$$\mathcal{T}_{\mathrm{pl-at}}\vec{\mathcal{E}}_{\vec{k}_\perp,p,+} = \exp(ik_z z_{\mathrm{at}})\vec{\mathcal{E}}_{\vec{k}_\perp,p,+} \ , \tag{II.13}$$

$$\mathcal{T}_{\mathrm{at-pl}}\vec{\mathcal{E}}_{\vec{k}_\perp,p,-} = \exp(ik_z z_{\mathrm{at}})\vec{\mathcal{E}}_{\vec{k}_\perp,p,-} \ . \tag{II.14}$$

We will suppose that the surface of the material medium is ideally flat, so that reflection is specular. Therefore the reflection operator on the plane $\mathcal{R}_{\mathrm{pl}}$ preserves the polarization p and the transverse wavevector $\vec{k}_\perp$:

$$\mathcal{R}_{\mathrm{pl}}\vec{\mathcal{E}}_{\vec{k}_\perp,p,-} = \rho^p(\vec{k}_\perp,\omega)\vec{\mathcal{E}}_{\vec{k}_\perp,p,+} \ . \tag{II.15}$$

The reflection coefficients $\rho^p(\vec{k}_\perp, \omega)$ for various types of materials will be given in section II.2.a.

The reflection operator on the atom $\mathcal{R}_{\rm at}$ gives the field which is reflected downwards by the atom when it is hit by an electromagnetic wave traveling upwards. We follow the derivation of [170] to compute the matrix elements of this operator. We suppose that the wavelengths involved are large compared to the size of the atom and treat it in the dipolar approximation. The electric field $\vec{\mathcal{E}}_{\rm in}$ deforms the electron cloud, giving rise to a dipole oscillating at frequency ω and of amplitude

$$\vec{d} = \alpha(\omega)\vec{\mathcal{E}}_{\rm in}(\vec{r}_{\rm at}) \ , \tag{II.16}$$

where $\alpha(\omega)$ is the *dynamic polarizability*. The radiation emitted downwards by this oscillating dipole forms the reflected wave $\vec{\mathcal{E}}_{\rm refl}$.

The expression of the dynamic polarizability can be obtained by treating the electromagnetic field as a time dependent perturbation on the ground state $|\psi_0\rangle$ of the atom [130]:

$$\alpha(\omega) = \frac{e^2}{m}\sum_n \frac{f_n}{\omega - \omega_n} \ , \qquad f_n = \frac{2m\omega_n}{\hbar}|\langle\psi_n|\hat{Z}|\psi_0\rangle|^2 \ . \tag{II.17}$$

Here $\omega_n = \hbar^{-1}(E_n - E_0)$ is the transition frequency to the $n^{\rm th}$ excited state $|\psi_n\rangle$ and each term is weighed by an *oscillator strength* f_n.

In calculations, we will use the dynamic polarizability of ground state hydrogen given in [171]. We assume that hydrogen and antihydrogen are symmetric with respect to the electromagnetic interaction, at least at the level of precision relevant to GBAR. We therefore take the dynamic polarizability of antihydrogen equal to that of hydrogen[1]. For ground state (anti)hydrogen, the value of the static polarizability is known exactly:

$$\frac{\alpha_{\rm H}(\omega = 0)}{4\pi\varepsilon_0} = \frac{9}{2}\,{\rm a_0}^3 \ . \tag{II.18}$$

The electric field created by the dipole is given by:

$$\vec{\mathcal{E}}_{\rm dipole}(\vec{r}) = \frac{1}{4\pi\varepsilon_0}\vec{\nabla}\wedge\vec{\nabla}\wedge\left(\vec{d}\,\frac{\exp\left(i\omega||\vec{r}-\vec{r}_{\rm at}||/c\right)}{||\vec{r}-\vec{r}_{\rm at}||}\right) \ . \tag{II.19}$$

This can be written as a sum over plane waves using Weyl's plane wave expansion:

$$\frac{\exp\left(i\omega\sqrt{x^2+y^2+z^2}/c\right)}{\sqrt{x^2+y^2+z^2}} = 2i\pi\iint\frac{{\rm d}k_x}{2\pi}\frac{{\rm d}k_y}{2\pi}\frac{\exp(i(k_x x + k_y y + k_z|z|))}{k_z} \ , \tag{II.20}$$

$$\text{where } k_z \equiv \begin{cases}\sqrt{(\omega/c)^2 - k_x^2 - k_y^2} & \text{if } (\omega/c)^2 > k_x^2 + k_y^2 \\ i\sqrt{k_x^2 + k_y^2 - (\omega/c)^2} & \text{if } (\omega/c)^2 < k_x^2 + k_y^2\end{cases} \tag{II.21}$$

[1] Since many of our results will be equally valid for hydrogen and antihydrogen, we will use the shorthand "(anti)hydrogen".

The field reflected downwards ($z < z_{\rm at}$) is therefore

$$\vec{\mathcal{E}}_{\rm refl}(\vec{r}) = \frac{i}{2\varepsilon_0}\iint \frac{\mathrm{d}^2\vec{k}_\perp}{(2\pi)^2}\frac{1}{k_z}\vec{\nabla}\wedge\vec{\nabla}\wedge\left(\vec{d}\,e^{i\vec{k}_-\cdot(\vec{r}-\vec{r}_{\rm at})}\right) \tag{II.22}$$

$$= \frac{i}{2\varepsilon_0}\iint \frac{\mathrm{d}^2\vec{k}_\perp}{(2\pi)^2}\frac{1}{k_z}\left((\vec{k}_-)^2\vec{d} - (\vec{k}_-\cdot\vec{d})\vec{k}_-\right)e^{i\vec{k}_-\cdot(\vec{r}-\vec{r}_{\rm at})}\ . \tag{II.23}$$

We recognize the projection of the dipole on the plane orthogonal to $\vec{k}_-$:

$$\vec{d} - \frac{1}{(\vec{k}_-)^2}\left(\vec{d}\cdot\vec{k}_-\right)\vec{k}_- = \sum_p \left(\vec{d}\cdot\vec{\epsilon}_{\vec{k}_\perp,p,-}\right)\vec{\epsilon}_{\vec{k}_\perp,p,-} \tag{II.24}$$

The wave reflected by the dipole for an incoming plane wave $\vec{\mathcal{E}}_{\rm in} = \vec{\mathcal{E}}_{\vec{k}'_\perp,p',+}$ is thus

$$\vec{\mathcal{E}}_{\rm refl} = \sum_p \iint \frac{\mathrm{d}^2\vec{k}_\perp}{(2\pi)^2}\frac{i\omega^2\alpha(\omega)}{2\varepsilon_0 c^2 k_z}\left(\vec{\epsilon}_{\vec{k}_\perp,p,-}\cdot\vec{\epsilon}_{\vec{k}'_\perp,p',+}\right)e^{i\vec{r}_{\rm at}\cdot(\vec{k}'_+-\vec{k}_-)}\vec{\mathcal{E}}_{\vec{k}_\perp,p,-}\ . \tag{II.25}$$

The coefficients of this sum are the matrix elements of the atom's reflection operator. To be more precise, since we did the calculation in the plane's reference frame, they are the matrix elements of $\mathcal{T}_{\rm pl-at}\mathcal{R}_{\rm at}\mathcal{T}_{\rm at-pl}$:

$$\left(\mathcal{T}_{\rm pl-at}\mathcal{R}_{\rm at}\mathcal{T}_{\rm at-pl}\right)_{\vec{k}_\perp,p,-;\vec{k}'_\perp,p',+} = \frac{i\omega^2\alpha(\omega)}{2\varepsilon_0 c^2 k_z}\left(\vec{\epsilon}_{\vec{k}_\perp,p,-}\cdot\vec{\epsilon}_{\vec{k}'_\perp,p',+}\right)e^{i\vec{r}_{\rm at}\cdot(\vec{k}'_+-\vec{k}_-)}\ . \tag{II.26}$$

II.1.c Expression of the Casimir-Polder potential

Since the Casimir free energy $\mathcal{F}_{\rm Cas}$ will play the role of a potential in the Schrödinger equation describing the motion of the atom, we will denote it V from now on. Moreover, the height of the atom $z_{\rm at}$ will simply be denoted z.

Out of resonance, a single atom is a very poor reflector. Therefore we only need to consider a single scattering process on the atom and we can linearize the logarithm in the expression of the Casimir-Polder potential (II.8):

$$V(z) \underset{||\mathcal{R}_{\rm at}||\ll 1}{\simeq} -\hbar\int_0^\infty \frac{\mathrm{d}\xi}{2\pi}\,\mathrm{Tr}\left(\mathcal{R}_{\rm pl}\mathcal{T}_{\rm pl-at}\mathcal{R}_{\rm at}\mathcal{T}_{\rm at-pl}\right)\ . \tag{II.27}$$

Writing the trace explicitly as a sum over the polarization $p = \mathrm{TE}, \mathrm{TM}$ and the transverse wavevector $\vec{k}_\perp$ and evaluating the reflection and translation operators at the imaginary frequency $\omega = i\xi$, we obtain

$$V(z) = \frac{\hbar}{c^2}\int_0^\infty \mathrm{d}\xi \iint \frac{\mathrm{d}^2\vec{k}_\perp}{(2\pi)^2}\frac{\alpha}{4\pi\varepsilon_0}\frac{\xi^2}{\kappa_z}e^{-2\kappa_z z}\left[\rho^{\rm TE} - \left(1+\frac{2c^2k_\perp^2}{\xi^2}\right)\rho^{\rm TM}\right]\ , \tag{II.28}$$

$$\kappa_z \equiv -ik_z = \sqrt{\xi^2/c^2 + k_\perp^2} \tag{II.29}$$

We have left out the arguments of $\alpha(i\xi)$ and $\rho^p(\vec{k}_\perp, i\xi)$ for the sake of readability and we have used

$$\vec{\epsilon}_{\vec{k}_\perp,p,+} \cdot \vec{\epsilon}_{\vec{k}_\perp,p,-} = \begin{cases} 1 & \text{if } p = \text{TE} , \\ -1 - 2c^2k_\perp^2/\xi^2 & \text{if } p = \text{TM} . \end{cases} \tag{II.30}$$

If the reflection coefficients are independent of the direction of $\vec{k}_\perp$, which will always be the case in this work, we can further simplify:

$$V(z) = \frac{\hbar}{c^2}\int_0^\infty \mathrm{d}\xi \int_0^\infty \frac{k_\perp \mathrm{d}k_\perp}{2\pi} \frac{\alpha}{4\pi\varepsilon_0}\frac{\xi^2}{\kappa_z} e^{-2\kappa_z z}\left[\rho^{\text{TE}} - \left(1 + \frac{2c^2k_\perp^2}{\xi^2}\right)\rho^{\text{TM}}\right] . \tag{II.31}$$

The integral can be rewritten in a more convenient form for numerical evaluation by introducing dimensionless variables $q = k_\perp z$ and $u = \xi z/c$:

$$V(z) = \frac{\hbar c}{2\pi z^4}\int_0^\infty \mathrm{d}u \int_0^\infty \mathrm{d}q \frac{\alpha}{4\pi\varepsilon_0}\frac{qu^2 e^{-2\sqrt{q^2+u^2}}}{\sqrt{q^2+u^2}}\left[\rho^{\text{TE}} - \left(1 + \frac{2q^2}{u^2}\right)\rho^{\text{TM}}\right] . \tag{II.32}$$

II.2 Casimir-Polder potential near various surfaces

The properties of the mirror enter the expression of the Casimir-Polder energy through the reflection coefficients ρ^p. They can be very different from one material to another, leading to different Casimir-Polder interaction strengths [172].

II.2.a Thick and thin slabs

In this section we consider homogeneous, isotropic, linear and non-magnetic materials whose optical response can be described by their relative permittivity (or dielectric constant) $\varepsilon(\omega)$ which we will assume independent of temperature.

All interfaces are supposed to be perfectly plane and orthogonal to the z-axis. Corrections due to roughness or curvature [170, 173] are not considered here. In this framework, the reflection coefficients are obtained by enforcing continuity relations for the electromagnetic field at each interface. For a semi-infinite bulk, we obtain the well-known Fresnel reflection coefficients:

$$\rho_\infty^{\text{TE}}(\vec{k}_\perp,\omega) = \frac{k_z - K_z}{k_z + K_z} , \qquad \rho_\infty^{\text{TM}}(\vec{k}_\perp,\omega) = \frac{\varepsilon(\omega)k_z - K_z}{\varepsilon(\omega)k_z + K_z} , \tag{II.33}$$

where K_z is the longitudinal wavevector inside the medium:

$$K_z = \sqrt{\varepsilon(\omega)(\omega/c)^2 - (\vec{k}_\perp)^2} . \tag{II.34}$$

For a material slab of finite thickness d suspended in vacuum we have [174–176]:

$$\rho_d^p(\vec{k}_\perp,\omega) = \frac{1 - \exp(2idK_z)}{1 - (\rho_\infty^p)^2\exp(2idK_z)}\rho_\infty^p . \tag{II.35}$$

Optical response of the mirror

The dielectric constant which enters the expression of the reflection coefficients is evaluated at imaginary frequency $\omega = i\xi$. We will consider that the causality of the optical response ensures that the following relation holds:

$$\varepsilon(i\xi) = 1 + \frac{2}{\pi}\int_0^\infty \frac{\omega\,\mathrm{Im}(\varepsilon(\omega))}{\omega^2+\xi^2}\mathrm{d}\omega\ . \tag{II.36}$$

This formula is particularly useful to obtain $\varepsilon(i\xi)$ from tabulated values of $\varepsilon(\omega)$ [177].

Since all frequencies are present in the spectrum of vacuum fluctuations, the Casimir force is the result of an integration over a broad frequency band. On the one hand this means that the optical response of the interacting objects must be known over a wide range of frequencies. On the other hand, details of this optical response are generally averaged out. It is therefore sufficient to work with models of the relative permittivity which reproduce its main features.

In practice, we use models which give the dielectric constant as a sum of Lorentzian functions, each corresponding to an absorption resonance. In such simple models, the analytical continuation simply consists in making the replacement $\omega \to i\xi$. Moreover, the dissipative part of the permittivity can safely be neglected on the imaginary frequency axis. Note that for the interaction of two metal planes, the situation is more subtle [169].

In numerical calculations we use the following models:

- A *perfect* or *ideal mirror* is a material with a very high dielectric constant, so that the electric field cannot penetrate it and is perfectly reflected: $\rho^{\mathrm{TM}} = -\rho^{\mathrm{TE}} = 1$. Metals with a high conductivity behave as perfect mirrors below their plasma frequency, therefore perfect mirrors are sometimes referred to somewhat abusively as "perfectly conducting" media.

- For intrinsic silicon, we use the Drude-Lorentz model which features one resonance [178]:
$$\varepsilon(i\xi) = \varepsilon(\infty) + \frac{\varepsilon(0)-\varepsilon(\infty)}{1+(\xi/\omega_0)^2} \tag{II.37}$$
with $\varepsilon(0) = 11.87$, $\varepsilon(\infty) = 1.035$ and $\omega_0 = 6.6\times10^{15}$ rad.s^{-1}.

- For amorphous silica the relative permittivity is approximated by a Sellmeier model with three resonances [179]:
$$\varepsilon(i\xi) = 1 + \frac{B_1}{1+(\xi/\omega_1)^2} + \frac{B_2}{1+(\xi/\omega_2)^2} + \frac{B_3}{1+(\xi/\omega_3)^2} \tag{II.38}$$
with the following parameters:

i	1	2	3
B_i	0.6967	0.4082	0.8908
ω_i (10^{16} rad.s^{-1})	2.727	1.629	0.01903

- Diamond is also described by a Sellmeier model with two resonant frequencies [180]:

$$\varepsilon(i\xi) = B_0 + \frac{B_1}{1+(\xi/\omega_1)^2} + \frac{B_2}{1+(\xi/\omega_2)^2} \ , \tag{II.39}$$

with the following parameters:

i	0	1	2
B_i	2.3098	3.3566	3.2567
ω_i (10^{15} rad.s^{-1})		14.3235	0.0376730

- Finally, the relative permittivity of liquid water at 30°C is obtained by applying the Kramers-Kronig relation (II.36) to the data tabulated in [178].

Asymptotic behaviors

Above a characteristic frequency Ω, the electrons of the atom and mirror can no longer follow the oscillations of the field so that both the atom and the mirror become transparent. Therefore frequencies above Ω do not contribute to the integral (II.31). This frequency scale defines an atom-surface separation $\Lambda \equiv c/\Omega$ at which the behavior of the Casimir-Polder potential changes.

We first examine the short distance behavior $z \ll \Lambda$. Notice that this limit also corresponds formally to $c \to \infty$, meaning that it disregards the finite propagation time between the atom and plane. For this reason it is known as the *non-retarded* limit. We will also suppose that the distance z is smaller than the slab width d, so that $\rho_d^p \simeq \rho_\infty^p$. Starting from (II.31) we again make the change to the variable $q = k_\perp z$ but keep ξ as the other integration variable:

$$V(z) = \frac{\hbar}{2\pi c^2 z}\int_0^\infty \mathrm{d}\xi \int_0^\infty \mathrm{d}q \frac{\alpha}{4\pi\varepsilon_0} \frac{q\xi^2 e^{-2\sqrt{q^2+\xi^2 z^2/c^2}}}{\sqrt{q^2+\xi^2 z^2/c^2}} \left[\rho_\infty^{\mathrm{TE}} - \left(1+\frac{2q^2c^2}{\xi^2 z^2}\right)\rho_\infty^{\mathrm{TM}}\right] \ . \tag{II.40}$$

The reflection coefficients are evaluated at $\omega = i\xi$:

$$\rho_\infty^{\mathrm{TE}} = \frac{\sqrt{q^2+\xi^2 z^2/c^2} - \sqrt{q^2+\varepsilon(i\xi)\xi^2 z^2/c^2}}{\sqrt{q^2+\xi^2 z^2/c^2} + \sqrt{q^2+\varepsilon(i\xi)\xi^2 z^2/c^2}} \ , \tag{II.41}$$

$$\rho_\infty^{\mathrm{TM}} = \frac{\varepsilon(i\xi)\sqrt{q^2+\xi^2 z^2/c^2} - \sqrt{q^2+\varepsilon(i\xi)\xi^2 z^2/c^2}}{\varepsilon(i\xi)\sqrt{q^2+\xi^2 z^2/c^2} + \sqrt{q^2+\varepsilon(i\xi)\xi^2 z^2/c^2}} \ . \tag{II.42}$$

They have the following asymptotic behavior when z/Λ goes to zero:

$$\rho_\infty^{\mathrm{TE}} \underset{z/\Lambda\to 0}{\to} 0 \ , \qquad \rho_\infty^{\mathrm{TM}} \underset{z/\Lambda\to 0}{\to} \frac{\varepsilon(i\xi)-1}{\varepsilon(i\xi)+1} \ , \tag{II.43}$$

so that we end up with

$$V(z) \underset{z\ll d,\Lambda}{\simeq} -\frac{\hbar}{\pi z^3}\int_0^\infty \mathrm{d}q\ q^2 e^{-2q} \int_0^\infty \mathrm{d}\xi \frac{\alpha}{4\pi\varepsilon_0}\frac{\varepsilon(i\xi)-1}{\varepsilon(i\xi)+1} \ . \tag{II.44}$$

The integral over q evaluates to $\frac{1}{4}$, which leaves us with the final result:

$$V(z) \underset{z\ll d,\Lambda}{\simeq} -\frac{C_3}{z^3}\ , \qquad C_3 = \frac{\hbar}{4\pi}\int_0^\infty \mathrm{d}\xi\ \frac{\alpha(i\xi)}{4\pi\varepsilon_0}\frac{\varepsilon(i\xi)-1}{\varepsilon(i\xi)+1}\ . \tag{II.45}$$

This limit corresponds to the instantaneous interaction of the atom's and medium's induced dipoles, which is the well known non-retarded London-van der Waals interaction.

We now study the opposite limit $z \gg \Lambda$. In this case we start with the dimensionless expression (II.32) and introduce another change of variables to $r \equiv \sqrt{q^2+u^2}$ and $s \equiv \sqrt{q^2+u^2}/u$:

$$V(z) = \frac{\hbar c}{2\pi z^4}\int_0^\infty \mathrm{d}r\ r^3 e^{-2r}\int_1^\infty \frac{\mathrm{d}s}{s^4}\frac{\alpha}{4\pi\varepsilon_0}\left(\rho^{\mathrm{TE}} + (1-2s^2)\rho^{\mathrm{TM}}\right)\ . \tag{II.46}$$

The exponential term e^{-2r} suppresses the integrand if the value of r is too large. Since $\xi = crs/z$ and $k_\perp = r\sqrt{1-s^2}/z$ tend towards zero as z goes to infinity, r remaining finite, we can replace the reflection coefficients and polarizability by their low-frequency limit. We then need to distinguish between thick and thin slabs depending on how the distance z compares with the slab width d.

If z remains small compared to the slab width ($z \ll d$), which is generally the case, we can use the low frequency limit of the Fresnel coefficients:

$$\rho_\infty^{\mathrm{TE}} \to \frac{s-\sqrt{s^2+\varepsilon(0)-1}}{s+\sqrt{s^2+\varepsilon(0)-1}}\ , \tag{II.47}$$

$$\rho_\infty^{\mathrm{TM}} \to \frac{\varepsilon(0)s-\sqrt{s^2+\varepsilon(0)-1}}{\varepsilon(0)s+\sqrt{s^2+\varepsilon(0)-1}}\ , \tag{II.48}$$

and we find

$$V(z) \underset{\Lambda\ll z\ll d}{\simeq} -\frac{C_4}{z^4}\ , \qquad C_4 = \frac{3\hbar c}{16\pi}\frac{\alpha(0)}{4\pi\varepsilon_0}f(\varepsilon(0))\ , \tag{II.49}$$

with

$$f(\varepsilon(0)) \equiv -\int_1^\infty \frac{\mathrm{d}s}{s^4}\left(\frac{s-\sqrt{s^2+\varepsilon(0)+1}}{s+\sqrt{s^2+\varepsilon(0)+1}} + \left(1-2s^2\right)\frac{\varepsilon(0)s-\sqrt{s^2+\varepsilon(0)-1}}{\varepsilon(0)s+\sqrt{s^2+\varepsilon(0)-1}}\right)\ . \tag{II.50}$$

The function $f(\varepsilon(0))$ grows from 0 for a transparent medium ($\varepsilon(0) = 1$) to 2 when $\varepsilon(0) \to \infty$. The latter limit, corresponds to an ideal mirror and we denote $C_{4,\mathrm{id}}$ the corresponding coefficient. It was first computed by Casimir and Polder in their seminal paper [64]:

$$C_{4,\mathrm{id}} = \frac{3\hbar c}{8\pi}\frac{\alpha(0)}{2\pi\varepsilon_0} = 73.6 \text{ a.u. for (anti)hydrogen.} \tag{II.51}$$

In the following, we will often use $V_{\mathrm{id}}(z) \equiv -C_{4,\mathrm{id}}/z^4$ as a reference.

For a thin slab, that is if $z \gg d$, the reflection coefficients have the following behavior:

$$\rho_d^p \to \frac{2dr}{sz}\frac{\sqrt{s^2+\varepsilon(0)+1}}{1-(\rho_\infty^p)^2}\rho_\infty^p \tag{II.52}$$

and after integration we obtain

$$V(z) \underset{z\gg d,\Lambda}{\simeq} -\frac{C_5}{z^5}\ , \qquad C_5 = \frac{\hbar c d}{40\pi}\frac{\alpha(0)}{4\pi\varepsilon_0}\left(14\varepsilon(0) - 5 - \frac{9}{\varepsilon(0)}\right)\ . \tag{II.53}$$

The exponent -5 can be found by supposing that the Casimir-Polder potential is additive and taking the difference between the potentials created by two semi-infinite media whose surfaces are separated by a distance d:

$$V(z) = -\frac{C_4}{z^4} + \frac{C_4}{(z+d)^4} \underset{z\gg d}{\simeq} -\frac{4dC_4}{z^5}\ . \tag{II.54}$$

The fact that this simple calculation does not give the correct value of C_5 shows that dispersion forces are not additive [181–183]. These long-distance limits are referred to as *retarded* since at large separations the finite speed of light comes into play.

The Casimir-Polder potential near a thick mirror is sometimes approximated by

$$V(z) \simeq -\frac{C_4}{z^3(z + C_4/C_3)} = -\left(\frac{z^3}{C_3} + \frac{z^4}{C_4}\right)^{-1}\ . \tag{II.55}$$

This form has the correct asymptotic behavior in the short and long distance limits but we will not use it here as we have checked it to be a poor approximation of the potential in the intermediate distance range $z \simeq C_4/C_3$.

Casimir-Polder potential for thick and thin slabs

We now present the potential curves computed using equation (II.32) for the interaction between an (anti)hydrogen atom and material slabs of various compositions and widths.

Figure II.2 shows the Casimir-Polder potential $V(z)$ near various thick material slabs. In the right hand panel, we take the ratio of $V(z)$ to the retarded interaction with a perfect mirror $V_{4,\mathrm{id}}(z) = -C_{4,\mathrm{id}}/z^4$ to highlight the van der Waals and retarded regimes. These ratios tend to linear variations $C_3 z/C_{4,\mathrm{id}}$ at small distances and constant values $C_4/C_{4,\mathrm{id}}$ for large separations. The ratio $C_4/C_{4,\mathrm{id}}$ is smaller than one for real materials, with lower values corresponding to a weaker coupling of the mirror to the electromagnetic field.

We will show in section II.3.e that weak Casimir-Polder interactions are associated with large quantum reflection probabilities, which makes weakly interacting mirrors of particular interest. With this in mind, we have calculated the Casimir-Polder potential near thin slabs. Thin slabs cannot accommodate modes of large wavelength and are therefore transparent at low frequencies. This results in a reduction of the Casimir-Polder potential at long distance, as shown in figure II.3. Again we normalize the potential by $V_{\mathrm{id}}(z)$ so that the retarded regime is characterized by the inverse law $C_5/C_{4,\mathrm{id}} z$.

We note however that the Casimir-Polder potential is affected by the finite thickness of the slab only at distances that are large compared to the slab width. This means that to obtain a significant reduction of the Casimir-Polder potential in the 10-100 nm

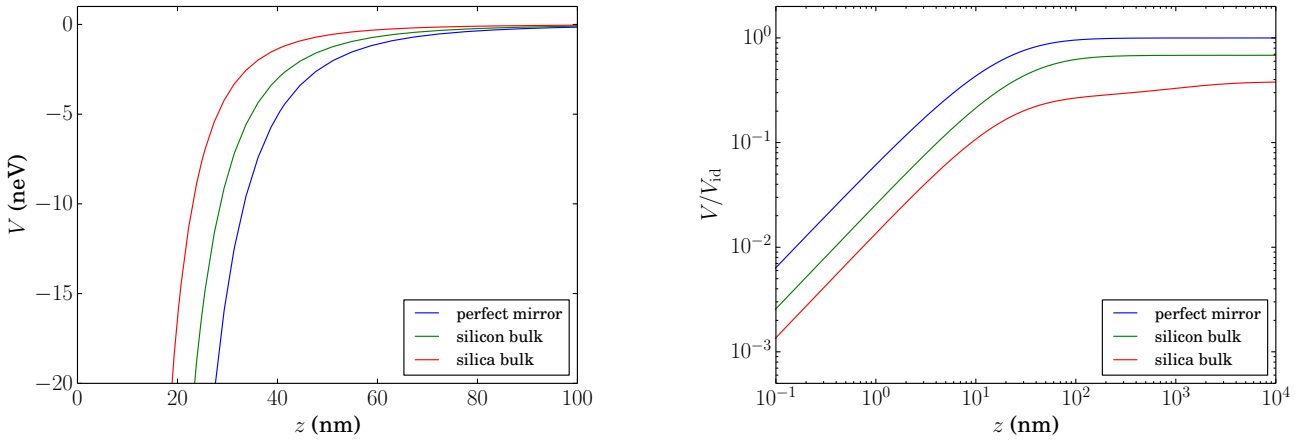

Figure II.2: Left panel: Casimir-Polder potential $V(z)$ between an (anti)hydrogen atom and a thick mirror (from bottom to top, blue: perfect mirror, green: silicon bulk, red: silica bulk). Right panel: ratio $V(z)/V_{\rm id}(z)$ (same color code).

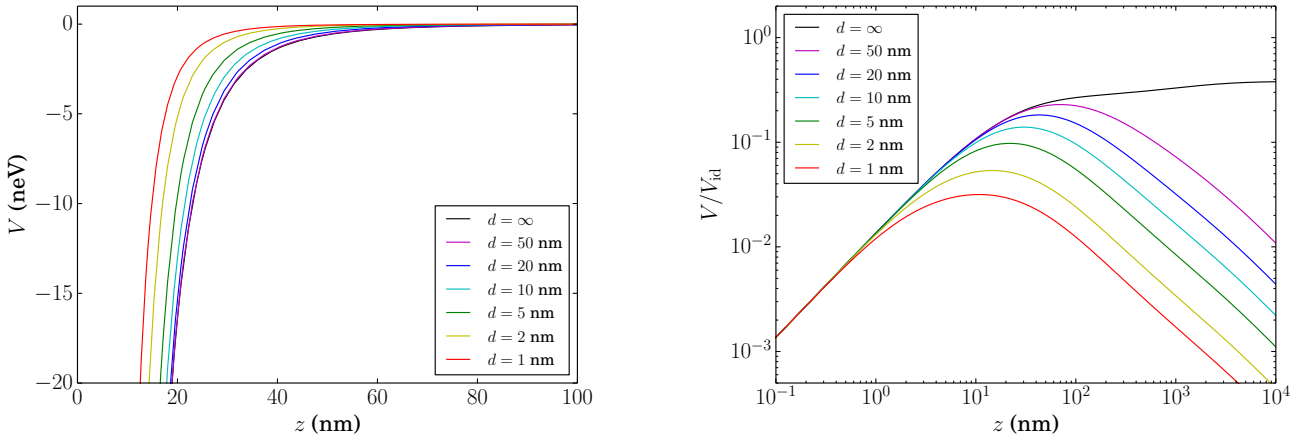

Figure II.3: Left panel: Casimir-Polder potential $V(z)$ between an (anti)hydrogen atom and thin silica slabs of various widths d (from bottom to top, black: thick slab, purple: $d = 50$ nm, blue: $d = 20$ nm, cyan: $d = 10$ nm, green: $d = 5$ nm, yellow: $d = 2$ nm, red: $d = 1$ nm). Right panel: ratio $V(z)/V_{\rm id}(z)$ (same color code).

range relevant to quantum reflection, the slab's width must be on the order of 1-10 nm. Suspending such a slab in vacuum is likely to be of insuperable technical difficulty.

Another idea would be to deposit a thin layer of material on a substrate to form an anti-reflective coating. However, such anti-reflective effects are very dependent on the wavelength and are averaged out in the integration over frequencies which enters the calculation of the Casimir-Polder potential.

For completeness, numerical values of constants C_3, C_4 and C_5/d for (anti)hydrogen near a material wall are given in table II.1.

material	perfect mirror	silicon	silica
C_3 (a.u.)	0.2500	0.1007	0.05327
C_4 (a.u.)	73.61	50.28	28.11
C_5/d (a.u.)	/	787.2	166.5

Table II.1: Constants C_3,C_4 and C_5/d describing the short and long range behavior of the potential felt by (anti)hydrogen near various thin or thick slabs.

II.2.b Potential near an undoped graphene sheet

Given the difficulty of creating free-standing slabs of nanometric width, it is natural to turn to graphene sheets which are only one atomic layer thick but extremely resistant mechanically. The electrons in graphene behave like 2D relativistic fermions which can be described by a Dirac model [184]. The corresponding reflection coefficients, evaluated at imaginary frequency, are given in [185]:

$$\rho^{\mathrm{TE}} = \frac{-\alpha\Phi}{2\kappa_z + \alpha\Phi}, \qquad \rho^{\mathrm{TM}} = \frac{\alpha\kappa_z\Phi}{2\tilde{\kappa_z}^2 + \alpha\kappa_z\Phi}\ , \tag{II.56}$$

where

$$\kappa_z \equiv \sqrt{\frac{\xi^2}{c^2} + k_\perp^2}\ , \qquad \tilde{\kappa_z} \equiv \sqrt{\frac{\xi^2}{c^2} + \frac{v_F^2}{c^2}k_\perp^2}\ , \tag{II.57}$$

$$\Phi \equiv 4\left(\frac{\Delta}{\hbar c} + \frac{\tilde{\kappa_z}^2 - 4(\Delta/\hbar c)^2}{2\tilde{\kappa_z}}\arctan\left(\frac{\hbar c\tilde{\kappa_z}}{2\Delta}\right)\right)\ . \tag{II.58}$$

Here $\alpha \equiv \frac{1}{4\pi\varepsilon_0}\frac{e^2}{\hbar c}$ is the fine structure constant, $v_F = 10^6$ m.s^{-1} the Fermi velocity and Δ the gap energy. For undoped graphene the numerical value of Δ is not precisely known but it is much smaller than 0.1 eV. Its precise value only affects the potential beyond the region which is important for quantum reflection, so it will not concern us here.

In contrast to the "ordinary" mirrors considered previously, the reflection coefficients on graphene depend significantly on temperature [186]. In this work we consider only the zero temperature case.

The Casimir-Polder potential between an (anti)hydrogen atom and a graphene sheet is presented in figure II.4. We note that the extreme thinness of the sheet is somewhat

compensated by a strong coupling of the electrons to the electromagnetic field, yielding a potential comparable to that of nanometric silica slabs in the 1-100 nm separation regime.

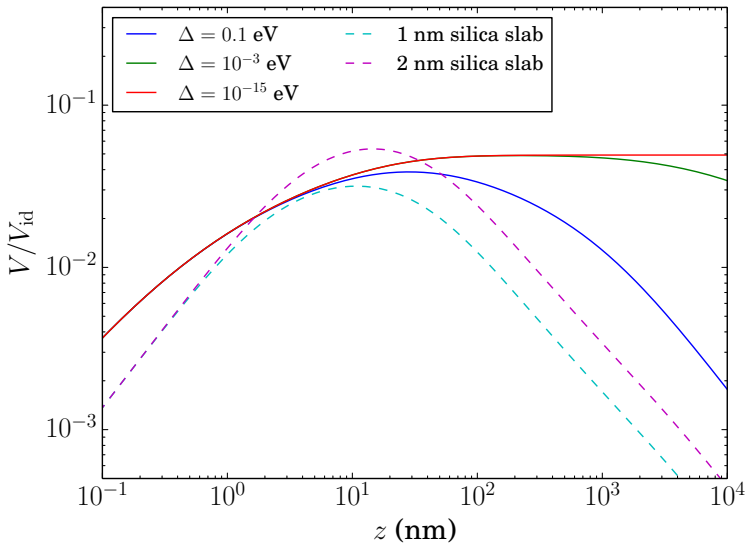

Figure II.4: Ratio $V(z)/V_{\mathrm{id}}(z)$ for the zero-temperature Casimir-Polder potential $V(z)$ between (anti)hydrogen and a suspended graphene sheet described by a Dirac model with different gap parameters (from top to bottom: red: $\Delta = 0.1$ eV, green: $\Delta = 10^{-3}$ eV), blue: $\Delta = 10^{-15}$ eV). The potential near silica slabs of width $d = 1$ and 2 nm is also plotted for comparison.

II.2.c Effective medium treatment of porous materials

Another family of candidates for weak Casimir-Polder interactions are very low density materials. These media incorporate a large fraction of gas or vacuum in a solid host matrix. They can consist in regular or random arrays of nanometric pores, ridges or pillars or in powder- or snow-like assemblies of nanoparticles. We refer to them generically as nanoporous materials, the porosity ϕ being the fraction of the total volume occupied by gas or vacuum. Such materials are inhomogeneous by nature, but from a distance much larger than the size of these inhomogeneities they can be expected to resemble an homogeneous medium with a dramatically reduced dielectric susceptibility.

In this work, we will consider only materials with a sufficiently random structure to avoid diffraction effects:

- Silica aerogels are well-known nanoporous materials because of their numerous applications. They are usually produced by supercritically drying a silica gel, a

process which removes the liquid component while leaving the silica matrix undamaged. Properties of the resulting medium such as porosity and pore size depend on the fabrication technique. Porosities as high as 98% and pore sizes in the 5-100 nm range can typically be achieved [187].

- Porous silicon can be obtained by anodization or etching of a silicon wafer. Porosities up to 95% are obtained with pore sizes typically ranging from 2 to 50 nm [188, 189].

- Diamond nanoparticles formed by explosive shock have been the subject of many studies [190, 191]. These particles have sizes of a few nanometers and consist of a diamond nucleus (with diamond density) within a thin onion-like shell with complex chemical composition and lower density [192]. Powders of diamond nanoparticles have notably been used as extremely efficient reflectors of slow neutrons [193, 194]. The density of such powders can be tuned between 5% and 15% of bulk diamond density by pressing the sample or blowing air through it [195].

- Very diffuse powders of frozen water nanoparticles can be obtained from "impurity-helium gels" [196]. These gels are formed by condensing a vapor of helium and the impurity (here water) on a superfluid helium surface at 1.6 K. Impurity-helium gels are being considered for use as neutron moderators and have been characterized by neutron scattering. After evaporation of the helium, a powder of ice nanoparticles with a mean diameter of 6-10 nm is obtained. Little optical data is available for ice at such temperatures. We will therefore be using the dielectric constant of liquid water (see section II.2.a) to describe the ice nanoparticles. Our calculations should thus be considered as preliminary and a direct measurement of the permittivity of these powders is desirable.

To compute the Casimir-Polder potential, we need the optical response of these materials over a broad range of frequencies. If the wavelengths involved are larger than the size of inhomogeneities, we can use an effective medium approximation, where the composite medium is replaced by a homogeneous effective medium. Several approximations can be used to express the relative permittivity ε_{eff} of the effective medium in terms of the dielectric constants of the original constituents:

- For a host material containing non-overlapping spherical inclusions of another material, application of the Clausius-Mossoti relation yields the Maxwell-Garnett formula [197]:
$$\frac{\varepsilon_{\text{eff}} - \varepsilon_h}{\varepsilon_{\text{eff}} + 2\varepsilon_h} = \phi_i \frac{\varepsilon_i - \varepsilon_h}{\varepsilon_i + 2\varepsilon_h} \ , \tag{II.59}$$
where ε_h and ε_i are the dielectric constants of the host and inclusions respectively and ϕ_i is the volume fraction of inclusions.

- The Bruggeman model [198] requires that the average polarization of spherical inclusions embedded in the effective medium vanish. For a mixture of materials

with relative permittivities ε_1 and ε_2 and volume fractions ϕ_1 and ϕ_2 ($\phi_1+\phi_2=1$), the effective relative permittivity is the solution of the equation:

$$\phi_1 \frac{\varepsilon_1 - \varepsilon_{\text{eff}}}{\varepsilon_1 + 2\varepsilon_{\text{eff}}} + \phi_2 \frac{\varepsilon_2 - \varepsilon_{\text{eff}}}{\varepsilon_2 + 2\varepsilon_{\text{eff}}} = 0 \ . \tag{II.60}$$

- Landau and Lifshitz have proposed another effective model based on the idea that the cubic root of the dielectric constant is approximately additive [174]:

$$\varepsilon_{\text{eff}}^{1/3} = \phi_1 \ \varepsilon_1^{1/3} + \phi_2 \ \varepsilon_2^{1/3} \ . \tag{II.61}$$

The Maxwell-Garnett model has already been used to describe aerogels in the Casimir-related literature, either as air inclusions in a solid matrix [199] or as silica inclusions in air [200]. Since we want to vary the porosity over a wide range of values, we prefer a model which treats the two components symmetrically. We choose the Bruggeman model over the Landau-Lifshitz model because of its clear physical interpretation. However, as shown in figure II.5, the three models give very similar results so that our particular choice has little impact on the computed Casimir-Polder potential.

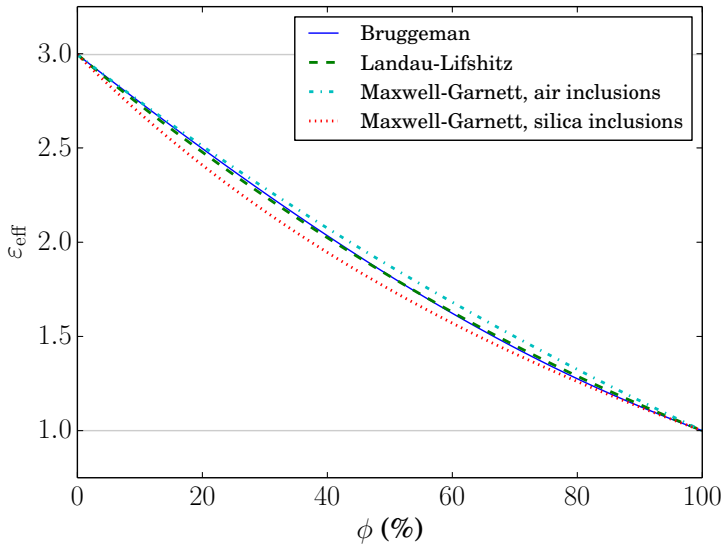

Figure II.5: Comparison of effective medium models for the effective static relative permittivity $\varepsilon_{\text{eff}}(0)$ of a silica aerogel as a function of its porosity ϕ: Bruggeman (blue full line), Landau-Lifshitz (green dashed line), Maxwell-Garnett with air inclusions in a silica matrix (cyan dot-dashed line), Maxwell-Garnett with silica inclusions in air (red dotted line).

Such effective models are valid when the size of the medium's inhomogeneities is sufficiently small compared with the wavelengths involved in the physical process of

interest. In our case we expect that they will allow a good estimation of the Casimir-Polder potential for separations larger than ~ 100 nm. Similarly, porous materials are likely to have a rough surface but we will assume that it does not affect the potential on distances larger than the scale of the roughness, so we maintain our assumption of a plane surface. Given these assumptions, our results should be taken as a first estimation of the Casimir-Polder potential with low-density materials.

A more rigorous study of the Casimir-Polder potential near a random medium shows that the fluctuations ΔV of the potential scale with the separation z and the density n of scatterers in the medium as [201, 202]

$$\frac{\Delta V}{V} \propto (nz^3)^{-1/2} \ . \tag{II.62}$$

This supports the idea that these fluctuations can be neglected when the atom-plane separation z is much larger than the typical distance between scatterers $n^{-1/3}$.

Figure II.6 shows the Casimir-Polder potential between an (anti)hydrogen atom and silica aerogels of various porosities ϕ. In figure II.7, we compare the potentials associated with bulk and nanoporous mirrors made from silica, silicon or diamond. Finally, in table II.2, we collect values of the coefficient C_4 characterizing the strength of the long-distance interaction.

As expected, we observe a drastic reduction of the potential as the porosity increases and the medium's optical response diminishes but the shape and relative positions of the curves are preserved.

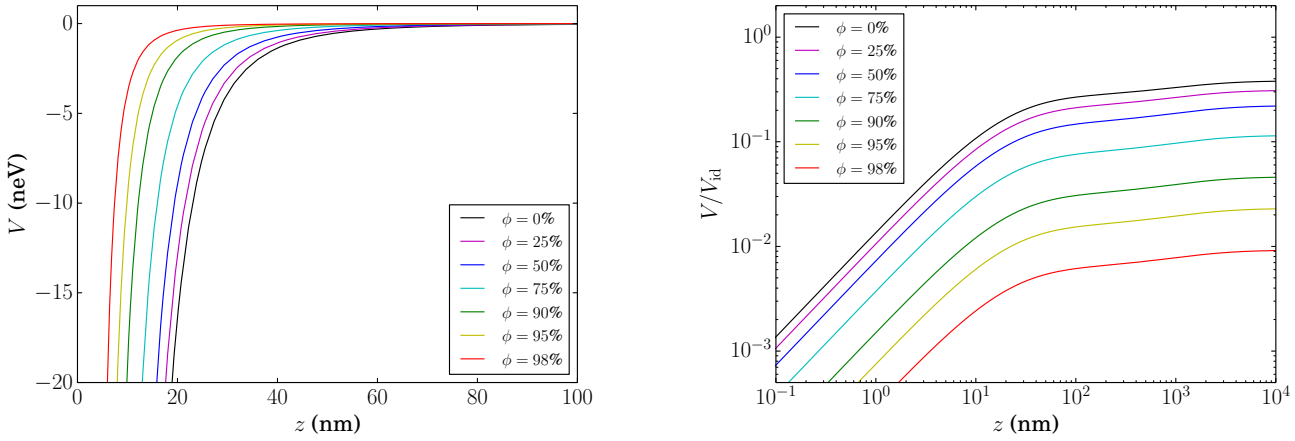

Figure II.6: Left panel: Casimir-Polder potential $V(z)$ between an (anti)hydrogen atom and nanoporous silica mirrors of various porosities ϕ (from bottom to top, black: silica bulk, purple: $\phi = 25$ %, blue: $\phi = 50$ %, cyan: $\phi = 75$ %, green: $\phi = 90$ %, yellow: $\phi = 95$ %, red: $\phi = 98$ %). Right panel: ratio $V(z)/V_{\text{id}}(z)$ (same color code).

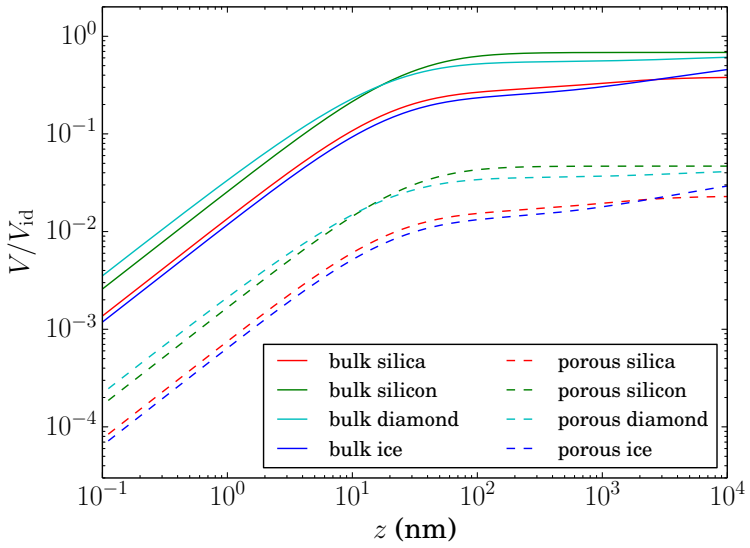

Figure II.7: Normalized Casimir-Polder potential $V(z)/V_{\mathrm{id}}(z)$ between an (anti)hydrogen atom and various bulk (full lines) and nanoporous materials of porosity $\phi = 95\%$ (dashed lines). Red: silica, green: silicon, cyan: diamond, blue: ice.

porosity	ϕ	0%	25%	50%	75%	90%	95%	98%
silica	(a.u.)	28.1	22.9	16.3	8.47	3.40	1.70	0.68
ice	(a.u.)	54.9	51.2	43.5	23.4	8.19	3.89	1.51
silicon	(a.u.)	50.3	45.4	36.3	19.2	7.14	3.45	/
diamond	(a.u.)	46.8	41.6	32.4	17.1	6.51	3.17	/

Table II.2: C_4 coefficients characterizing the long distance behavior of the Casimir-Polder interaction between an (anti)hydrogen atom and nanoporous silica, ice, diamond and silicon media with various porosities ϕ.

II.3 One-way quantum reflection

We are now ready to tackle the problem of atoms scattering from the Casimir-Polder potential near surfaces. In this section we consider atoms with positive energy E incident on a potential $V(z)$ given by the Casimir-Polder interaction only. The situation is represented in figure II.8 and it is described by the Schrödinger equation

$$-\frac{\hbar^2}{2m}\frac{\mathrm{d}^2\psi_E}{\mathrm{d}z^2}(z) + V(z)\psi_E(z) = E\psi_E(z)\ . \tag{II.63}$$

defined on the positive real axis $z > 0$. There is no classical turning point and the atom can be considered as free sufficiently far from the surface. If we denote $\kappa \equiv \hbar^{-1}\sqrt{2mE}$ the wavevector at infinity, the solutions of the Schrödinger equation have the following asymptotic behavior:

$$\psi(z) \underset{z\to\infty}{\simeq} \frac{\mathcal{N}}{\sqrt{\kappa}}\left(e^{-i\kappa z} + re^{i\kappa z}\right)\ . \tag{II.64}$$

The first term corresponds to the incoming matter wave, the second to the reflected wave. The reflection coefficient r depends on the choice of a boundary condition at the surface for the Schrödinger equation. In this section we will suppose that the surface is perfectly absorbing, so that the matter wave can impinge on the Casimir-Polder potential only from the right, hence the name *one-way quantum reflection*. This condition is certainly enforced for antihydrogen, which is annihilated as soon as it touches the matter plate. We will elaborate on this point in section II.3.b and consider more general situations in section II.4.

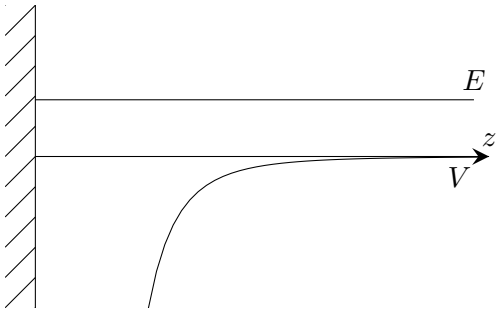

Figure II.8: Schematic representation of scattering of an atom with energy E on the Casimir-Polder potential $V(z)$.

II.3.a Behavior of the badlands function

We have seen in chapter I that the badlands function discriminates between regions where waves propagate classically and those where quantum reflection can occur. We therefore start by plotting the badlands function $Q(z)$ for different mirror materials and

atom energies. We recall that

$$Q(z) = \frac{\hbar^2}{2m} \frac{4(V(z) - E)V''(z) - 5V'(z)^2}{16(E - V(z))^3} \ . \tag{II.65}$$

In figure II.9 we consider a thick silica mirror and vary the energy of the incoming atom whereas in II.10 the energy is kept constant but we change the material medium.

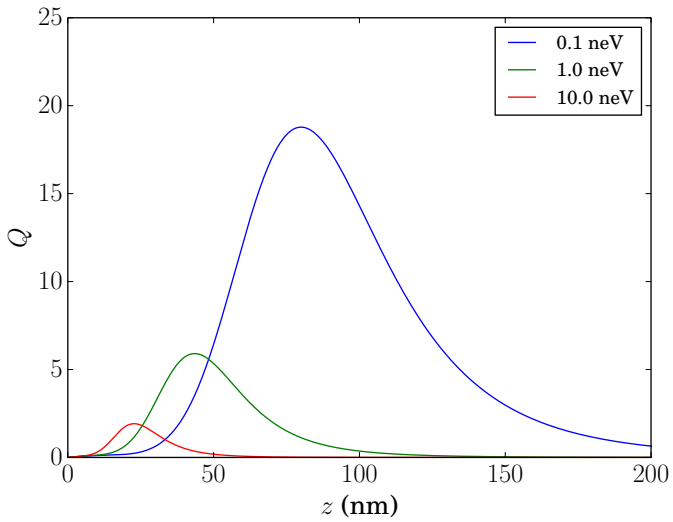

Figure II.9: Badlands function $Q(z)$ for the Casimir-Polder potential between a silica bulk and an antihydrogen atom with energies $E = 0.1$, 1.0 and 10.0 neV. The badlands peak moves away from the surface and becomes larger as the energy is reduced.

We can already make several important observations:

- First of all, the badlands function consists of a single peak and vanishes both as the distance goes to infinity and as it goes to zero. Indeed, the atom is a free particle when it is sufficiently far from the surface so that the semiclassical approximation is valid in that limit. The fact that it is also valid when the atom is very close to the surface is perhaps more surprising. Actually, the behavior of the badlands function depends on the relative magnitudes of k_{dB} and its derivatives. For potentials diverging like $-C_n/z^n$ at the surface, the fact that $k_{\mathrm{dB}}(z)$ is large prevails and the badlands function tends to zero if $n > 2$. This is the case in the short distance, van der Waals limit of the Casimir-Polder potential ($n = 3$). We conclude that there is a single badlands region and that on both sides of this region, waves propagate semiclassically, in a well defined direction. We will refer to the classical region near the surface as the *cliff side* and to the classical region far from the surface as the *far end*, as shown in figure II.11.

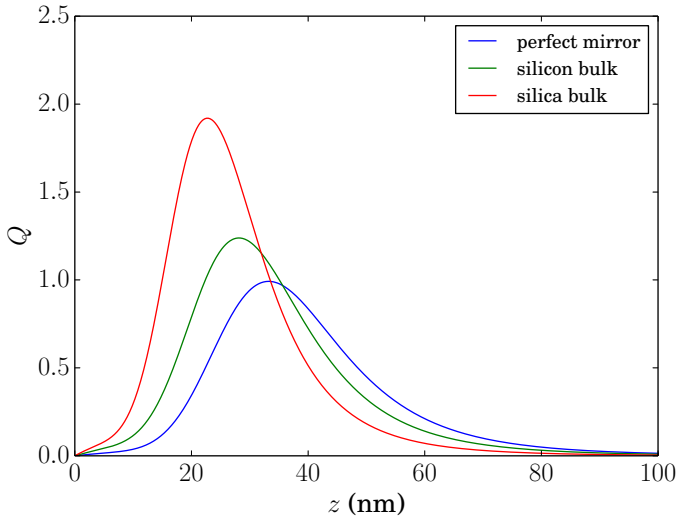

Figure II.10: Badlands function $Q(z)$ for the Casimir-Polder potential between an antihydrogen atom with energy $E = 10$ neV and perfect, silicon and silica mirrors. The badlands peak moves towards the surface and becomes larger as the potential strength is reduced.

- Closer examination reveals that the badlands peak is centered around the point where $|V(z)| = E$. It moves away from the surface when the energy is reduced for a given potential, and closer to it if the potential is weakened while the energy is kept fixed.

- Finally, it is particularly instructive to look at the peak value of the badlands function. Indeed, we have seen in section I.3.d that after a Liouville transformation to the WKB coordinate the badlands function plays the role of a potential. In the present case, the Liouville-transformed potential is a barrier and the peak value of the badlands function fixes its height. Higher badland peaks are therefore expected to be associated with greater reflection probabilities. We observe that the badlands peak grows as the energy is decreased, signaling the failure of the semiclassical approximation in the quantum regime. More surprisingly, the peak value of the badlands function also grows when the potential is weakened. Indeed the peak is the smallest for a perfect mirror and it is larger for a silica bulk than for a silicon bulk. We can thus expect more quantum reflection from weaker potentials. Explicit calculations (see section II.3.e) will confirm that this is indeed the case.

II.3.b Boundary condition on the surface

As mentioned above, in the present section we are assuming that the surface absorbs atoms perfectly. We have just shown that it is meaningful to speak of waves moving

towards and away from the surface on the cliff-side since the badlands function vanishes there. The relative amplitude of these two waves depends on the very short range interactions between the atom and surface. Such interactions are notoriously difficult to describe since they involve many competing elastic and inelastic phenomena. For example the atom might be reflected elastically by the Coulomb repulsion of electronic clouds, but it could also loose energy to phonons in the medium and be adsorbed on the surface. The atom will also be affected by the roughness of the surface, with the possibility of being reflected non specularly. The situation is much simpler in the case of an anti-atom since annihilation occurs as soon as it comes in contact with the surface.

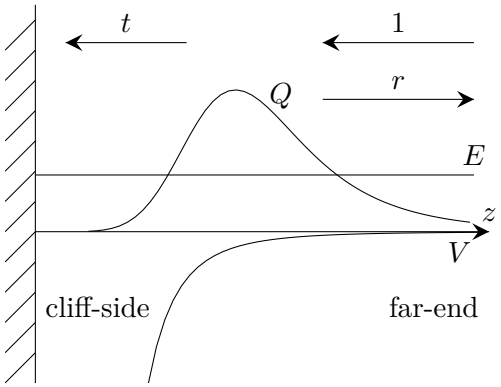

Figure II.11: Scattering on the Casimir-Polder potential: the incident wave is supposed to have amplitude 1 and there is no wave coming back from the surface, r and t denote respectively the reflection and transmission amplitudes for the badlands region.

In this section, we are making the strong assumption that there is no coherent reflection on the surface. This corresponds to a purely absorbing boundary conditions on the surface:

$$\psi(z) \underset{z\to 0}{\simeq} \mathcal{N} t \psi^{-}_{\mathrm{WKB}}(z) \tag{II.66}$$

$$\text{or} \quad a_+(z=0) = 0 \ , \quad a_-(z=0) = \mathcal{N} t \tag{II.67}$$

where t is the transmission coefficient[2]. Under these conditions, the atom can cross the badlands region only once, and only towards the surface. Although this assumption is justified for an anti-atom, it is an approximation in the case of real atoms, and we will show in section II.4 that if there is some coherent reflection from the surface then the reflection probability can be affected.

We now present two ways of solving the Schrödinger equation describing the quantum reflection. The first makes use of the differential equations which couple incident and reflected WKB waves. The second exploits the Liouville transformation to the WKB coordinate.

[2]In numerical calculations, it is convenient to set the product $\mathcal{N} t$ equal to one.

II.3.c Using the coupled equations for WKB waves

Before demonstrating the usefulness of Liouville transformations to solve quantum reflection problems, we describe a more standard approach. It consists in solving the coupled differential equations for the space-dependent amplitudes of the incoming and outgoing WKB waves, as presented in section I.2.c. We will use Berry and Mount's version of the coupled equations (equations (I.75)):

$$a'_{\pm}(z) = \frac{k'_{\mathrm{dB}}(z)}{2k_{\mathrm{dB}}(z)} a_{\mp}(z) \exp(\mp 2i\phi_{\mathrm{dB}}(z)) \ . \tag{II.68}$$

The expectation is that these amplitudes have smoother variations than the rapidly oscillating wavefunction. However, one is still confronted with the fact that the WKB phase $\phi_{\mathrm{dB}}(z)$ diverges near the surface. To bypass this difficulty, we use an analytical solution which is valid close to the surface. On the cliff-side, the energy E is negligible compared to the potential which takes its van der Waals form $V(z) \simeq -C_3/z^3$. In this limit, the WKB phase (I.54) is

$$\phi_{\mathrm{dB}}(z) \simeq \frac{1}{\hbar}\sqrt{\frac{8mC_3}{z_0}} - \frac{1}{\hbar}\sqrt{\frac{8mC_3}{z}} \ , \tag{II.69}$$

so that the coupled differential equations (II.68) simplify to

$$a'_{\pm}(z) = \frac{-3}{4z} \exp\left(\mp \frac{2i}{\hbar}\sqrt{\frac{8mC_3}{z_0}} \pm \frac{2i}{\hbar}\sqrt{\frac{8mC_3}{z}} \right) a_{\mp}(z) \tag{II.70}$$

We introduce the new variable $x \equiv \hbar^{-1}\sqrt{8mC_3/z}$ and obtain

$$a'_{\pm}(x) = \frac{3}{2x} \exp\left(\pm 2i(x - x_0)\right) a_{\mp}(x) \ , \tag{II.71}$$

which we can rewrite as two decoupled second order differential equations:

$$x^2 a''_{\pm}(x) + \left(x \mp 2ix^2\right) a'_{\pm}(x) - \frac{9}{4} a_{\pm}(x) = 0 \ . \tag{II.72}$$

With the following definitions: $a_{\pm}(x) \equiv x^{3/2} f_{\pm}(t)$, $t \equiv \pm 2ix$, these equations are mapped onto the Kummer equation:

$$t f''_{\pm}(t) + (b - t)\, f'_{\pm}(t) - a f_{\pm}(t) = 0 \tag{II.73}$$

with parameters $a = 3/2$ and $b = 4$. A pair of independent solutions is given by Kummer's confluent hypergeometric functions $M(a, b, t)$[3] and $U(a, b, t)$ [1]. The solutions corresponding to the boundary conditions $a_+(z = 0) = 0$ and $a_-(z = 0) = \mathcal{N} t = 1$ are

$$a_+(x) = -2(1 + i)x^{3/2}\left[U\left(\frac{3}{2}, 4, 2ix\right) - \frac{i\sqrt{\pi}}{8} M\left(\frac{3}{2}, 4, 2ix\right) \right] e^{-2ix_0} \ , \tag{II.74a}$$

$$a_-(x) = -2(1 + i)x^{3/2} U\left(\frac{3}{2}, 4, -2ix\right) \ . \tag{II.74b}$$

[3] Kummer's M function is also known as the ${}_1F_1$ hypergeometric function.

These functions can be evaluated at a finite distance from the surface and used as boundary conditions for the numerical resolution of equations (II.68), thereby circumventing the singularity at the origin.

On the cliff-side, the equations are better behaved when expressed in the variable $x = \hbar^{-1}\sqrt{8mC_3/z}$. It is therefore more convenient to solve equations (II.68) in terms of this variable close to the surface:

$$a'_{\pm}(x) = \frac{k'_{\mathrm{dB}}(x)}{2k_{\mathrm{dB}}(x)} \exp\left(\mp 2i\phi_{\mathrm{dB}}(x)\right) a_{\mp}(x) \ . \tag{II.75}$$

As we move away from the surface and the potential becomes comparable to the energy, we can switch back to the original variable z, which is the more appropriate choice far from the surface, where the WKB phase is proportional to z.

To sum up, the procedure to numerically solve the Schrödinger equation is the following:

- use a fifth order polynomial spline to create an interpolating function $V(z)$ from the values of the potential computed beforehand using equation (II.32),
- find points z_i, z_m and z_f (and the corresponding x_i, x_m and x_f) such that $|V(z_i)| \gg E$, $|V(z_m)| \sim E$ and $|V(z_f)| \ll E$,
- obtain the initial values $a_{\pm}(x_i)$ using the analytical expression (II.74),
- integrate equations (II.75) for $a_{\pm}(x)$ from x_i to x_m,
- integrate equations (II.68) for $a_{\pm}(z)$ from z_m to z_f,
- evaluate the reflection and transmission amplitudes:

$$r \approx \frac{a_+(z_f)}{a_-(z_f)} \qquad \text{and} \qquad t \approx \frac{1}{a_-(z_f)} \ . \tag{II.76}$$

Although this procedure gives good results, it is not completely satisfactory. First, it depends on being able to find an analytical solution of the equations on the cliff-side. Moreover, it requires changing variables in the middle of the numerical integration in order to avoid too fast oscillations of the complex exponential in (II.68). The equations are best behaved when written in a variable which resembles the WKB phase locally (x on the cliff-side, z in the far end). This prompts us to express the scattering problem directly in the WKB coordinate using a Liouville transformation.

II.3.d Liouville transformation from a well to a wall

We now apply the techniques developed in sections I.3.a and I.3.d to the quantum reflection problem. In the following we fix the origin of WKB phase by imposing:

$$\phi_{\mathrm{dB}}(z) \underset{z\to\infty}{\simeq} \kappa z \ , \qquad \kappa \equiv \hbar^{-1}\sqrt{2mE} \ . \tag{II.77}$$

As in section I.3.d, we define the new coordinate to be

$$\boldsymbol{z} \equiv \phi_{\mathrm{dB}}(z) \ , \tag{II.78}$$

where we have taken the proportionality constant $\varkappa$ equal to 1.

For the Casimir-Polder potential, the WKB phase grows continuously from $-\infty$ at the surface to $+\infty$ infinitely far from it, therefore the new coordinate $\boldsymbol{z}$ spans the whole real axis. As we have seen in section I.2.b, the badlands function $Q(z)$ for the Casimir-Polder potential is a peaked function which vanishes both in the far-end and at the cliff-side. This function plays the role of a potential in the transformed equation (I.115). In striking contrast with the original quantum reflection problem, the transformed problem can have classical turning points where $\boldsymbol{F} = 0$ if the peak of the badlands function is higher than 1. Therefore our initial problem of scattering on a potential well has been mapped onto a problem of scattering on a barrier associated with a radically different semiclassical picture. Classically, there is no reflection on the well and total reflection on the barrier (provided it is higher than the energy) but the quantum scattering amplitudes are exactly the same.

To illustrate this point, we go back to the examples of section II.3.a where we had observed the variation of the badlands function with respects to energy and potential strength. We first consider (anti)hydrogen impinging on a silica bulk with energies $E = 0.1, 1$ and 10 neV. The top panel of figure II.12 shows the shape of the potential and three horizontal lines corresponding to the energies. The middle panel gives the WKB phase $\phi_{\mathrm{dB}}(z)$ which will be used as the new variable. Finally, in the bottom panel, we plot the badlands function in terms of the new variable and a horizontal line which represents the new "energy", equal to one in all three cases. The Liouville transformation ensures that the scattering problems presented in the top and bottom panels are equivalent.

As we had noted in section II.3.a, the badlands peak becomes taller when the energy is reduced. Since the "energy" in the transformed problem is always equal to 1, we expect more reflection from the higher peaks, and hence for atoms with lower energies. This is confirmed by the values obtained for the reflection probability: R =88.1, 67.7 and 33.1% for $E = 0.1, 1$ and 10 neV respectively.

We similarly illustrate the effect of varying potential strength in figure II.13, where we give the example of (anti)hydrogen impinging on an ideal mirror, silicon and silica bulks with an energy $E = 10$ neV. As observed in section II.3.a, the WKB approximation grows worse as the Casimir-Polder potentials is weakened. In the transformed problem this translates into a potential barrier which is taller for silica than for silicon and ideal mirrors. The corresponding values of the reflection probability are R =33.1, 19.7 and 14.0% respectively.

Finally we compare the wavefunctions in two equivalent problems. Figure II.14 shows the potential and wavefunction for (anti)hydrogen scattering on a perfect mirror with energy $E = 1$ neV in the original (left panel) and WKB (right panel) coordinates. The rapid oscillations of the wavefunction near the surface in the initial situation are mapped to simple sinusoids in the WKB coordinate.

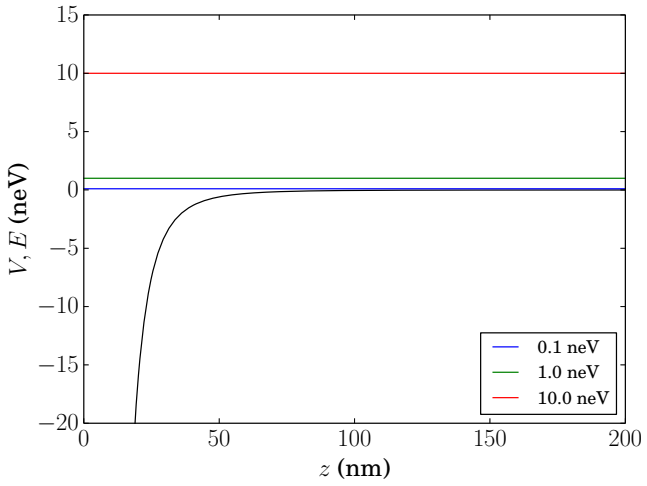

(a) The original scattering problems: (anti)hydrogen atom impinging on a silica bulk with energy $E = 0.1, 1$ and 10 neV.

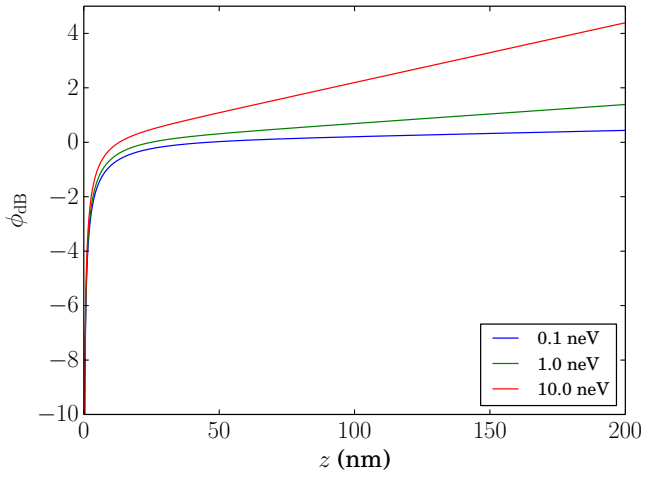

(b) The new coordinate $\boldsymbol{z} = \phi_{\mathrm{dB}}(z)$ for the three situations shown in (a), notice that $\phi_{\mathrm{dB}} \simeq \kappa z$ in the far-end.

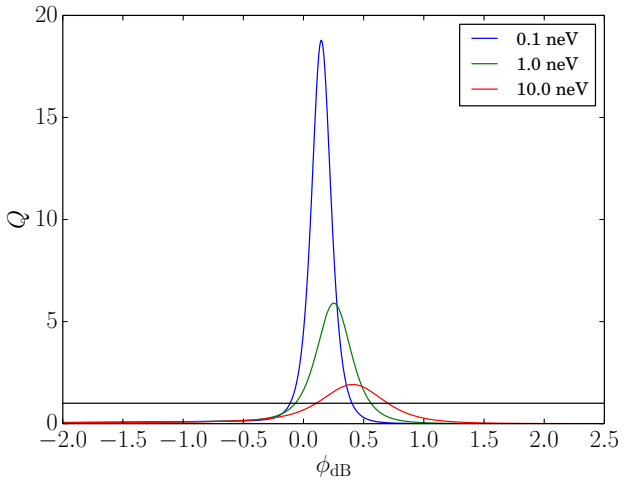

(c) The transformed problems: energy $\boldsymbol{E} = 1$ and potential $\boldsymbol{V} = Q$ versus the WKB coordinate $\boldsymbol{z} = \phi_{\mathrm{dB}}$. The new energy is equal to one in all three cases but the three original energies $E = 0.1, 1$ and 10 neV each give a different badlands peak.

Figure II.12: Liouville transformation to the WKB coordinate applied to the Schrödinger equations describing an (anti)hydrogen atom impinging on a silica bulk with energies $E = 0.1,\ 1$ and 10 neV (blue, green and red lines respectively).

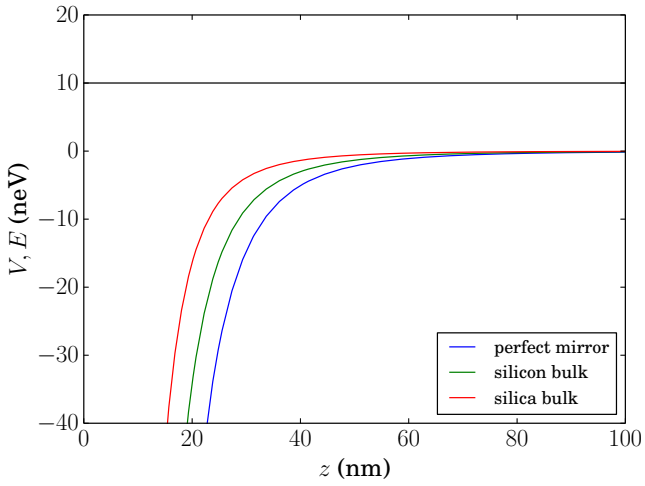

(a) The original scattering problems: (anti)hydrogen atom impinging on perfect, silicon and silica mirrors with energy $E = 10$ neV.

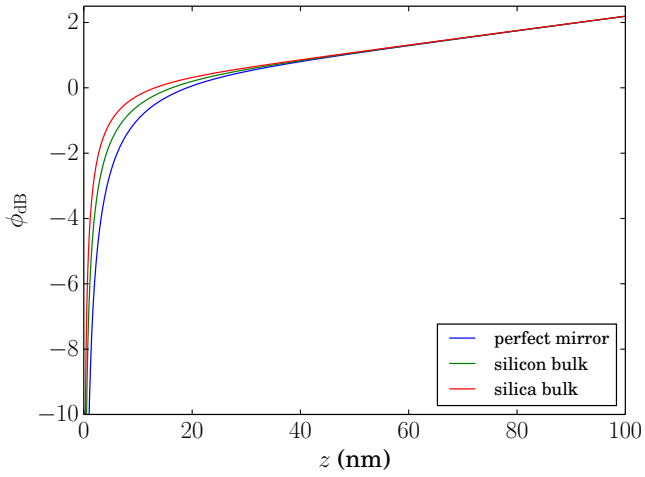

(b) The new coordinate $\boldsymbol{z} = \phi_{\mathrm{dB}}(z)$ for the three situations shown in (a).

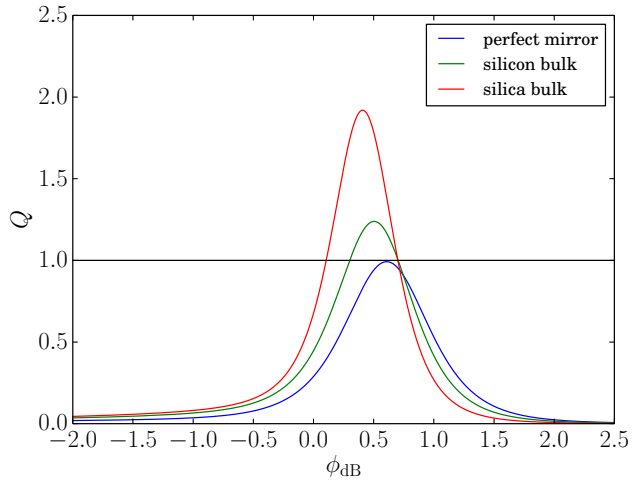

(c) The transformed problems: energy $\boldsymbol{E} = 1$ and potential $\boldsymbol{V} = Q$ versus the WKB coordinate $\boldsymbol{z} = \phi_{\mathrm{dB}}$. The new energy is equal to one in all three cases but the three original potentials, for ideal, silicon and silica mirrors, each give a different badlands peak.

Figure II.13: Liouville transformation to the WKB coordinate applied to the Schrödinger equations describing an (anti)hydrogen atom impinging on a on perfect mirror (blue), a silicon bulk (green) and a silica bulk (red) with energy $E = 10$ neV.

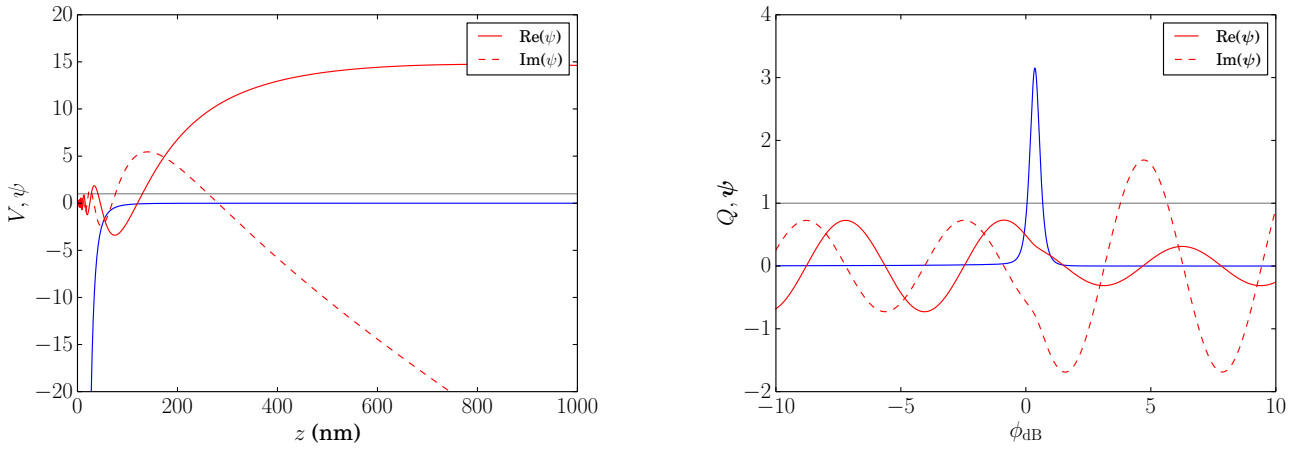

Figure II.14: Wavefunction of (anti)hydrogen scattering on a perfect mirror with energy $E = 1$ neV in the original (left panel) and WKB coordinates (right panel).

The above results are obtained through the following numerical procedure:

- use a fifth order polynomial spline to create an interpolating function $V(z)$ from the values of the potential computed beforehand using equation (II.32),
- integrate

$$z'(\boldsymbol{z}) = \frac{1}{k_{\mathrm{dB}}(z(\boldsymbol{z}))} \tag{II.79}$$

  to obtain the inverse coordinate change $z(\boldsymbol{z})$, the result is a list of values of z corresponding to a given grid $\boldsymbol{z}$
- translate the origin of the $\boldsymbol{z}$-grid in order to have $\boldsymbol{z} \simeq \kappa z$ as $z \to \infty$,
- calculate $Q(z)$ from E, $V(z)$ and its derivatives,
- solve the transformed Schrödinger equation $\boldsymbol{\psi}''(\boldsymbol{z}) + (1 - Q(z(\boldsymbol{z})))\boldsymbol{\psi}(\boldsymbol{z}) = 0$ with the boundary condition $\boldsymbol{\psi}(\boldsymbol{z}) \simeq \exp(-i\boldsymbol{z})$ for the first $\boldsymbol{z}$-grid point,
- evaluate the Wronskians $\mathcal{W}(\boldsymbol{\psi}, \exp(-i\boldsymbol{z}))$ and $\mathcal{W}(\boldsymbol{\psi}, \exp(i\boldsymbol{z}))$ at the last $\boldsymbol{z}$-grid point to extract reflection and transmission coefficients.

The method exposed here allows an exact evaluation of the reflection and transmission coefficients.

It is tempting to compare these results with the estimates given by the semiclassical Gamow-Gurney-Condon formula for the transmission through a barrier [129, 203]:

$$|t|^2 \simeq e^{-2\Phi} \ , \qquad \Phi \equiv \int_{z_1}^{z_2} \sqrt{\boldsymbol{V}(\boldsymbol{z}) - \boldsymbol{E}}\, \mathrm{d}\boldsymbol{z} \tag{II.80}$$

Φ is the imaginary action integral which runs under the barrier, between the two turning points z_1 and z_2. The semiclassical formula turns out to be a poor approximation, as could be expected since Φ is not invariant under Liouville transformations whereas T is. This is particularly flagrant in the examples shown here since a Liouville transformation can relate a quantum reflection problem where Φ is not defined to a tunneling problem where Φ is large, yet both have the same scattering amplitudes.

II.3.e Reflection probabilities

In this section, we present the one-way reflection probability $R \equiv |r|^2$ of (anti)hydrogen atoms on various surfaces, corresponding to the potentials computed in the first part of this work. For the moment, we do not discuss the phase of r, which is not directly observable in a one-way quantum reflection experiment. These probabilities can be calculated equivalently using the techniques discussed in section II.3.c and II.3.d.

We first plot the reflection probability on various thick slabs in figure II.15. The following observations can already be made on this first plot:

- The quantum reflection probability vanishes for large energies, where the classical behavior is recovered.
- On the contrary, the reflection probability tends to unity at low energies, signaling purely quantum behavior in that regime.
- Bad reflectors of the electromagnetic field such as silica turn out to be better reflectors for atoms. While this seems counterintuitive at first, it was to be expected from the results of the previous section, where we have shown that scattering on a weaker potential is equivalent to scattering on a taller barrier after Liouville transformation.

In figure II.16 we present the reflection probability as a function of energy for (anti)hydrogen impinging on thin silica slabs. It appears that slabs must be extremely thin, typically less than 10 nm thick, to get a notable increase of reflectivity. As discussed earlier, this seems extremely challenging from an experimental point of view. On the same graph, we show the reflection probability on graphene, which turns out to depend very little on the gap parameter Δ. It is comparable to the reflection probability on an (unrealistic) 1 nm silica slab.

We will not discuss nanoporous materials in this section. As mentioned in II.2.c, a simple effective description of such media is valid only at distances from the surface that are sufficiently large compared to the size of inhomogeneities in the medium. Therefore, it is necessary to consider low energies in order to have a valid description of quantum reflection on such media. Indeed we have seen in section II.3.a that quantum reflection occurs further afar from the surface as the energy is reduced. We will therefore postpone the discussion of reflection on nanoporous materials to the next section, where we consider the low energy limit of quantum reflection.

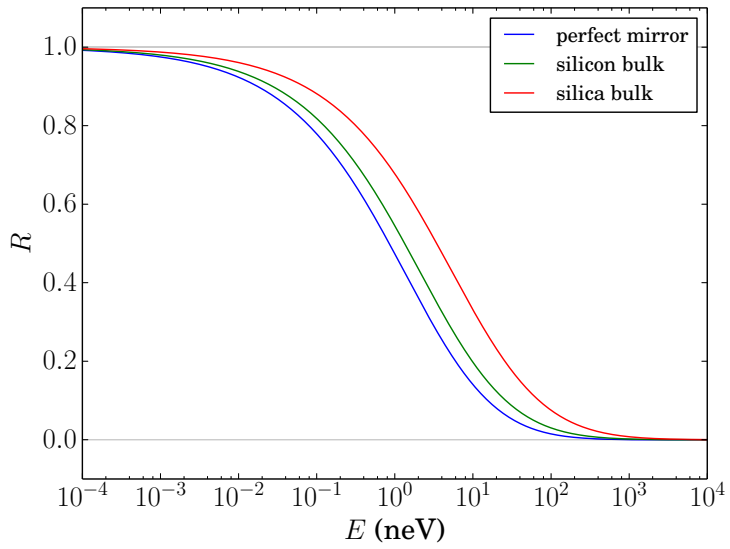

Figure II.15: Reflection probability versus energy of an antihydrogen atom impinging on a thick material medium (top: silica, middle: silicon, bottom: perfect mirror).

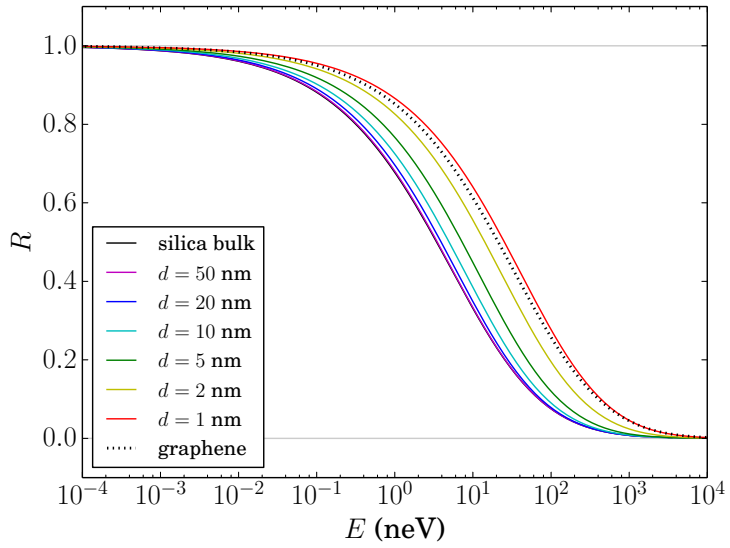

Figure II.16: Reflection probability versus energy for (anti)hydrogen falling on silica slabs of various thicknesses (from bottom to top the slab width is infinite, 50 nm, 20 nm, 10 nm, 5 nm, 2 nm, 1 nm) and graphene ($\Delta = 10^{-15}$ eV, black dotted line).

II.3.f Scattering lengths

In section I.4, we have shown that low energy scattering on a localized potential could be described in terms of a single complex parameter, the scattering length a. If ℓ is a characteristic length scale of the potential, the reflection coefficient is then given by:

$$r \underset{\kappa\ell\ll 1}{\simeq} -\exp\left(-2i\kappa a\right) , \qquad R \underset{\kappa\ell\ll 1}{\simeq} \exp\left(-4\kappa b\right) , \qquad b \equiv -\,\mathrm{Im}(a) . \tag{II.81}$$

In figure II.17 , we plot $-\log(-r)/2i\kappa$ as a function of energy for different materials, and show that it indeed goes to a constant value a in the limit $E \to 0$. The tables II.3 and II.4 below collect the values of the scattering length for some of the various potentials that have been addressed in this work.

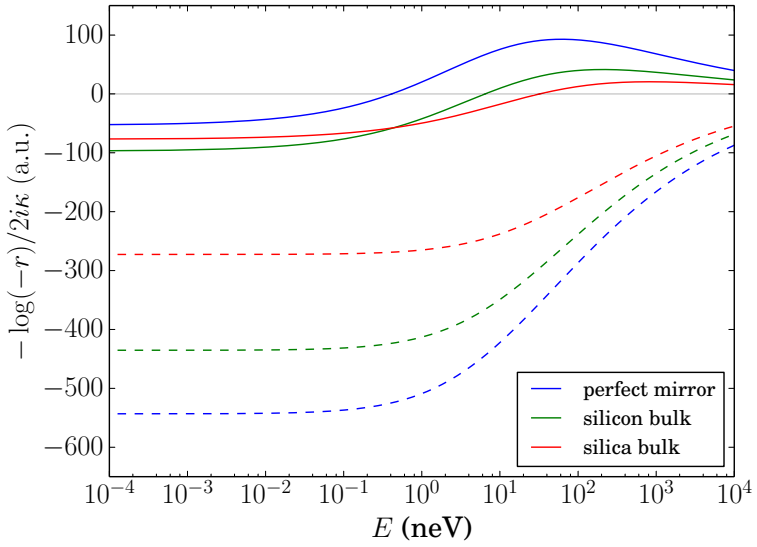

Figure II.17: Real (full lines) and imaginary (dashed lines) part of $-\log(-r)/2i\kappa$ for antihydrogen impinging on perfect (blue), silicon (green) and silica (red) mirrors.

	perfect mirror	silicon	silica	graphene
Re(a) (a.u.)	-53.0	-97.2	-77.0	-15.4
Im(a) (a.u.)	-543.0	-435.2	-272.6	-109.7

Table II.3: Scattering length of (anti)hydrogen on various thick slabs and graphene (with gap parameter $\Delta = 10^{-15}$ eV).

As expected, the imaginary part of the scattering length draws nearer to zero when the potential strength is reduced, that is for thinner slabs or materials that couple weakly to the electromagnetic field. This corresponds to a higher reflection probability. The

slab width	silicon (a.u.)		silica (a.u.)	
	Re(a)	Im(a)	Re(a)	Im(a)
1 nm	3.0	-178.1	6.5	-97.9
2 nm	1.6	-231.8	7.5	-130.3
5 nm	-6.5	-311.2	3.2	-181.9
10 nm	-21.8	-367.8	-9.3	-221.1
20 nm	-45.2	-408.0	-29.1	-250.1
50 nm	-73.1	-429.7	-53.3	-267.4
100 nm	-85.0	-433.7	-64.4	-271.2
∞	-97.2	-435.2	-77.0	-272.6

Table II.4: Real and imaginary parts of the scattering length for (anti)hydrogen interacting with a thin silicon or silica slab.

real part of the scattering length grows from negative to small positive values when the slab width is reduced.

As discussed in section II.2.c, quantum reflection calculations for nanoporous media should be performed at low enough energy to limit the influence of the short range potential which is affected by inhomogeneities in the medium. Figure II.18 shows the evolution of b with the porosity of various porous media : silica aerogel, porous silicon and diamond nanoparticle powder. These materials exhibit remarkably high reflection probabilities. For example, the parameter b (and therefore also the transmission probability $1 - R \simeq 4\kappa b$) is divided by a factor 20 when comparing bulk silica to 98% porosity aerogel.

Quantum reflection experiments have been performed by Pasquini et al. with condensates of sodium atoms on a nanostructured silicon surface and a silica aerogel [103]. They observed a reflection probability of ∼60% on the nanostructured silicon surface, compared with ∼15% on bulk silicon. However, no reflection was observed on the aerogel, possibly because of uncontrolled surface charges. This is a serious issue to be solved in order to observe the spectacular enhancement of reflection predicted here.

The fact that quantum reflection increases as matter is removed from the mirror begs the following question: what happens if the mirror is removed altogether? It is clear that some of the assumptions we have made must break down in that limit. Indeed, as the Casimir-Polder interaction is reduced and the atom is allowed to come closer to the surface, there must be a point where the mirror can no longer be considered homogeneous nor perfectly plane, or when the description of the atom as a dipole is no longer valid.

II.3.g Comparison with model potentials

We have seen in the previous section that at low energy quantum reflection can be described in terms of a complex scattering length. Since the reflection occurs farther from the surface as the energy goes to zero, one expects this near-threshold behavior to be governed by the tail of the potential [114, 117, 204]. In particular, for a thick

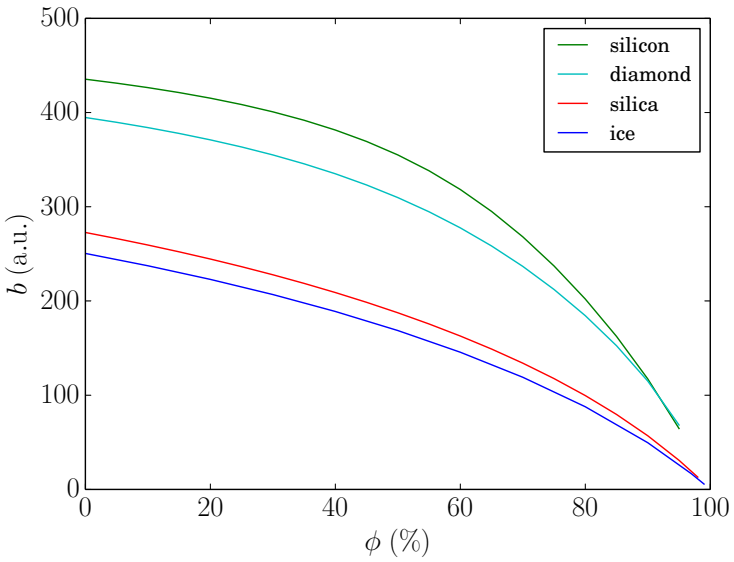

Figure II.18: Parameter b characterizing low energy scattering of (anti)hydrogen on silica aerogel (red) , porous silicon (green) and ice and diamond nanoparticle powders (dark and light blue, respectively) as a function of the material's porosity.

mirrors, the Casimir-Polder potential decays as $V(z) \simeq -C_4/z^4$ in the far-end. We therefore expect this "C_4 potential" to be relevant to low energy scattering on such mirrors.

Potentials of the form $V(z) = -C_n/z^n$ are said to be *homogeneous* because they obey the following scaling property:

$$V(\alpha z) = \alpha^{-n} V(z) \ . \tag{II.82}$$

Analytical results can be obtained for such potentials, we have collected them in appendix B. In particular, the scattering length can be computed exactly for homogeneous potentials. For the C_4 potential we find $a = -i\hbar^{-1}\sqrt{2mC_4}$. Comparison with the values obtained for real potentials shows that this is at most a crude approximation: the real part of the scattering length is non-zero and its imaginary part differs significantly.

Analytical calculations can also be carried out for the "$C_3 - C_4$ model", which interpolates between the short and long range behaviors of the Casimir-Polder potential:

$$V(z) = -\frac{C_4}{z^3(z + C_4/C_3)} \ . \tag{II.83}$$

The scattering length is then [119, 124]

$$a = -\frac{C_4}{2C_3}\left(1 + 2\rho\frac{H_1^{(1)'}(\chi)}{H_1^{(1)}(\chi)}\right) \ , \qquad \chi \equiv \frac{2C_3}{\hbar}\sqrt{\frac{2m}{C_4}} \ , \tag{II.84}$$

where $H_1^{(1)}$ is the Hankel function of order one of the first kind [1]. Although this model predicts a non-zero real part for the scattering length, it still fails to give the correct values. Comparison of the exact scattering lengths with both models is given in table II.5.

		perfect	silicon	silica
exact	Re(a) (a.u.)	-53.0	-97.2	-77.0
	Im(a) (a.u.)	-543.0	-435.2	-272.6
C_4	Re(a) (a.u.)	0	0	0
	Im(a) (a.u.)	-520.0	-429.8	-321.3
$C_3 - C_4$	Re(a) (a.u.)	-70.0	-103.7	-96.8
	Im(a) (a.u.)	-505.6	-389.0	-270.0

Table II.5: Real and imaginary parts of the scattering length for various materials. The first line is the exact numerical result, the second and third lines are the analytic results for a C_4 potential and the $C_3 - C_4$ potential, respectively.

A precise evaluation of the scattering length thus requires the knowledge of the exact potential from cliff-side to far-end. However, we should not hastily conclude that contrary to our initial supposition, the C_4 potential tail is irrelevant to near-threshold scattering. On the contrary, we will show that if we go beyond the simple reasoning presented above, the C_4 model can be used to make accurate estimations of the reflection probability over a large range of energies.

Let us study the C_4 model in more detail. We start by identifying the relevant length scales:

- the inverse of the wavevector at infinity:

$$\frac{1}{\kappa} \equiv \frac{\hbar}{\sqrt{2mE}} \ , \tag{II.85}$$

- the length scale associated with the strength of the potential:

$$\ell \equiv \frac{\sqrt{2mC_4}}{\hbar} \ , \tag{II.86}$$

- the distance at which $E = |V|$:

$$\sigma \equiv \sqrt{\frac{\ell}{\kappa}} = \left(\frac{C_4}{E}\right)^{1/4} \ . \tag{II.87}$$

From these length scales, one can form a single dimensionless parameter $\kappa\ell$. We also define the dimensionless coordinate $u \equiv \ln(z/\sigma)$.

The Schrödinger equation reads

$$\psi''(z) + \left(\kappa^2 - \frac{\ell^2}{z^4}\right)\psi(z) = 0 \ , \tag{II.88}$$

so that the WKB wavevector and phase are

$$k_{\mathrm{dB}}(z) = \kappa\sqrt{1+e^{-4u}}\ , \qquad \phi_{\mathrm{dB}}(z) = \sqrt{\kappa\ell}\int_{u_0}^{u}\sqrt{2\cosh(2\upsilon)}\ \mathrm{d}\upsilon\ , \tag{II.89}$$

where u_0 is chosen to enforce $\phi_{\mathrm{dB}}(z) \underset{z\to\infty}{\simeq} \kappa z$. The integral for the WKB phase can be expressed in terms of the hypergeometric function (defined as in [1]):

$$\phi_{\mathrm{dB}}(z) = \sqrt{\kappa\ell}\ e^{u} F\left(\frac{-1}{2},\frac{-1}{4};\frac{3}{4};-e^{-4u}\right) \tag{II.90}$$

For $\varkappa = \sqrt{\kappa\ell}$ the WKB coordinate depends only on u:

$$\boldsymbol{z} = \frac{\phi_{\mathrm{dB}}(z)}{\varkappa} = e^{u} F\left(\frac{-1}{2},\frac{-1}{4};\frac{3}{4};-e^{-4u}\right) \tag{II.91}$$

and the same is true for the potential:

$$\boldsymbol{V}(\boldsymbol{z}) = \kappa\ell Q(z) = \frac{5}{8\cosh(2u)^3}\ . \tag{II.92}$$

Therefore $\boldsymbol{V}(\boldsymbol{z})$ is a universal function, plotted in figure II.19, that is independent of the parameters of the problem. $\boldsymbol{V}$ reaches its maximum value $5/8$ for $u=0$, that is

$$z=\sigma, \qquad \boldsymbol{z}=\boldsymbol{\sigma} \equiv F\left(\frac{-1}{2},\frac{-1}{4};\frac{3}{4};-1\right) = \frac{\Gamma(3/4)^2}{\sqrt{\pi}} \simeq 0.847213\ . \tag{II.93}$$

$\boldsymbol{V}(\boldsymbol{z})$ is symmetric around this maximum as can be seen by taking $u\to -u$:

$$\boldsymbol{V} = \frac{5}{8\cosh(2u)^3} \underset{u\to -u}{\longrightarrow} \boldsymbol{V}\ , \tag{II.94}$$

$$\boldsymbol{z}-\boldsymbol{\sigma} = \int_0^u \sqrt{2\cosh(2\upsilon)}\ \mathrm{d}\upsilon \underset{u\to -u}{\longrightarrow} \boldsymbol{\sigma}-\boldsymbol{z}\ , \tag{II.95}$$

so that

$$\boldsymbol{V}(\boldsymbol{\sigma}+\boldsymbol{z}) = \boldsymbol{V}(\boldsymbol{\sigma}-\boldsymbol{z})\ . \tag{II.96}$$

At the far-end ($z\to\infty,\ u\to\infty$), the WKB coordinate has the following asymptotic behavior:

$$\boldsymbol{z} \underset{u\to\infty}{\simeq} e^{u}\ , \tag{II.97}$$

from which we deduce the behavior of the universal potential function:

$$\boldsymbol{V}(\boldsymbol{z}) \underset{\boldsymbol{z}\to\infty}{\simeq} \frac{5}{\boldsymbol{z}^6}\ . \tag{II.98}$$

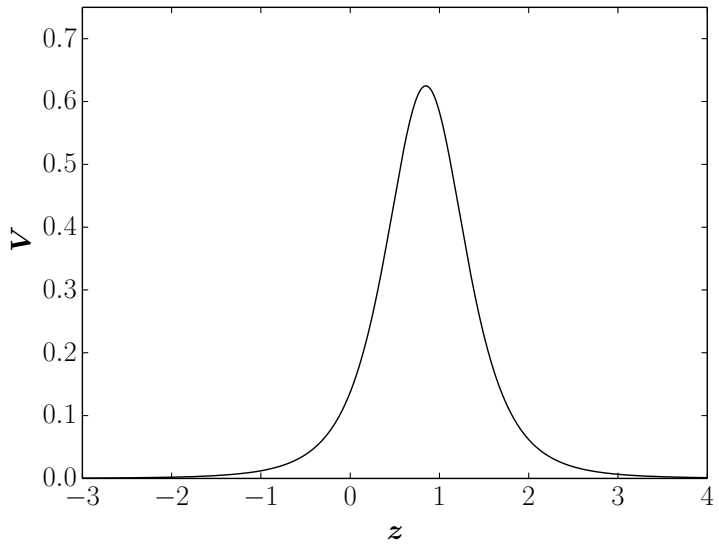

Figure II.19: Universal transformed potential function $\boldsymbol{V}(\boldsymbol{z})$ for a C_4 potential.

Using the symmetry (II.94) we easily obtain the asymptotic behaviors at the cliff-side:

$$\boldsymbol{z} \underset{u\to-\infty}{\simeq} 2\boldsymbol{\sigma} - e^{-u} , \qquad \boldsymbol{V}(\boldsymbol{z}) \underset{z\to-\infty}{\simeq} \frac{5}{(2\boldsymbol{\sigma}-\boldsymbol{z})^6} . \tag{II.99}$$

Finally, the integral of $\boldsymbol{V}$ over the $\boldsymbol{z}$ axis can be computed exactly:

$$\int_{-\infty}^{\infty} \boldsymbol{V}(\boldsymbol{z})\,\mathrm{d}\boldsymbol{z} = \frac{5\Gamma(5/4)^2}{3\sqrt{\pi}} \simeq 0.772531 . \tag{II.100}$$

With our choice of WKB coordinate, the potential $\boldsymbol{V}(\boldsymbol{z})$ is a universal function. As a consequence, the whole dependence on the parameters of the original problem lies in the energy $\boldsymbol{E} = \kappa\ell$. In particular the reflection and transmission coefficients are functions of $\kappa\ell$ only. These functions can be obtained by solving the Schrödinger equation and varying the parameter $\kappa\ell$. This can be done numerically or by using the analytical solution to the Schrödinger equation (II.88) in terms of Mathieu functions, which is given in appendix B.

Within the C_4 model, the variation of the reflection probability with the original potential strength (measured by ℓ) and energy (measured by κ) is evident: changing these parameters modifies the transformed energy $\boldsymbol{E} = \kappa\ell$ but not the potential peak $\boldsymbol{V}$, so that the lower the product $\kappa\ell$ is, the greater the reflection becomes.

A natural question is now whether we can find a similar unique parameter to describe reflection on realistic Casimir-Polder potentials. We have seen that at low energies the reflection probability is determined by the product κb, where b is the imaginary part of

the scattering length in absolute value (section (II.3.f)). Moreover in the special case of the C_4 potential, $b = \ell$. It is therefore natural to perform the Liouville transformation to the WKB coordinate with the proportionality factor $\varkappa = \sqrt{\kappa b}$. The results are presented in figures II.20 and II.21.

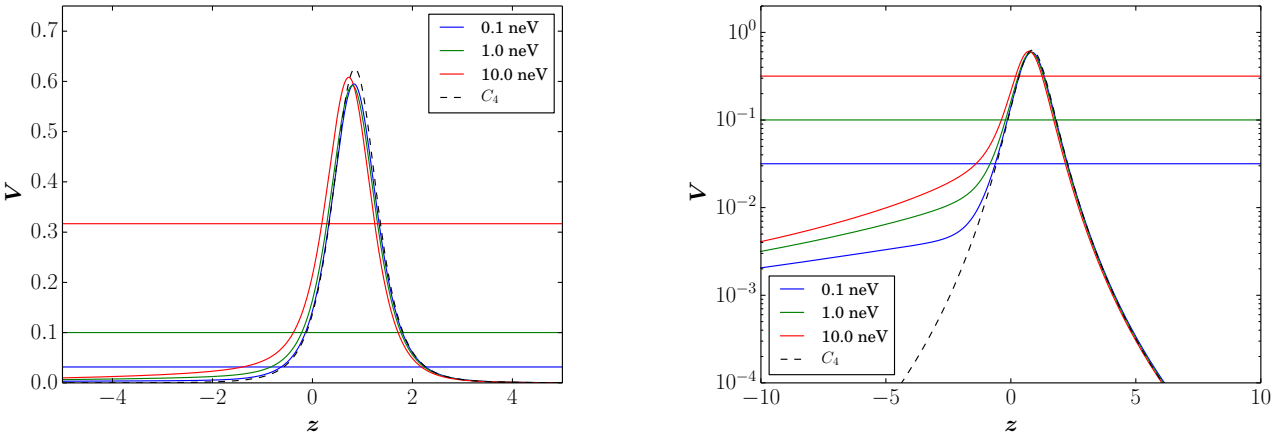

Figure II.20: Left panel: transformed energy $\boldsymbol{E}$ and potential $\boldsymbol{V}(\boldsymbol{z})$ with a scaling factor $\varkappa = \sqrt{\kappa b}$ for (anti)hydrogen impinging on a silica bulk with energies $E = 0.1, 1$ and 10 neV (blue, green and red lines respectively). The universal potential function $\boldsymbol{V}(\boldsymbol{z})$ is shown for comparison (dashed black line). Right panel: the same with a vertical logarithmic scale to emphasize differences in the wings of the potential function.

We observe that with this choice of scaling, the transformed potential functions $\boldsymbol{V}(\boldsymbol{z})$ corresponding to various original energies E and potentials $V(z)$ all approximately collapse onto the universal function for a C_4 potential plotted as a dotted line. More precise inspection of the curves in logarithmic scale shows deviations from this behavior on the cliff-side, where the C_4 model is a poor representation of the real potential.

Changing the original energy and potential therefore leaves the transformed potential peak almost unchanged but modifies the transformed energy $\boldsymbol{E} = \kappa b$. As a consequence, we expect the scattering amplitudes to tend towards universal functions of κb. We show that this is the case by replotting the reflection probability on a perfect mirror, silicon and silica as a function of κb in figure II.22.

Again we observe a collapse of the curves on the universal reflectivity curve calculated for a C_4 potential. Comparison with the low energy behavior $R \simeq e^{-4\kappa b}$ shows that the agreement between exact results and the C_4 model goes far beyond the domain of validity of the scattering length approximation. Use of a vertical logarithmic scale in figure II.22 shows that deviations from the universal C_4 curves occur at high energy. This is consistent with the fact that higher energy collisions sample regions of the potential that are closer to the surface and therefore badly described by the C_4 model.

It is remarkable that this universal scaling behavior also applies to potentials which

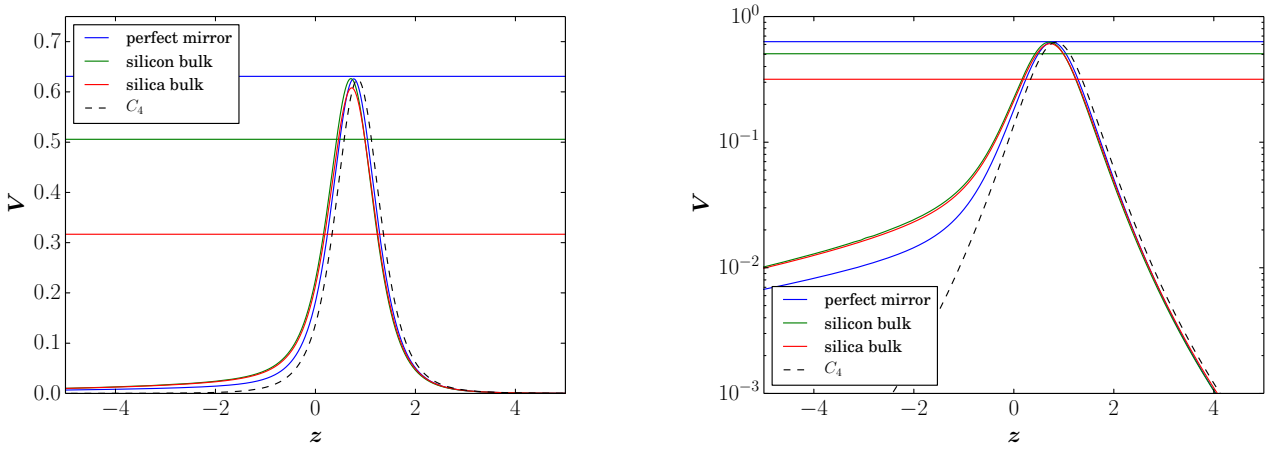

Figure II.21: Left panel: transformed energy $\boldsymbol{E}$ and potential $\boldsymbol{V}(\boldsymbol{z})$ with a scaling factor $\varkappa = \sqrt{\kappa b}$ for (anti)hydrogen impinging on a silica bulk with energy $E = 10$ neV on a perfect mirror(blue line), a silicon bulk (green line) and a silica bulk (red line). The universal potential function $\boldsymbol{V}(\boldsymbol{z})$ is shown for comparison (dashed black line). Right panel: the same with a vertical logarithmic scale to emphasize differences in the wings of the potential function.

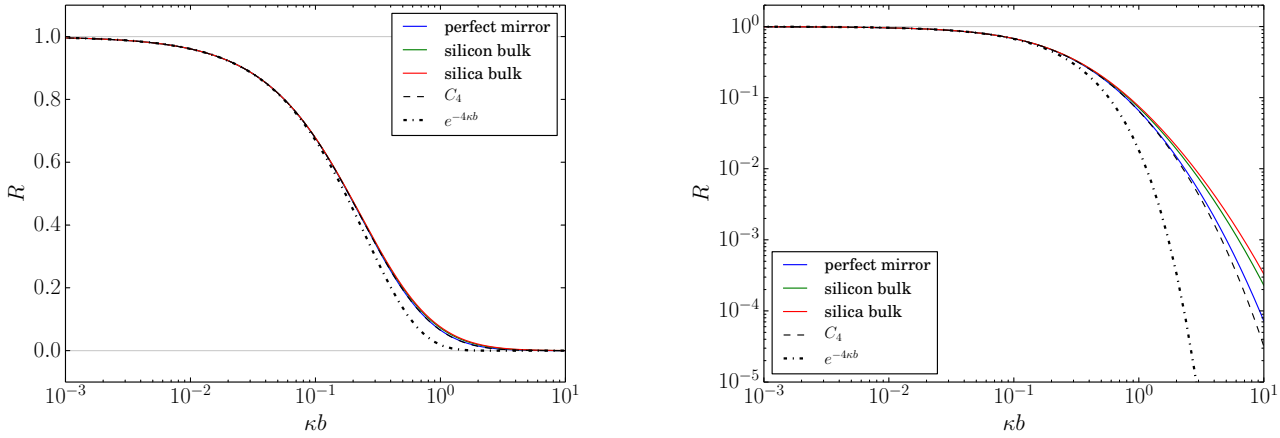

Figure II.22: Left panel: Reflection probability on a perfect mirror, silicon and silica bulks (blue, green and red lines respectively) as a function of the parameter κb. The corresponding curves for reflection in the C_4 model (black dashed line) and in the scattering length approximation (black dot-dashed line) are shown for comparison. Right panel: the same curves, plotted with a vertical logarithmic scale to emphasize deviations from the universal behavior at high energy.

do not exhibit long-range C_4 behavior, for example the potential near matter slabs which decreases as $-C_5/z^5$ in the far-end.

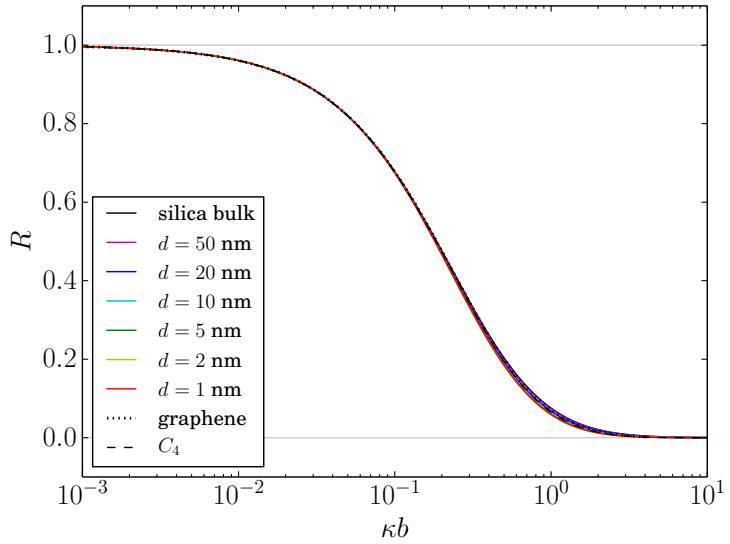

Figure II.23: Reflection probability on silica slabs of various widths (black: thick slab, purple: $d = 50$ nm, blue: $d = 20$ nm, cyan: $d = 10$ nm, green: $d = 5$ nm, yellow: $d = 2$ nm, red: $d = 1$ nm) and graphene ($\Delta = 10^{-15}$ eV, black dotted line) as a function of κb. The corresponding curve for reflection in the C_4 model is shown for comparison (black dashed line).

II.3.h Consequences for GBAR

In the GBAR experiment, annihilation of the anti-atom on the surface ensures that quantum reflection is "one-way". However, at this point we have not included the gravitational potential to which the anti-atom is also submitted in GBAR. Nevertheless, we will show in section III.3 that a particle dropped from a macroscopic height H in the Earth's gravity field can be treated as a plane wave of energy $E = m\bar{g}H$ over the range of the Casimir-Polder potential. The results presented above therefore have implications for the GBAR experiment:

- For fall heights on the order of 10 cm, which is typical of the GBAR setup, the atom has a kinetic energy of the order of 10 neV, so a significant amount of reflection (15-30%) is to be expected.
- The material used for the detection plate has an effect on quantum reflection and metallic surfaces should be used if we want to minimize reflection.

- Higher energy atoms are more likely to be detected in the GBAR experiment, which means that the higher end of the initial energy distribution of dropped atoms will tend to be overrepresented in the results. This will induce a bias which has to be accounted for when extracting the gravitational acceleration $\overline{g}$ from the experimental data.

At first, quantum reflection appears as a hindrance in the GBAR detection scheme. However, both for GBAR and other experiments, reaching high reflection probabilities could be a major advantage since it would allow to trap and guide antimatter with material walls. Potential applications such as a velocity selector for GBAR and antihydrogen quantum bouncing ball experiments will be discussed in chapter IV.

II.4 Two-way quantum reflection

In the previous section, we have solved the quantum reflection problem with full absorption on the surface. To our knowledge, all studies of quantum reflection to date use this boundary condition. This assumption is motivated by the loss of atoms reaching the surface through mechanisms such as annihilation, sticking or non-specular reflection. However it overlooks the possibility of elastic scattering from a very short range repulsive potential.

A detailed description of the mechanisms at work near the surface is far beyond the scope of this thesis. However, we will examine the effect of a modification of the boundary condition at the surface on quantum reflection. The sensitivity of the quantum reflection probability to such a change could explain the difficulty of accurately modeling the results of experiments with matter atoms [96–98].

II.4.a Changing the boundary condition on the surface

We have seen that reflection from the Casimir-Polder potential occurs in the badlands region, some distance away from the surface. This means that we can treat reflection from the Casimir-Polder potential and from the surface itself separately. Scattering on the Casimir-Polder potential is described by a scattering matrix relating the amplitudes of waves propagating away and towards the badlands region, as sketched in figure II.24:

$$\begin{pmatrix} a_+^{\text{out}} \\ a_-^{\text{out}} \end{pmatrix} \equiv \mathcal{S} \begin{pmatrix} a_+^{\text{in}} \\ a_-^{\text{in}} \end{pmatrix} , \qquad \mathcal{S} \equiv \begin{pmatrix} \bar{t} & r \\ \bar{r} & t \end{pmatrix} \tag{II.101}$$

These amplitudes are identical in the original problem and after a Liouville transformation.

We model the effect of short range interactions at the surface by fixing the ratio of the counterpropagating waves in the cliff-side region:

$$a_+^{\text{in}} = \eta a_-^{\text{out}} , \tag{II.102}$$

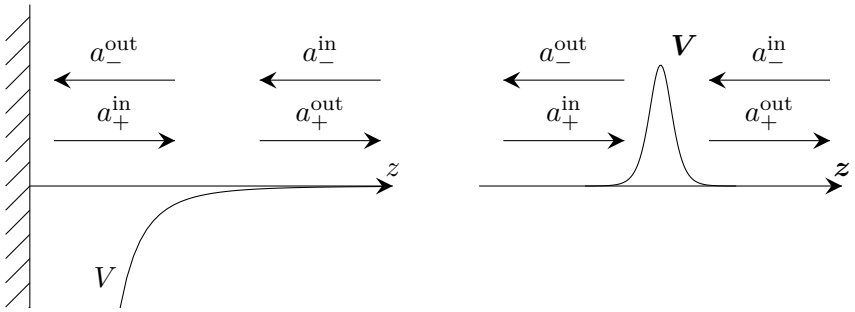

Figure II.24: Amplitudes of the waves incoming on and outgoing from the badlands region, in the original (left) and Liouville-transformed (right) scattering problem.

where η is supposed to be to be a complex number of modulus smaller or equal to one, possibly dependent on the energy. If $|\eta| = 1$, the scattering on the surface is purely elastic whereas for $|\eta| < 1$, part of the particle flux is lost at the surface. Full absorption at the surface, which we have considered in the previous section, corresponds to $\eta = 0$.

II.4.b Successive scattering processes

We solve the linear system of equations formed by the definition of the $\mathcal{S}$-matrix and the relation between a_+^{in} and a_-^{out} to obtain the overall reflection coefficient

$$r_\eta \equiv \frac{a_+^{\text{out}}}{a_-^{\text{in}}} = \frac{r - \eta r\bar{r} + \eta t\bar{t}}{1 - \eta\bar{r}} \ . \tag{II.103}$$

This result can also be written as a sum over the number of successive scattering processes on the surface on the one hand and on the badlands on the other hand:

$$r_\eta = r + t\eta\bar{t} + t\eta\bar{r}\eta\bar{t} + t\eta\bar{r}\eta\bar{r}\eta\bar{t} + \cdots = r + t\eta\left(\sum_{n=0}^{\infty}(\bar{r}\eta)^n\right)\bar{t} \tag{II.104}$$

The scattering matrix obeys unitarity and reciprocity relations which follow from conservation of probability and time-reversal symmetry (see appendix A). Applying these relations, we find that the reflection and transmission coefficients on one side of the badlands can be related to those on the other side:

$$\bar{r} = -r^* t/t^* \ , \qquad\qquad \bar{t} = t \ . \tag{II.105}$$

We can therefore express r_η in terms of r, t and η only:

$$r_\eta = \frac{r + \eta t/t^*}{1 + \eta r^* t/t^*} \ . \tag{II.106}$$

Given a value of η, the "two-way" reflection coefficient r_η can thus be immediately calculated from the "one-way" scattering amplitudes r and t. If $\eta = 0$ we recover the

situation of the previous section and $r_0 = r$. In the opposite case where $|\eta| = 1$, the whole scattering process is unitary and the probability density conserved so that $|r_\eta| = 1$.

It is instructive to write the transmission probability $1 - |r_\eta|^2$ as a function of the amplitudes and phases of r, t and η:

$$1 - |r_\eta|^2 = \frac{A}{1 + F\cos^2(\theta/2)} \ , \tag{II.107}$$

$$\theta \equiv \arg(r) - \arg(\eta) - 2\arg(t) \ , \tag{II.108}$$

$$A \equiv \frac{(1-|r|^2)(1-|\eta|^2)}{(1-|r\eta|)^2} \qquad \text{and} \qquad F \equiv \frac{4|r\eta|}{(1-|r\eta|)^2} \ . \tag{II.109}$$

This type of formula typically describes transmission of light through a Fabry-Perot cavity, formed by two partially reflective mirrors facing each other. When the wavelength of the light is tuned to the cavity length, amplitude builds up within the cavity and transmission is enhanced. Here the matter wave plays the role of light while the two mirrors are replaced by the surface and badlands respectively.

In figure II.25 we plot the transmission probability as a function of the phase θ, for $|r|^2 = 50\%$ and various values of $|\eta|^2$. The modulation of the transmission probability when θ varies can be understood in the following way: θ is the phase difference between a matter wave that is directly reflected off the badlands ($\arg(r)$) and one that escapes the "cavity" after one round trip ($2\arg(t) + \arg(\eta)$). When $\theta = 2k\pi$, $k \in \mathbb{Z}$, the two interfere constructively and reflection is maximal. Conversely, when $\theta = (2k+1)\pi$ reflection is minimal, the incoming wave matches a resonance of the "cavity" so that transmission is enhanced. These resonances are sharper for higher values of the coefficient of finesse F, corresponding to fewer losses on both sides of the "cavity".

Figure II.26 shows the modulus squared wavefunction in WKB coordinates in the resonant and non-resonant case and the relative weights of the counterpropagating waves. Notice the build-up of amplitude within the cavity in the resonant case and the associated increase in the net current directed towards the surface.

If the phase of η is unknown, the interference between the matter waves that are reflected off the Casimir-Polder and off the short range potentials can lead to either an increase or a reduction of the reflection probability compared to the fully absorbing case ($\eta = 0$), within the following bounds:

$$\left(\frac{|r| - |\eta|}{1 - |r\eta|}\right)^2 \leq |r_\eta|^2 \leq \left(\frac{|r| + |\eta|}{1 + |r\eta|}\right)^2 \ . \tag{II.110}$$

Figure II.27 shows the range of values that $|r_\eta|^2$ can take for hydrogen reflected off a perfect mirror for small, fixed values of $|\eta|^2$. It appears that even small values of $|\eta|^2$ can lead to sizable variations of the reflection probability.

Quantum reflection experiments attempting to probe the Casimir-Polder potential should therefore use atoms and surfaces such that there is full absorption upon contact, in order to be free of uncontrolled effects on the surface. Metastable atoms [96], fragile

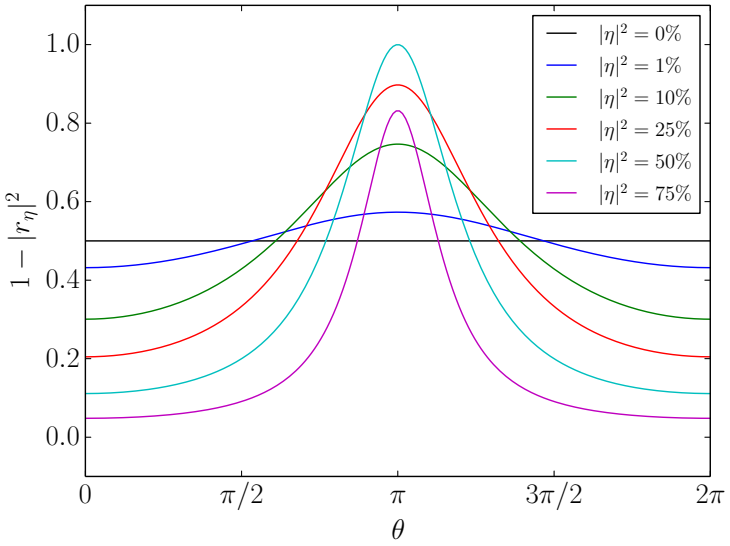

Figure II.25: Transmission probability $1 - |r_\eta|^2$ as a function of the phase θ, for $|r|^2 = 50\%$ and $|\eta|^2 = 0\%$ (black), 1% (blue), 10% (green), 25% (red), 50% (cyan) and 75% (magenta).

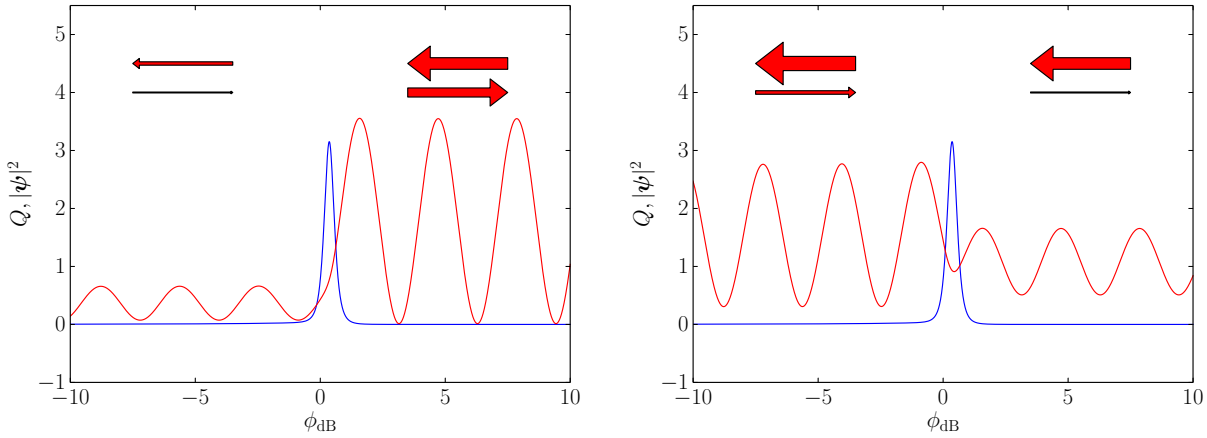

Figure II.26: Modulus squared of the wavefunction of (anti)hydrogen scattering on a perfect mirror with energy $E = 1$ neV and $|\eta|^2 = 25\%$, in the WKB coordinate. In the left panel the phase of η is chosen such that $\theta = 0$ whereas in the right panel it is such that $\theta = \pi$ so that the cavity is resonant. The arrows' relative widths correspond to the amplitudes of the counterpropagating waves on both sides of the badlands region (the amplitude arriving from the right is the same in both cases).

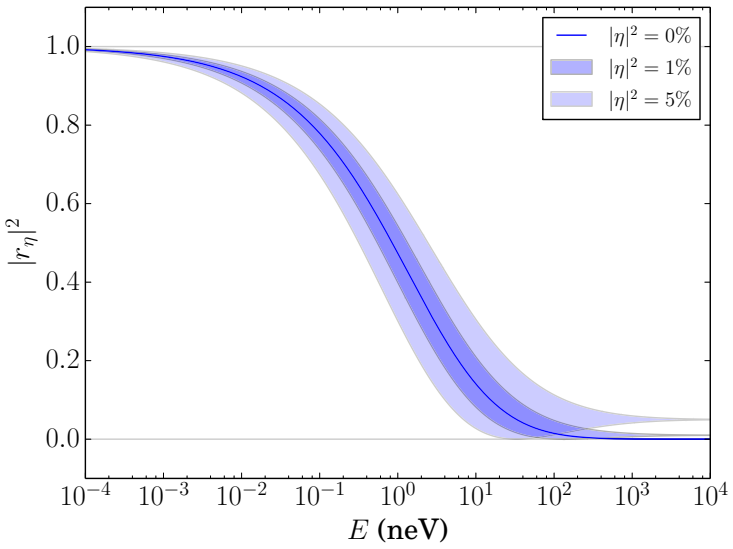

Figure II.27: Bounds on the reflection probability of hydrogen on a perfect mirror if the probability of reflection on the surface is fixed to $|\eta|^2 = 0, 1$ or 5%.

dimers or trimers [106] and rough surfaces [97] have been used to that purpose. Antimatter atoms are ideal candidates for such "clean" measurements since they are annihilated upon contact with the surface.

Conclusion

The scattering approach to Casimir forces has allowed us to take into account the dielectric properties of the mirror in our calculation of the Casimir-Polder potential between an (anti)hydrogen atom and a wide variety of surfaces. We have observed that quantum reflection on these potentials also depends on the optical response of the mirror. In particular, the reflection probability increases for mirrors that couple weakly to the electromagnetic field. For this reason, graphene sheets and nanoporous materials are interesting for applications where a large reflection probability is needed.

By performing a Liouville transformation to the WKB coordinate we have been able to to reinterpret quantum reflection on the Casimir-Polder potential well as reflection on a potential barrier. Although both situations are antinomic from a semiclassical point of view, they lead to the same quantum scattering amplitudes. In addition to providing a convenient way of solving the Schrödinger equation, the Liouville transformation method has allowed us to show that the quantum reflection probability depends essentially only on the product κb, where $\kappa = \hbar^{-1}\sqrt{2mE}$ depends on energy while b is a characteristic length scale associated with the potential.

Finally, we have shown that including reflection from the surface leads to resonance effects in the "cavity" formed by the surface on one side and the badlands on the other. This can result in a significant increase or decrease of the reflection probability compared with the case where the surface is absorbing.

Chapter III

Quantum free fall

Until now, we have analyzed scattering on the surface while disregarding the free fall which precedes. In this chapter, we shift our focus from the surface to the particle falling freely in a uniform gravitational field. We first solve the time-dependent Schrödinger equation in a linear potential by showing that it is equivalent to the free equation in an accelerated frame. We then present a phase space approach to the problem which demonstrates that quantum free fall can be described in terms of classical trajectories. Based on these results, we discuss the effect of classical and quantum uncertainties in the initial state of a dropped atom on the arrival time of the wavepacket at a given plane. We will end this chapter with a description of stationary states in the gravitational field. These states will be particularly relevant when we reintroduce the surface in the next chapter.

III.1 Free fall of a matter wave

III.1.a Schrödinger equation in an accelerated frame

The solution of the Schrödinger equation in a uniform gravitational field can be obtained from the solution of the free equation after transformation to a uniformly accelerated frame [37, 38]. In this sense, non-relativistic quantum mechanics is compatible with the weak equivalence principle.

To see this, we first place ourselves in an inertial reference frame with coordinate z_0. In this frame the quantum state of the particle is $|\psi_0\rangle$ and it evolves with the free Schrödinger equation

$$i\hbar\frac{\mathrm{d}}{\mathrm{d}t}|\psi_0\rangle = \hat{H}_0|\psi_0\rangle = \frac{\hat{P}^2}{2m}|\psi_0\rangle \ , \tag{III.1}$$

where the Hamiltonian $\hat{H}_0$ depends only on the momentum operator $\hat{P}$ and not on the position operator $\hat{Z}$.

We now consider a moving frame the origin of which lies in $z_0 = \zeta(t)$ at a time t. The position z and momentum p in the moving frame are thus related to the position

and momentum in the inertial frame through

$$z = z_0 - \zeta(t) \ , \qquad p = p_0 - m\zeta'(t) \ . \tag{III.2}$$

The quantum state in the moving frame $|\psi\rangle$ is related to $|\psi_0\rangle$ by a time-dependent unitary operator $\hat{O}(t)$ which remains to be specified:

$$|\psi\rangle = \hat{O}(t)\,|\psi_0\rangle \ , \qquad \hat{O}(t)^\dagger \hat{O}(t) = \hat{O}(t)\hat{O}(t)^\dagger = \hat{1} \ , \tag{III.3}$$

To lighten the notation, we hereafter leave the time dependence implicit when there is no risk of confusion.

To find $\hat{O}$, we impose that averages of the position and momentum operators transform according to (III.2):

$$\langle\psi|\,\hat{Z}\,|\psi\rangle = \langle\psi_0|\,\hat{O}^\dagger\hat{Z}\hat{O}\,|\psi_0\rangle = \langle\psi_0|\,\hat{Z}\,|\psi_0\rangle - \zeta\,\langle\psi_0|\psi_0\rangle \ , \tag{III.4}$$

$$\langle\psi|\,\hat{P}\,|\psi\rangle = \langle\psi_0|\,\hat{O}^\dagger\hat{P}\hat{O}\,|\psi_0\rangle = \langle\psi_0|\,\hat{P}\,|\psi_0\rangle - m\zeta'\,\langle\psi_0|\psi_0\rangle \ . \tag{III.5}$$

This being true for all $|\psi_0\rangle$, it follows that

$$\hat{O}^\dagger\hat{Z}\hat{O} = \hat{Z} - \zeta \ , \qquad \hat{O}^\dagger\hat{P}\hat{O} = \hat{P} - m\zeta' \ , \tag{III.6}$$

$$\hat{O}\hat{Z}\hat{O}^\dagger = \hat{Z} + \zeta \ , \qquad \hat{O}\hat{P}\hat{O}^\dagger = \hat{P} + m\zeta' \ . \tag{III.7}$$

We find a suitable unitary operator $\hat{O}$ by combining translation operators in coordinate and momentum space:

$$\hat{T} \equiv \exp\left(\frac{i}{\hbar}\zeta\hat{P}\right) \ , \qquad \hat{T}\,|z_0\rangle = |z_0 - \zeta\rangle \equiv |z\rangle \ , \tag{III.8}$$

$$\hat{S} \equiv \exp\left(\frac{-i}{\hbar}m\zeta'\hat{Z}\right) \ , \qquad \hat{S}\,|p_0\rangle = |p_0 - m\zeta'\rangle \equiv |p\rangle \ . \tag{III.9}$$

We choose for example:

$$\hat{O} \equiv \exp\left(\frac{i}{\hbar}\left(\zeta\hat{P} - m\zeta'\hat{Z} + f\right)\right) \tag{III.10}$$

where the time-dependent function $f = f(t)$ is left unspecified for the moment. The Zassenhaus formula[1] can be used to express $\hat{O}$ in terms of $\hat{S}$ and $\hat{T}$. For two operators $\hat{X}$ and $\hat{Y}$ which both commute with their commutator $[\hat{X}, \hat{Y}]$, we have:

$$\exp\left(\hat{X} + \hat{Y}\right) = \exp\left(\hat{X}\right)\exp\left(\hat{Y}\right)\exp\left(-\frac{1}{2}[\hat{X}, \hat{Y}]\right) \tag{III.11}$$

Since $[\hat{Z}, \hat{P}] = i\hbar$, changing the ordering of $\hat{S}$ and $\hat{T}$ only leads to the introduction of extra time-dependent factors:

$$\hat{O} = \hat{T}\hat{S}\exp\left(\frac{i}{\hbar}\left(f + \frac{m}{2}\zeta\zeta'\right)\right) = \hat{S}\hat{T}\exp\left(\frac{i}{\hbar}\left(f - \frac{m}{2}\zeta\zeta'\right)\right) \ . \tag{III.12}$$

[1] The Zassenhaus formula is a dual form of the well-known Baker–Campbell–Hausdorff formula (see [205]).

With these expressions, we easily show that the action of $\hat{O}$ on the coordinate and momentum bases is

$$\hat{O}\,|z_0\rangle = \exp\left(\frac{i}{\hbar}\left(-m\zeta' z_0 + f + \frac{m}{2}\zeta\zeta'\right)\right)|z_0 - \zeta\rangle \tag{III.13}$$

$$= \exp\left(\frac{i}{\hbar}\left(-m\zeta' z + f - \frac{m}{2}\zeta\zeta'\right)\right)|z\rangle \ , \tag{III.14}$$

$$\hat{O}\,|p_0\rangle = \exp\left(\frac{i}{\hbar}\left(\zeta p_0 + f - \frac{m}{2}\zeta\zeta'\right)\right)|p_0 - m\zeta'\rangle \tag{III.15}$$

$$= \exp\left(\frac{i}{\hbar}\left(\zeta p + f + \frac{m}{2}\zeta\zeta'\right)\right)|p\rangle \ , \tag{III.16}$$

so that equations (III.6) are indeed verified.

By taking the time derivative of equation (III.3) we find that the state vector in the moving frame obeys a modified Schrödinger equation:

$$i\hbar\frac{\mathrm{d}}{\mathrm{d}t}|\psi\rangle = \left(\hat{O}\hat{H}_0\hat{O}^\dagger + i\hbar\frac{\mathrm{d}\hat{O}}{\mathrm{d}t}\hat{O}^\dagger\right)|\psi\rangle \tag{III.17}$$

$$= \left(\frac{\hat{P}^2}{2m} + m\zeta''\hat{Z} - f' + \frac{m}{2}\zeta\zeta''\right)|\psi\rangle \ . \tag{III.18}$$

We can now choose the function f conveniently of the form

$$f(t) = \frac{m}{2}\int^t \zeta(\tau)\zeta''(\tau)\,\mathrm{d}\tau \ . \tag{III.19}$$

This choice suppresses the term proportional to the identity and we are left with the Schrödinger equation for a particle in a linear potential:

$$i\hbar\frac{\mathrm{d}}{\mathrm{d}t}|\psi\rangle = \left(\frac{\hat{P}^2}{2m} + m\zeta''\hat{Z}\right)|\psi\rangle \ . \tag{III.20}$$

The solution $|\psi(t)\rangle$ to this equation can be expressed in terms of the free evolution operator $\hat{U}_0(t)$ and the initial state $|\psi(0)\rangle$:

$$|\psi(t)\rangle = \hat{O}(t)\,|\psi_0(t)\rangle = \hat{O}(t)\hat{U}_0(t)\,|\psi_0(0)\rangle = \hat{O}(t)\hat{U}_0(t)\hat{O}(0)^\dagger\,|\psi(0)\rangle \ , \tag{III.21}$$

$$\hat{U}_0(t) \equiv \exp\left(\frac{-i}{\hbar}\hat{H}_0 t\right) = \exp\left(\frac{-i}{\hbar}\frac{\hat{P}^2}{2m}t\right) \ , \tag{III.22}$$

so that we can read off the evolution operator in the linear potential:

$$|\psi(t)\rangle = \hat{U}(t)\,|\psi(0)\rangle \ , \qquad \hat{U}(t) = \hat{O}(t)\hat{U}_0(t)\hat{O}(0)^\dagger \ . \tag{III.23}$$

The wavefunctions in the two frames are related through:

$$\psi(z,t) = \langle z|\psi\rangle = \langle z|\hat{O}|\psi_0\rangle = \langle z+\zeta|\psi_0\rangle\exp\left(\frac{-i}{\hbar}\left(m\zeta' z - f + \frac{m}{2}\zeta\zeta'\right)\right) \tag{III.24}$$

$$= \psi_0(z+\zeta,t)\exp\left(\frac{-i}{\hbar}\left(m\zeta' z - f + \frac{m}{2}\zeta\zeta'\right)\right) \ , \tag{III.25}$$

where ψ_0 evolves with the free Hamiltonian $\hat{H}_0$.

In momentum space the free evolution is diagonal so that we can give the wavefunction at time t directly in terms of the initial wavefunction:

$$\psi_p(p,t) = \langle p|\psi\rangle = \langle p|\hat{O}|\psi_0\rangle = \langle p + m\zeta'|\psi_0\rangle \exp\left(\frac{i}{\hbar}\left(\zeta p + f + \frac{m}{2}\zeta\zeta'\right)\right) \tag{III.26}$$

$$= \psi_{p,0}(p + m\zeta', t) \exp\left(\frac{i}{\hbar}\left(\zeta p + f + \frac{m}{2}\zeta\zeta'\right)\right) \tag{III.27}$$

$$= \psi_p(p + m\zeta', 0) \exp\left(\frac{-i}{\hbar}\frac{(p+m\zeta')^2}{2m}t\right) \exp\left(\frac{i}{\hbar}\left(\zeta p + f + \frac{m}{2}\zeta\zeta'\right)\right) . \tag{III.28}$$

III.1.b Particle in a uniform gravity field

We now consider a freely falling test particle, typically an antihydrogen atom, and denote $\overline{g}$ its gravitational acceleration. This corresponds to the choice $\zeta(t) = \overline{g}t^2/2$ in the equations of the previous section. The Schrödinger equation then reads

$$i\hbar\frac{\partial}{\partial t}\psi(z,t) = -\frac{\hbar^2}{2m}\frac{\partial^2\psi}{\partial z^2}(z,t) + m\overline{g}z\psi(z,t) . \tag{III.29}$$

The characteristic length and time scales associated with this equation are

$$z_g \equiv \left(\frac{\hbar^2}{2m^2\overline{g}}\right)^{1/3} , \qquad t_g \equiv \left(\frac{2\hbar}{m\overline{g}^2}\right)^{1/3} . \tag{III.30}$$

The associated momentum and energy scales are

$$p_g \equiv \frac{\hbar}{z_g} = (2\hbar m^2\overline{g})^{1/3} , \qquad E_g \equiv \frac{\hbar}{t_g} = \left(\frac{\hbar^2 m\overline{g}^2}{2}\right)^{1/3} . \tag{III.31}$$

We will use these quantities as our units in plots. If m is the mass of hydrogen and $\overline{g} = g$, their numerical values in the S.I. system are[2]:

$$z_g \approx 5.87 \times 10^{-6} \text{ m} , \qquad t_g \approx 1.09 \times 10^{-3} \text{ s} , \tag{III.32}$$

$$p_g \approx 1.80 \times 10^{-29} \text{ kg.m.s}^{-1} , \qquad E_g \approx 9.64 \times 10^{-32} \text{ J} . \tag{III.33}$$

With our choice of $\zeta(t)$, the function $f(t)$ is given by (see equation (III.19))

$$f(t) = \frac{m\overline{g}^2t^3}{12} . \tag{III.34}$$

We can write the wavefunction in coordinate space in terms of the solution $\psi_0(z,t)$ of the free equation:

$$\psi(z,t) = \psi_0\left(z + \frac{\overline{g}t^2}{2}, t\right) \exp\left(\frac{-i}{\hbar}\left(m\overline{g}tz + \frac{m\overline{g}^2t^3}{6}\right)\right) . \tag{III.35}$$

[2]Energies are more conveniently expressed in nanoelectronvolts: $E_g \approx 6.02 \times 10^{-4}$ neV.

In momentum space the wavefunction can be written directly in terms of the initial wavefunction:

$$\psi_p(p,t) = \psi_p(p + m\overline{g}t, 0) \exp\left(\frac{-i}{\hbar}\left(\frac{p^2 t}{2m} + \frac{\overline{g}t^2 p}{2} + \frac{m\overline{g}^2 t^3}{6}\right)\right) . \tag{III.36}$$

The evolution operator is

$$\hat{U}(t) = \hat{T}\hat{S}\hat{U}_0 \exp\left(\frac{i}{\hbar}\frac{m\overline{g}^2 t^3}{3}\right) = \hat{S}\hat{T}\hat{U}_0 \exp\left(\frac{-i}{\hbar}\frac{m\overline{g}^2 t^3}{6}\right) , \tag{III.37}$$

$$\hat{S} = \exp\left(-\frac{i}{\hbar} m\overline{g}t\hat{Z}\right) , \qquad \hat{T} = \exp\left(\frac{i}{\hbar}\frac{\overline{g}t^2}{2}\hat{P}\right) . \tag{III.38}$$

Evaluating it between an initial and a final momentum state gives the propagator in momentum space:

$$\begin{aligned} K_p(p_f, p_i, t) &\equiv \langle p_f|\hat{U}(t)|p_i\rangle \\ &= \exp\left(\frac{-i}{\hbar}\left(\frac{p_f^2 t}{2m} + \frac{\overline{g}t^2 p_f}{2} + \frac{m\overline{g}^2 t^3}{6}\right)\right)\delta(p_f + m\overline{g}t - p_i) . \end{aligned} \tag{III.39}$$

In coordinate space the propagator is expressed in terms of the free propagator:

$$\begin{aligned} K(z_f, z_i, t) &\equiv \langle z_f|\hat{U}(t)|z_i\rangle \\ &= K_0\left(z_f + \frac{\overline{g}t^2}{2}, z_i, t\right)\exp\left(\frac{-i}{\hbar}\left(m\overline{g}t z_f + \frac{m\overline{g}^2 t^3}{6}\right)\right) , \end{aligned} \tag{III.40}$$

with

$$K_0(z_f, z_i, t) \equiv \langle z_f|\hat{U}_0(t)|z_i\rangle = \int \frac{\mathrm{d}p}{2\pi}\langle z_f|p\rangle \exp\left(\frac{-i}{\hbar}\frac{p^2}{2m}t\right)\langle p|z_i\rangle \tag{III.41}$$

$$= \sqrt{\frac{m}{2i\pi\hbar t}}\exp\left(\frac{i}{\hbar}\frac{m(z_f - z_i)^2}{2t}\right) , \tag{III.42}$$

therefore,

$$K(z_f, z_i, t) = \sqrt{\frac{m}{2i\pi\hbar t}}\exp\left(\frac{i}{\hbar}\left(\frac{m(z_f - z_i)^2}{2t} - \frac{m\overline{g}(z_f + z_i)t}{2} - \frac{m\overline{g}^2 t^3}{24}\right)\right) . \tag{III.43}$$

$$\tag{III.44}$$

We recognize that

$$K(z_f, z_i, t) = \sqrt{\frac{m}{2i\pi\hbar t}}\exp\left(\frac{i}{\hbar}S_{\mathrm{cl}}(z_f, z_i, t)\right) , \tag{III.45}$$

with $S_{\rm cl}(z_f, z_i, t)$ Hamilton's principal function associated with the classical trajectory joining points z_i and z_f in time t:

$$S_{\rm cl}(z_f, z_i, t) = \int_0^t \left(\frac{m}{2} \left(\frac{{\rm d}z_{\rm cl}}{{\rm d}\tau}(\tau) \right)^2 - m\overline{g} z_{\rm cl}(\tau) \right) {\rm d}\tau \ , \tag{III.46}$$

where

$$z_{cl}(\tau) = z_i + v_i \tau - \frac{\overline{g}\tau^2}{2} \ , \qquad\qquad v_i = \frac{z_f - z_i}{t} + \frac{\overline{g}t}{2} \ . \tag{III.47}$$

The fact that the phase of the quantum propagator is proportional to the action associated with the classical trajectory is a well known property of systems with Hamiltonians that are at most quadratic in position and momentum [206].

III.1.c Wigner function

We have just seen that the propagator (III.45) in a uniform field can be written in terms of the classical action. Quantum states thus propagate classically in a linear potential. However, the state itself can be highly non-classical. This is best seen in the phase space formulation of quantum mechanics introduced by Wigner [207], as discussed in particular in [41].

The Wigner phase space quasi-distribution or *Wigner function* is a mixed position-momentum representation of the density matrix $\hat{\rho}$. It is equivalent to the density matrix, meaning that it can describe both quantum superpositions and statistical ensembles [208]. Its proximity to the classical phase space distribution makes the Wigner function an ideal tool to study the classical limit [209], but we stress that it is a fully quantum object.

The Wigner function is a real function of the pair of conjugate variables z and p defined by

$$W(z,p,t) \equiv \frac{1}{2\pi\hbar} \int {\rm d}\zeta \, \langle z + \zeta/2 | \hat{\rho}(t) | z - \zeta/2 \rangle \, e^{-ip\zeta/\hbar} \ , \tag{III.48}$$

which is easily shown to be equivalent to the dual definition

$$W(z,p,t) \equiv \frac{1}{2\pi\hbar} \int \frac{{\rm d}\varpi}{2\pi\hbar} \, \langle p + \varpi/2 | \hat{\rho}(t) | p - \varpi/2 \rangle \, e^{i\varpi z/\hbar} \ . \tag{III.49}$$

For a pure state $\hat{\rho} = |\psi\rangle \langle\psi|$, we get

$$W(z,p,t) = \frac{1}{2\pi\hbar} \int {\rm d}\zeta \ \psi(z + \zeta/2, t) \psi^*(z - \zeta/2, t) e^{-ip\zeta/\hbar} \tag{III.50}$$

$$= \frac{1}{2\pi\hbar} \int \frac{{\rm d}\varpi}{2\pi\hbar} \psi(p + \varpi/2, t) \psi^*(p - \varpi/2, t) e^{i\varpi z/\hbar} \ . \tag{III.51}$$

Unlike the classical phase space distribution function, the Wigner function is not a proper probability density, in particular it can take negative values [210, 211]. Nevertheless, it is known as a quasi-probability distribution since it can be used to write averages of observables on phase space:

$$\langle \hat{A} \rangle \equiv \mathrm{Tr}(\hat{\rho}\hat{A}) = \int \mathrm{d}z\, \mathrm{d}p\; W(z,p,t) A_W(z,p,t) \;, \tag{III.52}$$

where $A_W(z,p,t)$ is the Weyl transform of the observable:

$$A_W(z,p,t) \equiv \int \mathrm{d}\zeta\; \langle z+\zeta/2|\hat{A}(t)|z-\zeta/2\rangle\, e^{-ip\zeta/\hbar} \;. \tag{III.53}$$

In particular the marginals of the Wigner function give the probability densities in position and momentum space:

$$\int W(z,p,t)\; \mathrm{d}z = \frac{1}{2\pi\hbar} \langle p|\hat{\rho}|p\rangle \;, \qquad \int W(z,p,t)\; \mathrm{d}p = \langle z|\hat{\rho}|z\rangle \;, \tag{III.54}$$

and the current can be expressed as

$$j(z,t) = \int \frac{p}{m} W(z,p,t)\; \mathrm{d}p \;. \tag{III.55}$$

To obtain the evolution equation of the Wigner function, we start with the von Neumann equation for the density matrix:

$$i\hbar \frac{\mathrm{d}\hat{\rho}}{\mathrm{d}t} = [\hat{H}, \hat{\rho}] = \left(\frac{\hat{P}^2}{2m} + V(\hat{Z}) \right) \hat{\rho} - \hat{\rho} \left(\frac{\hat{P}^2}{2m} + V(\hat{Z}) \right) \;. \tag{III.56}$$

Using the momentum and position representations to treat the kinetic and potential terms respectively, one shows that the Wigner function obeys an equation known as the quantum Liouville or Wigner equation:

$$\frac{\partial W}{\partial t}(z,p,t) = -\frac{p}{m} \frac{\partial W}{\partial z}(z,p,t) + \Theta[V] W(z,p,t) \;, \tag{III.57}$$

where we used the shorthand notation

$$\Theta[V] W(z,p,t) \equiv \frac{-i}{2\pi\hbar^2} \int \mathrm{d}\zeta\, [V(z+\zeta/2) - V(z-\zeta/2)] \times \langle z+\zeta/2|\hat{\rho}|z-\zeta/2\rangle\, e^{-ip\zeta/\hbar} \;. \tag{III.58}$$

If V is infinitely differentiable, $\Theta[V]$ can be written as a pseudo-differential operator:

$$\Theta[V] = \frac{i}{\hbar} \left[V\left(z - \frac{i\hbar}{2} \frac{\partial}{\partial p} \right) - V\left(z + \frac{i\hbar}{2} \frac{\partial}{\partial p} \right) \right] \tag{III.59}$$

$$= \sum_{n=0}^{\infty} \frac{(-\hbar^2/4)^n}{(2n+1)!} \frac{\partial^{2n+1} V}{\partial z^{2n+1}}(z) \left(\frac{\partial}{\partial p} \right)^{2n+1} \;. \tag{III.60}$$

Another possible representation is

$$\Theta[V]W(z,p,t) = \int \mathrm{d}\varpi \; W(z,p+\varpi,t)J(z,\varpi) \; , \tag{III.61}$$

with

$$J(z,\varpi) = \frac{1}{2\pi\hbar^2}\int \mathrm{d}\zeta \, [V(z+\zeta/2) - V(z-\zeta/2)] \sin(\varpi\zeta/\hbar) \; , \tag{III.62}$$

provided this last integral is defined.

If the potential $V(z)$ is at most quadratic, the pseudo-differential operator reduces to its zeroth order term and the *quantum* Liouville equation reduces to the *classical* Liouville equation which describes the evolution of a classical phase space density in a potential $V(z)$:

$$\frac{\partial}{\partial t}W(z,p,t) = -\frac{p}{m}\frac{\partial W}{\partial z}(z,p,t) + \frac{\mathrm{d}V}{\mathrm{d}z}(z)\frac{\partial W}{\partial p}(z,p,t) \; . \tag{III.63}$$

In this case the exact quantum evolution can be expressed in terms of classical trajectories. Indeed, if the functions $z_{\mathrm{cl}}(t), p_{\mathrm{cl}}(t)$ obey the classical equations of motion

$$\frac{\mathrm{d}z_{\mathrm{cl}}}{\mathrm{d}t} = \frac{p_{\mathrm{cl}}}{m} \qquad \text{and} \qquad \frac{\mathrm{d}p_{\mathrm{cl}}}{\mathrm{d}t} = -\frac{\mathrm{d}V}{\mathrm{d}z}(z_{\mathrm{cl}}) \; , \tag{III.64}$$

then

$$\frac{\mathrm{d}W}{\mathrm{d}t}(z_{\mathrm{cl}}(t), p_{\mathrm{cl}}(t), t) = \frac{\partial W}{\partial t} + \frac{\mathrm{d}z_{\mathrm{cl}}}{\mathrm{d}t}\frac{\partial W}{\partial z} + \frac{\mathrm{d}p_{\mathrm{cl}}}{\mathrm{d}t}\frac{\partial W}{\partial p} = 0 \; , \tag{III.65}$$

so that

$$W(z_{\mathrm{cl}}(t), p_{\mathrm{cl}}(t), t) = W(z_{\mathrm{cl}}(t-\tau), p_{\mathrm{cl}}(t-\tau), t-\tau) \; . \tag{III.66}$$

In particular, for a linear gravitational potential $V(z) = m\overline{g}z$, the equation is

$$\frac{\partial W}{\partial t}(z,p,t) = -\frac{p}{m}\frac{\partial W}{\partial z}(z,p,t) + m\overline{g}\frac{\partial W}{\partial p}(z,p,t) \tag{III.67}$$

and

$$z_{\mathrm{cl}}(t-\tau) = z_{\mathrm{cl}}(t) - \frac{p_{\mathrm{cl}}(t)}{m}\tau - \frac{1}{2}\overline{g}\tau^2 \; , \qquad p_{\mathrm{cl}}(t-\tau) = p_{\mathrm{cl}}(t) + m\overline{g}\tau \; , \tag{III.68}$$

so that (replacing $z_c l(t), p_{\mathrm{cl}}(t)$ by z, p)

$$W(z,p,t) = W\left(z - \frac{p\tau}{m} - \frac{\overline{g}\tau^2}{2}, \; p + m\overline{g}\tau, \; t-\tau\right) \; . \tag{III.69}$$

As noticed by the authors of [41], this evolution can be seen as the composition of a translation $\hat{D}$ and a shear $\hat{S}$ in phase space:

$$W(z,p,t) = \hat{D}(\tau)\hat{S}(\tau)W(z,p,t-\tau) \; , \tag{III.70}$$

$$\hat{S}(\tau) : (z,p) \mapsto (z - p\tau/m, p) \; , \tag{III.71}$$

$$\hat{D}(\tau) : (z,p) \mapsto (z + \overline{g}\tau^2/2, p + m\overline{g}\tau) \; . \tag{III.72}$$

Moreover, this evolution is easily generalized to three dimensions ($\vec{g} \equiv -\overline{g}\vec{e}_z$):

$$W(\vec{r},\vec{p},t) = W\left(\vec{r} - \frac{\vec{p}\tau}{m} + \frac{\vec{g}\tau^2}{2},\ \vec{p} - m\vec{g}\tau,\ t-\tau\right) . \tag{III.73}$$

Instead of relating the Wigner function at two different times, one might want to connect its values at two different heights. We make the replacement $p\tau/m + \overline{g}\tau^2/2 \to \zeta$ in equation (III.69) and find two possible expressions:

$$W(z,p,t) = W\left(z-\zeta,\ \sqrt{p^2+2m^2\overline{g}\zeta},\ t + \frac{p}{m\overline{g}} - \frac{1}{m\overline{g}}\sqrt{p^2+2m^2\overline{g}\zeta}\right) \tag{III.74}$$

$$= W\left(z-\zeta,\ -\sqrt{p^2+2m^2\overline{g}\zeta},\ t + \frac{p}{m\overline{g}} + \frac{1}{m\overline{g}}\sqrt{p^2+2m^2\overline{g}\zeta}\right) , \tag{III.75}$$

along with the requirement that $p^2 + 2m^2\overline{g}\zeta \geq 0$. Indeed, one must keep in mind that a classical particle must have enough energy to reach a given plane, and if it does, then it crosses the plane twice: once going upwards and once going downwards.

The fact that the Wigner function propagates like a classical phase space distribution in a linear potential will prove useful in upcoming calculations. However, one must keep in mind that the Wigner function describes a quantum state. For instance, in contrast with a classical distribution, it is constrained by Heisenberg's uncertainty principle.

III.1.d Free falling wavefunctions

Based on the results of the previous sections, we now present two notable time-dependent solutions of the Schrödinger equation with a linear potential.

The first is a plane wave which initially has no momentum:

$$\psi_p(p,0) = \mathcal{N}\delta(p) . \tag{III.76}$$

Applying the results of section III.1.b we find

$$\psi(z,t) = \int \frac{\mathrm{d}p}{2\pi\hbar}\psi_p(z,t)e^{ipz/\hbar} = \frac{\mathcal{N}}{2\pi\hbar}\exp\left(-\frac{i}{\hbar}\left(m\overline{g}tz + \frac{m\overline{g}^2t^3}{6}\right)\right) . \tag{III.77}$$

The momentum of the plane wave thus follows the classical law $p_{\mathrm{cl}}(t) = -m\overline{g}t$ [212].

The second solution is more physical and more relevant to our purposes. It is the wavefunction of a particle dropped from a harmonic trap. The ground state wavefunction of a harmonic trap of frequency ω and centered at height H is a Gaussian:

$$\psi(z) = \left(\frac{m\omega}{\hbar\pi}\right)^{1/4}\exp\left(-\frac{m\omega}{2\hbar}(z-H)^2\right) , \tag{III.78}$$

$$\psi_p(p) = \left(\frac{4\pi\hbar}{m\omega}\right)^{1/4}\exp\left(-\frac{p^2}{2\hbar m\omega} - i\frac{pH}{\hbar}\right) . \tag{III.79}$$

Its position and momentum uncertainties are

$$\Delta z = \left(\int |\psi(z)|^2 (z-H)^2 \, \mathrm{d}z \right)^{1/2} = \sqrt{\frac{\hbar}{2m\omega}} \, , \tag{III.80}$$

$$\Delta p = \left(\int |\psi_p(p)|^2 p^2 \, \mathrm{d}p \right)^{1/2} = \sqrt{\frac{\hbar m\omega}{2}} \, , \tag{III.81}$$

and they saturate Heisenberg's uncertainty principle: $\Delta z \Delta p = \hbar/2$.

Suppose at first that there is no gravity. If the trapping potential is turned off at time $t = 0$, the wavefunction expands freely:

$$\psi_0(z,t) = \left(\frac{m\omega}{\hbar\pi(1+i\omega t)^2} \right)^{1/4} \exp\left(-\frac{m\omega}{2\hbar(1+i\omega t)} (z-H)^2 \right) \, . \tag{III.82}$$

In the presence of gravity, the evolved wavefunction is given by equation (III.35):

$$\psi(z,t) = \left(\frac{m\omega}{\hbar\pi(1+i\omega t)^2} \right)^{1/4} \exp\left(-\frac{m\omega}{2\hbar(1+i\omega t)} (z-H+\bar{g}t^2/2)^2 \right) \times \exp\left(-\frac{i}{\hbar} \left(m\bar{g}zt + \frac{m\bar{g}^2 t^3}{6} \right) \right) \, , \tag{III.83}$$

or in momentum space (see equation (III.36)):

$$\psi_p(p,t) = \left(\frac{4\hbar\pi}{m\omega} \right)^{1/4} \exp\left(-\frac{(p+m\bar{g}t)^2}{2m\hbar\omega} - \frac{i}{\hbar}(p+m\bar{g}t)H \right) \times \exp\left(-\frac{i}{\hbar} \left(\frac{p^2 t}{2m} + \frac{\bar{g}t^2 p}{2} + \frac{m\bar{g}^2 t^3}{6} \right) \right) \, . \tag{III.84}$$

Due to the presence of phase factors, these wavefunctions do not give an intuitive picture of the evolution. The Wigner function, in contrast, has the advantage of being free of cumbersome phases. It is initially equal to:

$$W(z,p,0) = \frac{1}{\pi\hbar} \exp\left(-\frac{p^2}{m\hbar\omega} - \frac{m\omega}{\hbar}(z-H)^2 \right) \tag{III.85}$$

so that after a free fall time t it becomes (see equation (III.69)):

$$W(z,p,t) = \frac{1}{\pi\hbar} \exp\left[-\frac{(p+m\bar{g}t)^2}{m\hbar\omega} - \frac{m\omega}{\hbar} \left(z - H - \frac{pt}{m} - \frac{\bar{g}t^2}{2} \right)^2 \right] \, . \tag{III.86}$$

The Wigner quasi-distribution and its marginal distributions are plotted in figure III.1 at times $t = 0$, $T_H/2$ and T_H, where $T_H \equiv \sqrt{2H/\bar{g}}$ is the free fall time of a classical particle dropped with no initial velocity. We can note that the momentum distribution is centered on the classical momentum $z_{\mathrm{cl}}(t) = -m\bar{g}t$ and that it keeps its shape. The center of the position distribution also moves along the classical trajectory $z_{\mathrm{cl}}(t) - \bar{g}t^2/2$ but the wavepacket spreads as it falls.

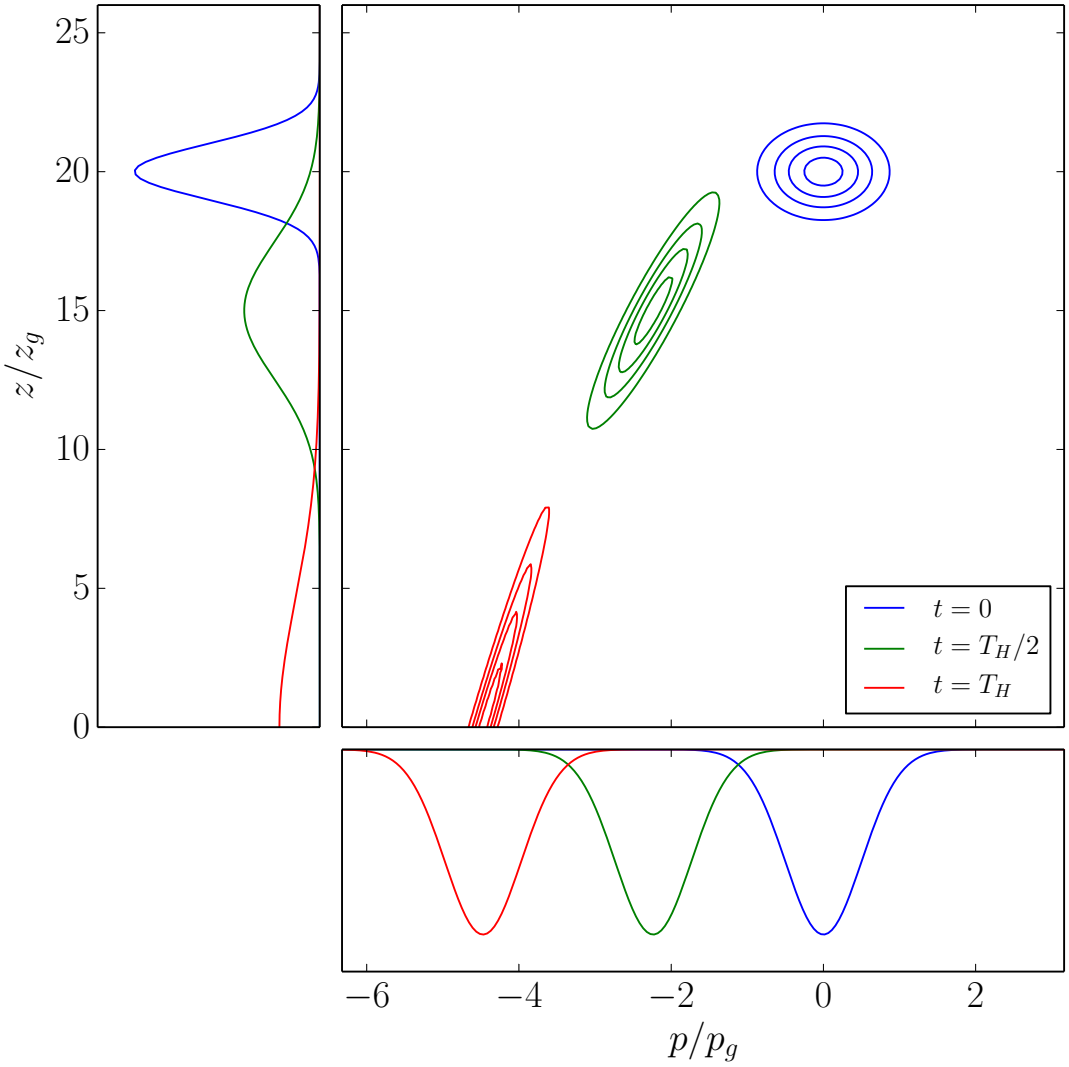

Figure III.1: Freely falling Gaussian wavepacket dropped from height $H = 20z_g$ with no average velocity, at times $t = 0$ (blue), $T_H/2$ (green) and T_H (red). Central panel: Wigner function, left panel: probability density in coordinate space, bottom panel: probability density in momentum space.

III.2 Propagation of errors for the fall of a wavepacket

Tests of the weak equivalence principle which time the free fall of a test mass are often limited by the control over the initial dropping time, position and velocity. For this reason, the most precise tests of the equivalence principle on macroscopic masses are performed using torsion pendulums [7, 213]. For microscopic test masses this is no longer possible and a precise control of the initial conditions is essential.

For a quantum particle, there are two types of uncertainties on the initial position and velocity:

- classical uncertainties on the central position and velocity of the wave packet, which might be due to vibrations of the trap in which the particle is held for example,
- quantum uncertainties corresponding to the width of the wavepacket itself in position and momentum space,

While there is no fundamental restriction on how well the central position and velocity of the wave packet are defined, the quantum uncertainties are constrained by Heisenberg's uncertainty principle:

$$\Delta z \Delta v \geq \frac{\hbar}{2m} \ . \tag{III.87}$$

In an experiment where an atom is prepared in a trap and then dropped on a detection plate, both types of uncertainties will result in a spread of the arrival time distribution. In this section we will determine this spread supposing that the particle is dropped from a height $\simeq H$ with initial velocity $\simeq 0$ and that it is detected by an ideal detector as it crosses the plane $z = 0$.

III.2.a A first, simple calculation

We have shown that the quantum phase space quasi-distribution $W(z, p, t)$ obeys classical equations of motion in a uniform gravity field. It follows that we can do all calculations based on classical trajectories, by treating classical and quantum uncertainties on the same footing.

Classically, a particle with initial position z_i and initial velocity v_i follows the trajectory:

$$z(\tau) = z_i + v_i\tau - \frac{\overline{g}\tau^2}{2} \tag{III.88}$$

Therefore a particle dropped from $z_i = H + \delta z$ with velocity $v_i = 0 + \delta v$ reaches $z = 0$ at time $T = T_H + \delta t$ with

$$T_H = \sqrt{\frac{2H}{\overline{g}}} \qquad \text{and} \qquad \delta t = \frac{\delta z + T_H \delta v}{\overline{g} T_H} \tag{III.89}$$

at first order in the small errors δz, δv.

If δz, δv are independent and normally distributed with standard deviations Δz, Δv, the variance ΔT^2 on the arrival time is given by:

$$\Delta T^2 = \left(\frac{\Delta z}{\overline{g} T_H}\right)^2 + \left(\frac{\Delta v}{\overline{g}}\right)^2 \tag{III.90}$$

and so the relative uncertainty on the arrival time is:

$$\frac{\Delta T}{T_H} = \sqrt{\left(\frac{\Delta z}{2H}\right)^2 + \left(\frac{\Delta v}{v_H}\right)^2}\ , \qquad v_H \equiv \sqrt{2\overline{g}H}\ . \tag{III.91}$$

For a quantum wavepacket, in the best possible case, Δz and Δv are of purely quantum origin and they saturate the Heisenberg inequality (III.87). The uncertainty on the arrival time (III.91) can then be expressed in terms of Δz only

$$\frac{\Delta T}{T_H} = \sqrt{\left(\frac{\Delta z}{2H}\right)^2 + \left(\frac{\hbar}{2mv_H \Delta z}\right)^2} \tag{III.92}$$

and it reaches an optimum for

$$\Delta z_{\rm opt} = \sqrt{\frac{\hbar H}{m v_H}}\ , \qquad \omega_{\rm opt} = \frac{1}{T_H} = \frac{1}{t_g}\sqrt{\frac{z_g}{H}}\ . \tag{III.93}$$

The corresponding optimum resolution for the free fall measurement is:

$$\left(\frac{\Delta T}{T_H}\right)_{\rm opt} = \sqrt{\frac{\hbar}{2mv_H H}}\ . \tag{III.94}$$

The larger the product $mv_H H$ is with respect to $\hbar/2$, the better this optimal resolution becomes.

III.2.b Quantum probability current through a surface

We now proceed to a more precise calculation of the arrival time distribution. In the absence of quantum reflection from the detector, the arrival time distribution on a detector placed in the plane $z = 0$ is given by the probability current distribution $|j(0,t)|$. It can be calculated directly from its definition (I.21) and the expression of the falling wavefunction or alternatively with the help of the Wigner function:

$$j(z,t) = \int \frac{p}{m} W(z,p,t)\ {\rm d}p\ . \tag{III.95}$$

This integral can be performed exactly in the case of the Gaussian wavepacket considered in section III.1.d. The Wigner function (III.86) at height $z = 0$ is then a Gaussian function of p:

$$W(0,p,t) = \frac{1}{\pi\hbar} \exp\left(-\frac{m\omega}{\hbar(1+\omega^2 t^2)}\left(H - \frac{\overline{g}t^2}{2}\right)^2\right) \exp\left(-\frac{(p-p_{\rm max})^2}{2\Delta^2}\right)\ , \tag{III.96}$$

with mean value

$$p_{\max}(t) = -\frac{m\omega^2 t}{1+\omega^2 t^2}\left(H + \frac{\overline{g}t^2}{2} + \frac{\overline{g}}{\omega^2}\right) \tag{III.97}$$

and variance

$$\Delta^2(t) = \frac{m\hbar\omega}{2(1+\omega^2 t^2)} \ . \tag{III.98}$$

Therefore, the probability current crossing the detection plane at height $z = 0$ is given by

$$j(0,t) = \frac{p_{\max}(t)}{m}\int W(0,p,t)\ \mathrm{d}p = \frac{p_{\max}(t)}{m}|\psi(0,t)|^2 \tag{III.99}$$

$$= -\sqrt{\frac{m\omega^5 t^2}{\hbar\pi(1+\omega^2 t^2)^3}}\left(H + \frac{\overline{g}t^2}{2} + \frac{\overline{g}}{\omega^2}\right)\exp\left[-\frac{m\omega}{\hbar(1+\omega^2 t^2)}\left(\frac{\overline{g}t^2}{2} - H\right)^2\right] \ . \tag{III.100}$$

Expanding the argument of the exponential to second order in $\delta t = t - T_H$ we recover the result (III.90) of the previous section:

$$\frac{m\omega}{\hbar(1+\omega^2 t^2)}\left(\frac{\overline{g}t^2}{2} - H\right)^2 \underset{\delta t \ll T_H}{\simeq} \frac{\delta t^2}{2\Delta T^2} \ , \tag{III.101}$$

$$\Delta T^2 = \frac{\hbar}{4m\omega\overline{g}H} + \frac{\hbar\omega}{2m\overline{g}^2} = \left(\frac{\Delta z}{\overline{g}T_H}\right)^2 + \left(\frac{\Delta p}{m\overline{g}}\right)^2 \ . \tag{III.102}$$

In figure III.2 we plot the Wigner function and arrival time distribution of various Gaussian wavepackets. For values of ω smaller than the optimal value ω_{opt} (equation (III.93)), the spread in arrival times is dominated by the initial position dispersion. On the other hand, if ω is larger than ω_{opt} the initial velocity dispersion dominates.

We can also derive an approximate expression for the current at the detection plane for a non-Gaussian wavepacket if it is initially well localized compared with the drop height. To do so, we write the current in terms of the initial Wigner function:

$$j(0,t) = \int \frac{p}{m} W\left(-\frac{pt}{m} - \frac{\overline{g}t^2}{2},\ p + m\overline{g}t, 0\right)\mathrm{d}p \ . \tag{III.103}$$

We change the integration variable to $\zeta = -pt/m - \overline{g}t^2/2$:

$$j(0,t) = -\int \frac{m}{t^2}\left(\zeta + \frac{\overline{g}t^2}{2}\right) W\left(\zeta,\ \frac{m}{t}\left(\frac{\overline{g}t^2}{2} - \zeta\right), 0\right)\mathrm{d}\zeta \ . \tag{III.104}$$

We can now use the fact that $W(z,p,0)$ is peaked around $z = H$ to obtain the approximate expression:

$$j(0,t) \simeq -\frac{m}{t^2}\left(H + \frac{gt^2}{2}\right)\int W\left(\zeta,\ \frac{m}{t}\left(\frac{\overline{g}t^2}{2} - H\right), 0\right)\mathrm{d}\zeta \tag{III.105}$$

$$\simeq -\frac{m}{t^2}\left(H + \frac{\overline{g}t^2}{2}\right)\left|\psi_p\left(\frac{m}{t}\left(\frac{\overline{g}t^2}{2} - H\right), 0\right)\right|^2 \ . \tag{III.106}$$

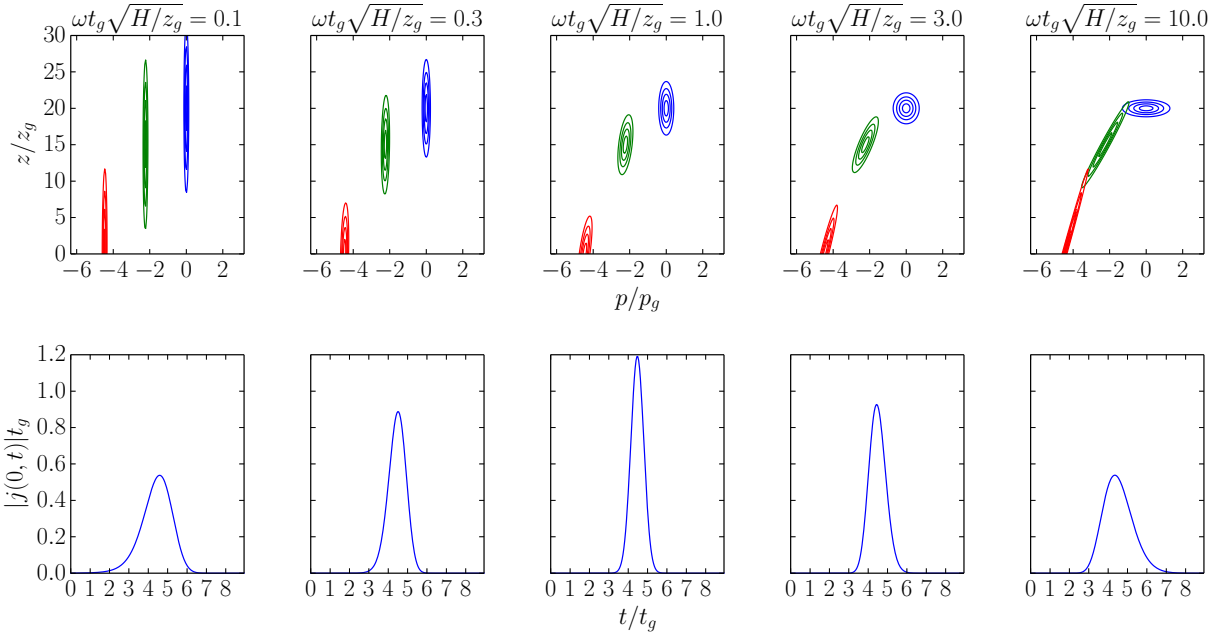

Figure III.2: Gaussian wavepackets of various initial widths dropped from $H = 20z_g$. The top row shows the Wigner function at times $t = 0$ (blue), $T_H/2$ (green) and T_H (red). the bottom row is the distribution of arrival times at the plane $z = 0$. On the left hand side, the uncertainty on the arrival time is dominated by the initial position uncertainty whereas on the right hand side it is dominated by the momentum uncertainty. The central plot shows the optimal case $\omega_{\text{opt}} = t_g^{-1}\sqrt{z_g/H}$ (see equation (III.93)).

If the packet is dropped with no initial velocity, $|\psi_p(p,0)|^2$ is peaked around $p=0$, so that the time arrival distribution is peaked around the classical arrival time T_H. We can thus write $t = T_H + \delta T$ and expand for $\delta T \ll T_H$ small:

$$j(0,t) \simeq -m\overline{g}\,|\psi_p(m\overline{g}\delta T, 0)|^2 \ . \tag{III.107}$$

The shape of the arrival time distribution is therefore given by the momentum distribution of the initial state. In particular an initial velocity dispersion Δv translates into a spread of arrival times $\Delta T = \Delta v/\overline{g}$. Again we recover the simple result of the previous section in the case where the velocity dispersion is dominant.

III.2.c Squeezed arrival time distribution

We have presented the Gaussian wavepacket satisfying (III.93) as optimal. However this result was derived assuming no initial correlations between position and momentum. Introducing such correlations allows us to focus the wavepacket on the detector and to make the arrival time distribution arbitrarily narrow.

To do so, we use our knowledge of the Wigner function's evolution to tailor the initial state so that at time $t = T_H$, the Wigner function is squeezed along the z direction [208]:

$$W(z,p,t=T_H) = \frac{1}{\pi\hbar}\exp\left(-\frac{z^2}{2\sigma^2} - \frac{2\sigma^2(p-mv_H)^2}{\hbar^2}\right) \tag{III.108}$$

with σ arbitrarily small, leading to an arbitrarily narrow arrival time distribution, $\Delta T \simeq \sigma/v_H$. The initial and final Wigner functions are related through

$$W(z,p,t=T_H) = W\left(z - \frac{pT_H}{m} - \frac{\overline{g}T_H^2}{2}, p + m\overline{g}T_H, 0\right) \tag{III.109}$$

so that the initial state is

$$W(z,p,0) = \frac{1}{\pi\hbar}\exp\left(-\frac{1}{2\sigma^2}\left(z + \frac{pT_H}{m} - H\right)^2 - \frac{2\sigma^2 p^2}{\hbar^2}\right) \tag{III.110}$$

The limitation of this calculation is that it does not tell us how to prepare such an initial state, which happens to be particularly extended both in position and momentum space, as can be observed in figure III.3.

III.3 Stationary states

III.3.a Airy wavefunctions

Although we have already exposed exact solutions of the time-dependent Schrödinger equation, it is also interesting to look at stationary solutions $\psi(z,t) = \psi_E(z)\exp(-iEt/\hbar)$ which obey the time-independent equation:

$$-\frac{\hbar^2}{2m}\frac{\mathrm{d}^2}{\mathrm{d}z^2}\psi_E(z) + m\overline{g}z\psi_E(z) = E\psi_E(z) \tag{III.111}$$

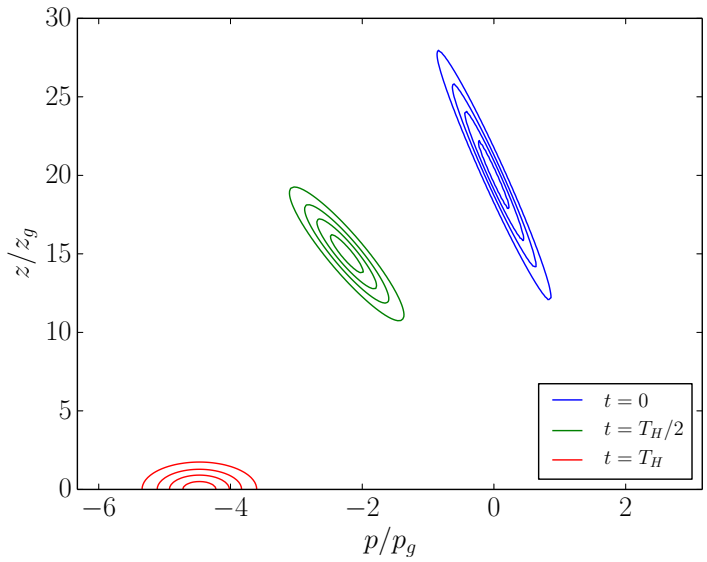

Figure III.3: Evolution of the Wigner function initially given by equation (III.110) and which is tailored to focus at the detection plane ($H = 20z_g, \sigma = z_g$).

When written in terms of the dimensionless variables,

$$x \equiv z/z_g - E/E_g \ , \qquad\qquad y(x) \equiv \psi_E(z) \ , \tag{III.112}$$

the Schrödinger equation becomes the Airy equation:

$$y''(x) - xy(x) = 0 \tag{III.113}$$

A pair of independent solutions are the Airy functions Ai and Bi, so that the general solution of the Schrödinger equation is:

$$\psi_E(z) = A\,\mathrm{Ai}\left(\frac{z}{z_g} - \frac{E}{E_g}\right) + B\,\mathrm{Bi}\left(\frac{z}{z_g} - \frac{E}{E_g}\right) \ . \tag{III.114}$$

The Airy functions are plotted in figure III.4. They exhibit oscillatory behavior on the negative real line, which corresponds to the classically allowed region:

$$\mathrm{Ai}(-x) \underset{x\to\infty}{\simeq} \frac{1}{\sqrt{\pi}x^{1/4}} \cos\left(\frac{2}{3}x^{3/2} - \frac{\pi}{4}\right) \ , \tag{III.115}$$

$$\mathrm{Bi}(-x) \underset{x\to\infty}{\simeq} \frac{-1}{\sqrt{\pi}x^{1/4}} \sin\left(\frac{2}{3}x^{3/2} - \frac{\pi}{4}\right) \ . \tag{III.116}$$

For positive x, Ai tends exponentially to zero whereas Bi diverges:

$$\mathrm{Ai}(x) \underset{x\to\infty}{\simeq} \frac{\exp\left(-\frac{2}{3}x^{3/2}\right)}{2\sqrt{\pi}x^{1/4}} \ , \qquad\qquad \mathrm{Bi}(x) \underset{x\to\infty}{\simeq} \frac{\exp\left(\frac{2}{3}x^{3/2}\right)}{\sqrt{\pi}x^{1/4}} \ . \tag{III.117}$$

More properties of the Airy functions can be found in appendix C, in the NIST Handbook of Mathematical Functions [1] and in the extensive work of Vallée and Soares [214]. Let us simply mention here that the first Airy function can be written as a Fourier integral:

$$\mathrm{Ai}(x) = \int_{-\infty}^{\infty} \frac{\mathrm{d}k}{2\pi} \exp\left(i\frac{k^3}{3} + ikx\right) \ , \tag{III.118}$$

which is easily seen to be a solution of equation (III.113).

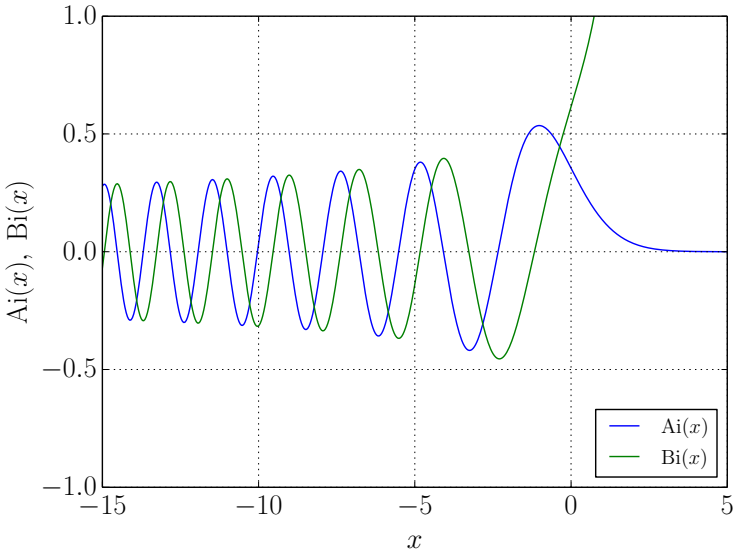

Figure III.4: The Airy functions Ai and Bi.

If the position of the particle is not bounded from below, the only boundary condition when solving the Schrödinger equation is that the wavefunction must decay above the classical turning point. Therefore, the coefficient of the Bi function must vanish and the eigenstates $|E\rangle$ have the following wavefunction:

$$\psi_E(z) = \langle z|E\rangle = \frac{1}{\sqrt{E_g z_g}} \mathrm{Ai}\left(\frac{z}{z_g} - \frac{E}{E_g}\right) \tag{III.119}$$

It is remarkable that all eigenstates have the same functional form and are related to one another by a translation along the z axis. This is of course a consequence of the invariance of the force field under translations.

III.3.b Decompositions on the stationary state basis

With the chosen normalization we have the following orthogonality properties:

$$\int_{-\infty}^{+\infty} \psi_E(z)\psi_{E'}(z)\ \mathrm{d}z = \delta(E-E')\ , \tag{III.120}$$

$$\int_{-\infty}^{+\infty} \psi_E(z)\psi_E(z')\ \mathrm{d}E = \delta(z-z')\ . \tag{III.121}$$

The first equation allows us to decompose a wavefunction on the basis of Airy functions:

$$\psi(z,t) = \int w(E)\psi_E(z)e^{-iEt/\hbar}\ \mathrm{d}E\ , \quad \text{with} \quad w(E) = \int_{-\infty}^{+\infty} \psi(z,0)\psi_E(z)\ \mathrm{d}z\ . \tag{III.122}$$

For example, the weighing function for the Gaussian wavepacket (III.78) can be obtained analytically:

$$w(E) = \frac{1}{\sqrt{E_g z_g}}\left(\frac{4\pi\hbar}{m\omega}\right)^{1/4} \mathrm{Ai}\left(\frac{H}{z_g} - \frac{E}{E_g} + \frac{\hbar^2}{4m^2\omega^2 z_g^4}\right) \times \exp\left(\frac{\hbar}{2m\omega z_g^2}\left(\frac{H}{z_g} - \frac{E}{E_g} + \frac{\hbar^2}{6m^2\omega^2 z_g^4}\right)\right)\ . \tag{III.123}$$

The second equation corresponds to the closure relation

$$\int |E\rangle\langle E|\ \mathrm{d}E = \hat{1}\ . \tag{III.124}$$

It can be used to express the propagator in terms of the eigenstates:

$$K(z_f, z_i, t) = \int_{-\infty}^{\infty} \psi_E(z_f)\psi_E(z_i)e^{-iEt/\hbar}\ \mathrm{d}E\ . \tag{III.125}$$

Using the expression of ψ_E as a Fourier integral one can show that this is indeed equal to equation (III.44).

Similarly, we can obtain the decomposition of the Wigner function on the eigenstate basis by inserting two closure relations in the definition of the Wigner function (III.48). We find that

$$W(z,p,t) = \iint \mathrm{d}E\,\mathrm{d}E'\ \langle E|\hat{\rho}(t)|E'\rangle\ W_{E,E'}(z,p) \tag{III.126}$$

$$= \iint \mathrm{d}E\,\mathrm{d}E'\ \langle E|\hat{\rho}(0)|E'\rangle\ e^{-i(E-E')t/\hbar} W_{E,E'}(z,p)\ , \tag{III.127}$$

where

$$W_{E,E'}(z,p) \equiv \frac{1}{2\pi\hbar}\int \mathrm{d}\zeta\ \psi_E(z+\zeta/2)\psi^*_{E'}(z-\zeta/2)e^{-ip\zeta/\hbar}\ . \tag{III.128}$$

Thanks to the special relation between position and energy in this problem, we have

$$W_{E,E'}(z,p) = \exp\left(\frac{-i}{\hbar}\frac{E-E'}{m\bar{g}}p\right) W_{0,0}\left(z - \frac{E+E'}{2m\bar{g}}, p\right) . \tag{III.129}$$

The integral

$$W_{0,0}(z,p) = \frac{1}{2\pi\hbar z_g E_g}\int \mathrm{d}\zeta\, \mathrm{Ai}\left(\frac{z+\zeta/2}{z_g}\right) \mathrm{Ai}\left(\frac{z-\zeta/2}{z_g}\right) e^{-ip\zeta/\hbar} \tag{III.130}$$

is given in [214]:

$$W_{0,0}(z,p) = \frac{1}{2^{1/3}\pi\hbar E_g}\,\mathrm{Ai}\left(\frac{2^{2/3}}{E_g}\left(\frac{p^2}{2m} + m\bar{g}z\right)\right) , \tag{III.131}$$

so that finally

$$W_{E,E'}(z,p) = \frac{1}{2^{1/3}\pi\hbar E_g}\exp\left(\frac{-i}{\hbar}\frac{E-E'}{m\bar{g}}p\right)\mathrm{Ai}\left(\frac{2^{2/3}}{E_g}\left(\frac{p^2}{2m} + m\bar{g}z - \frac{E+E'}{2}\right)\right) . \tag{III.132}$$

This generalizes the expression of $W_{E,E}(z,p)$ given by Kajari *et al.* in [41]. In accordance with equation (III.69) we have the relation:

$$W_{E,E'}(z,p)e^{-i(E-E')t/\hbar} = W_{E,E'}\left(z - \frac{pt}{m} - \frac{\bar{g}t^2}{2}, p + m\bar{g}t\right) . \tag{III.133}$$

III.3.c WKB approximation

It is interesting to see how the eigenstates of the linear potential compares to the WKB approximation discussed in section I.2.a. Taking the classical turning point $z_t \equiv E/m\bar{g}$ as the phase reference we have[3]

$$\phi_{\mathrm{dB}}(z) = \frac{1}{\hbar}\int_{z_t}^{z}\sqrt{2m(E - m\bar{g}\zeta)}\,\mathrm{d}\zeta \tag{III.134}$$

$$= -\frac{2}{3}\left(\sqrt{\frac{E}{E_g} - \frac{z}{z_g}}\right)^3 \tag{III.135}$$

and

$$Q(z) = \frac{\hbar^2}{2m}\frac{5m^2\bar{g}^2}{16(m\bar{g}z - E)^3} . \tag{III.136}$$

The badlands function diverges at the turning point but tends to zero on either side, so that the WKB approximation become increasingly precise as we move away from z_t.

[3] We use the principal square root to obtain well defined expressions on both sides of the turning point.

In fact the asymptotic expressions given in equations (III.116) and (III.117) are simply superpositions of WKB waves:

$$\psi^{\pm}_{\rm WKB} \underset{z<z_t}{=} \left(\frac{\hbar^2}{2m(E-m\bar{g}z)}\right)^{1/4} \exp\left(\mp i\frac{2}{3}\left(\frac{E}{E_g}-\frac{z}{z_g}\right)^{3/2}\right) , \tag{III.137}$$

$$\psi^{\pm}_{\rm WKB} \underset{z>z_t}{=} \left(\frac{\hbar^2}{2m(m\bar{g}z-E)}\right)^{1/4} \exp\left(\pm\frac{2}{3}\left(\frac{z}{z_g}-\frac{E}{E_g}\right)^{3/2}\right) . \tag{III.138}$$

Below the turning point, the stationary state $\psi_E(z)$ therefore corresponds to a balanced sum of rising and falling waves.

If we place ourselves at a distance $H \gg z_g$ below the turning point so that the WKB approximation is valid, then for small variations $\delta z \ll H$ around that point, the solutions of the Schrödinger equation in the linear potential resemble plane waves of energy $m\bar{g}H$:

$$\text{if } z = z_t - H + \delta z \ , \qquad z_t - z \gg z_g \ , \qquad \delta z \ll H \ , \tag{III.139}$$

$$\begin{aligned} &\mathrm{Ai}\left(\frac{z}{z_g}-\frac{E}{E_g}\right) \pm i\,\mathrm{Bi}\left(\frac{z}{z_g}-\frac{E}{E_g}\right) \\ &\qquad \simeq \frac{1}{\sqrt{\pi}}\left(\frac{z_g}{H}\right)^{1/4} \exp\left(\mp\frac{2i}{3}\left(\frac{H}{z_g}\right)^{3/2} \pm i\frac{\pi}{4}\right) \\ &\qquad\qquad \times \exp\left(\pm\frac{i}{\hbar}\sqrt{2m^2\bar{g}H}\delta z\right) . \end{aligned} \tag{III.140}$$

Therefore, under these conditions, we can locally expand a wavepacket as a sum over up- and downward traveling plane waves. This observation justifies the approximation made in section II.3.e, where a particle falling from a height $H \gg z_g$ was treated as a plane wave of energy $m\bar{g}H$ over the range ℓ of the Casimir-Polder potential ($\ell \ll H$).

Conclusion

One can argue that non-relativistic quantum mechanics is compatible with the weak equivalence principle in the sense that acceleration and gravity are equivalent. Although the wavefunction of a free falling particle depends explicitly on its inertial mass, this dependence is the same as that of a freely expanding wavepacket. This is consistent with the fact that the Wigner function representing the quantum state propagates along classical trajectories. Building on these results, we have described how the arrival time distribution of a falling particle at a given plane reflects the variance of its wavefunction in position and momentum space. This sets limits on the precision with which the value of $\bar{g}$ that can be determined in a free fall experiment. Finally, we have studied stationary states in the gravitational potential which will play a prominent role in the upcoming chapter.

Chapter IV
Quantum bouncers

In this last chapter, we combine the elements that we have studied separately in the previous chapters. We study quantum particles in a gravitational potential with their motion now constrained by the introduction of one or two horizontal mirrors.

A quantum bouncer is the quantum analogue of a ball bouncing on a horizontal surface. On most of its trajectory it is subject only to the gravitational field but an extra interaction causes it to reverse its direction when it reaches the surface. The quantum bouncer is thus trapped from above by gravity and from below by reflection on the mirror. The quantized states in this potential well are known as *gravitationally bound states* .

We study these bound states within a simple yet particularly instructive toy model where reflection on the surface is modeled by an infinite potential step [215]. We will also examine the case where a second reflective or absorbing surface is added above the first one.

We then turn to the case of an atom which bounces above a mirror thanks to quantum reflection from the Casimir-Polder potential. This system can be described by supposing that we can decouple gravity and the atom-surface interaction. We also develop an alternative, unified treatment, by means of a Liouville transformation to the Langer coordinate.

Finally, we apply the ideas developed in the course of the chapter to propose a way of improving the resolution of the GBAR experiment. The idea is to use the quantum bounces of antihydrogen to shape the velocity distribution of the dropped atom and thus achieve a better control on the initial conditions of the free fall [216, 217].

IV.1 Toy models

We start by considering reflection an infinite potential step. This idealized situation is convenient for calculations but it is also a good description for ultracold neutrons bouncing on a material surface. Indeed the neutrons interact via the strong interaction with the nuclei of the mirror. The effective potential obtained after averaging over the spatial extension of the neutron's wavefunction is a sharp step known as the Fermi

potential. Since the potential step is larger than the energy of the ultracold neutrons, the interaction results in a perfect reflection, which is used in ultracold neutron physics [218, 219]. We first consider only one mirror and will examine the case of a waveguide formed by two mirrors or one mirror and an absorber in the following section.

IV.1.a Infinite step

The potential corresponding to our first quantum bouncer model is

$$V(z) = \begin{cases} m\bar{g}z & \text{if } z > 0 \\ +\infty & \text{otherwise.} \end{cases} \tag{IV.1}$$

The stationary solutions of the Schrödinger equation in the presence of the infinite wall are obtained from the unconstrained solutions $\psi_E(z)$ described in section III.3 (equation (III.119)) by requiring that the wavefunction vanish at the wall [52, 215]:

$$\psi_n(z) \propto \begin{cases} \mathrm{Ai}\left(\frac{z}{z_g} - \frac{E_n}{E_g}\right) & \text{if } z > 0\ , \\ 0 & \text{otherwise.} \end{cases} \tag{IV.2}$$

Therefore, the energies E_n correspond to zeros of the Airy function:

$$E_n = a_n E_g\ , \qquad \mathrm{Ai}(-a_n) = 0\ , \qquad n \in \mathbb{N}\ . \tag{IV.3}$$

The Airy function has a countable infinity of zeros on the negative real axis (see figure III.4). The first few are given in table IV.1. From the asymptotic form of the Airy function at negative infinity (III.116), we deduce an asymptotic expression for the zeros for large n:

$$a_n \underset{n\to\infty}{\simeq} \left(\frac{3\pi}{2}\left(n - \frac{1}{4}\right)\right)^{2/3}\ . \tag{IV.4}$$

Comparing with the exact values from table IV.1, we see that this is in fact a good approximation even for small values of n.

n	1	2	3	4	5	6	7	8
a_n	2.338	4.088	5.521	6.787	7.944	9.023	10.040	11.009
$\left(\frac{3\pi}{2}\left(n-\frac{1}{4}\right)\right)^{2/3}$	2.320	4.082	5.517	6.784	7.942	9.021	10.039	11.008

Table IV.1: First zeros of the Airy functions: $\mathrm{Ai}(-a_n) = 0$, compared with the asymptotic expression (IV.4).

The wavefunctions of the gravitationally bound states are

$$\psi_n(z) \equiv \frac{\Theta(z)}{\sqrt{z_g}\,\mathrm{Ai}'(-a_n)}\,\mathrm{Ai}\left(\frac{z}{z_g} - a_n\right)\ , \tag{IV.5}$$

where $\Theta(z)$ is the Heaviside step function. The wavefunctions of the first states are plotted in figure IV.1. We have chosen the normalization such that the wavefunctions satisfy the orthogonality relation

$$\int_{-\infty}^{+\infty} \psi_m(z)\psi_n(z)\ \mathrm{d}z = \delta_{m,n}. \tag{IV.6}$$

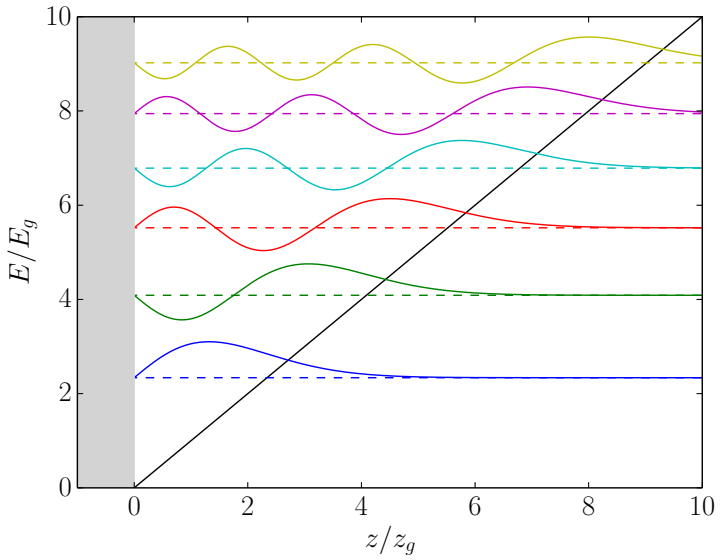

Figure IV.1: Wavefunctions of the first six gravitationally bound states.

To characterize the quantum bouncer's eigenstates, we calculate the following averages, using mathematical results from [214, 220, 221]. The n^{th} state has a mean altitude

$$\langle\psi_n|\hat{Z}|\psi_n\rangle = \frac{2a_n}{3}z_g \tag{IV.7}$$

and a dispersion

$$\Delta z_n = \sqrt{\langle\psi_n|\hat{Z}^2|\psi_n\rangle - \langle\psi_n|\hat{Z}|\psi_n\rangle^2} = \frac{2a_n}{3\sqrt{5}}z_g\ . \tag{IV.8}$$

Its average momentum is zero:

$$\langle\psi_n|\hat{P}|\psi_n\rangle = 0 \tag{IV.9}$$

and its momentum dispersion is

$$\Delta p_n = \sqrt{\langle\psi_n|\hat{P}^2|\psi_n\rangle} = \sqrt{\frac{a_n}{3}}p_g\ . \tag{IV.10}$$

Note that both Δz_n and Δp_n increase with n and that the product

$$\Delta z_n \Delta p_n = \frac{4\, a_n^{3/2}}{3\sqrt{15}} \times \frac{\hbar}{2} \tag{IV.11}$$

does not reach the minimum of Heisenberg's uncertainty principle.

Using the orthogonality relation (IV.6), we can write the decomposition of any wavefunction with support on $\mathbb{R}_+$ on the bound states:

$$\psi(z) = \sum_n C_n \psi_n(z) \qquad C_n = \int_0^\infty \frac{\psi(z)}{\sqrt{z_g}\,\mathrm{Ai}'(-a_n)}\,\mathrm{Ai}\left(\frac{z}{z_g} - a_n\right) \mathrm{d}z \tag{IV.12}$$

For example, we take a Gaussian wavefunction (III.78) centered around a height H that is much larger than its width $\Delta z = \sqrt{\hbar/2m\omega}$. Since it assumes negligible values outside $\mathbb{R}_+$, we can extend the integral (IV.12) to $\mathbb{R}$. Based on the result for the unconstrained stationary states (III.123), we find that the expansion coefficients are:

$$\begin{aligned} C_n = &\frac{1}{\sqrt{z_g}\,\mathrm{Ai}'(-a_n)}\,\mathrm{Ai}\left(\frac{H}{z_g} - a_n + \frac{\hbar^2}{4m^2\omega^2 z_g^4}\right) \\ &\times \left(\frac{4\pi\hbar}{m\omega}\right)^{1/4} \exp\left(\frac{\hbar}{2m\omega z_g^2}\left(\frac{H}{z_g} - a_n + \frac{\hbar^2}{6m^2\omega^2 z_g^4}\right)\right) . \end{aligned} \tag{IV.13}$$

Another interesting analytical result is the decomposition of a gravitationally bound state on a basis of states that are shifted downwards relative to it. For example, we consider a particle in a bound state above a surface of equation $z = H$:

$$\psi_n^H(z) = \frac{\Theta(z-H)}{\sqrt{z_g}\,\mathrm{Ai}'(-a_n)}\,\mathrm{Ai}\left(\frac{z-H}{z_g} - a_n\right) . \tag{IV.14}$$

The particle is moving horizontally towards the top of a step of height H. When it reaches the step, it is projected onto the states defined with reference to the plane $z = 0$:

$$\psi_n^H(z) == \sum_m C_{nm}(H)\psi_m^0(z) . \tag{IV.15}$$

Using (IV.6) and results on integrals of Airy functions we find the expression of the coefficients

$$C_{nm}(H) = \int_{-\infty}^{\infty} \psi_n^H(z)\psi_m^0(z)\,\mathrm{d}z = \left(\frac{H}{z_g} + a_n - a_m\right)^{-1} \frac{\mathrm{Ai}\left(\frac{H}{z_g} - a_m\right)}{\mathrm{Ai}'\left(-a_m\right)} \tag{IV.16}$$

The time evolution of the probability density $|\psi(z,t)|^2$ of a state that has fallen off the edge of a step is shown in figure IV.2. Before the time $t = 0$, the particle is in the 2^{nd} gravitationally bound state on top of the step. For $t > 0$, the probability density roughly follows the trajectory of a classical bouncing ball but exhibits complex interference patterns.

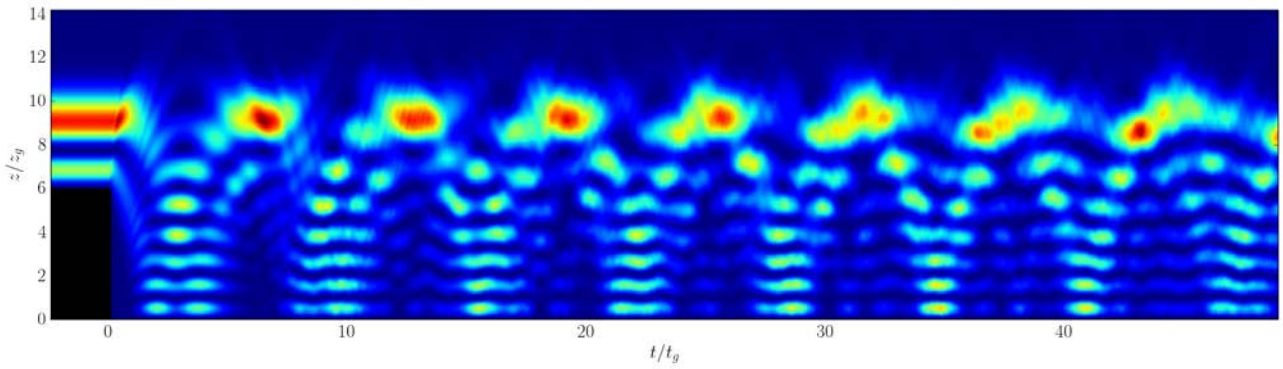

Figure IV.2: Probability density $|\psi(z,t)|^2$ of the state obtained by dropping the second gravitationally bound state from a step of height $H = 6z_g$

If a bound state falls from an infinitely high step, it should be projected on the set of unconstrained stationary states $\psi_E(z)$ given by equation (III.119):

$$\text{if} \quad \psi(z,0) = \psi_n(z) \ , \tag{IV.17}$$

$$\text{then} \quad \psi(z,t) = \int C_n(E)\psi_E(z)e^{-iEt/\hbar}\,\mathrm{d}E \quad \text{for} \quad t > 0 \ , \tag{IV.18}$$

$$\text{with} \quad C_n(E) = \int_{-\infty}^{\infty} \psi_n(z)\psi_E(z)\,\mathrm{d}z = \frac{\sqrt{E_g}}{E - E_n}\,\mathrm{Ai}\left(-\frac{E}{E_g}\right) \ . \tag{IV.19}$$

If an ideal detector is placed at a height $H \gg a_n z_g$ below the top of the step, the width of the time of arrival distribution of such a wavepacket is given by formulas (III.107) and (IV.10):

$$\Delta T_n = \frac{\Delta p_n}{m\bar{g}} = \sqrt{\frac{a_n}{3}}t_g \ . \tag{IV.20}$$

IV.1.b Waveguide

In the previous section, the quantum bouncer was trapped from below by an impenetrable barrier and from above by the gravitational field only. There are interesting situations where the motion is constrained from the top by a second surface. In this section we will consider both impenetrable and absorbing top surfaces.

We first consider a particle whose motion is constrained by two impenetrable barriers at heights 0 and h. For $0 < z < h$, solutions of the Schrödinger equation are of the form

$$\psi_n(z) = A_n\,\mathrm{Ai}\left(\frac{z}{z_g} - \frac{E_n}{E_g}\right) + B_n\,\mathrm{Bi}\left(\frac{z}{z_g} - \frac{E_n}{E_g}\right) \ , \tag{IV.21}$$

with the requirement that $\psi_n(0) = \psi_n(h) = 0$. These conditions form a system of two linear equations for A_n and B_n, which has a non-trivial solution if the following

determinant cancels:

$$\mathrm{Ai}\left(-\frac{E_n}{E_g}\right)\mathrm{Bi}\left(\frac{h}{z_g}-\frac{E_n}{E_g}\right)-\mathrm{Ai}\left(\frac{h}{z_g}-\frac{E_n}{E_g}\right)\mathrm{Bi}\left(-\frac{E_n}{E_g}\right)=0\ . \tag{IV.22}$$

This condition selects the eigenenergies E_n. For $0<z<h$ the wavefunction is given by

$$\psi_n(z)=\mathcal{N}\left[\mathrm{Bi}\left(-\frac{E_n}{E_g}\right)\mathrm{Ai}\left(\frac{z}{z_g}-\frac{E_n}{E_g}\right)-\mathrm{Ai}\left(-\frac{E_n}{E_g}\right)\mathrm{Bi}\left(\frac{z}{z_g}-\frac{E_n}{E_g}\right)\right] \tag{IV.23}$$

and it vanishes elsewhere. The normalization condition $\int_0^h|\psi_n(z)|\,\mathrm{d}z=1$ yields[1]

$$\mathcal{N}=\frac{\pi}{\sqrt{z_g}}\left(1-\frac{\mathrm{Bi}\left(-\frac{E_n}{E_g}\right)^2}{\mathrm{Bi}\left(\frac{h}{z_g}-\frac{E_n}{E_g}\right)^2}\right)^{-1/2} \tag{IV.24}$$

We plot the corresponding wavefunctions in figure IV.3. While the low lying states resemble that of the unconstrained quantum bouncer (see figure IV.1), the higher energy states resemble infinite square well states.

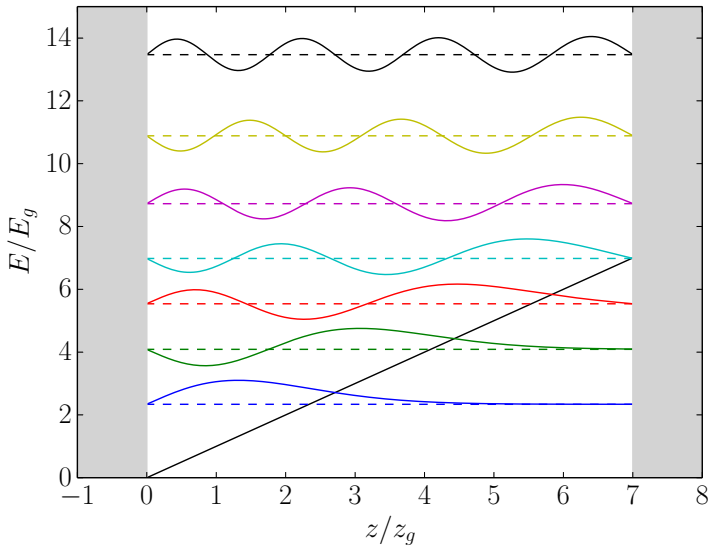

Figure IV.3: Wavefunctions of the first seven states in an impenetrable waveguide of height $h=7z_g$.

Another possibility is to replace the top mirror by an absorber which suppresses particles that come into contact with it. Such a device can be used to prepare particles

[1] We again use results from [214] and the Wronskian $\mathcal{W}(\mathrm{Ai},\mathrm{Bi})=\pi^{-1}$

in the first gravitationally bound states by suppressing higher energy states which overlap with the absorber. This is precisely what was done by Nesvizhevsky and collaborators to observe the gravitationally bound states of neutrons [53–55]. As the distance between mirror and absorber was increased, transmission through the device was seen to increase by steps, corresponding to one more gravitationally bound state fitting inside the device.

Transmission through such a waveguide can be modeled phenomenologically by supposing that the particles are in the unperturbed gravitationally bound states (IV.5) but that they decay at a rate Γ_n which increases with the overlap of wavefunction $\psi_n(z)$ with the top wall. If the horizontal motion of the particles is classical, with a velocity V, then after traveling a distance L the state ψ_n is suppressed by a factor $\exp(-\Gamma_n L/V)$, and this suppression is larger for larger values of n [222, 223].

IV.2 Atom bouncing above a real surface

So far we have supposed ideal reflection of the quantum bouncer on the mirror. This is a good enough model for neutrons, which are reflected off a high and steep potential step. In the case of atoms, quantum reflection on the Casimir-Polder potential is the mechanism responsible for the bounces. The atoms no longer reflect off a sharp step and they have a finite probability of being transmitted across the badlands. If we suppose that the particle is lost upon hitting the surface, then the bouncer is not in a stationary state anymore, but in a slowly decaying *quasi-stationary state*.

To see this, we study the Schrödinger equation in the presence of both gravity and the Casimir-Polder potential $V(z)$:

$$-\frac{\hbar^2}{2m}\frac{\mathrm{d}^2\psi}{\mathrm{d}z^2}(z) + \left(m\bar{g}z + V(z)\right)\psi(z) = E\psi(z)\ . \tag{IV.25}$$

IV.2.a Quasi-stationary states

In a first approach to the problem, we take advantage of the difference between the length and energy scales characterizing the gravitational and Casimir-Polder interactions. Indeed, for an (anti)hydrogen atom dropped from $H \sim 10$ cm, the free fall height is much larger than the quantum length scale $z_g \approx 5.8$ μm, which is itself much larger than the range of the Casimir-Polder interaction $\ell \sim 30$ nm.

Following the method initially proposed by Voronin *et al.* [124–126], we will consider solutions of the Schrödinger equation in the Casimir-Polder potential alone on the one hand and in the gravitational field alone on the other hand and then match them.

In the absence of gravity, we have seen in chapter II (equation (II.64)) that the solutions of the Schrödinger equation far from the surface are of the form

$$\psi(z) \simeq \frac{\mathcal{N}}{\sqrt{\kappa}}\left(e^{-i\kappa z} + re^{i\kappa z}\right) \tag{IV.26}$$

If $|r| < 1$, they correspond to a non-zero current flowing towards the surface, which is fed by a source at infinity.

In the region dominated by gravity, the wavefunction is a linear combination of Airy functions (see section III.3):

$$\psi(z) \simeq A_E \operatorname{Ai}\left(\frac{z}{z_g} - \frac{E}{E_g}\right) + B_E \operatorname{Bi}\left(\frac{z}{z_g} - \frac{E}{E_g}\right) \tag{IV.27}$$

and the requirement that the wavefunction vanish as $z \to \infty$, so that $B_E = 0$, precludes the existence of a non zero current if E is real.

Given that solutions of the time-independent Schrödinger equation have a uniform current, it is clear that we cannot match (IV.26) and (IV.27) as such. This is not surprising: if the wavefunction is absorbed by the surface but no amplitude arrives from infinity to compensate this loss, the system cannot be in a stationary state.

A way around this problem is to allow the energy to be complex, denoting it $E^\star = \epsilon - i\hbar\gamma/2$. The corresponding solutions of the time-dependent equation are no longer stationary but decay slowly at a rate γ:

$$\psi(z,t) = \psi_{E^\star}(z)\exp(-iE^\star t) = \psi_{E^\star}(z)\exp(-i\epsilon t/\hbar)\exp(-\gamma t/2)\ , \tag{IV.28}$$

$$|\psi(z,t)|^2 \propto \exp(-\gamma t)\ . \tag{IV.29}$$

They are known as quasi-stationary states [129].

The Airy functions can be analytically continued to the complex plane (see appendix C) and the requirement that the wavefunction vanish at infinity still entails $B_{E^\star} = 0$. However, the analytical continuation of (IV.26) to complex E is not straightforward in general. At low enough energies though, we can use the scattering length approximation (see section I.4) in which the reflection coefficient has a simple energy dependence:

$$r \simeq -\exp\left(-2ia\hbar^{-1}\sqrt{2mE^\star}\right)\ . \tag{IV.30}$$

We choose a matching point z_m satisfying

$$\ell \ll z_m \ll 1/\kappa \qquad \text{and} \qquad z_m \ll z_g\ , \tag{IV.31}$$

$$\text{or, put otherwise,} \tag{IV.32}$$

$$\ell \ll z_m \ll z_g \qquad \text{and} \qquad E \ll \frac{\hbar^2}{2mz_m^2}\ . \tag{IV.33}$$

Around z_m the wavefunctions (IV.26) and (IV.27) can both be linearized:

$$\psi(z) \underset{z\simeq z_m}{\simeq} C\left(1 - \frac{z}{a}\right) \tag{IV.34}$$

$$\psi(z) \underset{z\simeq z_m}{\simeq} A_{E^\star} \operatorname{Ai}\left(-\frac{E^\star}{E_g}\right) + A_{E^\star}\frac{z}{z_g}\operatorname{Ai}'\left(-\frac{E^\star}{E_g}\right) \tag{IV.35}$$

Equating the two, we find that

$$\operatorname{Ai}\left(-\frac{E^\star}{E_g}\right) + \frac{a}{z_g}\operatorname{Ai}'\left(-\frac{E^\star}{E_g}\right) = 0 \underset{|a|\ll z_g}{\simeq} \operatorname{Ai}\left(\frac{a}{z_g} - \frac{E^\star}{E_g}\right)\ . \tag{IV.36}$$

This last equation determines the energy in terms of the zeros of the Airy function:

$$E_n^\star = a_n E_g + m\bar{g}a \ . \tag{IV.37}$$

In the region dominated by gravity, the corresponding wavefunctions are

$$\psi_n(z) \propto \mathrm{Ai}\left(\frac{z-a}{z_g} - a_n\right) \ . \tag{IV.38}$$

The effect of the Casimir-Polder potential is therefore to displace all the energies of the ideal quantum bouncer by the same amount $m\bar{g}a$. While the real part of the scattering length contributes a (small) energy shift $m\bar{g}\,\mathrm{Re}(a)$, its imaginary part $\mathrm{Im}(a) = -b$ is associated with a decay rate $\gamma = 2\hbar^{-1}m\bar{g}b$, or a lifetime $\tau \equiv 1/\gamma = \hbar/2m\bar{g}b$.

Remarkably, the transition frequencies between gravitationally bound states

$$\omega_{mn} \equiv \frac{1}{\hbar}\left(E_n^\star - E_m^\star\right) = \frac{E_g}{\hbar}\left(a_n - a_m\right) \tag{IV.39}$$

are independent of the scattering length a and are the same as in the ideal model of section IV.1.a. Therefore, spectroscopy experiments which induce transitions between these states give direct access to the value of E_g and are not affected by the details of the interaction with the surface [124–126]. This is true as long as the scattering length approximation is valid, *i.e.* for

$$\hbar^{-1}\sqrt{2ma_nE_g}\ell \ll 1 \ , \qquad \text{that is} \qquad n \ll \frac{2}{3\pi}\left(\frac{\hbar^2}{2m\ell^2E_g}\right)^{3/2} \sim 10^6 \ . \tag{IV.40}$$

Finally, we note that the lifetime of the quasi-stationary states can be calculated classically. The duration of a bounce of height H is $2\sqrt{2H/\bar{g}}$. The probability of transmission through the badlands at each bounce is $1 - R \simeq 4\kappa b$, with $\kappa = \sqrt{2mE} = m\sqrt{2\bar{g}H}$. Therefore the decay rate is

$$\gamma = \frac{\text{transmission probability for each bounce}}{\text{duration of a bounce}} = \frac{2m\bar{g}b}{\hbar} \tag{IV.41}$$

The fact that all states have same lifetime can be interpreted classically by the compensation of the lower reflection probability at higher energies by less frequent bounces.

IV.2.b Resonances in Langer coordinate

We now tackle the problem in a more systematic and unified way which does not rely on the scattering length approximation or on a matching procedure. In the spirit of section II.3, we reinterpret quantum reflection of gravitationally bound atoms as reflection on a potential barrier. Since the Schrödinger equation (IV.25) has a single turning point z_t such that $m\bar{g}z_t + V(z_t) = E$, we use a Liouville transformation to the Langer coordinate (see section I.3.e).

In the definition (I.131) of the Langer coordinate $\boldsymbol{z}$, we choose $\alpha = -1$ and $\boldsymbol{z}_t = 0$ to obtain simple dimensionless equations:

$$\boldsymbol{z}'(z) \equiv \sqrt{\frac{-F(z)}{\boldsymbol{z}}} \ , \qquad \text{for} \qquad z \neq z_t \ , \tag{IV.42}$$

$$\boldsymbol{z}'(z_t) \equiv -F'(z_t)^{1/3} \ , \qquad \boldsymbol{z}(z_t) = 0 \ , \tag{IV.43}$$

$$\boldsymbol{F}(\boldsymbol{z}) = -\boldsymbol{z} + \frac{1}{2}\{z, \boldsymbol{z}\} = -\boldsymbol{z} - \frac{5}{16\boldsymbol{z}^2} + \boldsymbol{z}Q(z) \ . \tag{IV.44}$$

The new coordinate $\boldsymbol{z}$ spans the whole real axis. The function $\boldsymbol{V}(\boldsymbol{z}) = -\boldsymbol{F}(\boldsymbol{z})$ can be seen as a potential in the transformed equation, the new energy being equal to zero: $\boldsymbol{E} = 0$. In figure IV.4 we plot this potential for an (anti)hydrogen atom above a silica mirror with energy $E = 1,\ 5$ and $10\ E_g$. It differs from a linear potential only in a localized region around $\boldsymbol{z} \simeq -E/E_g$, where it exhibits a large peak, analogous to the badlands peak responsible for quantum reflection in the absence of gravity.

The physical picture is clear: the peak forms a barrier which holds the wavefunction against gravity for some time before it escapes by tunneling. We can therefore expect a resonant behavior, with resonances when the original energy E is such that the well formed by gravity on the one side and the quantum reflection barrier on the other holds a bound state with energy $\boldsymbol{E} = 0$. These resonances are of course associated with the quasi-stationary states displayed in the previous section and their signature can be seen in the scattering amplitudes associated with the peak, as we will now show.

On both sides of the peak, the wavefunction can be written as a superposition of Airy functions, and we choose the combinations corresponding to upward and downward waves as our basis (see equation (III.140)):

$$\boldsymbol{\psi}(\boldsymbol{z}) \simeq a_+ \, \mathrm{Ci}^+(\boldsymbol{z}) + a_- \, \mathrm{Ci}^-(\boldsymbol{z}) \ , \tag{IV.45}$$

$$\mathrm{Ci}^\pm \equiv \mathrm{Ai}(\boldsymbol{z}) \pm i \, \mathrm{Bi}(\boldsymbol{z}) \ . \tag{IV.46}$$

We then define the scattering matrix in the usual way (see section I.2.d):

$$\begin{pmatrix} a_+^{\mathrm{out}} \\ a_-^{\mathrm{out}} \end{pmatrix} \equiv \mathcal{S} \begin{pmatrix} a_+^{\mathrm{in}} \\ a_-^{\mathrm{in}} \end{pmatrix} \ , \qquad \mathcal{S} \equiv \begin{pmatrix} \bar{t} & r \\ \bar{r} & t \end{pmatrix} \ . \tag{IV.47}$$

where a_+^{in} and a_-^{out} are associated with the left side of the peak and a_-^{in} and a_+^{out} are associated with its right side (see figure I.5).

Our objective is to compute these scattering amplitudes. In practice, this is done by the following numerical procedure:

- use a fifth order polynomial spline to create an interpolating function $V(z)$ from the values of the potential computed beforehand using equation (II.32),
- find the turning point z_t such that $V(z_t) + m\bar{g}z_t = E$,

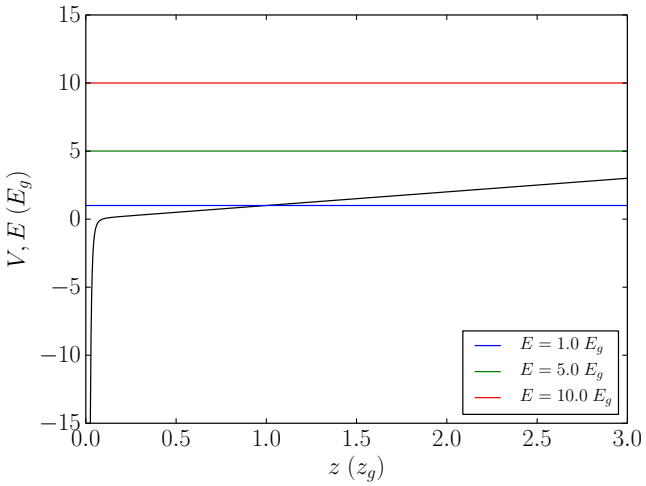

(a) The original scattering problems: (anti)hydrogen atom with energy $E = 1,\ 5$ or $10\ E_g$ in the gravity field above a silica bulk.

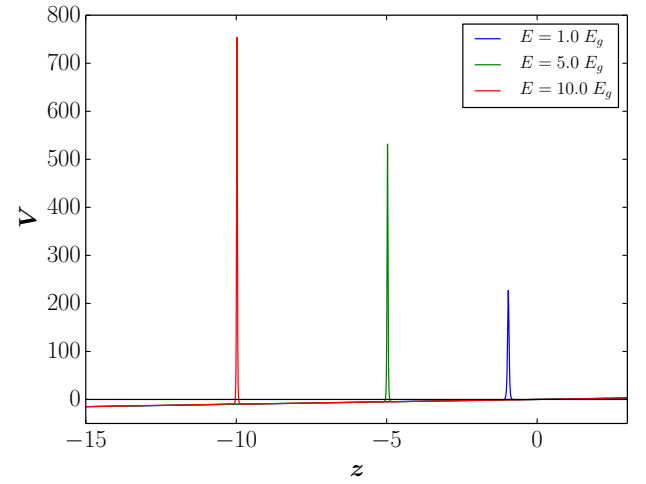

(b) The transformed problems: energy $\boldsymbol{E} = 0$ and potential $\boldsymbol{V}$ versus the Langer coordinate $\boldsymbol{z}$. The new energy is equal to zero in all three cases but the three original energies $E = 1,\ 5$ and $10\ E_g$ each give a different potential.

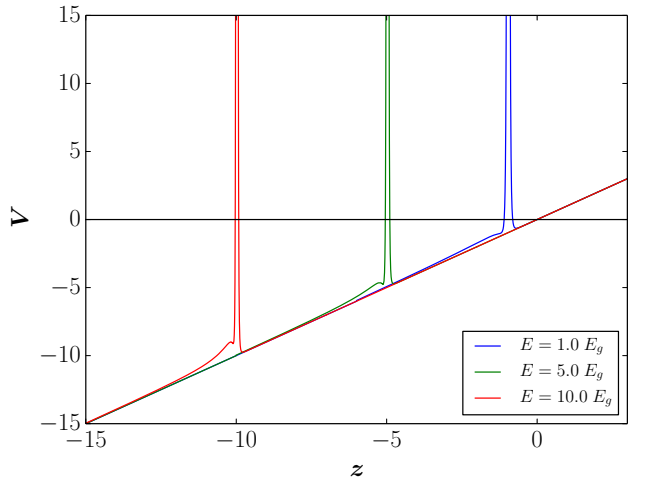

(c) Same as above, zoomed in.

Figure IV.4: Liouville transformation to the Langer coordinate applied to the Schrödinger equations describing an (anti)hydrogen atom impinging on a silica bulk with energies $E = 1,\ 5$ and $10\ E_g$ (blue, green and red lines respectively).

- integrate

$$z'(\boldsymbol{z}) = \sqrt{\frac{-\boldsymbol{z}}{F(z(\boldsymbol{z}))}} \ , \qquad \text{for} \qquad \boldsymbol{z} \neq 0 \ , \tag{IV.48}$$

$$z'(0) = -F'(z_t)^{-1/3} \ , \qquad z(0) = z_t \ , \tag{IV.49}$$

  to obtain the inverse coordinate change $z(\boldsymbol{z})$,

- calculate the new potential using the expression

$$\boldsymbol{V}(\boldsymbol{z}) = \boldsymbol{z} + \frac{5}{16\boldsymbol{z}^2} - \boldsymbol{z}Q(z) \ . \tag{IV.50}$$

  This is preferable to computing the Schwarzian derivative $\boldsymbol{V}(\boldsymbol{z}) = -\frac{1}{2}\{z, \boldsymbol{z}\}$ which involves third derivatives. However, one must be careful of the large cancellation between the two last terms near the turning point.

- Solve the new Schrödinger equation with a purely outgoing boundary condition:

$$\boldsymbol{\psi}''(\boldsymbol{z}) - \boldsymbol{V}(\boldsymbol{z})\boldsymbol{\psi}(\boldsymbol{z}) = 0 \ , \tag{IV.51}$$

$$\boldsymbol{\psi}(\boldsymbol{z}) = \mathrm{Ci}^-(\boldsymbol{z}) \text{ on the left of the peak } (a_+^{\mathrm{in}} = 0 \text{ and } a_-^{\mathrm{out}} = 1), \tag{IV.52}$$

- evaluate the Wronskians $\mathcal{W}(\boldsymbol{\psi}, \mathrm{Ci}^{\pm})$ on the right side of the peak to extract a_-^{in} and a_+^{out}. All scattering amplitudes can then be retrieved:

$$r = a_+^{\mathrm{out}}/a_-^{\mathrm{in}} \ , \qquad t = \bar{t} = 1/a_-^{\mathrm{in}} \ , \qquad \bar{r} = -r^*t/t^* \ . \tag{IV.53}$$

Note that the solution of the Schrödinger equation that we are computing is unphysical in the sense that it diverges for $\boldsymbol{z} \to \infty$. This is a consequence of the fact that we are looking for stationary solutions to a problem with a net outgoing current. Such solutions can only exist if sources balance the loss of amplitude. In the absence of a gravitational field, the system could be fed by a plane wave arriving from the right; this is no longer possible in the presence of gravity. However, our objective here is only to retrieve the scattering amplitudes. These amplitudes can then be included in a broader problem including the appropriate sources and sinks, but they already contain significant information about the system by themselves.

The quasi-stationary states introduced in the previous section satisfy simultaneously two conditions, they vanish asymptotically at infinity and obey a fully absorbing boundary condition at the surface:

$$a_+^{\mathrm{out}} = a_-^{\mathrm{in}} = 1 \ , \qquad a_+^{\mathrm{in}} = 0 \ . \tag{IV.54}$$

As we have seen, this can only be fulfilled for complex energies $E_n^\star = \epsilon_n - i\hbar\gamma_n/2$. From the conditions (IV.54) we deduce that the reflection coefficient on the right side of the

peak satisfies $r(E_n^\star) = 1$. Expanding formally, we find that in the vicinity of $E_n^\star$, the reflection coefficient for a real energy E is

$$r(E) \underset{E\simeq E_n^\star}{\simeq} 1 + (E - E_n^\star)\frac{\mathrm{d}r}{\mathrm{d}E}\Big|_{E_n^\star} . \tag{IV.55}$$

We define the closed-loop function of the cavity as a sum over the number of round trips in the cavity:

$$\frac{1}{1-r} = 1 + r + r^2 + \dots \underset{E\simeq E_n^\star}{\simeq} \left(\frac{\mathrm{d}r}{\mathrm{d}E}\Big|_{E_n^\star}\right)^{-1} \frac{1}{E_n^\star - E} \tag{IV.56}$$

This function has poles at the energies $E_n^\star$ of the quasi-stationary states. On the real axis, the proximity of these poles results in Lorentzian resonances of the squared modulus of the closed-loop function:

$$\left|\frac{1}{1-r}\right|^2 \underset{E\simeq E_n^\star}{\simeq} \frac{A_n}{(E-\epsilon_n)^2 + \hbar^2\gamma_n^2/4} , \qquad A_n = \left|\frac{\mathrm{d}r}{\mathrm{d}E}\Big|_{E_n^\star}\right|^{-2} . \tag{IV.57}$$

Figure IV.5 shows the first ten resonance peaks of the absolute square of the closed-loop function for (anti)hydrogen interacting with a perfect mirror. The parameters ϵ_n, γ_n and A_n can be retrieved by fitting a Lorentzian curve to each of these peaks. In figure IV.6 we show a close up on the third peak and the fitting function, for (anti)hydrogen interacting with a perfect mirror, a silicon bulk or a silica bulk.

We observe that, for a given mirror, all peaks have the same width and are slightly shifted by the same amount relative to the ideal quantum bouncer energies $E_g a_n$. In figure IV.7 we compare the fitted values $E_n^\star = \epsilon_n - i\hbar\gamma_n/2$ with the expression $E_n^\star = E_g a_n + m\bar{g}a$ derived in the previous section. The agreement is particularly good for the imaginary part but less so for the real energy shift. If precise values of the resonant energies are needed, the unified treatment of quantum reflection and gravity described in this section should be preferred over the matching procedure of section IV.2.a.

IV.3 Shaping the distribution of vertical velocities of $\overline{\mathrm{H}}$ in GBAR

We now apply the arguments developed in the previous sections to the GBAR experiment. In particular, we show how the GBAR experiment can take advantage of the quantum bounces of antihydrogen to improve its resolution. The idea is to reduce the initial velocity dispersion of the falling atom and thereby achieve a smaller uncertainty on the arrival time of the particle.

IV.3.a Limits on the precision of GBAR

Let us first recall a few numbers that are typically considered for the experiment. We will use these figures in our numerical applications. The ion trap from which $\overline{\mathrm{H}}$ is dropped is centered at a height $H = 10$ cm above the detection plate. In general, the precision of

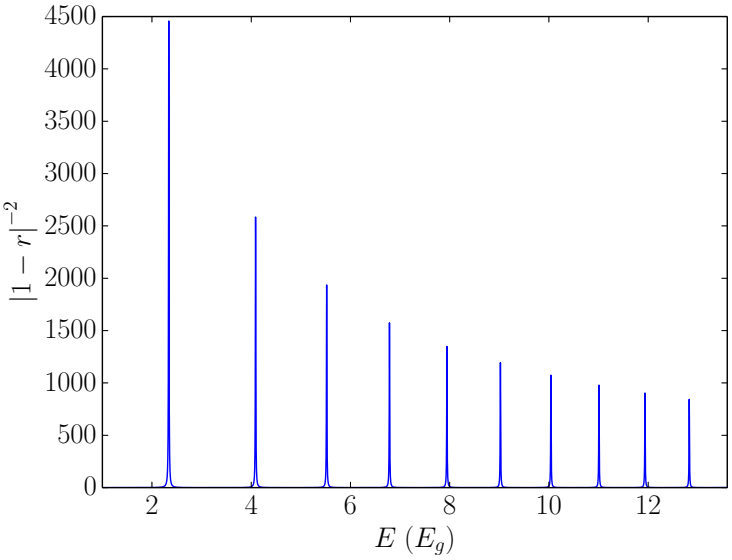

Figure IV.5: Squared modulus of the closed loop function (IV.56) as a function of energy for (anti)hydrogen interacting with a perfect mirror.

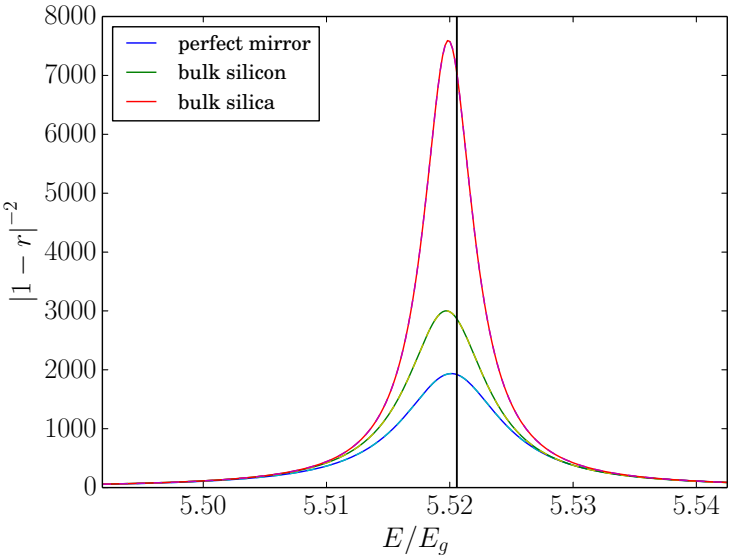

Figure IV.6: Third peak (full line) and Lorentzian fit (dashed line) of the absolute square of the closed-loop function for (anti)hydrogen interacting with a perfect mirror (blue), a silicon bulk (green) or a silica bulk (red). The vertical line indicates the position of the ideal quantum bouncer energy $E_g a_2$.

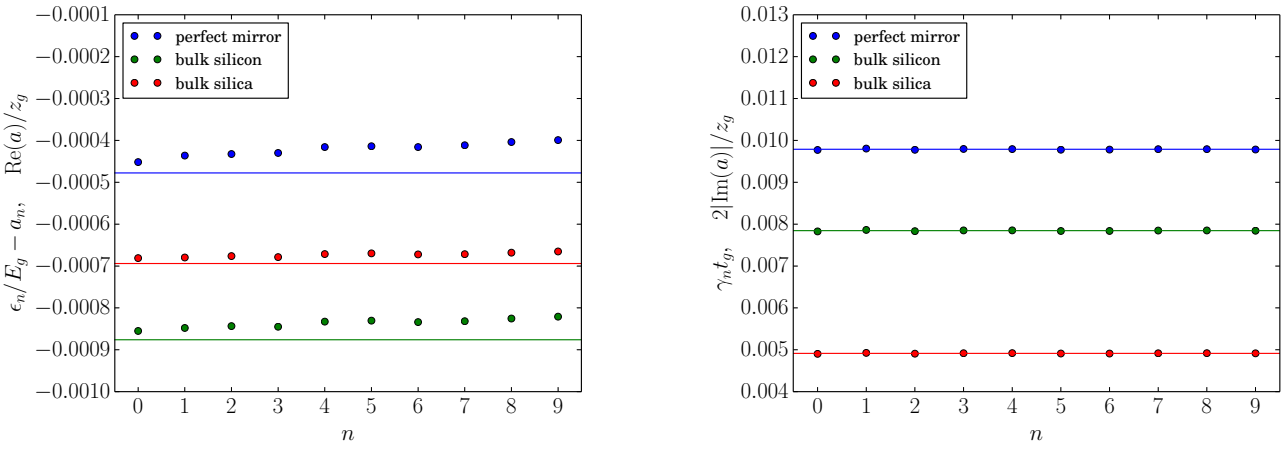

Figure IV.7: Values of the real (left panel) and imaginary (right panel) parts of the energy shift $E_n^\star - a_n E_g$ of the quasi-stationary states of (anti)hydrogen interacting with a perfect mirror (blue), a silicon bulk (green) or a silica bulk (red), in units of E_g. The values predicted by the matching procedure of section IV.2.a are shown as horizontal lines for comparison.

a free fall experiment increases when the dropping height increases. In GBAR, the free fall height is limited by the size of the vacuum vessel. Assuming $\overline{g} = g$ (which we will do in numerical calculations), this corresponds to a time of free fall $T_H \approx 0.14$ s and an arrival velocity $v_H \approx 1.4$ m.s^{-1} for a classical particle with no initial velocity.

The ELENA ring is expected to provide a pulse of antiprotons every 110 s and a single cold antihydrogen atom can be prepared per pulse. Therefore, on the order of $N_{\mathrm{tot}} = 7500$ atoms can be cooled in ten days of continuous operation.

If we assume that the initial velocity distribution of the atoms is centered on zero and that the height H is well defined, the estimated value of $\overline{g}$ after a single free fall of duration T is $\overline{g} \approx 2H/T^2$, and the relative uncertainty on that value is

$$\frac{\Delta\overline{g}}{\overline{g}} = 2\frac{\Delta T}{T_H} \ . \tag{IV.58}$$

After N_{tot} independent events, it is reduced to

$$\frac{1}{\sqrt{N_{\mathrm{tot}}}}\frac{\Delta\overline{g}}{\overline{g}} = \frac{2}{\sqrt{N_{\mathrm{tot}}}}\frac{\Delta T}{T_H} \ . \tag{IV.59}$$

We have considered only statistical fluctuations here. A few possible systematic effects are discussed below.

In the GBAR experiment, the uncertainty ΔT on the free fall time originates from various sources:

- uncertainty on the start time of the free fall, that is the time at which the extra positron is photodetached,
- finite resolution on the measurement of the annihilation time, which marks the end of the free fall,
- momentum kick by the antihydrogen atom received during the photodetachment process,
- width of the position and momentum distributions of the quantum wavepacket.

In order to minimize the uncertainty on the starting time of the free fall, the photodetachment will be performed by a series of short, well separated laser pulses. The start time is thus defined with high precision and there is no ambiguity on which shot triggered the free fall. The free fall time is less than 150 ms and we have approximately 100 s between antiproton pulses. If 100 μs laser shots are repeated every 500 ms during 100 s, the free fall start time can be located unambiguously within one 100 μs time interval and the photodetachment efficiency over the whole 100 s is larger than 90 % [224]. The associated uncertainty on the free fall time is thus:

$$\Delta T_{\text{start}} \approx \frac{100\ \mu\text{s}}{\sqrt{12}}\ . \tag{IV.60}$$

The photodetachment process is also responsible for an initial velocity dispersion because of the recoils associated with the photon absorption and positron emission. The photodetachment cross section is larger for higher energy photons, but the energy in excess of the photodetachment threshold is converted to kinetic energy. Therefore a trade-off has to be made between the photodetachment efficiency and minimization of the velocity dispersion. Calculations show that a photodetachment rate of 130 s^{-1} can be achieved with a 1 W laser beam tuned 10 μeV above the threshold energy E_T=0.76 eV and focused on a 10 μm $\times$10 μm area covering the Paul trap center. If the laser beam is horizontally polarized, these settings lead to a vertical velocity dispersion on the order of 0.5 m.s^{-1} [224]. The resulting uncertainty on the free fall time is

$$\Delta T_{\text{recoil}} \approx 50\ \text{ms}\ . \tag{IV.61}$$

This figure disregards a possible systematic effect whereby the atom would recoil in a preferred direction. Such an effect would evidently be hugely detrimental to GBAR. We will come back to this point later.

We now consider the uncertainty associated with the extension of the quantum wavepacket in coordinate and momentum space. Before the free fall, the Paul trap holds the $\overline{\text{H}}^+$ ion in a harmonic potential. The operation of the Paul trap requires different horizontal and vertical trapping frequencies, that we denote ω and Ω respectively [2].

[2] In general, we will use uppercase and lowercase letters to denote quantities relating to the horizontal and vertical directions, respectively.

Typically, $2 < \Omega/\omega < 4$ [225]. The ground state wavefunction of this trap is a Gaussian

$$\psi(x,y,z) = \left(\frac{m^3\omega\Omega^2}{\pi^3\hbar^3}\right)^{1/4} \exp\left(-\frac{m\omega}{2\hbar}(z-H)^2 - \frac{m\Omega}{2\hbar}\rho^2\right) , \qquad \rho = \sqrt{x^2+y^2} , \tag{IV.62}$$

with vertical position and velocity dispersions

$$\Delta z = \sqrt{\frac{\hbar}{2m\omega}} , \qquad \Delta v = \sqrt{\frac{\hbar\omega}{2m}} \tag{IV.63}$$

and a horizontal root mean square (rms) velocity

$$V_{\rm rms} = \sqrt{\frac{\hbar\Omega}{m}} . \tag{IV.64}$$

The range of trap frequencies that can be used is limited by the residual kinetic energy of the atoms after cooling. In GBAR, the considered frequency range for vertical trapping is 0.1 MHz $< \omega/2\pi <$ 1 MHz, so that one gets 0.22 μm $> \Delta z >$ 0.07 μm , 0.14 m/s $< \Delta v <$ 0.44 m/s and 0.28 m/s $< V_{\rm rms} <$ 1.26 m/s. The uncertainty on the free fall time follows from formula (III.90):

$$\Delta T_{\rm quantum} \approx 10 - 40 \text{ ms} . \tag{IV.65}$$

For comparison, we recall the velocity and position dispersions which minimize the uncertainty on the arrival time, derived in section III.2.a:

$$\Delta z_{\rm opt} = \sqrt{\frac{\hbar H}{m v_H}} \approx 67 \ \mu\text{m} , \qquad \Delta v_{\rm opt} = \sqrt{\frac{\hbar v_H}{4mH}} \approx 0.47 \text{ mm.s}^{-1} . \tag{IV.66}$$

This corresponds to a wavepacket that is cooler than the planned performance of GBAR by orders of magnitude.

Leaving out any systematic effect due to photodetachment, the resolution of the GBAR experiment is thus limited by the velocity dispersion $\Delta v \approx 0.7$ m.s^{-1} due to both photodetachment recoil and quantum uncertainty:

$$\frac{1}{\sqrt{N_{\rm tot}}}\frac{\Delta\overline{g}}{\overline{g}} \simeq \frac{2}{\sqrt{N_{\rm tot}}}\frac{\Delta v}{v_H} \approx 1\% . \tag{IV.67}$$

Although it is not experimentally feasible to reduce this dispersion in GBAR, it is possible to improve the resolution by removing atoms with a large vertical velocity. Indeed, a reduction of the vertical velocity range from Δv to δv yields an improvement of the single-shot resolution by a factor scaling as $\delta v/\Delta v$ while the statistics are reduced by a factor scaling as $\sqrt{\delta v/\Delta v}$, so that an overall improvement is expected. As an additional benefit, if the central velocity of the velocity window δv can be selected, such a filtering scheme leads to a better control over a possible systematic effect associated with the photodetachment.

IV.3.b Velocity shaper for GBAR

The proposed device to realize the filtering of initial velocities in GBAR is inspired by the techniques used to observe the gravitationally bound states of ultracold neutrons [54, 55, 226, 227]. The idea is to send the particles in the waveguide between a smooth bottom mirror which reflects them and a rough top surface which acts as an absorber, as described in section IV.1.b.

Since $\overline{\mathrm{H}}$ does not leave the trap in a preferred horizontal direction (if we omit the possible anisotropy of the photodetachment kick), the shaping device should consist of two disks of radius R centered around the trap with a central opening of radius r to allow operation of the trap. One or several sectors could be removed to provide extra access to the trap and for testing purposes. A scheme of the proposed device is shown in figure IV.8, where relevant dimensions are introduced.

The bottom disk should be made of a rigid material such as sapphire and be coated with a metal to avoid stray charges in proximity of the ion trap. It should have a flat, horizontal and smooth upper surface to allow specular reflection of the anti-atoms: only the direction of the vertical velocity should be changed upon reflection, not its magnitude nor the horizontal velocity. In contrast, the lower surface of the top mirror should be rough so that reflection upon it mixes the horizontal and vertical velocity components and prevents the atom from leaving the device, leading ultimately to its annihilation. Therefore atoms with insufficient vertical velocity to reach the top disk would bounce with high probability on the bottom disk before exiting the device, whereas atoms with a larger vertical velocity would hit the top disk and thus be suppressed.

IV.3.c Classical trajectories in the shaper

If the height h of the slit formed by the two disks is small enough (on the order of several times z_g, that is tens of microns), the quantization of the vertical motion inside the waveguide should be taken into account using the notions from section IV.1.b. For the moment we assume that h is larger than 50 μm, and that the quantum motion can be described by an ensemble of classical trajectories, as in the case of a free fall without boundary conditions (see section III.1). This assumption allows us to determine the acceptance of the device based on a classical calculation. Moreover we will suppose that reflection on the lower surface and absorption on the top one are ideal.

As shown in figure IV.9, we take the detection plate as the origin of altitudes. The top surface of the bottom disk is located at a height $z = H$ and the center of the ion trap is in $z = H + z_0$. The extension of the wavepacket in the trap (~ 0.1 μm) being much smaller than all other lengths scales in the problem, it is neglected and we suppose that all particles leave from the same point. Denoting ρ the radial coordinate, we consider a particle initially in $\rho = 0$, $z = H + z_0$ with vertical and horizontal velocities $v = v_0$ and $V = V_0$ respectively. The horizontal velocity V is conserved throughout so that the horizontal coordinate follows $\rho(t) = Vt = V_0 t$.

A typical trajectory through the shaper is sketched in figure IV.9. The atom is

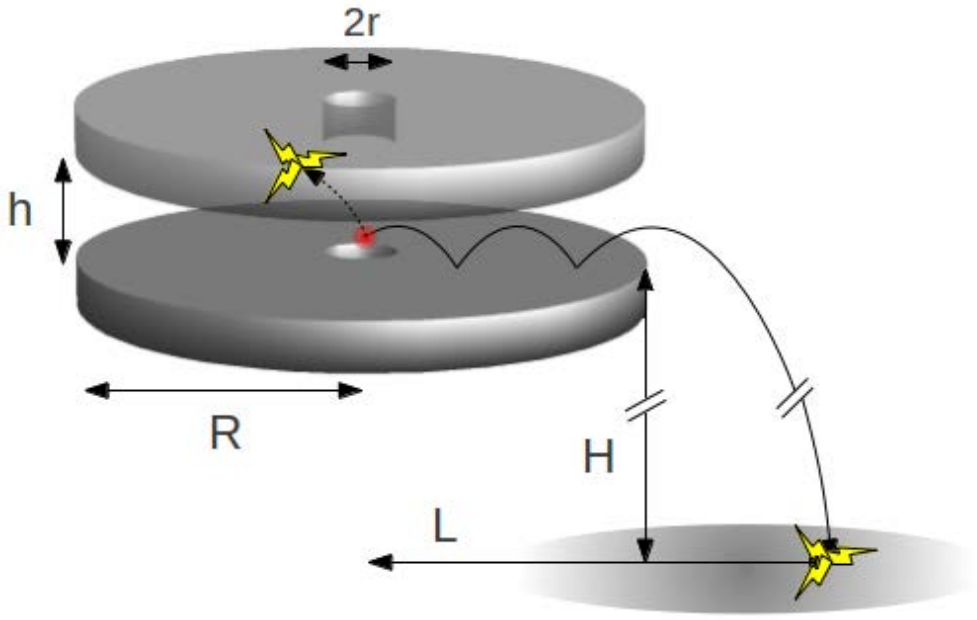

Figure IV.8: A scheme of principle of the proposed shaping device: an $\overline{\mathrm{H}}$ atom is released from the Paul trap (central spot) and it bounces a few times on the mirror surface of the bottom disk (arrows); if it scatters on the rough top surface, it annihilates (lightnings); otherwise, it escapes from the aperture between the two disks, and falls to the detection plate where it annihilates (lightning on the detection plate). R is the radius of the bottom and top disks, r is the radius of central openings in the disks, h is the distance between the top surface of the bottom disk and the bottom surface of the top disk, H is the distance between the top of the detection plate and the top of the bottom disk, L is the horizontal distance between the initial spot and the detection point.

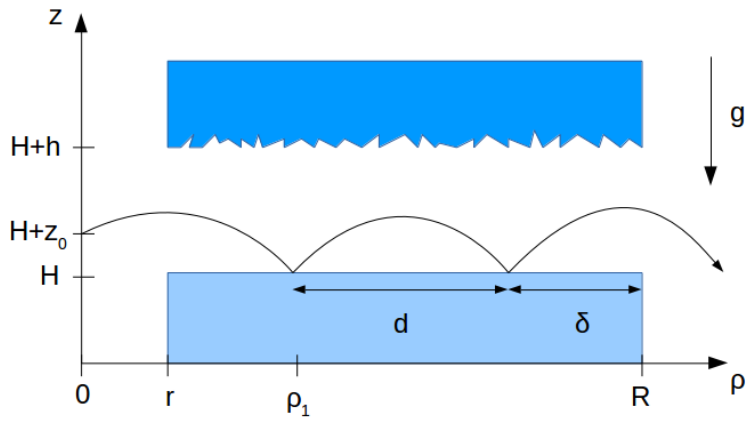

Figure IV.9: Example of a classical particle's trajectory in the shaping device.

released at time $t = 0$ and its trajectory before the first bounce is given by

$$z(t) = H + z_0 + v_0 t - \frac{1}{2}\overline{g}t^2 \ . \tag{IV.68}$$

The particle enters the waveguide at $\rho = r$ (i.e. $t = r/V$) provided that

$$0 < z_0 + \frac{v_0 r}{V} - \frac{\overline{g} r^2}{2V^2} < h \ . \tag{IV.69}$$

If it enters the guide, the time and position of the first bounce are given by solving $z(t_1) = H$ (with $t_1 > 0$):

$$t_1 = \frac{1}{\overline{g}}(v_0 + \sqrt{v_0^2 + 2\overline{g}z_0}) \ , \qquad \rho_1 = \frac{V}{\overline{g}}(v_0 + \sqrt{v_0^2 + 2\overline{g}z_0}) \tag{IV.70}$$

and the vertical speed $v_1 = v(t_1^+) = -v(t_1^-)$ at the bounce is

$$v_1 = |v_0 - \overline{g}t_1| = \sqrt{v_0^2 + 2\overline{g}z_0} \ . \tag{IV.71}$$

This vertical speed must be smaller than $\sqrt{2\overline{g}h}$ for the particle not to reach the absorber (assuming the guide is long enough), which yields a second condition:

$$\sqrt{v_0^2 + 2\overline{g}z_0} < \sqrt{2\overline{g}h} \ . \tag{IV.72}$$

The following bounces are identical, the time between two successive bounces is $T_{\text{bounce}} = 2v_1/\overline{g}$, the distance covered is $d = V\tau = 2Vv_1/\overline{g}$ and the maximum height reached is $v_1^2/2\overline{g}$. At the exit of the guide ($\rho = R$), the particle has bounced n times, with

$$R = \rho_1 + (n-1)d + \delta \ , \qquad \delta < d \ . \tag{IV.73}$$

This defines δ, the distance between the last bounce and the end of the guide. The particle exits the guide at a time δ/V after this last bounce. The particle crosses the surface $\rho = R$ at time $T_{\text{shaper}} = R/V$, at height $z_{\text{out}} = v_1\delta/V - \overline{g}\delta^2/2V^2$ and with a vertical velocity $v_{\text{out}} = v_1 - \overline{g}\delta/V$ which satisfy

$$H < z_{\text{out}} < H + h \ , \qquad -\sqrt{2\overline{g}h} < v_{\text{out}} < \sqrt{2\overline{g}h} \ . \tag{IV.74}$$

Let us now take a closer look at the two conditions on the particle's velocity, supposing the position z_0 of the trap is given. From (IV.72) we immediately get

$$|v_0| < \sqrt{2\overline{g}(h - z_0)} \ . \tag{IV.75}$$

If this is satisfied, so is the second inequality in (IV.69), so that finally the two conditions for the particle to exit the device are

$$|v_0| < \sqrt{2\overline{g}(h - z_0)} \ , \tag{IV.76}$$

$$v_0 > \frac{\overline{g}}{2}\frac{r}{V} - \frac{V}{r}z_0 \ . \tag{IV.77}$$

The number of atoms allowed through the shaping device is given by the following integral restricted to the domain defined by (IV.76) and (IV.77):

$$N = N_{\text{tot}} \iint \mathrm{d}v_0 \, \mathrm{d}V_0 \ 2\pi V_0 \sqrt{\frac{m^3}{\hbar^3\pi^3\omega\Omega^2}} \exp\left(-\frac{mv_0^2}{\hbar\omega} - \frac{mV_0^2}{\hbar\Omega}\right) \ . \tag{IV.78}$$

At the output of the device, the vertical velocities range from $-\sqrt{2\overline{g}h}$ to $+\sqrt{2\overline{g}h}$. Keeping this interval fixed, we want to maximize the transmission through the shaper. In particular we do not want to lose atoms that would otherwise make it through the shaper because of the central opening, in short the bond (IV.77) should not be limiting. Moreover the value of z_0 should be kept as small as possible in view of (IV.76). We therefore choose:

$$\frac{\overline{g}}{2}\frac{r}{V} - \frac{V}{r}z_0 = -\sqrt{2\overline{g}(h - z_0)} \ , \tag{IV.79}$$

which yields the smallest value of z_0 such that (IV.77) is automatically satisfied if (IV.76) is satisfied. We find:

$$z_0 = \frac{r}{V}\sqrt{2\overline{g}h} - \frac{\overline{g}r^2}{2V^2} \ , \tag{IV.80}$$

so that the bound on the initial vertical velocity is

$$|v_0| < \sqrt{2\overline{g}h} - \frac{\overline{g}r}{V} \ . \tag{IV.81}$$

The central radius r should thus be kept as small as possible, with ideally $r \ll V\sqrt{2h/\overline{g}}$.

The outer radius R of the disks should be sufficiently large to ensure that atoms with a too large vertical velocity touch the top disk. The time T_{shaper} spent in the shaper should therefore be larger than the time of the longest possible bounce, from which we deduce a lower bound for the disks' radius R:

$$T_{\text{shaper}} = \frac{R}{V} > 2\sqrt{\frac{2h}{\overline{g}}} \quad \Rightarrow \quad R > R_{\text{min}} = 2V\sqrt{\frac{2h}{\overline{g}}} \ . \tag{IV.82}$$

On the other hand R should not be too large since there is a small probability of loosing the atom at each bounce on the lower mirror. Of course V is randomly distributed and it should be replaced by its rms value when estimating the optimal values of z_0, r and R. Typically, z_0 can be neglected, r is in the millimeter range while R is in the centimeter range.

In GBAR, the annihilation signal is resolved in time and space. Therefore we have access to both the horizontal distance L from the center of the trap to the position of annihilation on the detection plate and the time T_{tot} taken by the anti-atom to go from one to the other. This gives us the atom's horizontal velocity $V = L/T_{\text{tot}}$, which allows to correct for the time spent inside the device before the free fall $T_{\text{shaper}} = R/V$:

$$T_{\text{free fall}} = T_{\text{tot}} - T_{\text{shaper}} \ . \tag{IV.83}$$

The proposed shaping device satisfies the requirements of reducing the vertical velocity range and fixing its central value. Not only does this lead to an improved resolution, as we show in the next section, but it also guarantees the experiment against any vertical asymmetry in the photodetachment recoil, which would seriously jeopardize the experiment otherwise.

IV.3.d Estimation of the statistical uncertainty

The position and velocity of the atom at the output of the shaping device are correlated. For example, an atom leaving the device at altitude $z = H+h$ can only have zero vertical velocity while an atom exiting at height $z = H$ has a maximal vertical velocity.

Here, for a first estimation of the performances of the shaping device, we suppose that the output velocity and position distributions are Gaussian and uncorrelated, with standard deviations $\delta v = \sqrt{2\overline{g}h/3}$ and $\delta z = h/\sqrt{12}$ respectively. This allows us to use the results of section III.2 on the free fall of Gaussian wavepackets to obtain the reduced spread of arrival times δT.

If we neglect quantum reflection on the detection plate, the spread of arrival times is given by equation (III.92), which in this case evaluates to

$$\frac{\delta T}{T_H} = \sqrt{\left(\frac{h}{4\sqrt{3}H}\right)^2 + \frac{h}{3H}} \ . \tag{IV.84}$$

If $h \ll H$, the spread in initial velocities dominates and

$$\frac{\delta T}{T_H} \underset{h\ll H}{\simeq} \sqrt{\frac{h}{3H}} \ . \tag{IV.85}$$

The corresponding accuracy on the value of $\overline{g}$ obtained after a single annihilation is

$$\frac{\delta\overline{g}}{\overline{g}} \simeq 2\sqrt{\frac{h}{3H}} \ . \tag{IV.86}$$

This simple estimation is not fundamentally modified when the quantum nature of the motion in the waveguide is taken into account. Indeed, suppose that the output state of the shaper is an incoherent superposition of the bound states which fit in the slit, that is states with

$$n \leq n_{\max} \ , \qquad\qquad a_{n_{\max}} z_g \approx h \ . \tag{IV.87}$$

This approximation can be justified qualitatively by considering that the effects of coherence are washed out in the averaging associated with free fall propagation as well as horizontal velocity dispersion. For the n^{th} gravitationally bound state, the width ΔT_n of the arrival time distribution after a free fall over a height H is given by formula (IV.20). If all states are equally populated, which is a natural assumption if the slit size is small compared with the size of the wavefunction which enters the device, the total dispersion is the quadratic sum

$$\frac{\delta T}{T_H} = \sqrt{\frac{1}{n_{\max}} \sum_{n=1}^{n_{\max}} \left(\frac{\Delta T_n}{T_H}\right)^2} = \sqrt{\frac{1}{n_{\max}} \sum_{n=1}^{n_{\max}} \frac{a_n z_g}{3H}} \ , \tag{IV.88}$$

In the limit where $n_{\max} \gg 1$, we can use the asymptotic expression (IV.4) for a_n and replace the sum by an integral to find

$$\frac{\delta T}{T_H} \simeq \sqrt{\frac{h}{5H}} \tag{IV.89}$$

which differs from the previous result only by a factor $\sqrt{5/3}$.

On the other hand, the proportion of atoms which exit the device also scales like $\sqrt{h/H}$. To be more specific, suppose that the trap is at the level of the bottom mirror, that is $z_0 = 0$, and that the effect of gravity over the short time r/V is small so the first term in (IV.77) can be omitted. Under these conditions the shaper selects velocities satisfying $0 < v_0 < \sqrt{2\overline{g}h}$ and if $\sqrt{2\overline{g}h} \ll \Delta v$ the integral (IV.78) is approximately:

$$\frac{N}{N_{\text{tot}}} \simeq \sqrt{\frac{h}{2\pi H}} \ . \tag{IV.90}$$

The achieved statistical accuracy with the shaper is therefore

$$\frac{1}{\sqrt{N}} \frac{\delta\overline{g}}{\overline{g}} \simeq \frac{2(2\pi)^{1/4}}{\sqrt{5N_{\text{tot}}}} \left(\frac{h}{H}\right)^{1/4} \tag{IV.91}$$

The best accuracy is therefore achieved for smaller slit sizes, keeping in mind that below a certain slit size, the quantization of the vertical motion in the shaper must be taken into account.

- If $h = 1$ mm, the fraction of selected atoms is $N/N_{\rm tot} \approx 4\%$ and the statistical accuracy is $\delta\overline{g}/\overline{g}\sqrt{N} \approx 0.5\%$, a twofold improvement on the original resolution. For a conducting mirror and a maximal vertical velocity $\sqrt{2\overline{g}h} \approx 0.14$ m/s, the reflection probability on the bottom mirror is 78%.
- For $h = 50$ μm, $N/N_{\rm tot} \approx 1\%$ and the statistical accuracy is $\delta\overline{g}/\overline{g}\sqrt{N} \approx 0.2\%$, which is a factor 5 better than the original experiment. The reflection probability for an atom with the maximal velocity $\sqrt{2gh} = 3.1 \times 10^{-2}$ m/s is 94% for a perfect mirror.
- For $h < 20$ μm, only atoms in the lowest quantum state can pass through the slit. The uncertainty on the free fall time of such an atom is given by equation (IV.20). It follows that the resolution on $\overline{g}$ after the measurement of a *single* free fall is $\delta\overline{g}/\overline{g} \approx 1.4\%$, a result comparable with the 1% accuracy expected for the original GBAR setup after 7500 free falls.

These estimations are preliminary and should be completed by simulations which take into account the following effects:

- position-momentum correlations at the exit of the device,
- loss of atoms because of shadowing by trap electrodes,
- finite size of the detection plate,
- annihilation on the bottom mirror,
- accuracy of the correction for the time spent in the shaping device,
- reflection on detection plate,
- defects in the geometry of the device, such as inclination of the disks and detection plate,
- vibrations of the device,
- effect of electrostatic patches on the mirror surfaces,
- diffraction of atoms on the mirror edges.

The first five points have already been included in Monte-Carlo simulations by Debu [228] which confirm our simple estimations. Further simulations should follow as the design of the experiment is refined.

It is probable that the experiment will first be operated without the shaping device, in order to keep the largest number of events. However, when sufficient control has been achieved over the previous stages of the experiment, the shaper should be inserted to ensure a fine control of the initial conditions of the free fall and in particular to avoid systematic effects caused by the photodetachment process.

On the long term, the shaping device could constitute a first step towards experiments with the gravitationally bound states of antimatter, which could push the resolution on $\overline{g}$ by several orders of magnitude [126, 229, 230].

Conclusion

A quantum particle bouncing on an infinite step in a linear potential is certainly a problem of theoretical and pedagogical interest, but not only. This physical system has actually been realized with ultracold neutrons and is a promising tool for precise measurements of gravity and short-range forces.

We have shown that quantum bouncers could also be realized with neutral atoms thanks to quantum reflection on the Casimir-Polder potential above a mirror. Since reflection no longer occurs on a sharp step and is not total, the energy levels of these bouncers receive a complex shift with respects to the ideal case. However, as all low-lying states are displaced by the same amount, the transition frequencies between these quasi-stationary states are universal.

We have suggested an interesting alternative approach to the problem by means of a Liouville transformation to the Langer coordinate. Quantum reflection was shown to be equivalent to reflection on a barrier and the quasi-stationary states could be interpreted as resonances of a lossy "cavity" formed by the gravitational potential on the one hand and the quantum reflection barrier on the other.

Finally we have shown that the quantum bounces of antihydrogen could be used to shape the initial velocity distribution in the GBAR experiment, allowing a more precise measurement of $\overline{g}$ and paving the way for future experiments with gravitationally bound state of antihydrogen.

Conclusions and perspectives

Our exploration of quantum reflection on the Casimir-Polder potential has taken us through three successive layers of quantum phenomena. First, the atom-mirror interaction arising from fluctuations of the quantized electromagnetic field. Next, the reflection of the atomic matter wave on this interaction potential. And finally, the quantum bounces of the atom in the gravity field above the mirror.

Casimir forces are efficiently calculated from the scattering properties of the interacting objects. We have used this scattering approach to compute the interaction energy between a hydrogen or antihydrogen atom and a variety of mirrors. We have especially stressed the dependence of the Casimir-Polder potential on the thickness, density and dielectric properties of the mirror.

Despite being attracted to the surface, the atom has a probability of being reflected before it even reaches it. To provide a thorough understanding of the quantum reflection phenomenon, we have introduced Liouville transformations of the Schrödinger equation. These transformations relate dissimilar potential landscapes which lead to identical scattering amplitudes. In particular, we have shown that scattering on the Casimir-Polder potential well was quantum mechanically equivalent to a collision with a repulsive wall; two problems that are antithetic from a semiclassical point of view. The barrier in the Liouville-transformed problem has a clear interpretation as a measure of the departure of the exact quantum equation from the semiclassical WKB approximation. Exploring the links between quantum reflection and other non-adiabatic phenomena could constitute a promising continuation of this work.

Using these tools, we have presented a quantitative study of quantum reflection of a hydrogen or antihydrogen atom on a variety of mirrors. We have been able to show that the reflection probabilities for a wide range of surfaces are well described by a one-parameter model based on the long-range C_4 potential. It transpired that bad reflectors of the electromagnetic field, which are associated with weak Casimir-Polder potentials, are highly reflective for atoms. This effect can be enhanced by decreasing the width or density of the mirror. In particular, nanoporous materials exhibit exceptionally high quantum reflection probabilities. In this context, a generalization of our calculations to non-specular quantum reflection on rough surfaces and inhomogeneous media would constitute an appealing objective for future work.

While most calculations to date assume that atoms are lost upon reaching the surface, we have also investigated the influence of coherent reflection from the surface. The

matter wave can become resonant with the cavity formed by the surface and the Casimir-Polder potential, similarly to the electromagnetic field inside a Fabry-Perot cavity. A small amount of coherent reflection from the surface may thus significantly alter the overall reflection probability.

The next step was to include the effect of gravity on the atomic wavepacket. In accordance with the equivalence principle, a matter wave in a uniform field behaves like a free particle seen from an accelerated coordinate frame. Although the wavepacket propagates classically, its quantum nature imposes that it is extended in phase space. This results in a spread of the time of arrival distribution on an ideal detector. Specifically, we have noted the adverse effect of the initial momentum dispersion on the precision of a quantum free fall experiment.

If the ideal detector is replaced by a reflective surface, the matter wave can bounce on top of it. The combination of a perfectly reflecting surface and gravity forms a potential well which holds gravitationally bound states. However, if the bounces are due to quantum reflection from the Casimir-Polder potential then reflection is partial and the atom can only bounce a finite amount of times before hitting the surface. The resulting quasi-stationary states can again be seen as resonances of a lossy cavity formed by gravity and the quantum reflection barrier.

Finally, we have exposed a scheme to improve the precision of the GBAR experiment by reducing the velocity dispersion of the falling atoms. This scheme relies on the quantum reflection of the antihydrogen atoms on a horizontal surface above which an absorber is placed to suppress atoms with a large vertical velocity. In addition to improving control on the initial conditions of the free fall, this scheme is a first step towards the observation of the quantized states of atoms or anti-atoms in the gravitational field. Such “quantum bouncer” experiments could take advantage of spectroscopic and interferometric measurement techniques to perform fundamental tests with an unprecedented resolution.

Appendices

A The Schrödinger equation in 1D

In this appendix, we compile mathematical results on the time-independent Schrödinger equation in one-dimension:

$$\psi''(z) + F(z)\psi(z) = 0 \ . \tag{A.1}$$

In particular, we focus on results relevant to scattering theory and on transformations of the equation.

A.1 Wronskians

We recall the definition of the Wronskian of two functions ψ_1 and ψ_2:

$$\mathcal{W}(\psi_1, \psi_2) \equiv \psi_1(z)\psi_2'(z) - \psi_1'(z)\psi_2(z) \ . \tag{A.2}$$

If ψ_1 and ψ_2 are solutions of (A.1), $\mathcal{W}(\psi_1, \psi_2)$ is independent of z so that the Wronskian is a bilinear skew-symmetric form on the space of solutions.

For a pair ψ^+, ψ^- of linearly independent solutions of (A.1), the Wronskian is non-zero:

$$\mathcal{W}(\psi^+, \psi^-) \equiv w \neq 0 \ . \tag{A.3}$$

ψ^+ and ψ^- form a basis in which any other solution ψ_a can be expressed:

$$\psi_a(z) = a_+\psi^+(z) + a_-\psi^-(z) \ . \tag{A.4}$$

The coefficients a_+ and a_- can be extracted using the Wronskian:

$$a_\pm = \frac{\mathcal{W}(\psi^\mp, \psi_a)}{\mathcal{W}(\psi^\mp, \psi^\pm)} = \mp\frac{1}{w}\mathcal{W}(\psi^\mp, \psi_a) \ . \tag{A.5}$$

This property allows one to express a change of basis in terms of Wronskians. In particular, the scattering and transfer matrices are changes between specific bases of solutions.

We introduce the following matrix notation ($\top$ symbolizes matrix transposition):

$$\psi_a(z) = [A|\Psi] = [\Psi|A] \ , \tag{A.6}$$

$$[A| \equiv \begin{pmatrix} a_+ & a_- \end{pmatrix} \ , \qquad |A] \equiv [A|^\top \qquad [\Psi| \equiv \begin{pmatrix} \psi^+ & \psi^- \end{pmatrix} \ , \qquad |\Psi] \equiv [\Psi|^\top \ . \tag{A.7}$$

In a given basis $\psi^\pm$, the Wronskian bilinear form has the following matrix representation:

$$\mathcal{W}(\psi_a, \psi_b) = [A|W|B] \ , \tag{A.8}$$

with W the skew-symmetric matrix:

$$W \equiv \begin{pmatrix} \mathcal{W}(\psi_+, \psi_+) & \mathcal{W}(\psi_+, \psi_-) \\ \mathcal{W}(\psi_-, \psi_+) & \mathcal{W}(\psi_-, \psi_-) \end{pmatrix} = wJ \ , \tag{A.9}$$

$$J \equiv \begin{pmatrix} 0 & 1 \\ -1 & 0 \end{pmatrix} \ , \qquad J^2 = -1 \ . \tag{A.10}$$

We introduce a new basis $\tilde{\psi}^\pm$ and the associated vector $|\tilde{\Psi}]$. The vector of coefficients of ψ_a in this new basis is $|\tilde{A}]$:

$$\psi_a(z) = [\tilde{\Psi}|\tilde{A}] = [\tilde{A}|\tilde{\Psi}] \ . \tag{A.11}$$

The two bases are related by an invertible matrix U:

$$|\tilde{A}] = U|A] \ , \qquad [\tilde{A}| = [A|U^\top \ , \tag{A.12}$$

$$|\tilde{\Psi}] = U^{-1\top}|\Psi] \ , \qquad [\tilde{\Psi}| = [\Psi|U^{-1} \ . \tag{A.13}$$

In the new basis, the Wronskian is represented by the matrix $\tilde{W}$:

$$\mathcal{W}(\psi_a, \psi_b) = [\tilde{A}|\tilde{W}|\tilde{B}] = [A|U^\top \tilde{W} U|B] = [A|W|B] \ , \tag{A.14}$$

$$W = U^\top \tilde{W} U \ , \qquad \tilde{W} = U^{-1\top} W U^{-1} \ . \tag{A.15}$$

A simple calculation shows that $\tilde{W}$ is of the same form as W:

$$\tilde{W} = \frac{1}{\det U} \begin{pmatrix} 0 & w \\ -w & 0 \end{pmatrix} = \begin{pmatrix} 0 & \tilde{w} \\ -\tilde{w} & 0 \end{pmatrix} \ . \tag{A.16}$$

Equation (A.15) can be used to obtain an expression of the matrix U when the wavefunctions $\psi^\pm$ and $\tilde{\psi}^\pm$ are known. Indeed, isolating U in (A.15) we have:

$$U = \tilde{W}^{-1} U^{-1\top} W \ . \tag{A.17}$$

$U^{-1\top}$ is the matrix of coefficients of $\tilde{\psi}^\pm$ in the $\psi^\pm$ basis so that $U^{-1\top}W$ is the matrix of Wronskians between $\tilde{\psi}^\pm$ and $\psi^\pm$:

$$U^{-1\top} W = \begin{pmatrix} \mathcal{W}(\tilde{\psi}^+, \psi^+) & \mathcal{W}(\tilde{\psi}^+, \psi^-) \\ \mathcal{W}(\tilde{\psi}^-, \psi^+) & \mathcal{W}(\tilde{\psi}^-, \psi^-) \end{pmatrix} \ . \tag{A.18}$$

Using the fact that $J^2 = -1$ we find:

$$U = \frac{-1}{\tilde{w}} J \begin{pmatrix} \mathcal{W}(\tilde{\psi}^+, \psi^+) & \mathcal{W}(\tilde{\psi}^+, \psi^-) \\ \mathcal{W}(\tilde{\psi}^-, \psi^+) & \mathcal{W}(\tilde{\psi}^-, \psi^-) \end{pmatrix} \tag{A.19}$$

$$= \frac{1}{\mathcal{W}(\tilde{\psi}^+, \tilde{\psi}^-)} \begin{pmatrix} \mathcal{W}(\psi^+, \tilde{\psi}^-) & \mathcal{W}(\psi^-, \tilde{\psi}^-) \\ \mathcal{W}(\tilde{\psi}^+, \psi^+) & \mathcal{W}(\tilde{\psi}^+, \psi^-) \end{pmatrix} . \tag{A.20}$$

At each point z_0, we can define a "fundamental basis" of solutions $C_{z_0}(z)$, $S_{z_0}(z)$ defined by:

$$C_{z_0}(z_0) = 1 , \qquad C'_{z_0}(z_0) = 0 , \tag{A.21}$$

$$S_{z_0}(z_0) = 0 , \qquad S'_{z_0}(z_0) = 1 . \tag{A.22}$$

In this basis a solution ψ is written:

$$\psi(z) = \psi(z_0) C_{z_0}(z) + \psi'(z_0) S_{z_0}(z) \tag{A.23}$$

and the Wronskian is represented by

$$W = \begin{pmatrix} 0 & 1 \\ -1 & 0 \end{pmatrix} . \tag{A.24}$$

Similarly, at each point z_0, we can define the "WKB basis" $\psi^{\rightarrow}_{z_0}(z), \psi^{\leftarrow}_{z_0}(z)$ as the pair of exact solutions of the Schrödinger equation which coincide with the WKB approximate wavefunctions in z_0:

$$\psi^{\rightarrow}_{z_0}(z_0) = \psi^{+}_{\mathrm{WKB}}(z_0) , \qquad \psi'^{\rightarrow}_{z_0}(z_0) = \psi'^{+}_{\mathrm{WKB}}(z_0) , \tag{A.25}$$

$$\psi^{\leftarrow}_{z_0}(z_0) = \psi^{-}_{\mathrm{WKB}}(z_0) , \qquad \psi'^{\leftarrow}_{z_0}(z_0) = \psi'^{-}_{\mathrm{WKB}}(z_0) . \tag{A.26}$$

This basis satisfies $\psi^{\rightarrow}_{z_0} = (\psi^{\leftarrow}_{z_0})^*$ so that

$$w = \mathcal{W}(\psi^{\rightarrow}_{z_0}, \psi^{\leftarrow}_{z_0}) = -2i , \qquad \text{therefore} \qquad W = -2iJ . \tag{A.27}$$

A solution $\psi(z)$ to the Schrödinger equation can be written in the WKB bases associated to any point z_0:

$$\psi(z) = a_-(z_0) \psi^{\leftarrow}_{z_0}(z) + a_+(z_0) \psi^{\rightarrow}_{z_0}(z) \tag{A.28}$$

where

$$a_-(z_0) = -\frac{1}{2i} \mathcal{W}(\psi^{\rightarrow}_{z_0}, \psi) , \qquad a_+(z_0) = \frac{1}{2i} \mathcal{W}(\psi^{\leftarrow}_{z_0}, \psi) . \tag{A.29}$$

In $z = z_0$, the basis functions have the same value as the WKB functions so that :

$$\psi(z_0) = a_-(z_0) \psi^{-}_{\mathrm{WKB}}(z_0) + a_+(z_0) \psi^{+}_{\mathrm{WKB}}(z_0) . \tag{A.30}$$

This is precisely the decomposition introduced by Kemble [139] and discussed in section I.2.c. Indeed, evaluating the Wronskians (A.29) in z_0, we recover equation (I.78):

$$a_\pm(z_0) = \pm\frac{1}{2i}\mathcal{W}(\psi^\mp_{\rm WKB}, \psi) \ . \tag{A.31}$$

The decomposition chosen by Berry and Mount [110] corresponds to a slightly different definition of the basis functions:

$$\psi^{\Rightarrow}_{z_0}(z_0) = \psi^+_{\rm WKB}(z_0) \ , \qquad \psi'^{\Rightarrow}_{z_0}(z_0) = ik_{\rm dB}(z_0)\psi^+_{\rm WKB}(z_0) \ , \tag{A.32}$$

$$\psi^{\Leftarrow}_{z_0}(z_0) = \psi^-_{\rm WKB}(z_0) \ , \qquad \psi'^{\Leftarrow}_{z_0}(z_0) = -ik_{\rm dB}(z_0)\psi^-_{\rm WKB}(z_0) \ . \tag{A.33}$$

With this definition, the basis functions have the same value as the WKB functions in z_0, so that (A.30) still holds, but their derivative is not equal to the derivative of the WKB functions.

A.2 Transfer and scattering matrices

Hereafter we will consider a situation where the physical domain is divided into a central "interaction" region and "asymptotic" regions on its left and right. For the moment, this division is rather arbitrary, we will see how it can be given physical meaning later on. We choose a reference point z_L (resp. z_R) and an associated basis $\psi^\pm_L$ (resp. $\psi^\pm_R$) in the left (resp. right) asymptotic region. In a very broad sense, the transfer matrix is the operator which performs the change between these two bases.

Let $a^L_\pm$, $a^R_\pm$ be the coefficients of a generic solution ψ_a in the left and right bases respectively and $|A_L]$, $|A_R]$ the associated vectors, the transfer matrix $\mathcal{T}$ is defined by

$$|A_R] = \mathcal{T}|A_L] \ . \tag{A.34}$$

It follows from (A.20) that the transfer matrix has the following expression in terms of the Wronskians of the basis functions:

$$\mathcal{T} = \frac{-1}{\mathcal{W}(\psi^+_L, \psi^-_L)} J \begin{pmatrix} \mathcal{W}(\psi^+_L, \psi^+_R) & \mathcal{W}(\psi^+_L, \psi^-_R) \\ \mathcal{W}(\psi^-_L, \psi^+_R) & \mathcal{W}(\psi^-_L, \psi^-_R) \end{pmatrix} \ . \tag{A.35}$$

Instead of associating a basis to each side of the interaction region, we can pair the wavefunctions $\psi^\pm_L$, $\psi^\pm_R$ depending on whether they are "propagating" towards the interaction region or away from it. At this point, the notion of propagation is purely conventional and we associate the plus (resp. minus) sign to "propagation" towards the right (resp. left). We therefore make the following identifications:

$$\psi^+_L \equiv \psi^+_{\rm in} \ , \qquad a^L_+ \equiv a^{\rm in}_+ \ , \tag{A.36}$$

$$\psi^+_R \equiv \psi^+_{\rm out} \ , \qquad a^R_+ \equiv a^{\rm out}_+ \ , \tag{A.37}$$

$$\psi^-_L \equiv \psi^-_{\rm out} \ , \qquad a^L_- \equiv a^{\rm out}_- \ , \tag{A.38}$$

$$\psi^-_R \equiv \psi^-_{\rm in} \ , \qquad a^R_- \equiv a^{\rm in}_- \ , \tag{A.39}$$

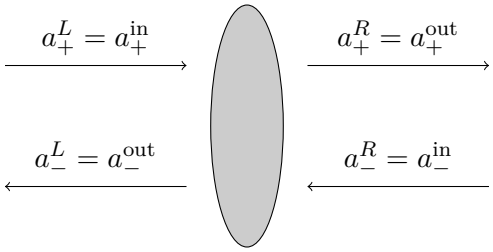

Figure 1: Diagram showing the amplitudes of leftward and rightward traveling waves on either side of the scattering region (depicted by the gray ellipse).

as sketched in figure 1.

The scattering matrix $\mathcal{S}$ relates the coefficients $|A_{\text{out}}]$ of a generic wavefunction ψ_a in the "out" basis $\psi_\pm^{\text{out}}$ to the coefficients $|A_{\text{in}}]$ of ψ_a in the "in" basis $\psi_\pm^{\text{in}}$:

$$|A_{\text{out}}] = \mathcal{S}|A_{\text{in}}] \ . \tag{A.40}$$

Its expression in terms of Wronskians follows from (A.20):

$$\mathcal{S} = \frac{-1}{\mathcal{W}(\psi_{\text{out}}^+, \psi_{\text{out}}^-)} J \begin{pmatrix} \mathcal{W}(\psi_{\text{out}}^+, \psi_{\text{in}}^+) & \mathcal{W}(\psi_{\text{out}}^+, \psi_{\text{in}}^-) \\ \mathcal{W}(\psi_{\text{out}}^-, \psi_{\text{in}}^+) & \mathcal{W}(\psi_{\text{out}}^-, \psi_{\text{in}}^-) \end{pmatrix} \ . \tag{A.41}$$

The matrices $\mathcal{S}$ and $\mathcal{T}$ contain the same information. The link between the two can be made explicit by rewriting the identifications (A.36) with the help of the projection matrices

$$\Pi^+ \equiv \begin{pmatrix} 1 & 0 \\ 0 & 0 \end{pmatrix} \qquad \text{and} \qquad \Pi^- \equiv \begin{pmatrix} 0 & 0 \\ 0 & 1 \end{pmatrix} \ . \tag{A.42}$$

We obtain:

$$\Pi^+|A_{\text{out}}] = \Pi^+|A_R] \ , \qquad \Pi^+|A_{\text{in}}] = \Pi^+|A_L] \ , \tag{A.43}$$

$$\Pi^-|A_{\text{out}}] = \Pi^-|A_L] \ , \qquad \Pi^-|A_{\text{in}}] = \Pi^-|A_R] \ . \tag{A.44}$$

$$\tag{A.45}$$

Summing these relations by pairs and using the fact that $\Pi^+ + \Pi^- = \mathcal{I}$, we find that

$$|A_{\text{out}}] = \left(\Pi^+\mathcal{T} + \Pi^-\right)|A_L] \ , \tag{A.46}$$

$$|A_{\text{in}}] = \left(\Pi^-\mathcal{T} + \Pi^+\right)|A_L] \ , \tag{A.47}$$

so that

$$\mathcal{S} = \left(\Pi^+\mathcal{T} + \Pi^-\right)\left(\Pi^-\mathcal{T} + \Pi^+\right)^{-1} \ . \tag{A.48}$$

Similarly, we find that

$$\mathcal{T} = \left(\Pi^+\mathcal{S} + \Pi^-\right)\left(\Pi^-\mathcal{S} + \Pi^+\right)^{-1} \ . \tag{A.49}$$

If we introduce the following notation for the matrix elements of $\mathcal{S}$ and $\mathcal{T}$,

$$\mathcal{S} \equiv \begin{pmatrix} \bar{t} & r \\ \bar{r} & t \end{pmatrix} \ , \qquad \mathcal{T} \equiv \begin{pmatrix} a & b \\ c & d \end{pmatrix} \ , \tag{A.50}$$

these relations yield:

$$\mathcal{S} = \frac{1}{d}\begin{pmatrix} \det\mathcal{T} & b \\ -c & 1 \end{pmatrix} \ , \qquad \mathcal{T} = \frac{1}{t}\begin{pmatrix} \det\mathcal{S} & r \\ -\bar{r} & 1 \end{pmatrix} \ . \tag{A.51}$$

Hitherto, the discussion has remained rather abstract. To give physical meaning to the transfer and scattering matrices, we must choose appropriate basis functions and define the "asymptotic regions" more precisely. In the present thesis, we ask that WKB approximation be valid in the asymptotic regions, i.e. that the badlands function $Q(z)$ vanish there (see section I.2.b). The natural basis wavefunctions are then those who match WKB wavefunctions on either side:

$$\psi_L^+ \equiv \psi_{\text{in}}^+ \equiv \psi_{z_L}^{\rightarrow} \ , \tag{A.52}$$
$$\psi_R^+ \equiv \psi_{\text{out}}^+ \equiv \psi_{z_R}^{\rightarrow} \ , \tag{A.53}$$
$$\psi_L^- \equiv \psi_{\text{out}}^- \equiv \psi_{z_L}^{\leftarrow} \ , \tag{A.54}$$
$$\psi_R^- \equiv \psi_{\text{in}}^- \equiv \psi_{z_R}^{\leftarrow} \ , \tag{A.55}$$

with the notations of the previous section. Since the WKB approximation is valid asymptotically, these definitions do not depend on the choice of the reference points z_L and z_R within each asymptotic region. Moreover, the direction of propagation of these waves is well defined in the asymptotic regions. With this choice, the scattering matrix effectively relates waves that are traveling towards the interaction region and away from it and its matrix elements are reflection and transmission coefficients.

A.3 Unitarity and reciprocity

The scattering and transfer matrices have specific mathematical properties which follow from current conservation and time reversal symmetry.

If $\psi^+ = (\psi^-)^*$, then the Wronskian $w = \mathcal{W}(\psi^+, \psi^-)$ is pure imaginary and the current associated with

$$\psi_a(z) = a_+\psi^+(z) + a_-\psi^-(z) \tag{A.56}$$

has the following simple expression:

$$j(\psi_a) = \frac{\hbar\varpi}{m}(|a_+|^2 - |a_-|^2) \ , \qquad \varpi \equiv iw/2 \in \mathbb{R} \ . \tag{A.57}$$

Since the current is conserved, we deduce

$$|a_+^L|^2 - |a_-^L|^2 = |a_+^R|^2 - |a_-^R|^2 \ , \tag{A.58}$$

which we rewrite

$$|a_+^{\rm out}|^2 - |a_-^{\rm out}|^2 = |a_+^{\rm in}|^2 - |a_-^{\rm in}|^2 \ , \tag{A.59}$$

or in matrix notation:

$$(|A_{\rm out}])^\dagger \, |A_{\rm out}] = (|A_{\rm in}])^\dagger \, |A_{\rm in}] \ . \tag{A.60}$$

We inject the definition of the scattering matrix:

$$(\mathcal{S}|A_{\rm in}])^\dagger \, \mathcal{S}|A_{\rm in}] = (|A_{\rm in}])^\dagger \, \mathcal{S}^\dagger \mathcal{S}|A_{\rm in}] = (|A_{\rm in}])^\dagger \, |A_{\rm in}] \ . \tag{A.61}$$

This being true for all $|A_{\rm in}]$, we deduce that $\mathcal{S}$ is unitary:

$$\mathcal{S}^\dagger \mathcal{S} = \mathcal{I} \ . \tag{A.62}$$

The transmission and reflection amplitudes thus obey

$$|r|^2 + |t|^2 = |\bar{r}|^2 + |\bar{t}|^2 = 1 \ , \tag{A.63}$$

$$\bar{t}^* r + \bar{r}^* t = 0 \ . \tag{A.64}$$

The time-dependent Schrödinger equation (I.12) can be time-reversed by taking its complex conjugate. For the time-independent equation, this means that if $\psi(z)$ is a solution, so is its complex conjugate $\psi^*(z)$. Complex conjugation switches the direction of the WKB waves: $(\psi^{\pm}_{\rm WKB})^* = \psi^{\mp}_{\rm WKB}$. Therefore equation (A.40) should also hold after the substitutions $a_+^{\rm in} \leftrightarrow (a_-^{\rm out})^*$ and $a_-^{\rm in} \leftrightarrow (a_+^{\rm out})^*$:

$$\begin{pmatrix} (a_-^{\rm in})^* \\ (a_+^{\rm in})^* \end{pmatrix} \equiv \mathcal{S} \begin{pmatrix} (a_-^{\rm out})^* \\ (a_+^{\rm out})^* \end{pmatrix} \tag{A.65}$$

If we introduce the matrix

$$M = \begin{pmatrix} 0 & 1 \\ 1 & 0 \end{pmatrix} \tag{A.66}$$

which exchanges the top and bottom elements of a vector, we find that

$$\mathcal{S}^* = M \mathcal{S}^{-1} M \ , \tag{A.67}$$

so that

$$t = t^* \det \mathcal{S} \ , \qquad \bar{t} = \bar{t}^* \det \mathcal{S} \ , \tag{A.68}$$

$$r = -\det \mathcal{S} \bar{r}^* \ , \qquad \bar{r} = -\det \mathcal{S} r^* \ . \tag{A.69}$$

In particular, it follows that

$$|\det \mathcal{S}|^2 = |r\bar{r} + t\bar{t}|^2 = 1 \ , \qquad \bar{r} = -tr^*/t^* \ . \tag{A.70}$$

These are known as reciprocity relations.

Finally, if we combine unitarity and reciprocity, we find that

$$t = \bar{t} \ , \quad \text{or equivalently,} \quad \det \mathcal{T} = 1 \ . \tag{A.71}$$

These properties can also be proven directly from the expression of the $\mathcal{S}$ and $\mathcal{T}$ matrices in terms of Wronskians.

A.4 Sturm-Liouville equations and their transformations

Sturm-Liouville equations are second-order linear differential equations of the form

$$\frac{\mathrm{d}}{\mathrm{d}x}\left(p(x)\frac{\mathrm{d}y}{\mathrm{d}x}(x)\right) + q(x)y(x) = 0 \ . \tag{A.72}$$

In the special case where $p(x) = 1$, the equation is said to be in Liouville normal form:

$$y''(x) + q(x)y(x) = 0 \ . \tag{A.73}$$

This is for example the case of the (time-independent) Schrödinger equation (A.1).

The Wronskian of two solutions of a Sturm-Liouville equation is defined as previously:

$$\mathcal{W}[y_1, y_2](x) \equiv y_1(x)y_2'(x) - y_1'(x)y_2(x) \ , \tag{A.74}$$

but we have adapted the notation to account for the fact that the Wronskian is not constant in general. Indeed, by taking its derivative we find that

$$\frac{\mathrm{d}}{\mathrm{d}x}\mathcal{W}[y_1, y_2](x) = -\frac{p'(x)}{p(x)}\mathcal{W}[y_1, y_2](x) \ , \tag{A.75}$$

so that the product $p(x)\mathcal{W}[y_1, y_2](x)$ is a constant. In particular, if the equation is in Liouville normal form, $p(x) = 1$ and so the Wronskian is constant.

We consider two elementary transformations which leave the form of the Sturm-Liouville equation (A.72) unchanged:

- A (spatially dependent) rescaling of the dependent variable: $Y(x) \equiv y(x)/\alpha(x)$. The equation becomes

$$\frac{\mathrm{d}}{\mathrm{d}x}\left(P(x)\frac{\mathrm{d}Y}{\mathrm{d}x}(x)\right) + Q(x)Y(x) = 0 \ , \tag{A.76}$$

$$P(x) = \alpha(x)^2 p(x) \ , \qquad Q(x) = \alpha(x)^2\left(q(x) + p(x)\frac{\alpha''(x)}{\alpha(x)} + p'(x)\frac{\alpha'(x)}{\alpha(x)}\right) \ . \tag{A.77}$$

- A change of the independent variable: $\overline{y}(\overline{x}(x)) \equiv y(x)$, with $\overline{x}(x)$ a smooth invertible function such that $\overline{x}'(x) > 0$. In this we obtain

$$\frac{\mathrm{d}}{\mathrm{d}\overline{x}}\left(\overline{p}(\overline{x})\frac{\mathrm{d}\overline{y}}{\mathrm{d}\overline{x}}(\overline{x})\right) + \overline{q}(\overline{x})\overline{y}(\overline{x}) = 0 \ , \tag{A.78}$$

$$\overline{p}(\overline{x}) = \overline{x}'(x)p(x) \ , \qquad \overline{q}(\overline{x}) = q(x)/\overline{x}'(x) \ . \tag{A.79}$$

Note that the product $p(x)\mathcal{W}[y_1, y_2](x)$ is invariant under both operations:

$$p(x)\mathcal{W}[y_1, y_2](x) = P(x)\mathcal{W}[Y_1, Y_2](x) = \overline{p}(\overline{x})\mathcal{W}[\overline{y}_1, \overline{y}_2](\overline{x}) \ . \tag{A.80}$$

We now apply both transformations successively: $\overline{Y}(\overline{x}(x)) \equiv Y(x) = y(x)/\alpha(x)$. We obtain

$$\frac{\mathrm{d}}{\mathrm{d}\overline{x}}\left(\overline{P}(\overline{x})\frac{\mathrm{d}\overline{Y}}{\mathrm{d}\overline{x}}(\overline{x})\right) + \overline{Q}(\overline{x})\overline{Y}(\overline{x}) = 0 \ , \tag{A.81}$$

$$\overline{P}(\overline{x}) = \overline{x}'(x)P(x) = \overline{x}'(x)\alpha(x)^2 p(x) \tag{A.82}$$

$$\overline{Q}(\overline{x}) = \frac{Q(x)}{\overline{x}'(x)} = \frac{\alpha(x)^2}{\overline{x}'(x)}\left(q(x) + p(x)\frac{\alpha''(x)}{\alpha(x)} + p'(x)\frac{\alpha'(x)}{\alpha(x)}\right) \ . \tag{A.83}$$

Liouville transformations are defined by $\overline{P}(\overline{x}) = p(x)$. Therefore they satisfy

$$\alpha(x) = \frac{1}{\sqrt{\overline{x}'(x)}} \ , \qquad \overline{Y}(\overline{x}(x)) = \sqrt{\overline{x}'(x)}y(x) \ , \tag{A.84}$$

$$\overline{Q}(\overline{x}) = \frac{1}{\overline{x}'(x)^2}\left(q(x) - \frac{p(x)}{2}\{\overline{x}, x\} - \frac{p'(x)}{2}\frac{\overline{x}''(x)}{\overline{x}(x)}\right) \ . \tag{A.85}$$

where

$$\{\overline{x}, x\} = \frac{\overline{x}'''(x)}{\overline{x}'(x)} - \frac{3}{2}\left(\frac{\overline{x}''(x)}{\overline{x}'(x)}\right)^2 \tag{A.86}$$

is the Schwarzian derivative of $\overline{x}$ with respect to x, which we discuss in the next section.

Since $\overline{P}(\overline{x}) = p(x)$, it follows from equation (A.80) that Liouville transformations preserve the Wronskian:

$$\mathcal{W}[\overline{Y}_1, \overline{Y}_2](\overline{x}) = \mathcal{W}[y_1, y_2](x) \ . \tag{A.87}$$

Moreover, equations in Liouville normal form remain in the same form after a Liouville transformation:

$$y''(x) + q(x)y(x) = 0 \to \overline{Y}''(\overline{x}) + \overline{Q}(\overline{x})\overline{Y}(\overline{x}) = 0 \ , \tag{A.88}$$

$$\overline{Q}(\overline{x}) = \frac{1}{\overline{x}'(x)^2}\left(q(x) - \frac{1}{2}\{\overline{x}, x\}\right) \ . \tag{A.89}$$

B Reflection from homogeneous potentials

Potentials of the form $V(z) = -C_n/z^n$ are said to be *homogeneous* because they obey a simple scaling property:

$$V(\alpha z) = \alpha^{-n} V(z) \ . \tag{B.1}$$

In this appendix, we consider homogeneous potentials with $n > 2$, which correspond to the typical asymptotic behavior of the Casimir-Polder potential. For example $n = 3$ corresponds to the non-retarded Van der Waals interaction, $n = 4$ to the retarded potential for a thick mirror and $n = 5$ to the retarded potential for a thin slab. For the sake of brevity, we will refer to these potentials simply as "C_n potential".

When considering the Schrödinger equation (I.14) with a homogeneous potential, the following length scales appear:

$$\frac{1}{\kappa} \equiv \frac{\hbar}{\sqrt{2mE}} \tag{B.2}$$

is the inverse of the wavevector at infinity,

$$\ell_n \equiv \left(\frac{2mC_n}{\hbar^2}\right)^{\frac{1}{n-2}} \tag{B.3}$$

measures the strength of the potential, and

$$\sigma_n \equiv \left(\frac{C_n}{E}\right)^{1/n} \tag{B.4}$$

is the distance at which $E = |V_n|$.

The Schrödinger equation can thus be written

$$\psi''(z) + \left(\kappa^2 + \frac{\ell_n^{n-2}}{z^n}\right)\psi(z) = 0 \ . \tag{B.5}$$

B.1 Scattering lengths

We start by considering the case of a particle near threshold, that is, the limit where the inverse wavevector $1/\kappa$ goes to infinity:

$$\psi''(z) + \frac{\ell_n^{n-2}}{z^n}\psi(z) \simeq 0 \tag{B.6}$$

This equation can be solved exactly [119, 231] by changing the coordinate and rescaling the wavefunction[3]:

$$s(z) \equiv \frac{2}{n-2}\left(\frac{\ell_n}{z}\right)^{\frac{n}{2}-1} \ , \tag{B.7}$$

$$\psi(z) \equiv \sqrt{z}\ \chi(s) \ . \tag{B.8}$$

[3] This is *not* a Liouville transformation.

We then obtain the Bessel equation [1]

$$s^2\chi''(s) + s\chi'(s) + (s^2 - \nu^2)\chi(s) = 0, \qquad \nu \equiv \frac{1}{n-2} \tag{B.9}$$

A general solution of that equation can be written as a linear combination of Hankel functions $H_\nu^{(1)}(s)$ and $H_\nu^{(2)}(s)$, so the general solution of the Schrödinger equation is:

$$\psi(z) = \sqrt{z}\left(AH_\nu^{(1)}(s) + BH_\nu^{(2)}(s)\right) \tag{B.10}$$

As we approach the surface, s goes to infinity and the Hankel functions have the following asymptotic behavior:

$$H_\nu^{(1),(2)}(s) \underset{s\to\infty}{\simeq} \sqrt{\frac{2}{\pi s}} \exp\left(\pm i\left(s - \frac{\nu\pi}{2} - \frac{\pi}{4}\right)\right) \ . \tag{B.11}$$

Recognizing that $s = -\phi_{\rm dB}(z) + \text{constant}$, we see that the term proportional to $H^{(1)}$ matches the incoming WKB wave near the surface, while the term proportional to $H^{(2)}$ matches the outgoing WKB wave. A fully absorbing boundary condition on the surface thus corresponds to $B = 0$.

In this case, the long distance behavior of the wavefunction is obtained from the $s \to 0$ expansion of the first Hankel function:

$$H_\nu^{(1)}(s) \underset{s\to 0}{\simeq} \begin{cases} -\dfrac{2i}{\pi s} + \dfrac{\pi + 2i(\gamma + \ln(s/2) - 1/2)}{2\pi} s & \text{if} \quad \nu = 1 \ , \\ -\dfrac{i}{\sin(\pi\nu)}\left(\dfrac{(s/2)^{-\nu}}{\Gamma(1-\nu)} - e^{-i\pi\nu}\dfrac{(s/2)^{\nu}}{\Gamma(1+\nu)}\right) & \text{if} \quad \nu < 1 \ . \end{cases} \tag{B.12}$$

The scattering length a can be read off by comparison with

$$\psi(z) \underset{\ell_n \ll z \ll \kappa^{-1}}{\simeq} \mathcal{N}\left(1 - \frac{z}{a}\right) \ . \tag{B.13}$$

We find

$$a = \begin{cases} \infty - i\pi\ell_3 & \text{if} \quad n = 3 \ , \\ \exp\left(\dfrac{-i\pi - 2\ln(n-2)}{n-2}\right)\dfrac{\Gamma(1 - 1/(n-2))}{\Gamma(1 + 1/(n-2))}\ell_n & \text{if} \quad n > 3 \ . \end{cases} \tag{B.14}$$

In table 2 we give the real and imaginary parts of the scattering length for $n = 3, 4, 5$.

n	3	4	5
$\mathrm{Re}(a)$	∞	0	$0.364506\ \ell_5$
$\mathrm{Im}(a)$	$-\pi\ell_3$	$-\ell_4$	$-0.631342\ \ell_5$

Table 2: Real and imaginary parts of the scattering length for homogeneous potentials.

The exact scattering length can also be calculated for the model potential

$$V(z) = \left(z^3/C_3 + z^4/C_4\right)^{-1} \tag{B.15}$$

which reproduces the short- and long-range limits of the Casimir-Polder potential near a thick mirror [119, 125]. In that case the zero-energy wavefunction is

$$\psi(z) \propto \sqrt{z\left(z + \frac{C_4}{C_3}\right)} H_1^{(1)}\left(2\sqrt{\ell_3\left(\frac{1}{z} + \frac{C_3}{C_4}\right)}\right) \tag{B.16}$$

and the scattering length is

$$a = -\frac{C_4}{2C_3}\left(1 + \eta\frac{H_1'^{(1)}(\eta)}{H_1^{(1)}(\eta)}\right), \qquad \eta = \frac{2C_3}{\hbar}\sqrt{\frac{2m}{C_4}} = 2\frac{\ell_3}{\ell_4} \tag{B.17}$$

In particular,

$$\mathrm{Im}(a) = -\frac{C_4}{\pi C_3 |H_1^{(1)}(\eta)|^2} \tag{B.18}$$

When $\eta \ll 1$, i.e. when ℓ_3 is small compared to ℓ_4, the C_3 potential is dominant and $\mathrm{Im}(a) \to -\pi\ell_3$, whereas for large values of η the C_4 regime dominates and $\mathrm{Im}(a) \to -\ell_4$.

B.2 Liouville transformation to the WKB coordinate

For the C_n potential, the WKB wavevector and phase are

$$k_{\mathrm{dB}}(z) = \kappa\sqrt{1 + \frac{1}{x^n}}\,, \quad x \equiv \frac{z}{\sigma_n}\,, \tag{B.19}$$

$$\phi_{\mathrm{dB}}(z) = \kappa\sigma_n \int_{x_0}^{x} \sqrt{1 + \frac{1}{x'^n}}\,\mathrm{d}x'\,, \tag{B.20}$$

where x_0 is chosen to enforce

$$\phi_{\mathrm{dB}}(z) - \kappa z \underset{z\to\infty}{\longrightarrow} 0 \tag{B.21}$$

For $n > 2$, we ϕ_{dB} can be expressed in terms of the hypergeometric function F, defined as in [1]:

$$\phi_{\mathrm{dB}} = \frac{nx\kappa\sigma_n}{n-2}\left(F\left(\frac{1}{2}, \frac{-1}{n}; 1 - \frac{1}{n}; \frac{-1}{x^n}\right) - \frac{2}{n}\sqrt{1 + \frac{1}{x^n}}\right)\,. \tag{B.22}$$

The badlands function has the following expression:

$$Q(z) = \frac{nx^{n-2}}{(\kappa\sigma_n)^2}\frac{4 - n + 4(1+n)x^n}{16\,(1+x^n)^3}\,. \tag{B.23}$$

It is a peaked function which reaches its maximum at

$$x_m = \left(\frac{5n^2 - 3n - 8 + \sqrt{3(7n^4 - 6n^3 - 13n^2)}}{4(n^2 + 3n + 2)} \right)^{1/n} . \tag{B.24}$$

Since Q scales as $(\kappa\sigma_n)^{-2}$, we define the WKB coordinate as

$$\boldsymbol{z} \equiv \frac{\phi_{\mathrm{dB}}(z)}{\kappa\sigma_n} . \tag{B.25}$$

The Liouville-transformed equation is then

$$\boldsymbol{\psi}''(\boldsymbol{z}) + \Big((\kappa\sigma_n)^2 - \boldsymbol{V}_n(\boldsymbol{z}) \Big) \boldsymbol{\psi}(\boldsymbol{z}) = 0 , \tag{B.26}$$

where the potential functions $\boldsymbol{V}_n(\boldsymbol{z})$ do not depend on any other parameter than n and have the following parametric expression:

$$\boldsymbol{z} = \frac{nx}{n-2} \left(F\left(\frac{1}{2}, \frac{-1}{n}; 1 - \frac{1}{n}; \frac{-1}{x^n} \right) - \frac{2}{n} \sqrt{1 + \frac{1}{x^n}} \right) , \tag{B.27}$$

$$\boldsymbol{V}_n = (nx^{n-2}) \frac{4 - n + 4(1+n)x^n}{16\,(1+x^n)^3} , \qquad x > 0 . \tag{B.28}$$

The universal functions $\boldsymbol{V}_n(\boldsymbol{z})$ are drawn on figure 2 for the cases $n = 3, 4, 5$.

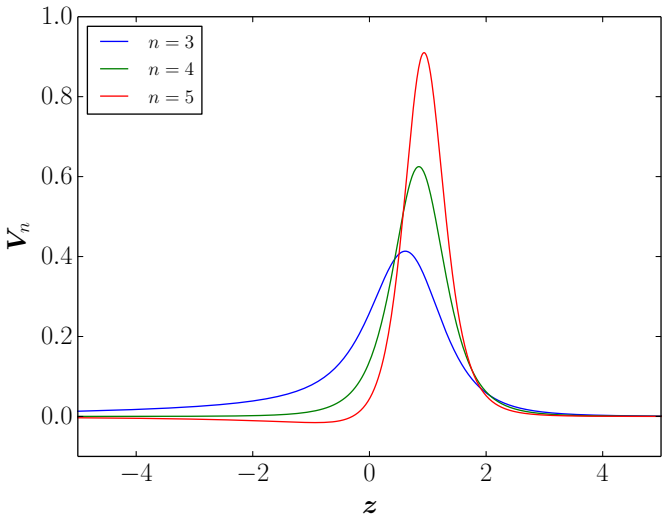

Figure 2: Plot of the universal functions $\boldsymbol{V}_n(\boldsymbol{z})$ for $n = 3, 4, 5$ (smallest to tallest).

The integrals of $\boldsymbol{V}_n(\boldsymbol{z})$ over the real axis are real numbers depending only on n and they can be expressed in terms of the Gamma function:

$$\int_{-\infty}^{\infty} \boldsymbol{V}_n(\boldsymbol{z})\, \mathrm{d}\boldsymbol{z} = \frac{n\sqrt{\pi}\Gamma\left(2+\frac{1}{n}\right)\sec\left(\frac{\pi}{n}\right)}{12\Gamma\left(\frac{1}{2}+\frac{1}{n}\right)} \ . \tag{B.29}$$

B.3 Exact solution for the C_4 potential

The Schrödinger equation with a C_4 potential admits an exact solution in terms of Mathieu functions [232–234]. From a practical point of view, this analytical method is not superior to a numerical resolution of the Schrödinger equation for the potential $V_4(z)$ or $\boldsymbol{V}_4(\boldsymbol{z})$, nevertheless we feel it is worth describing here.

The derivation presented here follows the work of [233] and uses results from [1, 235]. We start with the Schrödinger equation

$$\psi''(z) + \left(\kappa^2 - \frac{\ell^2}{z^4}\right)\psi(z) = 0 \ , \tag{B.30}$$

where we have dropped the index "4" in order to recover the notation of section II.3.g. We first perform a Liouville transformation:

$$z \to \tilde{z}(z) = \ln\frac{z}{\sigma} \ , \quad \psi(z) \to \tilde{\psi}(\tilde{z}) = \frac{\psi(z)}{\sqrt{z}} \ . \tag{B.31}$$

which transforms the equation (B.30) into the *modified Mathieu equation*:

$$\tilde{\psi}''(\tilde{z}) + (-a + 2q\cosh(2\tilde{z}))\,\tilde{\psi}(\tilde{z}) = 0 \ , \tag{B.32}$$

where $a \equiv \frac{1}{4}$ while $q \equiv \sqrt{\kappa\ell}$ is the only remaining parameter.

A pair of solutions to this equation can be written as series involving products of Bessel functions:

$$\tilde{\psi}^{(\pm)}(\tilde{z}) = \sum_{n=-\infty}^{\infty} (-1)^n A_n^{(\tau)} J_{\pm(n+\tau)}(\sqrt{q}e^{\tilde{z}}) J_{\pm n}(\sqrt{q}e^{-\tilde{z}}) \ . \tag{B.33}$$

Here τ is a complex parameter yet to be determined, known as the *Mathieu characteristic exponent*. The coefficients $A_n^{(\tau)}$ obey the following recurrence relation:

$$\left((\tau+2n)^2 - a\right) A_n^{(\tau)} + q\left(A_{n+1}^{(\tau)} + A_{n-1}^{(\tau)}\right) = 0 \ . \tag{B.34}$$

The infinite determinant associated with this system of equations must be zero for a non trivial solution to exist. Therefore τ must obey the following condition [236]:

$$\sin^2\left(\frac{\pi\tau}{2}\right) = \Delta\sin^2\left(\frac{\pi\sqrt{a}}{2}\right) = \frac{\Delta}{2} \tag{B.35}$$

where Δ is an infinite and convergent determinant. In practice, Δ can be approximated by the successive elements of the sequence Δ_n, defined by [233]:

$$\Delta_n \equiv Y_n(2X_n - Y_n) \ , \tag{B.36}$$

$$X_n \equiv X_{n-1} - Z_n Z_{n-1} X_{n-2} \ , \quad n \geq 1 \ , \qquad X_0 = X_{-1} \equiv 1 \ , \tag{B.37}$$

$$B_n \equiv B_{n-1} - Z_n Z_{n-1} Y_{n-2} \ , \quad n \geq 2 \ , \qquad Y_1 = Y_0 \equiv 1 \ , \tag{B.38}$$

$$Z_n \equiv \frac{q}{4n^2 - a} \ . \tag{B.39}$$

Alternatively, Mathematica provides a function `MathieuCharacteristicExponent[a,q]` which returns the value of τ.

The recurrence relation on the A_n allows us to write the ratios $A_n^{(\tau)}/A_{n-1}^{(\tau)}$ and $A_{-n}^{(\tau)}/A_{-(n-1)}^{(\tau)}$ as continued fractions:

$$\frac{A_n}{A_{n-1}} = \frac{-q}{(\tau + 2n)^2 - a + qA_{n+1}/A_n} \ , \tag{B.40}$$

$$\frac{A_{-n}}{A_{-(n-1)}} = \frac{-q}{(\tau + 2n)^2 - a + qA_{-(n+1)}/A_{-n}} \ . \tag{B.41}$$

These ratios go to 0 when $|n|$ increases so that we can truncate the continued fractions to obtain numerical values for $A_n^{(\tau)}$ (we fix the normalization by setting $A_0^{(\tau)} = 1$).

As a result of the invariance of equation (B.32) under parity $\tilde{z} \to -\tilde{z}$ (which is the symmetry discussed in II.3.g), $\tilde{\psi}^{(\pm)}(-\tilde{z})$ are also solutions, and one can show that:

$$\tilde{\psi}^{(\pm)}(\tilde{z}) = e^{\mp\sigma}\tilde{\psi}^{(\mp)}(-\tilde{z}), \quad \varsigma \equiv \ln \frac{\tilde{\psi}^{(-)}(0)}{\tilde{\psi}^{(+)}(0)}. \tag{B.42}$$

Using known results for the Bessel functions:

$$J_\nu(x) \underset{x\to\infty}{\simeq} \sqrt{\frac{2}{\pi x}} \cos\left(x - \frac{\nu\pi}{2} - \frac{\pi}{4}\right) \ , \quad J_n(0) = \delta_{n,0} \ , \tag{B.43}$$

we deduce the asymptotic behaviors:

$$\tilde{\psi}^{(\pm)}(\tilde{z}) \underset{\tilde{z}\to\infty}{\simeq} \sqrt{\frac{2}{\pi\sqrt{q}e^{\tilde{z}}}} \cos\left(\sqrt{q}e^{\tilde{z}} \mp \frac{\pi\tau}{2} - \frac{\pi}{4}\right) \ , \tag{B.44}$$

$$\tilde{\psi}^{(\pm)}(\tilde{z}) \underset{\tilde{z}\to-\infty}{\simeq} e^{\mp\varsigma}\sqrt{\frac{2}{\pi\sqrt{q}e^{-\tilde{z}}}} \cos\left(\sqrt{q}e^{-\tilde{z}} \pm \frac{\pi\tau}{2} - \frac{\pi}{4}\right) \ . \tag{B.45}$$

We now consider the solution $\psi_L^-(z)$ of the Schrödinger equation which matches an outgoing WKB wave near the surface. From equation (II.99), it follows that

$$\phi_{\mathrm{dB}}(z) \underset{z\to0}{\simeq} 2\kappa\ell\boldsymbol{\sigma} - \frac{\ell}{z} \ , \qquad \boldsymbol{\sigma} = \frac{\Gamma(3/4)^2}{\sqrt{\pi}} \ , \tag{B.46}$$

so that

$$\psi_L^-(z) \underset{z\to 0}{\simeq} \frac{tz}{\sqrt{\ell}} \exp\left(-i\left(2\kappa\ell\boldsymbol{\sigma} - \frac{\ell}{z}\right)\right) , \tag{B.47}$$

Far from the surface $\psi_L^-(z)$ takes the usual asymptotic form

$$\psi_L^-(z) \underset{z\to\infty}{\simeq} \frac{e^{-i\kappa z} + re^{i\kappa z}}{\sqrt{\kappa}} . \tag{B.48}$$

Matching the asymptotic form (B.47) to (B.45) and (B.44) to (B.48), we obtain the reflection and transmission amplitudes:

$$r = -i\frac{\sinh(\varsigma)}{\sinh(\varsigma + i\pi\tau)} , \qquad t = \frac{\sin(\pi\tau)e^{2i\kappa\ell\boldsymbol{\sigma}}}{\sinh(\varsigma + i\pi\tau)} . \tag{B.49}$$

We can easily check that $|r|^2 + |t|^2 = 1$. Note that these coefficients depend only on the parameter $\kappa\ell = 2m\hbar^{-2}\sqrt{EC_4}$. When $\kappa\ell$ goes to zero, r behaves as $(\kappa\ell - 1)/(\kappa\ell + 1)$, which agrees with the scattering length found in B.1 $a = -i\ell = -i\hbar^{-1}\sqrt{2mC_4}$. The quantum reflection probability $R = |r|^2$ is drawn on figure 3.

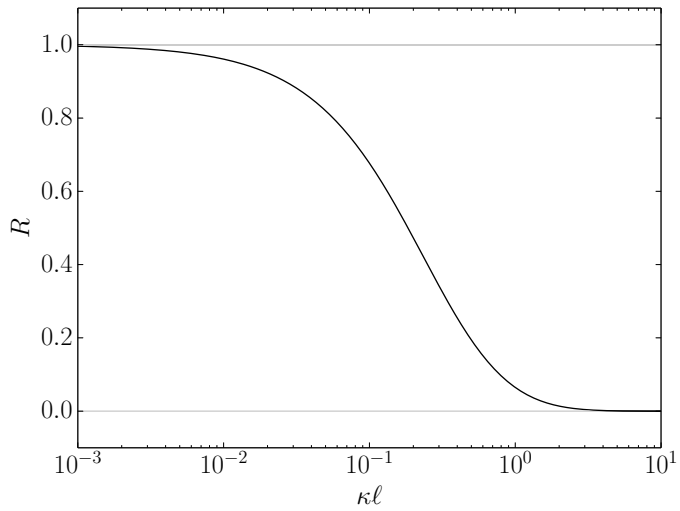

Figure 3: Quantum reflection probability R calculated for the C_4 model and shown as a function of the dimensionless parameter $\kappa\ell$.

C Airy functions

The Airy function was introduced by Airy in 1838 to describe optical caustics such as rainbows [237, 238]. It is a solution to the Airy equation:

$$y''(x) - xy(x) = 0 . \tag{C.1}$$

This equation appears in many areas of physics, in particular in the study of stationary quantum states in a uniform field (see section III.3). In this appendix, we compile useful mathematical properties of the solutions of the Airy equation. For a complete reference, we direct the reader to the NIST Handbook of Mathematical Functions [1] and to the book by Vallée and Soares [214] from which many of the following results are taken.

C.1 Definition

We can look for solutions of the Airy equation (C.1) under the form of a Laplace integral along a path $\mathcal{C}$ in the complex plane

$$f(x) \equiv \int_{\mathcal{C}} \frac{\mathrm{d}k}{2i\pi} g(k) e^{kx} \ . \tag{C.2}$$

We find that $f(x)$ is a solution of the Airy equation provided $g(k)$ obeys the first order equation

$$g'(k) + k^2 g(k) = 0 \tag{C.3}$$

and that $g(k)e^{kx}$ vanishes at the ends of $\mathcal{C}$. Therefore, solutions of equation (C.1) can be written

$$f(x) \equiv \int_{\mathcal{C}} \frac{\mathrm{d}k}{2i\pi} \exp\left(-\frac{k^3}{3} + kx\right) \tag{C.4}$$

with the extremities of $\mathcal{C}$ lying at infinity in the sectors where $k^3 > 0$. With $1, j \equiv \exp(2i\pi/3)$ and j^2 the cubic roots of unity, two independent solutions that are real on the real line are:

$$\mathrm{Ai}(x) \equiv \int_{j^2\infty}^{j\infty} \frac{\mathrm{d}k}{2i\pi} \exp\left(-\frac{k^3}{3} + kx\right) \tag{C.5}$$

$$\mathrm{Bi}(x) \equiv \int_{j\infty}^{\infty} \frac{\mathrm{d}k}{2\pi} \exp\left(-\frac{k^3}{3} + kx\right) + \int_{j^2\infty}^{\infty} \frac{\mathrm{d}k}{2\pi} \exp\left(-\frac{k^3}{3} + kx\right) \tag{C.6}$$

$$= ij^2 \,\mathrm{Ai}(j^2 x) - ij \,\mathrm{Ai}(jx) \tag{C.7}$$

The corresponding integration contours are shown in figure 4.

For a real x, one can deform the paths to run along the real and imaginary axes and obtain:

$$\mathrm{Ai}(x) = \int_{-\infty}^{\infty} \frac{\mathrm{d}k}{2\pi} \exp\left(i\frac{k^3}{3} + ikx\right) \tag{C.8}$$

$$= \frac{1}{\pi} \int_0^{\infty} \mathrm{d}k \cos\left(\frac{k^3}{3} + kx\right) \ . \tag{C.9}$$

$$\mathrm{Bi}(x) = \frac{1}{\pi} \int_0^{\infty} \mathrm{d}k \left(\exp\left(-\frac{k^3}{3} + kx\right) + \sin\left(\frac{k^3}{3} + kx\right)\right) \ . \tag{C.10}$$

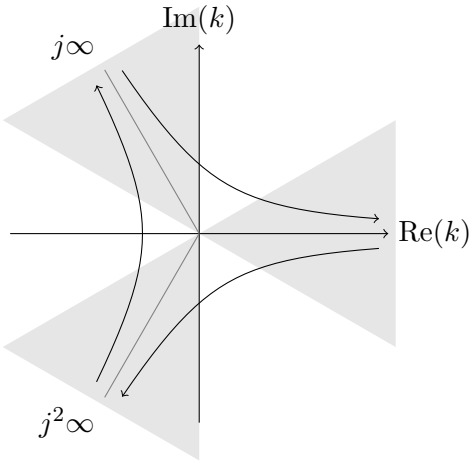

Figure 4: Integration contours used in the definition of the Airy functions.

Finally, the Wronskian of the two Airy functions is

$$\mathcal{W}\left(\mathrm{Ai},\mathrm{Bi}\right) = \frac{1}{\pi}\ . \tag{C.11}$$

C.2 Asymptotic behavior and zeros

For the sake of completeness, we recall the asymptotic behavior of the Airy functions, already discussed in section III.3:

$$\mathrm{Ai}(x) \underset{x\to\infty}{\simeq} \frac{1}{2\sqrt{\pi}\,x^{1/4}} \exp\left(-\frac{2}{3}x^{3/2}\right) \tag{C.12}$$

$$\mathrm{Bi}(x) \underset{x\to\infty}{\simeq} \frac{1}{2\sqrt{\pi}\,x^{1/4}} \exp\left(\frac{2}{3}x^{3/2}\right) \tag{C.13}$$

$$\mathrm{Ai}(-x) \underset{x\to\infty}{\simeq} \frac{1}{\sqrt{\pi}x^{1/4}} \sin\left(\frac{2}{3}x^{3/2}+\frac{\pi}{4}\right) \tag{C.14}$$

$$\mathrm{Bi}(-x) \underset{x\to\infty}{\simeq} \frac{1}{\sqrt{\pi}x^{1/4}} \cos\left(\frac{2}{3}x^{3/2}+\frac{\pi}{4}\right) \tag{C.15}$$

We deduce the following approximate expression for the zeros of the Airy function:

$$\mathrm{Ai}(-a_n) = 0\ , \qquad n\in\mathbb{N}\ , a_n \underset{n\to\infty}{\simeq} \left(\frac{3\pi}{2}\left(n-\frac{1}{4}\right)\right)^{2/3}\ . \tag{C.16}$$

The numerical value of the a_n and of their approximation can be found in table IV.1.

C.3 Integrals

We now list a number of integrals that are useful in calculations involving stationary states in a uniform field. In the following, $A(x)$ and $B(x)$ are arbitrary linear combinations of $\mathrm{Ai}(x)$ and $\mathrm{Bi}(x)$.

We recall the Fourier transform of the Airy function:

$$\mathrm{Ai}(x) = \int_{-\infty}^{\infty} \frac{\mathrm{d}k}{2\pi} \exp\left(i\frac{k^3}{3} + ikx\right) \ , \tag{C.17}$$

which can be generalized to

$$\int_{-\infty}^{+\infty} \frac{\mathrm{d}k}{2\pi} \exp\left[i\left(\frac{k^3}{3} + ak^2 + bk\right)\right] = \exp\left[ia\left(\frac{2a^2}{3} - b\right)\right] \mathrm{Ai}\left(b - a^2\right) \ . \tag{C.18}$$

The primitive of a product of Airy functions is particularly useful:

$$\int A(x+\beta_1)B(x+\beta_2)\ \mathrm{d}x = \begin{cases} (x+\beta)AB - A'B' & \text{if} \quad \beta_1 = \beta_2 = \beta \ , \\ \frac{1}{\beta_1 - \beta_2}\left(AB' - A'B\right) & \text{if} \quad \beta_1 \neq \beta_2 \ . \end{cases} \tag{C.19}$$

In particular we have

$$\int_{-\infty}^{+\infty} \mathrm{Ai}(x+\beta_1)\,\mathrm{Ai}(x+\beta_2)\ \mathrm{d}x = \delta(\beta_1 - \beta_2) \ , \tag{C.20}$$

$$\int_{0}^{\infty} \mathrm{Ai}(x-a_n)\,\mathrm{Ai}(x-a_m)\ \mathrm{d}x = \mathrm{Ai}'(-a_n)^2\delta_{m,n} \tag{C.21}$$

and

$$\int_{h}^{\infty} \mathrm{Ai}(x-h-a_n)\,\mathrm{Ai}(x-a_m)\ \mathrm{d}x = \frac{1}{h+a_n-a_m}\,\mathrm{Ai}'(-a_n)\,\mathrm{Ai}(h-a_m) \ . \tag{C.22}$$

The convolution product of an Airy function with a Gaussian is given by

$$\int_{-\infty}^{+\infty} \frac{e^{-y^2}}{\sqrt{\pi}}\,\mathrm{Ai}\left(\frac{x-y}{\alpha}\right)\mathrm{d}y = \exp\left(\frac{1}{4\alpha^3}\left(x + \frac{1}{24\alpha^3}\right)\right)\mathrm{Ai}\left(\frac{x}{\alpha} + \frac{1}{16\alpha^4}\right) \ . \tag{C.23}$$

The Wigner function associated with a stationary state in a linear potential can be computed using

$$\int_{-\infty}^{+\infty} \mathrm{Ai}\,(x+y)\,\mathrm{Ai}\,(x-y)\,e^{2iky}\ \mathrm{d}y = 2^{-1/3}\,\mathrm{Ai}\left(2^{2/3}\left(x+k^2\right)\right) \ . \tag{C.24}$$

C.4 Airy wavepackets

Airy functions also appear in the expression of the non-spreading, self-accelerating wavepackets discovered by Berry [239]. We start with a stationary solution of the Schrödinger equation in a linear potential (III.119) and replace the acceleration $\overline{g}$ by an arbitrary acceleration G (without loss of generality we take $E = 0$):

$$\psi(z,0) = \mathcal{N}\,\mathrm{Ai}\left(\left(\frac{2m^2G}{\hbar^2}\right)^{1/3} z\right) \ . \tag{C.25}$$

Letting this wavepacket evolve in the gravity field, we find that

$$\psi(z,t) = \mathcal{N}\,\mathrm{Ai}\left(\left(\frac{2m^2G}{\hbar^2}\right)^{1/3}\left(z - \frac{G-\overline{g}}{2}t^2\right)\right) \tag{C.26}$$

$$\times \exp\left[\frac{-i}{\hbar}\left(m(\overline{g}-G)tz + \frac{(\overline{g}-2G)(\overline{g}-G)mt^3}{6}\right)\right] \tag{C.27}$$

The wavepacket thus propagates without dispersion and with a uniform acceleration $G-\overline{g}$. This is also true in the absence of any external force ($\overline{g}=0$).

D Time dependent quantum harmonic oscillator

Quantum reflection can be interpreted as a transfer between incident and reflected waves due to spatial variations of the potential. It can thus be likened to non-adiabatic transitions between the states of a driven quantum system. In this appendix we explore the links between quantum reflection and (non-)adiabaticity by studying in detail the case of an oscillator with a time-dependent frequency.

The Hamiltonian of the system is

$$\hat{H}(t) = \frac{\hat{P}^2}{2m} + \frac{1}{2}m\omega(t)^2\hat{Z}^2 \tag{D.1}$$

and the associated time-dependent Schrödinger equation reads

$$i\hbar\frac{\partial\psi}{\partial t}(z,t) = -\frac{\hbar^2}{2m}\frac{\partial^2\psi}{\partial z^2}(z,t) + \frac{1}{2}m\omega(t)^2z^2\psi(z,t)\ . \tag{D.2}$$

The solutions to this equation can be written in terms of the classical trajectories $z_{\mathrm{cl}}(t)$ which solve the classical equation of motion

$$z''_{\mathrm{cl}}(t) + \omega(t)^2 z_{\mathrm{cl}}(t) = 0\ . \tag{D.3}$$

This classical equation is essentially identical to the time-independent Schrödinger equation describing one-dimensional scattering

$$\psi''(z) + F(z)\psi(z) = 0\ . \tag{D.4}$$

The results which we have obtained in our study of quantum reflection can thus be transposed to the time-dependent quantum harmonic oscillator. In particular we will underline the connection between quantum reflection and the parametric generation of quanta. Moreover we will investigate the effect of Liouville transformations of equation (D.3) on the quantum oscillator and establish a link with *shortcuts to adiabaticity*: choices of the function $\omega(t)$ such that the number of quanta in the system is the same in the initial and final states.

D.1 Solution in terms of classical trajectories

As mentioned earlier, the solution to the time-dependent quantum problem can be given in terms of solutions to the classical equation of motion (D.3). The derivation presented here is inspired by the work of Husimi [240].

The solution $\psi(z,t)$ of equation (D.2) given an initial state $\psi(z,0)$ is

$$\psi(z_f,t) = \int K(z_f,z_i,t)\psi(z_i,0)\ \mathrm{d}z_i\ . \tag{D.5}$$

Since the Hamiltonian is quadratic in $\hat{Z}$ and $\hat{P}$, the exact propagator $K(z_f,z_i,t)$ can be expressed in terms of Hamilton's principal function [206]:

$$K(z_f,z_i,t) = \frac{1}{\sqrt{2i\pi\hbar}}\left|\frac{\partial^2 S_{\mathrm{cl}}}{\partial z_i \partial z_f}\right|^{1/2} \exp\left(\frac{i}{\hbar}S_{\mathrm{cl}}(z_f,z_i,t)\right)\ , \tag{D.6}$$

where

$$S_{\mathrm{cl}}(z_f,z_i,t) = \int_0^t \left(\frac{1}{2}m z'_{\mathrm{cl}}(\tau)^2 - \frac{1}{2}m\omega(\tau)^2 z_{\mathrm{cl}}(\tau)^2\right)\mathrm{d}\tau \tag{D.7}$$

and $z_{\mathrm{cl}}(\tau)$ obeys the classical equation of motion (D.3) and the following boundary conditions:

$$z_{\mathrm{cl}}(0) = z_i\ , \qquad z_{\mathrm{cl}}(t) = z_f\ . \tag{D.8}$$

Using equation (D.3), we can write

$$S_{\mathrm{cl}}(z_f,z_i,t) = \int_0^t \frac{\mathrm{d}}{\mathrm{d}\tau}\left(\frac{1}{2}m z'_{\mathrm{cl}}(\tau) z_{\mathrm{cl}}(\tau)\right)\mathrm{d}\tau \tag{D.9}$$

$$= \frac{1}{2}m\left(z'_{\mathrm{cl}}(t)z_{\mathrm{cl}}(t) - z'_{\mathrm{cl}}(0)z_{\mathrm{cl}}(0)\right)\ . \tag{D.10}$$

It remains to rewrite this expression in terms of $z_f = z_{\mathrm{cl}}(t)$ and $z_i = z_{\mathrm{cl}}(0)$ only. To do so, we write a generic real solution $z_{\mathrm{cl}}(\tau)$ in terms of a fundamental complex solution of equation (D.3):

$$Z(\tau) \equiv X(\tau) + iY(\tau)\ , \tag{D.11}$$

$$Z(0) = 1\ , \qquad Z'(0) = -i\omega_0\ , \tag{D.12}$$

where ω_0 is an arbitrary frequency. Any classical trajectory $z_{\mathrm{cl}}(\tau)$ can then be written

$$z_{\mathrm{cl}}(\tau) = z_{\mathrm{cl}}(0)X(\tau) - \frac{z'_{\mathrm{cl}}(0)}{\omega_0}Y(\tau)\ . \tag{D.13}$$

We deduce

$$z'_{\mathrm{cl}}(0) = \omega_0\frac{z_{\mathrm{cl}}(0)X(t) - z_{\mathrm{cl}}(t)}{Y(t)}\ , \tag{D.14}$$

$$z'_{\mathrm{cl}}(t) = z_{\mathrm{cl}}(0)X'(t) - Y'(t)\frac{z_{\mathrm{cl}}(0)X(t) - z_{\mathrm{cl}}(t)}{Y(t)} \tag{D.15}$$

$$= \frac{\omega_0 z_{\mathrm{cl}}(0) + Y'(t)z_{\mathrm{cl}}(t)}{Y(t)}\ . \tag{D.16}$$

In the last equality, we have used the fact that the Wronskian $\mathcal{W}(Y,X) = \omega_0$ is a constant. Hamilton's principal function thus reads

$$S_{\rm cl}(z_f, z_i, t) = \frac{m}{2Y(t)}\left(Y'(t)z_f^2 + 2\omega_0 z_f z_i - \omega_0 X(t) z_i^2\right) \tag{D.17}$$

and we finally have

$$K(z_f, z_i, t) = \sqrt{\frac{m}{2i\pi\hbar Y(t)}}\exp\left(\frac{im}{2\hbar Y(t)}\left(Y'(t)z_f^2 + 2\omega_0 z_f z_i - \omega_0 X(t) z_i^2\right)\right) . \tag{D.18}$$

Equivalently, the time dependent quantum harmonic oscillator can be solved using the Wigner phase space quasi-distribution. For a quadratic Hamiltonian, the Wigner function $W(z,p,t)$ describing the quantum system obeys the classical Liouville equation (see section III.1.c):

$$\frac{\partial W}{\partial t}(z,p,t) = -\frac{p}{m}\frac{\partial W}{\partial z}(z,p,t) + m\omega(t)^2 z\frac{\partial W}{\partial p}(z,p,t) , \tag{D.19}$$

whose solution is

$$W(z_f, p_f, t) = W(z_i, p_i, 0) , \tag{D.20}$$

where z_i, p_i and z_f, p_f are the starting and end points of the classical trajectory $z_{\rm cl}(\tau), p_{\rm cl}(\tau)$ defined by equation (D.3) and $p_{\rm cl}(\tau) = m z'_{\rm cl}(\tau)$. Using again the solution $Z(\tau)$ defined by equation (D.12) we find that

$$W(z,p,t) = W\left(\frac{1}{m\omega_0}\,{\rm Im}\left(pZ(t) - mzZ'(t)\right),\ {\rm Re}\left(pZ(t) - mzZ'(t)\right),\ 0\right) . \tag{D.21}$$

D.2 Parametric creation of quanta

In this section, we will suppose that the frequency $\omega(t)$ of the oscillator remains constant outside a given time interval:

$$\omega(t) = \omega_0 \quad \text{for} \quad t < 0 , \tag{D.22}$$

$$\omega(t) = \omega_f \quad \text{for} \quad t > t_f > 0 . \tag{D.23}$$

Therefore, the function $Z(t)$ oscillates sinusoidally for $t < 0$ and $t > t_f$:

$$Z(t) = \exp(-i\omega_0 t) \qquad \text{for} \quad t < 0 , \tag{D.24}$$

$$Z(t) = \alpha\sqrt{\frac{\omega_0}{\omega_f}}\exp(-i\omega_f t) + \beta\sqrt{\frac{\omega_0}{\omega_f}}\exp(i\omega_f t) \qquad \text{for} \quad t > t_f . \tag{D.25}$$

The constants α and β depend on the form of $\omega(t)$ between $t = 0$ and t_f. They are analogous to the scattering amplitudes associated with equation (D.4). The fact that the Wronskian of $Z(t)$ and its complex conjugate $Z^*(t)$ is a constant entails

$$|\alpha|^2 - |\beta|^2 = 1 , \tag{D.26}$$

which is the counterpart of current conservation in quantum scattering.

We now suppose that the system starts off in an eigenstate of the *time-independent* harmonic oscillator of frequency ω_0. For $t < 0$, the Wigner function is thus given by [241]

$$W(z,p,t) = W_n\left(\frac{H_0(z,p)}{\hbar\omega_0}\right) \qquad (t<0)\ , \tag{D.27}$$

$$W_n(x) \equiv \frac{(-1)^n}{\hbar\pi}\exp(-2x)\,L_n(4x)\ , \qquad H_0(z,p) \equiv \frac{p^2}{2m}+\frac{1}{2}m\omega_0^2 z^2\ , \tag{D.28}$$

where L_n is the n^{th} Laguerre polynomial [1]. The initial energy is

$$E_0 = \iint \mathrm{d}z\,\mathrm{d}p\ H_0(z,p)W_n\left(\frac{H_0(z,p)}{\hbar\omega_0}\right) = \hbar\omega_0\left(n+\frac{1}{2}\right)\ . \tag{D.29}$$

During the subsequent evolution, the Wigner function reads (see equation (D.21))

$$W(z,p,t) = W_n\left(\frac{|pZ(t)-mzZ'(t)|^2}{2m\hbar\omega_0}\right)\ . \tag{D.30}$$

We now want to evaluate the energy for $t > t_f$:

$$E_f = \iint \mathrm{d}z\,\mathrm{d}p\ H_f(z,p)W(z,p,t)\ , \qquad H_f(z,p) \equiv \frac{p^2}{2m}+\frac{1}{2}m\omega_f^2 z^2\ . \tag{D.31}$$

Replacing $Z(t)$ by its final expression (D.25), we find

$$W(z,p,t) = W_n\left(\frac{H_f(z,p)}{\hbar\omega_f}\left(|\alpha|^2+|\beta|^2+2\,\mathrm{Re}\left(\frac{p+im\omega_f z}{p-im\omega_f z}\alpha\beta^* e^{-2i\omega_f t}\right)\right)\right)\ . \tag{D.32}$$

To evaluate the integral we change to cylindrical coordinates:

$$r\cos\theta \equiv \frac{p}{\sqrt{2m\hbar\omega_f}}\ , \qquad r\sin\theta \equiv \sqrt{\frac{m\omega_f}{2\hbar}}z\ , \tag{D.33}$$

$$E_f = \hbar\omega_f\int_0^\infty \mathrm{d}r\int_0^{2\pi}\mathrm{d}\theta\ r^3\,W_n\left(r^2\left(|\alpha|^2+|\beta|^2+2|\alpha\beta|\cos(2\theta+\arg(\alpha\beta^*)-2\omega_f t)\right)\right)\ . \tag{D.34}$$

We change the origin of angles and rescale the radius:

$$\theta' \equiv \theta+\frac{1}{2}\arg(\alpha\beta^*)-\omega_f t \qquad r' \equiv r\sqrt{|\alpha|^2+|\beta|^2+2|\alpha\beta|\cos(2\theta')}\ , \tag{D.35}$$

$$E_f = \hbar\omega_f\int_0^\infty \mathrm{d}r'\ r'^3 W_n\left(r'^2\right)\int_0^{2\pi}\mathrm{d}\theta'\left(|\alpha|^2+|\beta|^2+2|\alpha\beta|\cos(2\theta')\right)^{-2}\ . \tag{D.36}$$

The integral on θ' can be performed:

$$E_f = \left(|\alpha|^2 + |\beta|^2\right)^{-2} \left(1 - \frac{4|\alpha\beta|^2}{(|\alpha|^2 + |\beta|^2)^2}\right)^{-3/2} \hbar\omega_f \int_0^\infty 2\pi \mathrm{d}r'\, r'^3\, W_n\left(r'^2\right) \ . \tag{D.37}$$

Using equation (D.26) this simplifies to

$$E_f = (1 + 2|\beta|^2)\hbar\omega_f \int_0^\infty 2\pi \mathrm{d}r'\, r'^3\, W_n\left(r'^2\right) \ . \tag{D.38}$$

We can now transform the radial integral back into the form of (D.29) by defining

$$r' \cos\theta' \equiv \frac{p'}{\sqrt{2m\hbar\omega_f}} \ , \qquad\qquad r' \sin\theta' \equiv \sqrt{\frac{m\omega_f}{2\hbar}} z' \ , \tag{D.39}$$

and we get

$$E_f = (1 + 2|\beta|^2) \iint \mathrm{d}z'\, \mathrm{d}p'\ H_f(z', p') W_n\left(\frac{H_f(z', p')}{\hbar\omega_f}\right) \tag{D.40}$$

$$= (1 + 2|\beta|^2)\hbar\omega_f \left(n + \frac{1}{2}\right) \ . \tag{D.41}$$

The final energy E_f is thus always larger than the energy of the n^{th} eigenstate of the harmonic oscillator of frequency ω_f. The extra energy is measured by the amplitude β of the negative frequency component of the function $Z(t)$, that is, in the language of quantum reflection, the amplitude of the reflected wave.

The fact that a variation of the oscillator's frequency can lead to the generation of new quanta is highly reminiscent of scalar particle formation in an expanding metric [242–244] or in the presence of a moving mirror [245–248]. The amplitude β can be likened to a Bogoliubov coefficient linking "in" and "out" vacua.

It is natural to ask oneself under what conditions the amplitude β is equal to zero. The connection we have established with quantum reflection (and in this case, the absence thereof) provides a first answer: $\beta = 0$ if the WKB approximation can be applied to the classical equation of motion (D.3). Indeed, if this is the case, then

$$Z(t) \simeq \sqrt{\frac{\omega_0}{\omega(t)}} \exp\left(-i \int_0^t \omega(\tau)\ \mathrm{d}\tau\right) \tag{D.42}$$

and so for $t > t_f$,

$$Z(t) \simeq \sqrt{\frac{\omega_0}{\omega_f}} \exp\left(-i\omega_f t + i\delta\right) \ , \tag{D.43}$$

where δ is a real constant, so that

$$\alpha \simeq e^{i\delta} \ , \qquad\qquad \beta \simeq 0 \ , \qquad\qquad E_f \simeq \hbar\omega_f \left(n + \frac{1}{2}\right) \ . \tag{D.44}$$

Moreover, we have

$$W(z,p,t) \simeq W_n\left(\frac{1}{\hbar\omega(t)}\left(\frac{p^2}{2m}+\frac{1}{2}m\omega(t)^2z^2\right)\right) \tag{D.45}$$

so that at all times the system is in an instantaneous eigenstate of the system. The WKB approximation applied to the classical equation of motion is thus equivalent to the adiabatic approximation for the quantum oscillator.

The validity of the adiabatic approximation is therefore bound to that of the WKB approximation. It follows that the adiabatic approximation is valid provided the badlands function

$$Q(t) \equiv \frac{1}{2}\frac{\omega''(z)}{\omega(z)^3} - \frac{3}{4}\frac{\omega'(z)^2}{\omega(z)^4} \tag{D.46}$$

remains much smaller than 1 at all times.

D.3 Liouville transformations

Given that it has the same form as the Schrödinger equation (D.4), we can perform a Liouville transformation of the classical equation of motion (D.3) obeyed by the function $Z(t)$. In that aim, we introduce a new time coordinate $\tilde{t}(t)$ (with $\tilde{t}'(t) > 0$) and define

$$\tilde{Z}(\tilde{t}) = \sqrt{\tilde{t}'(t)}Z(t) \tag{D.47}$$

which obeys the transformed equation

$$\tilde{Z}''(\tilde{t}) + \tilde{\omega}(\tilde{t})^2\tilde{Z}(\tilde{t}) = 0\ , \qquad \tilde{\omega}(\tilde{t})^2 = \frac{\omega(t)^2 - \frac{1}{2}\{\tilde{t},t\}}{\tilde{t}'(t)^2}\ . \tag{D.48}$$

This new classical equation is associated with a Schrödinger equation

$$i\hbar\frac{\partial\tilde{\psi}}{\partial\tilde{t}}(\tilde{z},\tilde{t}) = -\frac{\hbar^2}{2m}\frac{\partial^2\tilde{\psi}}{\partial\tilde{z}^2}(\tilde{z},\tilde{t}) + \frac{1}{2}m\tilde{\omega}(\tilde{t})^2\tilde{z}^2\tilde{\psi}(\tilde{z},\tilde{t}) \tag{D.49}$$

the solutions of which we want to relate with solutions of the original equation (D.2). We will assume that in the vicinity of $t = 0$, we have $\tilde{t} = t$. This way the function

$$\tilde{Z}(\tilde{t}) \equiv \sqrt{\tilde{t}'(t)}Z(t) \tag{D.50}$$

has the same initial values as $Z(t)$:

$$\tilde{Z}(0) = 1\ , \qquad \tilde{Z}'(0) = -i\omega_0\ . \tag{D.51}$$

The propagator associated with equation (D.49) is thus

$$\tilde{K}(\tilde{z}_f,\tilde{z}_i,\tilde{t}) \equiv \sqrt{\frac{m}{2i\pi\hbar\tilde{Y}(\tilde{t})}}\exp\left(\frac{im}{2\hbar\tilde{Y}(\tilde{t})}\left(\tilde{Y}'(\tilde{t})\tilde{z}_f^2 + 2\omega_0\tilde{z}_f\tilde{z}_i - \omega_0\tilde{X}(\tilde{t})\tilde{z}_i^2\right)\right)\ . \tag{D.52}$$

We can write the propagator (D.18) associated with the original equation (D.2) in terms of this Liouville-transformed propagator:

$$K(z_f, z_i, t) = (\tilde{t}'(t))^{1/4} \sqrt{\frac{m}{2i\pi\hbar \tilde{Y}(\tilde{t})}} \exp\left(\frac{-im}{4\hbar}\frac{\tilde{t}''(t)}{\tilde{t}'(t)} z_f^2\right) \tag{D.53}$$

$$\times \exp\left(\frac{im}{2\hbar \tilde{Y}(\tilde{t})}\left(\tilde{Y}'(\tilde{t})\tilde{z}_f^2 + 2\omega_0 \tilde{z}_f \tilde{z}_i - \omega_0 \tilde{X}(\tilde{t})\tilde{z}_i^2\right)\right) \tag{D.54}$$

$$= (\tilde{t}'(t))^{1/4} \exp\left(\frac{-im}{4\hbar}\frac{\tilde{t}''(t)}{\tilde{t}'(t)} z_f^2\right) \tilde{K}\left(\tilde{z}_f, \tilde{z}_i, \tilde{t}\right) \ , \tag{D.55}$$

where $\tilde{z}_f \equiv \sqrt{\tilde{t}'(t)} z_f$ and $\tilde{z}_i \equiv \sqrt{\tilde{t}'(0)} z_i = z_i$. Given an initial wavefunction $\tilde{\psi}(\tilde{z}_i, 0)$ and the associated solution to equation (D.49)

$$\tilde{\psi}(\tilde{z}_f, \tilde{t}) = \int \tilde{K}\left(\tilde{z}_f, \tilde{z}_i, \tilde{t}\right) \tilde{\psi}(\tilde{z}_i, 0)\ \mathrm{d}\tilde{z}_i \ , \tag{D.56}$$

it follows that the wavefunction

$$\psi(z_f, t) \equiv (\tilde{t}'(t))^{1/4} \exp\left(\frac{-im}{4\hbar}\frac{\tilde{t}''(t)}{\tilde{t}'(t)} z_f^2\right) \tilde{\psi}(\tilde{z}_f, \tilde{t}) \tag{D.57}$$

is a solution of the original equation. Indeed,

$$\psi(z_f, t) = (\tilde{t}'(t))^{1/4} \exp\left(\frac{-im}{4\hbar}\frac{\tilde{t}''(t)}{\tilde{t}'(t)} z_f^2\right) \int \tilde{K}\left(\tilde{z}_f, \tilde{z}_i, \tilde{t}\right) \tilde{\psi}(\tilde{z}_i, 0)\ \mathrm{d}\tilde{z}_i \tag{D.58}$$

$$= \int K\left(z_f, z_i, t\right) \psi(z_i, 0)\ \mathrm{d}z_i \ , \tag{D.59}$$

where $\psi(z_i, 0) = \tilde{\psi}(\tilde{z}_i, 0)$. One can check explicitly that if $\tilde{\psi}(\tilde{x}, \tilde{t})$ is a solution of (D.49) then the ansatz

$$\psi(z, t) = \tilde{t}'(t)^{1/4} \exp\left(\frac{-im}{4\hbar}\frac{\tilde{t}''(t)}{\tilde{t}'(t)} z^2\right) \tilde{\psi}(\tilde{z}, \tilde{t}) \tag{D.60}$$

solves (D.2).

We can do the equivalent transformation in the Wigner function formalism. Replacing $Z(t)$ by its expression in terms of $\tilde{Z}(\tilde{t})$ in equation (D.21), we find that

$$W(z, p, t) = \tilde{W}\left(\tilde{z}(\tilde{t}), \tilde{p}(\tilde{t}), \tilde{t}\right) \ , \tag{D.61}$$

where

$$\tilde{z}(\tilde{t}) = z\sqrt{\tilde{t}'(t)} \ , \tag{D.62}$$

$$\tilde{p}(\tilde{t}) = m\tilde{z}'(\tilde{t}) = \frac{1}{\sqrt{\tilde{t}'(t)}}\left(p + mz\frac{\tilde{t}''(t)}{2\tilde{t}'(t)}\right) \tag{D.63}$$

and $\tilde{W}$ obeys

$$\frac{\partial \tilde{W}}{\partial \tilde{t}}(\tilde{z}, \tilde{p}, \tilde{t}) = -\frac{\tilde{p}}{m}\frac{\partial \tilde{W}}{\partial \tilde{z}}(\tilde{z}, \tilde{p}, \tilde{t}) + m\tilde{\omega}(\tilde{t})^2 \tilde{z}\frac{\partial \tilde{W}}{\partial \tilde{p}}(\tilde{z}, \tilde{p}, \tilde{t}) \ . \tag{D.64}$$

D.4 Shortcuts to adiabaticity

We have seen that provided the badlands function (D.46) remains small, the time-dependent harmonic oscillator stays in the instantaneous eigenstates of the system at all times. In general this is possible only for sufficiently slow variations of the oscillator frequency. In this section we will look for functions $\omega(t)$ such that the system eventually returns to its initial eigenstate (possibly at a different frequency) but does not necessarily remain in that state throughout the evolution. These are known as *shortcuts to adiabaticity* since the final state is identical to that which is obtained through adiabatic evolution but it can be reached in an arbitrarily short amount of time.

We are looking for functions $\omega(t)$ such that $\beta = 0$. Since β is invariant under Liouville transformations, all functions which are related to the constant function $\tilde{\omega}(\tilde{t}) = \omega_0$ by a Liouville transformation are adequate. We conclude from equation (D.48) that $\omega(t)$ must be such that

$$\omega(t)^2 = \omega_0^2 \tilde{t}'(t)^2 + \frac{1}{2}\{\tilde{t}, t\} \tag{D.65}$$

with $\tilde{t}(t)$ a smooth and strictly increasing function. Note that $\omega(t)^2$ can temporarily become negative, which corresponds to turning the harmonic trap into a repulsive parabolic barrier. For $\omega(t)$ to have the correct initial and final values, we also require

$$\tilde{t}(t) = t \qquad \text{for } t < 0 \ , \tag{D.66}$$

$$\tilde{t}(t) = \frac{\omega_f}{\omega_0} t + \text{constant} \qquad \text{for } t > t_f \ . \tag{D.67}$$

The exact solution of (D.3) is then the "WKB-like" function

$$Z(t) = \sqrt{\frac{\omega_0}{\Omega(t)}} \exp\left(-i \int_0^t \Omega(\tau)\, \mathrm{d}\tau\right) \ , \qquad \Omega(t) \equiv \omega_0 \tilde{t}'(t) \ . \tag{D.68}$$

In particular,

$$Z(t) \propto \exp\left(-i\omega_f t\right) \qquad \text{for } t > t_f \ , \tag{D.69}$$

so that β is indeed equal to zero.

In practice, one can start from a function $\Omega(t)$ which goes from ω_0 to ω_f in the desired amount of time and obtain the shortcut to adiabaticity as

$$\omega(t) = \Omega(t) + \frac{1}{2}\left(\frac{\Omega''(t)}{\Omega(t)} - \frac{3}{2}\frac{\Omega'(t)^2}{\Omega(t)^2}\right) \ . \tag{D.70}$$

Starting from a Hamiltonian

$$H_0(t) \equiv \frac{\hat{P}^2}{2m} + \frac{1}{2} m \Omega(t)^2 \hat{Z}^2 \ , \tag{D.71}$$

we have added an extra driving term

$$H_1(t) \equiv \frac{m}{4}\left(\frac{\Omega''(t)}{\Omega(t)} - \frac{3}{2}\frac{\Omega'(t)^2}{\Omega(t)^2}\right)\hat{Z}^2 \tag{D.72}$$

such that the exact evolution under $H_0 + H_1$ mimics the adiabatic evolution under H_0. This approach is known as transitionless quantum driving [249–251].

Another derivation of this shortcut to adiabaticity was proposed by Chen *et al.* [252, 253]. Based on the Lewis-Riesenfeld invariants of the harmonic oscillator [254], the authors introduce the ansatz

$$\psi(z,t) = \frac{1}{\sqrt{b(t)}}\Phi\left(\frac{z}{b(t)}, \int_0^t \frac{\mathrm{d}\tau}{b(\tau)^2}\right)\exp\left(i\frac{m}{2\hbar}\frac{b'(t)}{b(t)}z^2\right) , \tag{D.73}$$

where the function $b(t)$ obeys the Ermakov equation[4]:

$$b''(t) + \omega(t)^2 b(t) = \frac{\omega_0}{b(t)^3} \tag{D.74}$$

along with the boundary conditions

$$b(t) = 1 \quad \text{for } t < 0 , \qquad\qquad b(t) = \sqrt{\omega_0/\omega_f} \quad \text{for } t > t_f . \tag{D.75}$$

Under these conditions, $\psi(z,t)$ solves (D.2) provided that Φ is the wavefunction of an oscillator with a constant frequency ω_0. If we identify

$$b(t) \equiv \frac{1}{\sqrt{\tilde{t}'(t)}} , \tag{D.76}$$

we recognize that the ansatz (D.73) corresponds to the Liouville transformation rule for the wavefunction (D.60) and that the Ermakov equation (D.74) is equivalent to the condition (D.65) for $\omega(t)$ to be a shortcut to adiabaticity.

By means of a Liouville transformation of the classical equation of motion, we were thus able to derive shortcuts to adiabaticity for the time-dependent quantum harmonic oscillator. In the language of quantum reflection, these shortcuts correspond to "potentials" $\omega(t)^2$ which do not generate any reflection [255, 256]. Our approach highlights the links between the WKB and adiabatic approximations.

[4] This equation is sometimes also known as the Milne or Pinney equation.

List of publications

Articles in peer-reviewed journals

- G. Dufour, A. Gérardin, R. Guérout, A. Lambrecht, V. V. Nesvizhevsky, S. Reynaud, and A. Y. Voronin, "Quantum reflection of antihydrogen from the Casimir potential above matter slabs", Physical Review A **87**, 012901 (2013)
- G. Dufour, R. Guérout, A. Lambrecht, V. V. Nesvizhevsky, S. Reynaud, and A. Y. Voronin, "Quantum reflection of antihydrogen from nanoporous media", Physical Review A **87**, 022506 (février 19, 2013)
- G. Dufour, P. Debu, A. Lambrecht, V. V. Nesvizhevsky, S. Reynaud, and A. Y. Voronin, "Shaping the distribution of vertical velocities of antihydrogen in GBAR", European Physical Journal C **74**, 2731 (2014)
- G. Dufour, R. Guérout, A. Lambrecht, and S. Reynaud, "Quantum reflection and Liouville transformations from wells to walls", EPL (Europhysics Letters) **110**, 30007 (2015)
- G. Dufour, R. Guérout, A. Lambrecht, and S. Reynaud, "Liouville transformations and quantum reflection", Journal of Physics B: Atomic, Molecular and Optical Physics **48**, 155002 (2015)

Conference proceedings

- G. Dufour, R. Guérout, A. Lambrecht, V. Nesvizhevsky, S. Reynaud, and A. Voronin, "Quantum reflection of antihydrogen in the GBAR experiment", International Journal of Modern Physics: Conference Series **30**, 1460265 (2014)
- A. Y. Voronin, V. V. Nesvizhevsky, G. Dufour, P. Debu, A. Lambrecht, S. Reynaud, O. D. Dalkarov, E. A. Kupriyanova, and P. Froelich, "A spectroscopy approach to measure the gravitational mass of antihydrogen", International Journal of Modern Physics: Conference Series **30**, 1460266 (2014)
- P. Indelicato, G. Chardin, P. Grandemange, D. Lunney, V. Manea, A. Badertscher, P. Crivelli, A. Curioni, A. Marchionni, B. Rossi, A. Rubbia, V. Nesvizhevsky, D.

Brook-Roberge, P. Comini, P. Debu, P. Dupré, L. Liszkay, B. Mansoulié, P. Pérez, J.-M. Rey, B. Reymond, N. Ruiz, Y. Sacquin, B. Vallage, F. Biraben, P. Cladé, A. Douillet, G. Dufour, S. Guellati, L. Hilico, A. Lambrecht, R. Guérout, J.-P. Karr, F. Nez, S. Reynaud, C. I. Szabo, V.-Q. Tran, J. Trapateau, A. Mohri, Y. Yamazaki, M. Charlton, S. Eriksson, N. Madsen, D. P. van der Werf, N. Kuroda, H. Torii, Y. Nagashima, F. Schmidt-Kaler, J. Walz, S. Wolf, P.-A. Hervieux, G. Manfredi, A. Voronin, P. Froelich, S. Wronka, and M. Staszczak, "The GBAR project, or how does antimatter fall?", Hyperfine Interactions **228**, 141 (2014)

- G. Dufour, D. B. Cassidy, P. Crivelli, P. Debu, A. Lambrecht, V. V. Nesvizhevsky, S. Reynaud, A. Y. Voronin, and T. E. Wall, "Prospects for studies of the free fall and gravitational quantum states of antimatter", Advances in High Energy Physics **2015**, 379642 (2015)

- P. Pérez, D. Banerjee, F. Biraben, D. Brook-Roberge, M. Charlton, P. Cladé, P. Comini, P. Crivelli, O. Dalkarov, P. Debu, A. Douillet, G. Dufour, P. Dupré, S. Eriksson, P. Froelich, P. Grandemange, S. Guellati, R. Guérout, J. M. Heinrich, P.-A. Hervieux, L. Hilico, A. Husson, P. Indelicato, S. Jonsell, J.-P. Karr, K. Khabarova, N. Kolachevsky, N. Kuroda, A. Lambrecht, A. M. M. Leite, L. Liszkay, D. Lunney, N. Madsen, G. Manfredi, B. Mansoulié, Y. Matsuda, A. Mohri, T. Mortensen, Y. Nagashima, V. Nesvizhevsky, F. Nez, C. Regenfus, J.-M. Rey, J.-M. Reymond, S. Reynaud, A. Rubbia, Y. Sacquin, F. Schmidt-Kaler, N. Sillitoe, M. Staszczak, C. I. Szabo-Foster, H. Torii, B. Vallage, M. Valdes, D. P. V. der Werf, A. Voronin, J. Walz, S. Wolf, S. Wronka, and Y. Yamazaki, "The GBAR antimatter gravity experiment", Hyperfine Interactions **233**, 21 (2015)

- G. Dufour, R. Guérout, A. Lambrecht, and S. Reynaud, "Casimir effect and quantum reflection", to appear in the proceedings of the 50$^{\text{th}}$ Rencontres de Moriond

Résumé en français

La nature ondulatoire de la matière à l'échelle microscopique est à l'origine de nombreux phénomènes déroutants pour notre intuition classique : interférences, effet tunnel et principe d'incertitude de Heisenberg pour n'en citer que quelques uns. Cette thèse est consacrée à l'un de ces phénomènes : *la réflexion quantique*, c'est à dire la réflexion d'une onde de matière sur un potentiel qui ne réfléchirait pas une particule classique.

Le point de départ de ce travail est en apparence éloigné de ces considérations ; il s'agit d'une question qui occupe les physiciens depuis la découverte de l'antimatière dans les années 30 : est-ce que matière et antimatière chutent de la même manière dans le champ de gravité ? Le principe d'universalité de la chute libre le requiert mais cela n'a jamais été vérifié directement. Les progrès accomplis pour produire, piéger et refroidir des anti-particules permettront bientôt de donner une réponse expérimentale à cette question.

L'expérience GBAR [26, 27], actuellement en construction au CERN, consistera à mesurer le temps de chute d'un atome d'antihydrogène dans le champ de gravité de la Terre. Afin de pouvoir bénéficier des techniques de piégeage et de refroidissement des ions, c'est un ion positif d'antihydrogène, formé d'un antiproton et deux positrons, qui sera utilisé [28]. Une fois l'ion amené à une température de 10 μK dans un piège de Paul, une impulsion laser photodétache le positron excédentaire et l'atome neutre entame sa chute libre. L'annihilation de l'atome d'antihydrogène sur une plaque de détection située une dizaine de centimètres plus bas marque la fin de la chute.

Le fait que l'atome en chute libre ne soit pas une particule ponctuelle mais bien une onde de matière n'est pas sans conséquences pour l'expérience. Premièrement, sa position et sa vitesse initiales sont soumises au principe d'incertitude de Heisenberg. Cela se traduit par une dispersion des temps d'arrivée sur le détecteur. De plus, une onde de matière est susceptible de subir une réflexion quantique si elle rencontre de soudaines variations de potentiel. Or de telles variations ont lieu au voisinage de la plaque de détection, en raison de l'interaction de Casimir-Polder entre l'atome et la surface.

En effet, on sait depuis van der Waals qu'il existe des forces entre atomes et molécules neutres. En 1930, London montre que, bien que dépourvus de dipôle permanent, les atomes interagissent par le biais des fluctuations quantiques de leur nuage électronique [61]. Casimir et Polder généralisent ce résultat en tenant compte du temps que mettent les ondes électromagnétiques pour voyager d'un atome à l'autre [63, 64]. Casimir montrera ensuite que ces forces découlent de la modification de l'énergie de point-zéro du champ

électromagnétique lorsqu'on y déplace des objets et considérera le cas emblématique de deux miroirs qui s'attirent bien que placés dans le vide [65, 66]. L'énergie du vide a donc des conséquences au niveau macroscopique. Ces conséquences n'ont été observées directement et de façon conclusive qu'un demi-siècle après la prédiction de Casimir [67–69].

Pour revenir à GBAR, l'atome en chute libre subit une force de Casimir-Polder qui l'attire vers la plaque de détection. Cette force n'est significative qu'à des distances de quelques dizaines de nanomètres et son effet sur une particule classique ne serait qu'une modification imperceptible du temps de chute. En revanche, une onde de matière incidente sur le potentiel de Casimir-Polder est en partie réfléchie, ce qui se traduit par une probabilité de voir l'atome rebondir avant d'avoir atteint le détecteur [165].

C'est cette réflexion quantique que nous étudierons dans cette thèse. Nous commencerons par des considérations théoriques générales sur la réflexion quantique. Nous calculerons ensuite le potentiel de Casimir-Polder entre un atome d'hydrogène ou d'antihydrogène et diverses surfaces planes puis les probabilités de réflexion sur ces potentiels. Enfin nous nous intéresserons au mouvement d'un paquet d'onde quantique dans un champ de gravité, en présence ou non d'une surface réfléchissante.

Réflexion quantique

Équation de Schrödinger et approximation WKB

En mécanique classique, une particule de masse m et d'énergie E se déplaçant dans un potentiel unidimensionnel $V(z)$ a une quantité de mouvement

$$p_{\mathrm{cl}}(z) = \pm\sqrt{2m(E - V(z))} \ . \tag{1}$$

Le signe correspond à la direction de propagation et ne peut changer qu'en un *point de rebroussement classique*, c'est à dire un point où $V(z) = E$. Ces points de rebroussement délimitent les zones classiquement accessibles à la particule, où $E \geq V(z)$, et les zones classiquement interdites, où $E < V(z)$.

Ces frontières sont floutées pour une onde de matière décrite par une fonction d'onde $\psi(z)$ obéissant à l'équation de Schrödinger

$$-\frac{\hbar^2}{2m}\frac{\mathrm{d}^2\psi}{\mathrm{d}z^2}(z) + V(z)\psi(z) = E\psi(z) \ , \tag{2}$$

qu'on écrira de façon compacte

$$\psi''(z) + F(z)\psi(z) = 0 \ , \qquad F(z) \equiv \frac{2m}{\hbar^2}\left(E - V(z)\right) \ . \tag{3}$$

Par exemple, une particule quantique peut traverser une zone classiquement interdite par effet tunnel. Par ailleurs, une onde de matière peut être réfléchie en l'absence de point de rebroussement classique, c'est ce qu'on appellera la réflexion quantique.

La réflexion quantique peut être définie plus précisément comme un écart à l'approximation semiclassique de Wentzel, Kramers et Brillouin (WKB). Dans les régions accessibles classiquement ($V(z) > E$), les deux solutions approchées de l'équation de Schrödinger se propageant en sens inverse sont données par

$$\psi^{\pm}_{\mathrm{WKB}}(z) \equiv \frac{1}{\sqrt{k_{\mathrm{dB}}(z)}} \exp(\pm i\phi_{\mathrm{dB}}(z)) \ . \tag{4}$$

Le vecteur d'onde de de Broglie est défini par

$$k_{\mathrm{dB}} \equiv \frac{p_{\mathrm{cl}}(z)}{\hbar} = \sqrt{F(z)} \tag{5}$$

et la phase WKB en est une primitive[5]

$$\phi_{\mathrm{dB}}(z) \equiv \int_{z_0}^{z} k_{\mathrm{dB}}(\zeta)\ \mathrm{d}\zeta \tag{6}$$

Dans cette approximation, un paquet d'onde se propage sans réflexion, en suivant la trajectoire classique.

On peut voir la réflexion quantique comme un transfert d'amplitude d'une onde WKB vers l'autre. Pour ce faire, on écrit la solution exacte $\psi(z)$ de l'équation de Schrödinger comme une combinaison linéaire d'ondes WKB dont les coefficients peuvent varier :

$$\psi(z) \equiv a_+(z)\psi^{+}_{\mathrm{WKB}}(z) + a_-(z)\psi^{-}_{\mathrm{WKB}}(z) \ . \tag{7}$$

Les coefficients $a_{\pm}(z)$ obéissent alors à des équations différentielles couplées [110] :

$$a'_{\pm}(z) = \frac{k'_{\mathrm{dB}}(z)}{2k_{\mathrm{dB}}(z)} a_{\mp}(z) \exp(\mp 2i\phi_{\mathrm{dB}}(z)) \ . \tag{8}$$

Si l'approximation WKB est valide de part et d'autre d'une "région d'interaction", les coefficients $a_{\pm}(z)$ y tendent vers une limite finie. La matrice de diffusion ou matrice $\mathcal{S}$ relie les amplitudes des ondes quittant la région d'interaction à celles y entrant.

Les fonctions d'onde WKB obéissent à une équation de Schrödinger modifiée

$$\psi''(z) + F(z)\,(1 + Q(z))\,\psi(z) = 0 \ . \tag{9}$$

Le terme supplémentaire $Q(z)$ est appelé "fonction badlands" et s'exprime à l'aide de la dérivée Schwarzienne $\{\phi_{\mathrm{dB}}, z\}$ de la phase WKB :

$$Q(z) \equiv \frac{1}{2\phi'_{\mathrm{dB}}(z)} \{\phi_{\mathrm{dB}}, z\} \ , \tag{10}$$

$$\{\phi_{\mathrm{dB}}, z\} \equiv \frac{\phi'''_{\mathrm{dB}}(z)}{\phi'_{\mathrm{dB}}(z)} - \frac{3}{2}\frac{\phi''_{\mathrm{dB}}(z)^2}{\phi'_{\mathrm{dB}}(z)^2} \ . \tag{11}$$

On s'attend à ce que les solutions exactes de l'équation de Schrödinger s'écartent de l'approximation WKB dans les régions où la fonction badlands prend des valeurs significatives. C'est donc dans ces régions que la réflexion quantique peut avoir lieu. Ceci est clairement mis en évidence par une transformation de Liouville de l'équation de Schrödinger, comme nous allons le montrer après une brève présentation de ces transformations.

[5] Le choix du point z_0 est arbitraire.

Transformations de Liouville

Les transformations de Liouville consistent en un changement de coordonnée[6] $z \to \tilde{z}$ associé à une redéfinition de la fonction d'onde

$$\tilde{\psi}(\tilde{z}) \equiv \sqrt{\tilde{z}'(z)}\psi(z) \ . \tag{12}$$

La fonction $\tilde{\psi}(\tilde{z})$ obéit à une autre équation de Schrödinger

$$\tilde{\psi}''(\tilde{z}) + \tilde{F}(\tilde{z})\tilde{\psi}(\tilde{z}) = 0 \ , \tag{13}$$

où la fonction $\tilde{F}(\tilde{z})$ s'exprime notamment à l'aide de la dérivée Schwarzienne $\{\tilde{z}, z\}$ du changement de coordonnée [138] :

$$\tilde{F}(\tilde{z}) = \frac{F(z) - \frac{1}{2}\{\tilde{z}, z\}}{\tilde{z}'(z)^2} \ . \tag{14}$$

Les décompositions de la fonction d'onde sur une paire d'ondes contrapropageantes, telles que l'équation (7), sont préservées par les transformations de Liouville. Il s'ensuit que les amplitudes de diffusion regroupées dans la matrice $\mathcal{S}$ sont invariantes par transformation de Liouville.

On s'intéresse maintenant à la transformation de Liouville où la nouvelle coordonnée est la phase WKB (on utilisera des caractères gras pour désigner les quantités associées à ce choix de coordonnée) :

$$\boldsymbol{z}(z) \equiv \phi_{\mathrm{dB}}(z) \ , \qquad \boldsymbol{\psi}(\boldsymbol{z}) = \sqrt{k_{\mathrm{dB}}(z)}\psi(z) \ , \tag{15}$$

$$\boldsymbol{\psi}''(\boldsymbol{z}) + \boldsymbol{F}(\boldsymbol{z})\boldsymbol{\psi}(\boldsymbol{z}) = 0 \ , \qquad \boldsymbol{F}(\boldsymbol{z}) = 1 - Q(z) \ . \tag{16}$$

Par analogie avec l'équation (3), la fonction badlands joue le rôle d'un potentiel dans la nouvelle équation de Schrödinger, l'énergie étant égale à 1. Dans les régions où la fonction badlands s'annule, on trouve immédiatement

$$\boldsymbol{\psi}(\boldsymbol{z}) = a_+ \exp(i\boldsymbol{z}) + a_- \exp(-i\boldsymbol{z}) \ , \tag{17}$$

avec $a_\pm$ constants. On en déduit que l'approximation WKB y est valide :

$$\psi(z) = a_+\psi^+_{\mathrm{WKB}}(z) + a_-\psi^-_{\mathrm{WKB}}(z) \ . \tag{18}$$

En revanche, si $Q(z)$ n'est pas négligeable, la diffusion sur ce "potentiel" génère un échange entre les ondes se propageant vers la gauche et vers la droite. La forme de la fonction badlands est donc déterminante pour la réflexion quantique. Comme nous allons le voir par la suite, ce nouveau "potentiel" peut être significativement différent de l'original et offrir une vision plus intuitive de la réflexion quantique.

[6] On supposera que le changement de coordonné $\tilde{z}(z)$ est dérivable trois fois et vérifie $\tilde{z}'(z) > 0$.

Réflexion sur le potentiel de Casimir-Polder

L'interaction de Casimir-Polder entre un atome et un miroir matériel varie rapidement à courte distance et peut provoquer la réflexion quantique d'atomes suffisamment froids. Pour évaluer quantitativement la probabilité de réflexion, nous commençons par calculer le potentiel de Casimir-Polder, avant de résoudre l'équation de Schrödinger avec ce potentiel.

Calcul du potentiel

L'approche dite "de diffusion" permet de calculer la force de Casimir entre deux objets à partir des propriétés de diffusion électromagnétique de chacun d'eux [77, 79]. Pour un atome éloigné d'une distance z d'un miroir, le potentiel d'interaction à température nulle est donnée par [170]

$$V(z) = \frac{\hbar}{c^2}\int_0^\infty \mathrm{d}\xi \int_0^\infty \frac{k_\perp \mathrm{d}k_\perp}{2\pi}\frac{\alpha(i\xi)}{4\pi\varepsilon_0}\frac{\xi^2}{\kappa_z}e^{-2\kappa_z z}\left[\rho^{\mathrm{TE}} - \left(1+\frac{2c^2k_\perp^2}{\xi^2}\right)\rho^{\mathrm{TM}}\right] , \tag{19}$$

$$\kappa_z \equiv \sqrt{\xi^2/c^2 + k_\perp^2} . \tag{20}$$

Cette expression est obtenue après passage aux fréquences imaginaires $\omega = i\xi$. La polarisabilité $\alpha(i\xi)$ caractérise la réponse de l'atome au champ électromagnétique et les $\rho^p(k_\perp, i\xi)$ sont les coefficients de réflexion sur le miroir correspondant aux polarisations transverse électrique ($p = \mathrm{TE}$) et transverse magnétique ($p = \mathrm{TM}$). Par exemple, pour un miroir diélectrique infiniment épais de permittivité $\varepsilon(i\xi)$,

$$\rho^{\mathrm{TE}}(k_\perp, i\xi) = \frac{\kappa_z - K_z}{\kappa_z + K_z} , \qquad \rho^{\mathrm{TM}}(k_\perp, i\xi) = \frac{\varepsilon(i\xi)\kappa_z - K_z}{\varepsilon(i\xi)\kappa_z + K_z} , \tag{21}$$

$$K_z \equiv \sqrt{\varepsilon(i\xi)\xi^2/c^2 + k_\perp^2} . \tag{22}$$

Pour un tel miroir, on distingue deux régimes suivant la valeur de la distance z par rapport à une longueur d'onde Λ caractérisant la réponse optique de l'atome et du miroir [64] :

$$V(z) \underset{z\ll\Lambda}{\simeq} -\frac{C_3}{z^3} , \qquad V(z) \underset{z\gg\Lambda}{\simeq} -\frac{C_4}{z^4} . \tag{23}$$

À courte distance, l'interaction entre l'atome et la surface peut-être considérée comme instantanée. À grande distance il faut tenir compte du temps de propagation des ondes électromagnétiques mais seules les basses fréquences contribuent.

Les potentiels d'interaction entre un atome d'hydrogène ou d'antihydrogène[7] et un miroir épais de silicium, de silice ou un miroir parfait sont tracés figure 1. Un miroir parfait est défini par $\rho^{\mathrm{TM}} = -\rho^{\mathrm{TE}} = 1$ et constitue une idéalisation d'un miroir métallique

[7] On considérera qu'hydrogène et antihydrogène ont la même polarisabilité.

très bon conducteur. Pour un tel miroir,

$$C_4 = C_{4,\mathrm{id}} \equiv \frac{3\hbar c}{8\pi}\frac{\alpha(0)}{2\pi\varepsilon_0} = 73.6 \text{ a.u. pour l'(anti)hydrogène.} \tag{24}$$

On utilise $V_{\mathrm{id}}(z) \equiv -C_{4,\mathrm{id}}/z^4$ comme référence pour mettre en évidence les régimes retardé et non-retardé dans le panneau de droite de la figure 1.

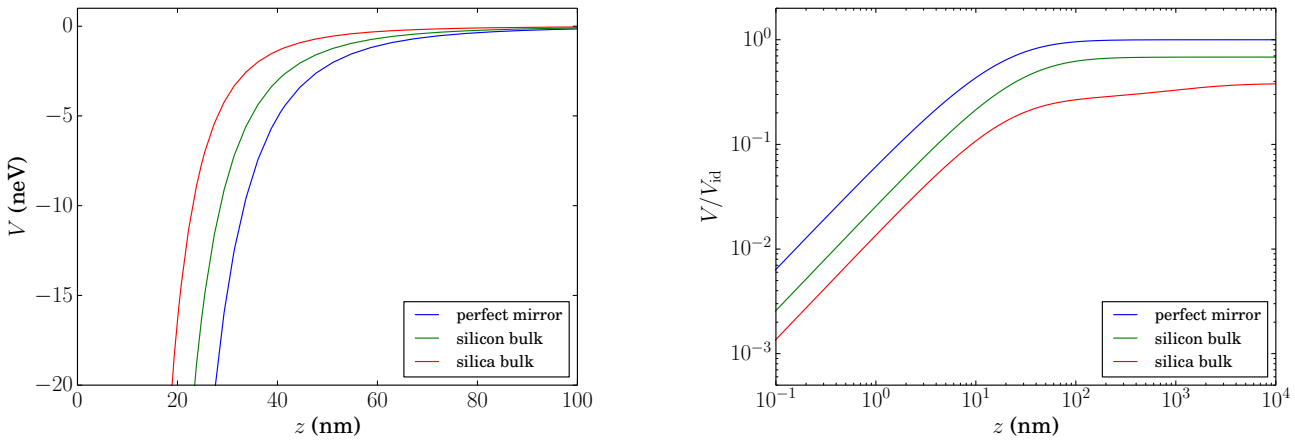

Figure 1 – Gauche : Potentiel de Casimir-Polder $V(z)$ entre un atome d'(anti)hydrogène et un miroir épais (bleu : miroir parfait, vert : silicium, rouge : silice). Droite : rapport $V(z)/V_{\mathrm{id}}(z)$ (même code couleur).

Nous verrons par la suite que les matériaux nanoporeux sont particulièrement intéressants du point de vue de la réflexion quantique. Ils sont composés d'une matrice solide qui emprisonne une grande quantité de gaz ou de vide. De tels matériaux sont par essence inhomogènes, mais leurs hétérogénéités sont de taille nanométrique, si bien qu'ils peuvent être considérés comme homogènes à une échelle plus grande. Plus la porosité ϕ du milieu est importante, plus sa permittivité effective est faible, ce qui conduit à des potentiels de Casimir-Polder très réduits [166]. La figure 2 montre par exemple le potentiel au voisinage d'aérogels de silice de différentes porosités.

Probabilité de réflexion

Nous voulons maintenant résoudre l'équation de Schrödinger (2) avec le potentiel de Casimir-Polder. L'étude de la fonction badlands (voir équation (10)) montre que celle-ci est piquée et qu'elle tend vers zéro à la fois à grande distance et sur la surface, comme schématisé figure 3. L'approximation WKB est donc valide de part et d'autre du pic et la direction de propagation des ondes y est bien définie.

On considère la solution de l'équation de Schrödinger (2) qui correspond à une surface parfaitement absorbante. C'est-à-dire que près de la surface la fonction d'onde est une

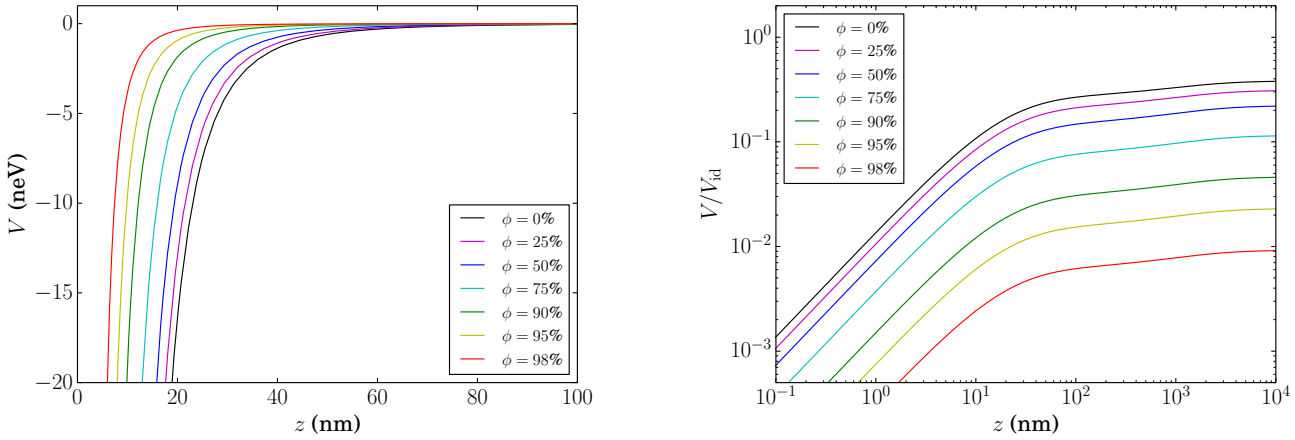

FIGURE 2 – Gauche : Potentiel de Casimir-Polder $V(z)$ entre un atome d'(anti)hydrogène et des miroirs de silice nanoporeuse de différentes porosités ϕ (noir : silice compacte, violet : $\phi = 25$ %, bleu : $\phi = 50$ %, cyan : $\phi = 75$ %, vert : $\phi = 90$ %, jaune : $\phi = 95$ %, rouge : $\phi = 98$ %). Droite : rapport $V(z)/V_{\mathrm{id}}(z)$ (même code couleur).

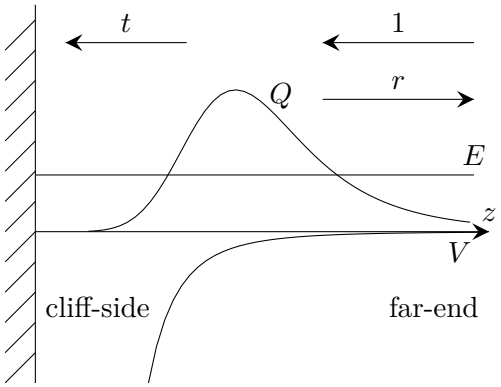

FIGURE 3 – Diffusion sur le potentiel de Casimir-Polder. De part et d'autre du pic de la fonction badlands l'amplitude des ondes se propageant vers la gauche et la droite est bien définie. Si la surface est absorbante, pour une onde incidente d'amplitude 1, l'onde réfléchie a une amplitude r et l'onde transmise a une amplitude t.

onde WKB se propageant vers la gauche :

$$\psi(z) \underset{z\to 0}{\simeq} \mathcal{N} t \psi^{-}_{\mathrm{WKB}}(z) \tag{25}$$

Loin de la surface, la fonction d'onde est la somme d'une onde incidente et d'une onde réfléchie :

$$\psi(z) \underset{z\to\infty}{\simeq} \mathcal{N}\left(\psi^{-}_{\mathrm{WKB}}(z) + r\psi^{+}_{\mathrm{WKB}}(z)\right) \tag{26}$$

$$= \frac{\mathcal{N}}{\sqrt{\kappa}}\left(e^{-i\kappa z} + re^{i\kappa z}\right) , \qquad \kappa \equiv \hbar^{-1}\sqrt{2mE} , \tag{27}$$

r et t sont respectivement les coefficients de réflexion et de transmission et $\mathcal{N}$ est une constante de normalisation.

Notre choix de condition aux limites absorbante est adapté pour l'antihydrogène, qui s'annihile au contact de la surface matérielle. Pour un atome de matière, la condition aux limites adaptée dépend du détail des interactions à très courte portée. Le coefficient de réflexion est alors modifié mais il peut s'exprimer en fonction des coefficients r et t calculés dans le cas d'une surface absorbante.

Pour résoudre l'équation de Schrödinger il est utile d'effectuer la transformation de Liouville (15) qui utilise la phase WKB comme coordonnée. L'équation transformée est définie sur tout l'axe réel, le potentiel y est partout régulier et s'annule en plus et moins l'infini (rappelons qu'il est égal à la fonction badlands). Les énergies et potentiels originaux et transformés sont tracés figure 4 pour divers miroirs et énergies.

On constate que les problèmes originaux et transformés sont très différents du point de vue de l'intuition classique : pour les premiers, la diffusion se fait sur un puits de potentiel et il n'y a pas de point de rebroussement classique ; pour les seconds, l'atome rencontre une barrière de potentiel qui peut être plus élevée que l'énergie. Malgré cela, ces situations sont parfaitement équivalentes pour ce qui est de la diffusion quantique [154, 155].

La probabilité de réflexion quantique de l'(anti)hydrogène sur des miroirs massifs est tracée figure 5. On y voit que la réflexion devient certaine à basse énergie et qu'elle reste significative dans la gamme d'énergie de GBAR (soit une dizaine de nanoélectronvolts). De plus, la dépendance en énergie de la probabilité de réflexion favorise la détection des atomes les plus énergétiques ; un biais qui devra être pris en compte dans l'analyse des données de GBAR.

La façon dont la probabilité de réflexion quantique $R \equiv |r|^2$ dépend de l'énergie et de la forme du potentiel n'est pas évidente dans le problème original. Après transformation, en revanche, il est tout de suite clair que les barrières les plus hautes sont associées aux plus grandes probabilités de réflexion. Or le pic de la fonction badlands est d'autant plus élevé que l'énergie est basse et que le potentiel est faible. Ainsi, à énergie fixée, la probabilité de réflexion est plus grande sur un miroir en silice que sur un miroir en silicium ou un miroir parfait, comme le montre la figure 5. Les matériaux nanoporeux interagissent très faiblement avec l'atome incident, ce qui conduit à des probabilités de réflexion quantique particulièrement élevées ; ils pourraient ainsi être utilisés pour piéger et guider des atomes d'antimatière [166].

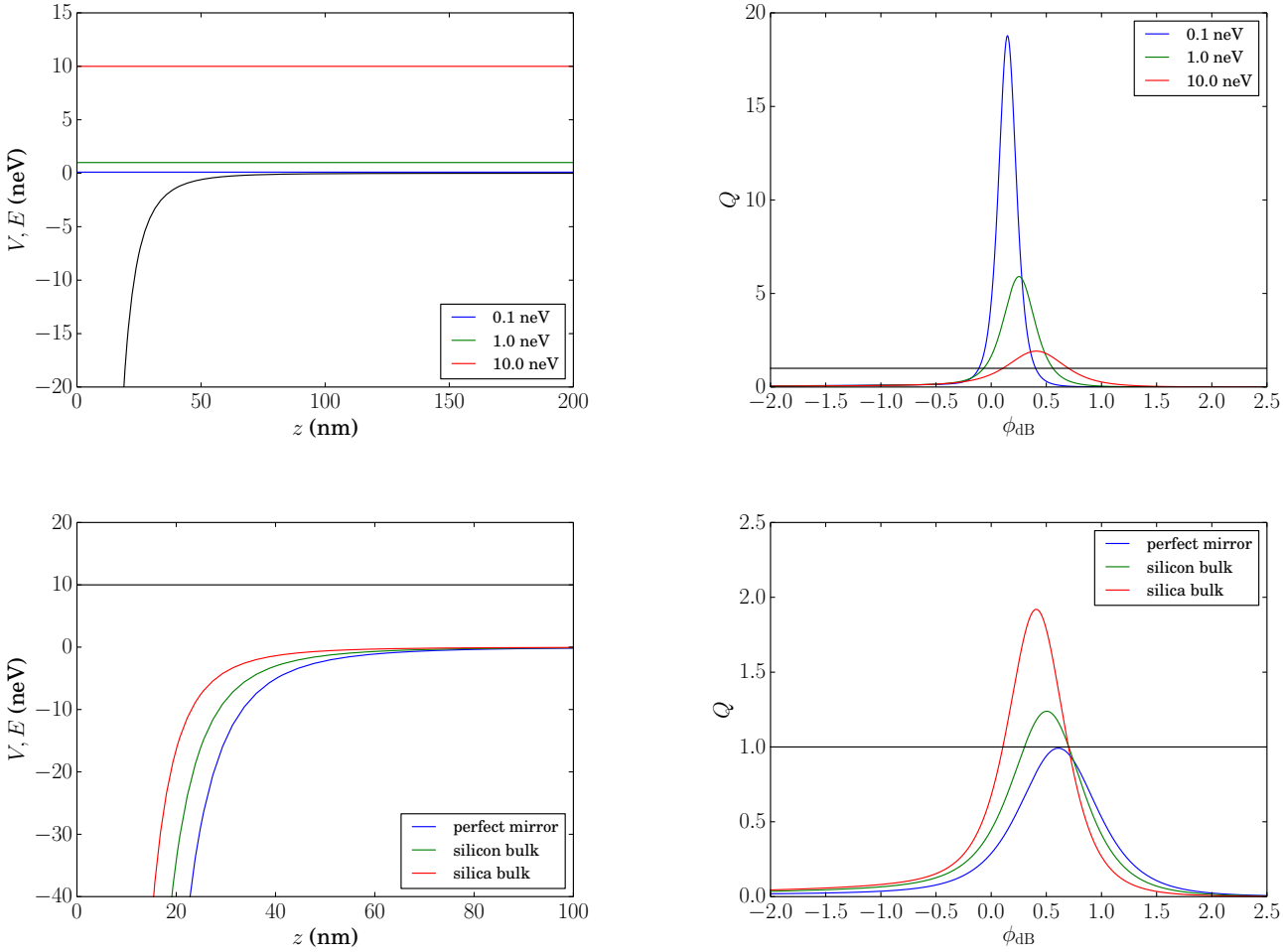

FIGURE 4 – Transformation de Liouville pour la diffusion d'un atome d'(anti)hydrogène sur le potentiel de Casimir-Polder. À gauche, les potentiels et énergies originaux ; à droite, les potentiels et énergies lorsque la phase WKB ϕ_{dB} est utilisée comme coordonnée. En haut : miroir épais en silice et atome d'énergie $E = 0.1,\ 1$ ou 10 neV (bleu, vert et rouge respectivement). En bas : atome d'énergie $E = 10$ neV, miroir parfait (bleu) ou miroir épais en silicium (vert) ou en silice (rouge).

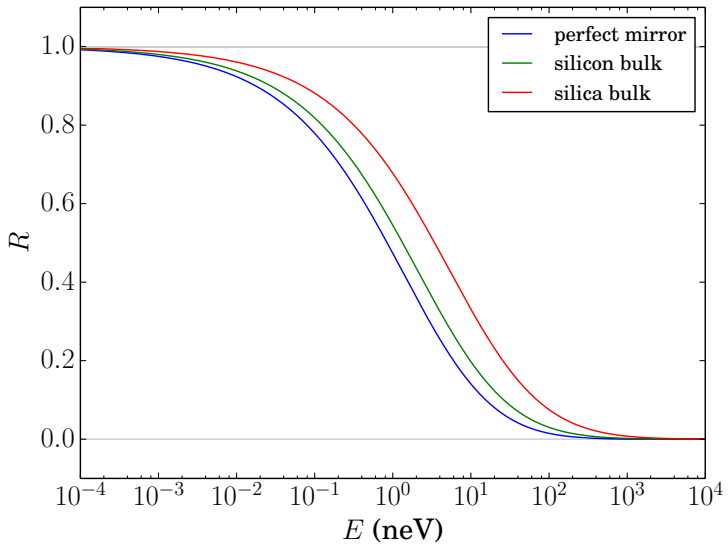

FIGURE 5 – Probabilité de réflexion en fonction de l'énergie d'un atome d'antihydrogène incident sur un miroir de silice (rouge), de silicium (vert) ou un miroir parfait (bleu).

Comme les interactions inter-atomiques dans un condensat de Bose-Einstein, l'interaction atome-surface à basse énergie est entièrement décrite par une longueur de diffusion notée a [124, 125]. Dans le régime où $\kappa^{-1} = \hbar(2mE)^{-1/2}$ est grand devant la portée du potentiel, on a

$$r \simeq \exp(-2i\kappa a) \ . \tag{28}$$

Si la surface est absorbante, la probabilité de réflexion R est inférieure à un, on en déduit que a est complexe, avec une partie imaginaire négative :

$$R \simeq \exp(-4\kappa b) \ , \qquad b \equiv -\operatorname{Im}(a) > 0 \ . \tag{29}$$

En traçant la probabilité de réflexion R en fonction du produit κb pour divers choix de miroir, on constate que toutes les courbes se superposent, même en dehors du domaine de validité de l'approximation de la longueur de diffusion. Avec une bonne approximation, la probabilité de réflexion quantique est donc une fonction universelle du paramètre κb. La forme de cette fonction est déterminée par la queue du potentiel $V(z) \propto z^{-4}$ [154, 155]. La connaissance du paramètre b permet ainsi d'évaluer la probabilité de réflexion rapidement et avec précision sur toute la gamme d'énergies où elle n'est pas négligeable. La figure 6 donne la valeur de b pour divers miroirs nanoporeux. On constate que b diminue lorsque la porosité du miroir augmente, ce qui indique une augmentation de la probabilité de réflexion quantique.

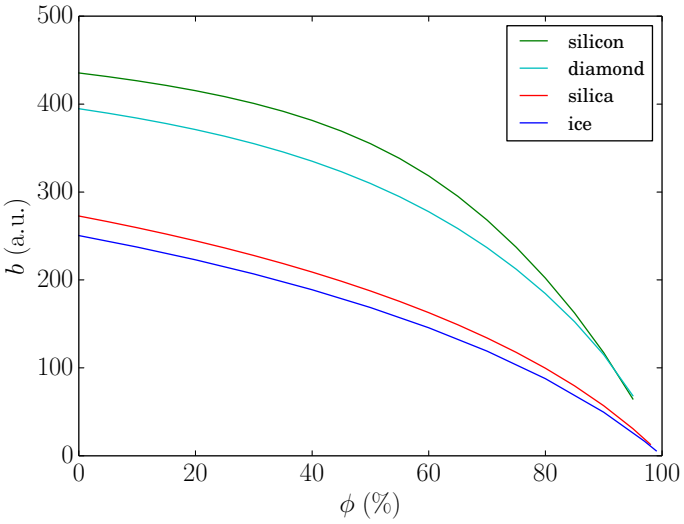

Figure 6 – Paramètre b caractérisant la diffusion à basse énergie d'un atome d'(anti)hydrogène sur un aérogel de silice (rouge) , du silicium poreux (vert) et une poudre de nanoparticules de glace (bleu foncé) ou de diamant (bleu clair), en fonction de la porosité du matériau.

Chute libre quantique

Jusqu'ici, nous n'avons pas inclus la gravité dans nos calculs. Dans un premier temps, nous nous éloignons de la surface pour considérer un paquet d'onde chutant dans l'espace libre. L'effet conjoint de la gravité et de la surface sera abordé dans la partie suivante.

En accord avec l'équivalence entre gravitation et accélération, l'équation de Schrödinger dans un champ de gravité uniforme est reliée à l'équation libre par un passage à un référentiel accéléré [37, 38]. Partant d'une solution $|\psi_0\rangle$ de l'équation libre

$$i\hbar\frac{\mathrm{d}}{\mathrm{d}t}|\psi_0\rangle = \hat{H}_0|\psi_0\rangle = \frac{\hat{P}^2}{2m}|\psi_0\rangle \ , \tag{30}$$

on définit

$$|\psi\rangle \equiv \hat{O}(t)|\psi_0\rangle \ , \qquad \hat{O}(t) \equiv \exp\left(\frac{i}{\hbar}\left(\frac{\overline{g}t^2}{2}\hat{P} - m\overline{g}t\hat{Z} + \frac{m\overline{g}^2t^3}{12}\right)\right) \ . \tag{31}$$

$\hat{O}$ est un opérateur unitaire qui effectue le changement de référentiel

$$\hat{O}(t)^\dagger\hat{Z}\hat{O}(t) = \hat{Z} - \frac{\overline{g}t^2}{2} \ , \qquad \hat{O}(t)^\dagger\hat{P}\hat{O}(t) = \hat{P} - m\overline{g}t \ . \tag{32}$$

Dans le nouveau référentiel, l'équation de Schrödinger s'écrit

$$i\hbar\frac{\mathrm{d}}{\mathrm{d}t}\left|\psi\right\rangle = \left(\hat{O}(t)\hat{H}_0\hat{O}(t)^\dagger + i\hbar\frac{\mathrm{d}\hat{O}}{\mathrm{d}t}(t)\,\hat{O}(t)^\dagger\right)\left|\psi\right\rangle \tag{33}$$

$$= \left(\frac{\hat{P}^2}{2m} + m\overline{g}\hat{Z}\right)\left|\psi\right\rangle \ . \tag{34}$$

Cette transformation permet d'exprimer facilement les solutions de l'équation dans le champ de gravité en fonction des solutions de l'équation libre.

Le problème peut aussi être abordé dans l'espace des phases à l'aide de la fonction de Wigner, définie à partir de la matrice densité $\hat{\rho}$ par

$$W(z,p,t) \equiv \frac{1}{2\pi\hbar}\int \mathrm{d}\zeta\, \langle z+\zeta/2|\hat{\rho}(t)|z-\zeta/2\rangle\, e^{-ip\zeta/\hbar} \ . \tag{35}$$

La fonction de Wigner obéit à une équation de Liouville quantique

$$\frac{\partial W}{\partial t}(z,p,t) = -\frac{p}{m}\frac{\partial W}{\partial z}(z,p,t) + \Theta[V]W(z,p,t) \ , \tag{36}$$

où $\Theta[V]$ est un opérateur pseudo-différentiel :

$$\Theta[V] = \frac{i}{\hbar}\left[V\left(z - \frac{i\hbar}{2}\frac{\partial}{\partial p}\right) - V\left(z + \frac{i\hbar}{2}\frac{\partial}{\partial p}\right)\right] \tag{37}$$

$$= \sum_{n=0}^{\infty}\frac{(-\hbar^2/4)^n}{(2n+1)!}\frac{\partial^{2n+1}V}{\partial z^{2n+1}}(z)\left(\frac{\partial}{\partial p}\right)^{2n+1} \ . \tag{38}$$

Pour un potentiel linéaire, la somme se réduit à son premier terme et on obtient l'équation de Liouville classique. Bien qu'elle reste un objet quantique, la fonction de Wigner se propage alors suivant les trajectoires classiques dans l'espace des phases [41]. On en déduit la fonction de Wigner au temps t en fonction de la condition initiale :

$$W(z,p,t) = W\left(z - \frac{pt}{m} - \frac{\overline{g}t^2}{2},\ p + m\overline{g}t,\ 0\right) \ . \tag{39}$$

Cette expression permet entre autres de calculer le courant à travers un plan horizontal d'altitude z, qui donne la distribution des temps d'arrivée d'une particule sur un détecteur idéal placé en z :

$$j(z,t) = \int \frac{p}{m}W\left(z,\ p,\ t\right)\mathrm{d}p = \int \frac{p}{m}W\left(z - \frac{pt}{m} - \frac{\overline{g}t^2}{2},\ p + m\overline{g}t, 0\right)\mathrm{d}p \ . \tag{40}$$

Pour un paquet d'onde initialement centré autour d'un point $(z,p) = (H,0)$ de l'espace des phases et de largeur $\Delta z \ll H$, on obtient l'expression approchée suivante pour la distribution des temps d'arrivée à l'altitude $z = 0$:

$$P(t) = |j(0,t)| \simeq m\overline{g}\left|\psi_p\left(m\overline{g}\left(t - \sqrt{2H/\overline{g}}\right)\right)\right|^2 \ , \tag{41}$$

où $|\psi_p(p,0)|^2$ est la distribution d'impulsion initiale.

Enfin, on peut aussi résoudre l'équation de Schrödinger dans un champ uniforme en en cherchant les solutions stationnaires, une approche qui nous sera utile par la suite. L'équation indépendante du temps s'écrit

$$-\frac{\hbar^2}{2m}\frac{\mathrm{d}^2}{\mathrm{d}z^2}\psi(z) + m\bar{g}z\psi(z) = E\psi(z) \tag{42}$$

et ses solutions s'expriment à l'aide de la fonction d'Airy [1, 214] :

$$\psi(z) = \frac{1}{\sqrt{E_g z_g}}\,\mathrm{Ai}\left(\frac{z}{z_g} - \frac{E}{E_g}\right)\,, \qquad z_g \equiv \left(\frac{\hbar^2}{2m^2\bar{g}}\right)^{1/3}\,, \quad E_g \equiv m\bar{g}z_g\,. \tag{43}$$

Cette fonction d'onde s'atténue exponentiellement au dessus du point de rebroussement classique $z_t = E/m\bar{g}$ et a un comportement oscillant en dessous.

Rebonds quantiques

États liés gravitationnellement

Dans cette dernière partie, on s'intéresse à l'effet conjoint de la gravité et de la réflexion sur une surface horizontale. Le système considéré est l'équivalent quantique d'une balle qui rebondit sur le sol. Dans un premier temps, on suppose que la réflexion est assurée par un mur de potentiel infini :

$$V(z) = \begin{cases} m\bar{g}z & \text{si } z > 0\,, \\ +\infty & \text{sinon.} \end{cases} \tag{44}$$

Par la suite, nous étudierons le cas où un atome rebondit sur un potentiel de Casimir-Polder.

Les états propres du puits de potentiel (44) sont obtenus en imposant à la fonction d'onde (43) de s'annuler en $z = 0$. On trouve[8]

$$\psi_n(z) \equiv \frac{\Theta(z)}{\sqrt{z_g}\,\mathrm{Ai}'(-E_n/E_g)}\,\mathrm{Ai}\left(\frac{z}{z_g} - \frac{E_n}{E_g}\right)\,, \tag{45}$$

où les énergies E_n s'expriment en fonction des zéros de la fonction d'Airy :

$$E_n \equiv a_n E_g \simeq \left(\frac{3\pi}{2}\left(n - \frac{1}{4}\right)\right)^{2/3} E_g\,, \qquad \mathrm{Ai}(-a_n) \equiv 0\,, \qquad n \in \mathbb{N}\,. \tag{46}$$

Ces fonctions d'ondes s'étendent sur une hauteur $h_n \equiv a_n z_g$. La réflexion sur la marche de potentiel étant parfaite, ces *états liés gravitationnellement* ont une durée de vie infinie.

[8] $\Theta(z)$ est la fonction "marche" de Heaviside.

En revanche, si la réflexion se fait sur un potentiel de Casimir-Polder, la réflexion n'est plus totale et une partie du paquet d'onde est absorbée par la surface.

En joignant la solution (43) de l'équation de Schrödinger dans le champ de gravité à la fonction d'onde dans le potentiel de Casimir-Polder dans l'approximation de la longueur de diffusion (équations (27) et (28)), on trouve les énergies propres suivantes [126] :

$$E_n^\star = a_n E_g + m\bar{g}a \equiv \epsilon_n - i\hbar\gamma_n/2 \tag{47}$$

$$\epsilon_n = a_n E_g + m\bar{g}\,\mathrm{Re}(a)\ , \qquad \gamma_n = -\hbar^{-1} m\bar{g}\,\mathrm{Im}(a)\ . \tag{48}$$

Ces énergies complexes correspondent à des états *quasi-stationnaires* qui décroissent sur une échelle de temps γ_n^{-1}. On remarque que les différences d'énergie $E_n^\star - E_m^\star$ sont identiques au cas idéal de la réflexion sur une marche infinie. L'étude des transitions entre états permettrait donc une mesure de $\bar{g}$ qui ne serait pas affectée par l'interaction de Casimir-Polder.

Le problème peut aussi être abordé de façon plus unifiée, sans découpler les effets de la gravité et du potentiel de Casimir-Polder, à l'aide d'une transformation de Liouville. La phase WKB ne peut être utilisée comme coordonnée dans ce cas en raison de l'existence d'un point de rebroussement classique z_t tel que

$$m\bar{g}z_t + V_{\mathrm{CP}}(z_t) = E\ . \tag{49}$$

On utilise plutôt la coordonnée "de Langer" [157] définie par

$$\boldsymbol{z}'(z) \equiv \sqrt{\frac{-F(z)}{\boldsymbol{z}}}\ , \qquad \text{for} \qquad z \neq z_t\ , \tag{50}$$

$$\boldsymbol{z}'(z_t) \equiv -F'(z_t)^{1/3}\ , \qquad \boldsymbol{z}(z_t) = 0\ , \tag{51}$$

$$\boldsymbol{F}(\boldsymbol{z}) = -\boldsymbol{z} + \frac{1}{2}\{z, \boldsymbol{z}\} = -\boldsymbol{z} - \frac{5}{16\boldsymbol{z}^2} + \boldsymbol{z}Q(z) \equiv -\boldsymbol{V}(\boldsymbol{z})\ . \tag{52}$$

Le résultat de la transformation est illustré par la figure 7. L'effet de la réflexion quantique se traduit par l'apparition d'un pic de potentiel qui s'ajoute à un potentiel linéaire s'étendant sur tout l'axe réel. Ainsi l'atome est piégé dans la cavité formée par la gravité d'un côté et la "barrière" de réflexion quantique de l'autre, barrière qu'il peut franchir par effet tunnel.

Les états quasi-stationnaires évoqués plus haut correspondent aux résonances de cette cavité. Pour le voir, on étudie le comportement de la fonction $(1-r)^{-1} = 1+r+r^2+\ldots$, où r est le coefficient de réflexion sur le côté droit de la barrière de réflexion quantique. Cette fonction somme les contributions des ondes ayant fait 0, 1, 2, ... tours dans la cavité ; elle a ses pôles aux énergies $E_n^\star$ des états quasi-stationnaires, si bien que pour une énergie réelle E proche de $E_n^\star = \epsilon_n - i\hbar\gamma_n/2$ on a

$$(1-r)^{-1} \underset{E\simeq E_n^\star}{\simeq} \left(\frac{\mathrm{d}r}{\mathrm{d}E}\Big|_{E_n^\star}\right)^{-1} \frac{1}{E_n^\star - E}\ , \tag{53}$$

$$|1-r|^{-2} \underset{E\simeq E_n^\star}{\simeq} \frac{A_n}{(E-\epsilon_n)^2 + \hbar^2\gamma_n^2/4}\ , \qquad A_n = \left|\frac{\mathrm{d}r}{\mathrm{d}E}\Big|_{E_n^\star}\right|^{-2}\ . \tag{54}$$

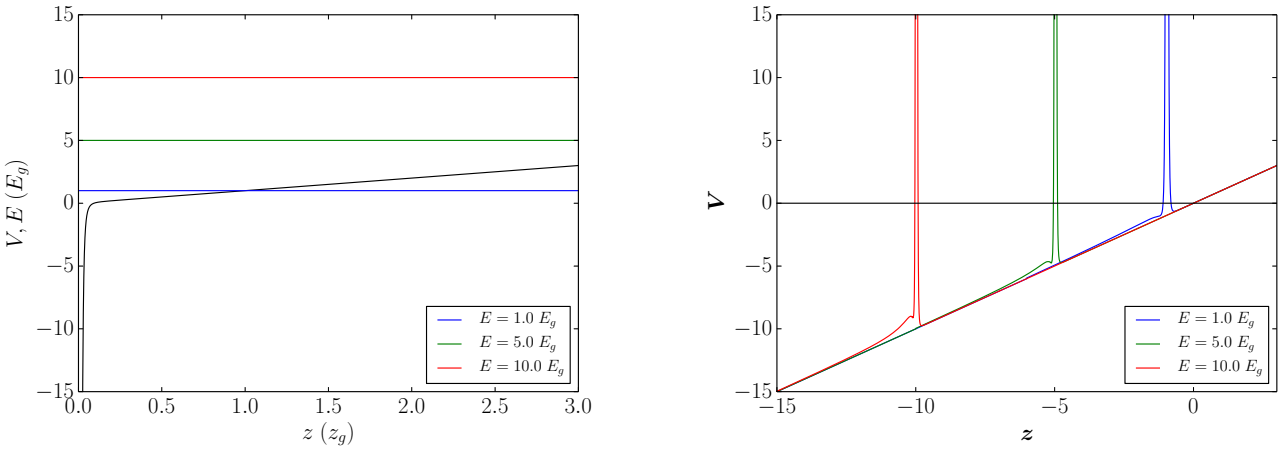

FIGURE 7 – Transformation de Liouville vers la coordonnée de Langer appliquée à l'équation de Schrödinger décrivant un atome d'(anti)hydrogène d'énergie $E = 1,\ 5$ ou $10\ E_g$ (lignes bleue, verte et rouge respectivement) au dessus d'un miroir en silice.

L'ajustement de la courbe de $|1 - r|^{-2}$ en fonction de E par des fonctions lorentziennes permet de déterminer les valeurs de ϵ_n et γ_n. On vérifie alors la validité des expressions (47) obtenues précédemment.

Façonnage de la distribution de vitesses dans GBAR

Pour finir, nous revenons à l'expérience GBAR et proposons un moyen d'en améliorer la résolution en utilisant les rebonds quantiques de l'antihydrogène [216]. L'incertitude ΔT sur le temps de chute de l'atome d'antihydrogène a plusieurs origines :

- l'incertitude sur l'instant du photodétachement qui marque le début de la chute libre,
- la résolution finie sur la mesure du temps d'annihilation qui marque la fin de la chute libre,
- la vitesse de recul communiquée à l'atome lors du photodétachment,
- la largeur des distributions de position et de vitesse du paquet d'onde quantique.

Pour l'expérience initialement prévue, les deux derniers points sont nettement dominants. Ils conduisent à une incertitude de l'ordre de $\Delta v \approx 0.7$ m.s^{-1} sur la vitesse verticale initiale de l'anti-atome. Pour $N_{\mathrm{tot}} = 7500$ chutes libres indépendantes sur une hauteur $H \approx 10$ cm, il en résulte une incertitude relative sur la valeur de $\overline{g}$ de

$$\frac{1}{\sqrt{N_{\mathrm{tot}}}}\frac{\Delta\overline{g}}{\overline{g}} \simeq \frac{2}{\sqrt{N_{\mathrm{tot}}}}\frac{\Delta v}{\sqrt{2\overline{g}H}} \approx 1\% \ . \tag{55}$$

En outre, une éventuelle asymétrie haut-bas du recul associé au photodétachement constitue un effet systématique difficile à évaluer.

Pour s'affranchir d'un tel effet tout en améliorant la précision de GBAR, on peut s'inspirer des expériences qui ont permis d'observer les états liés gravitationnellement de neutrons ultra-froids. Ces expériences consistent à faire passer les neutrons dans un guide d'onde constitué d'un "plancher" réfléchissant et d'un "plafond" absorbant dont on peut changer la hauteur. La transmission à travers un tel système augmente par à-coups à chaque fois que la hauteur h du plafond dépasse la taille $h_n = a_n z_g$ d'un nouvel état lié gravitationnellement [53–55].

Le dispositif proposé pour l'expérience GBAR est schématisé figure 8. Les atomes d'antihydrogène passent entre deux disques superposés jouant le rôle de miroir pour celui du bas (surface lisse) et d'absorbeur pour celui du haut (surface rugueuse). Dans un premier temps il sera utilisé dans un régime "classique", avec une hauteur h bien supérieure à la taille des premiers états gravitationnellement liés, si bien qu'on peut considérer que les atomes suivent des trajectoires classiques.

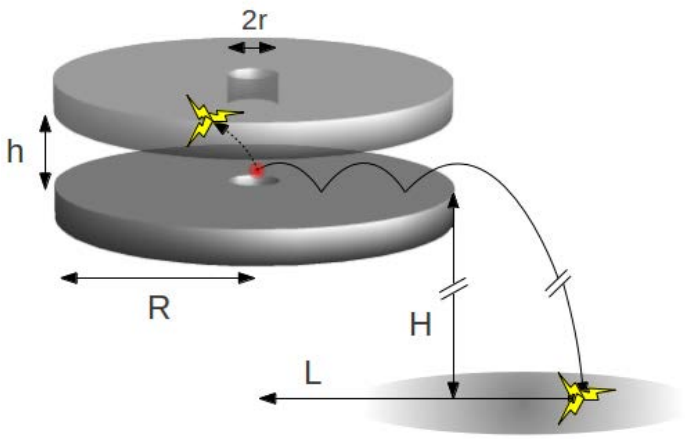

Figure 8 – Schéma de principe du système de façonnage de la distribution de vitesses. Un atome d'antihydrogène est libéré du piège de Paul (point central). Si sa vitesse verticale n'est pas trop importante, il rebondit sur le disque inférieur et sort d'entre les deux disques pour chuter librement vers la plaque de détection. En revanche si sa vitesse verticale est trop élevée, il rencontre le disque supérieur dont la surface est rugueuse, ce qui conduit à son annihilation.

À la sortie d'un tel dispositif, la position et la vitesse de l'atome sont comprises entre des bornes bien définies :

$$H < z_{\text{out}} < H + h \ , \qquad -\sqrt{2\bar{g}h} < v_{\text{out}} < \sqrt{2\bar{g}h} \ . \tag{56}$$

La fraction d'atomes sélectionnés par le dispositif est de l'ordre de $\sqrt{2\overline{g}h}/\Delta v$. Pour chacun de ces atomes, l'incertitude sur la durée de la chute libre est réduite d'un facteur de l'ordre de $\sqrt{2\overline{g}h}/\Delta v$. Au final, l'incertitude statistique (55) est réduite d'un facteur $\sim (2\overline{g}h/\Delta v^2)^{1/4}$.

Le façonnage de la distribution de vitesses des atomes d'antihydrogène permet une détermination plus précise de la valeur de $\overline{g}$ tout en l'affranchissant de tout effet systématique lié au photodétachement. Par ailleurs, à plus long terme, un tel dispositif peut être utilisé pour observer les états liés de l'antihydrogène dans le champ de gravité. Des mesures de spectroscopiques ou interférométriques sur ces états permettraient une détermination encore plus fine de $\overline{g}$ [126, 217, 229].

Conclusion

Notre exploration de la réflexion sur le potentiel de Casimir-Polder nous a conduit à étudier successivement trois phénomènes éminemment quantiques. En premier lieu, l'interaction entre l'atome et le miroir, qui résulte des fluctuations du champ électromagnétique quantifié. Ensuite, la diffusion de l'onde de matière atomique sur ce potentiel d'interaction. Enfin, les rebonds quantiques de l'atome dans le champ de gravité au dessus du miroir.

Ce travail a permis de déterminer l'impact de la réflexion quantique sur l'expérience GBAR et plus généralement d'évaluer les probabilités de réflexion quantique de l'antihydrogène sur diverses surfaces. Pour ce faire, nous avons développé une nouvelle approche basée sur les transformations de Liouville de l'équation de Schrödinger. L'inclusion de la gravité dans nos calculs a fait apparaître les états quasi-stationnaires de l'atome maintenu dans le champ de pesanteur par la réflexion quantique. L'utilisation d'un guide pour les atomes d'antihydrogène permettrait d'améliorer la précision de l'expérience GBAR et constituerait un premier pas vers l'observation de ces états.

Bibliography

[1] F. W. J. Olver, D. W. Lozier, R. F. Boisvert, and C. W. Clark, eds., *NIST Handbook of Mathematical Functions*, see also the online companion `http://dlmf.nist.gov/` (Cambridge University Press, New York, NY, 2010) (cited on pp. viii, 14, 60, 71, 72, 100, 141, 142, 144, 147, 153, 173).

[2] L. de Broglie, "Recherches sur la théorie des quanta", PhD Thesis (Université de Paris, 1924) (cited on p. 1).

[3] E. Schrödinger, "Quantisierung als Eigenwertproblem", Annalen der Physik **384**, 361 (1926) (cited on p. 1).

[4] P. A. M. Dirac, "The quantum theory of the electron", Proceedings of the Royal Society of London A: Mathematical, Physical and Engineering Sciences **117**, 610 (1928) (cited on p. 1).

[5] C. D. Anderson, "The apparent existence of easily deflectable positives", Science **76**, 238 (1932) (cited on p. 1).

[6] C. C. Speake and C. M. Will, "Tests of the weak equivalence principle", Classical and Quantum Gravity **29**, 180301 (2012) (cited on p. 2).

[7] T. A. Wagner, S. Schlamminger, J. H. Gundlach, and E. G. Adelberger, "Torsion-balance tests of the weak equivalence principle", Classical and Quantum Gravity **29**, 184002 (2012) (cited on pp. 2, 4, 94).

[8] S. Fray, C. A. Diez, T. W. Hänsch, and M. Weitz, "Atomic interferometer with amplitude gratings of light and its applications to atom based tests of the Equivalence Principle", Physical Review Letters **93**, 240404 (2004) (cited on pp. 2, 4).

[9] D. Schlippert, J. Hartwig, H. Albers, L. L. Richardson, C. Schubert, A. Roura, W. P. Schleich, W. Ertmer, and E. M. Rasel, "Quantum test of the universality of free fall", Physical Review Letters **112**, 203002 (2014) (cited on pp. 2, 4).

[10] J. Scherk, "Antigravity: A crazy idea?", Physics Letters B **88**, 265 (1979) (cited on p. 2).

[11] G. Chardin, "Motivations for antigravity in General Relativity", Hyperfine Interactions **109**, 83 (1997) (cited on p. 2).

[12] M. Villata, "CPT symmetry and antimatter gravity in general relativity", EPL (Europhysics Letters) **94**, 20001 (2011) (cited on p. 2).

[13] V. A. Kostelecký and J. D. Tasson, "Matter-gravity couplings and Lorentz violation", Physical Review D **83**, 016013 (2011) (cited on p. 2).

[14] A. Benoit-Lévy and G. Chardin, "Introducing the Dirac-Milne universe", Astronomy & Astrophysics **537**, A78 (2012) (cited on p. 2).

[15] M. M. Nieto and T. Goldman, "The arguments against "antigravity" and the gravitational acceleration of antimatter", Physics Reports **205**, 221 (1991) (cited on p. 2).

[16] E. G. Adelberger, B. R. Heckel, C. W. Stubbs, and Y. Su, "Does antimatter fall with the same acceleration as ordinary matter?", Physical Review Letters **66**, 850 (1991) (cited on p. 2).

[17] R. J. Hughes and M. H. Holzscheiter, "Constraints on the gravitational properties of antiprotons and positrons from cyclotron-frequency measurements", Physical Review Letters **66**, 854 (1991) (cited on p. 2).

[18] F. C. Witteborn and W. M. Fairbank, "Experimental comparison of the gravitational force on freely falling electrons and metallic electrons", Physical Review Letters **19**, 1049 (1967) (cited on p. 2).

[19] G. Baur et al., "Production of antihydrogen", Physics Letters B **368**, 251 (1996) (cited on p. 2).

[20] M. H. Holzscheiter, M. Charlton, and M. M. Nieto, "The route to ultra-low energy antihydrogen", Physics Reports **402**, 1 (2004) (cited on p. 2).

[21] M. Hori and J. Walz, "Physics at CERN's Antiproton Decelerator", Progress in Particle and Nuclear Physics **72**, 206 (2013) (cited on p. 2).

[22] The ALPHA Collaboration and A. E. Charman, "Description and first application of a new technique to measure the gravitational mass of antihydrogen", Nature Communications **4**, 1785 (2013) (cited on p. 2).

[23] S. Maury, W. Oelert, W. Bartmann, P. Belochitskii, H. Breuker, F. Butin, C. Carli, T. Eriksson, S. Pasinelli, and G. Tranquille, "ELENA: The extra low energy anti-proton facility at CERN", Hyperfine Interactions **229**, 105 (2014) (cited on p. 2).

[24] AEGIS Collaboration and M. G. Giammarchi, "AEGIS at CERN: Measuring antihydrogen fall", Few-Body Systems **54**, 779 (2012) (cited on p. 3).

[25] P. Hamilton, A. Zhmoginov, F. Robicheaux, J. Fajans, J. S. Wurtele, and H. Müller, "Antimatter interferometry for gravity measurements", Physical Review Letters **112**, 121102 (2014) (cited on p. 3).

[26] G. Chardin et al., *Proposal to measure the Gravitational Behaviour of Antihydrogen at Rest*, CERN-SPSC-2011-029. SPSC-P-342 (CERN, Geneva, 2011) (cited on pp. 3, 161).

[27] P. Pérez and Y. Sacquin, "The GBAR experiment: gravitational behaviour of antihydrogen at rest", Classical and Quantum Gravity **29** (2012) 10.1088/0264-9381/29/18/184008 (cited on pp. 3, 161).

[28] J. Walz and T. W. Hänsch, "A proposal to measure antimatter gravity using ultracold antihydrogen atoms", General Relativity and Gravitation **36**, 561 (2004) (cited on pp. 3, 161).

[29] P. Crivelli, U. Gendotti, A. Rubbia, L. Liszkay, P. Pérez, and C. Corbel, "Measurement of the orthopositronium confinement energy in mesoporous thin films", Physical Review A **81**, 052703 (2010) (cited on p. 3).

[30] P. Comini and P.-A. Hervieux, "$\bar{\mathrm{H}}^{+}$ ion production from collisions between antiprotons and excited positronium: cross sections calculations in the framework of the GBAR experiment", New Journal of Physics **15**, 095022 (2013) (cited on p. 3).

[31] L. Hilico, J.-P. Karr, A. Douillet, P. Indelicato, S. Wolf, and F. S. Kaler, "Preparing single ultra-cold antihydrogen atoms for free-fall in GBAR", International Journal of Modern Physics: Conference Series **30**, 1460269 (2014) (cited on p. 3).

[32] Y. Giomataris, P. Rebourgeard, J. P. Robert, and G. Charpak, "MICROMEGAS: a high-granularity position-sensitive gaseous detector for high particle-flux environments", Nuclear Instruments and Methods in Physics Research Section A: Accelerators, Spectrometers, Detectors and Associated Equipment **376**, 29 (1996) (cited on p. 3).

[33] D. Greenberger, "The role of equivalence in quantum mechanics", Annals of Physics **47**, 116 (1968) (cited on p. 4).

[34] L. Viola and R. Onofrio, "Testing the equivalence principle through freely falling quantum objects", Physical Review D **55**, 455 (1997) (cited on p. 4).

[35] M. M. Ali, A. S. Majumdar, D. Home, and A. K. Pan, "On the quantum analogue of Galileo's leaning tower experiment", Classical and Quantum Gravity **23**, 6493 (2006) (cited on p. 4).

[36] P. Chowdhury, D. Home, A. S. Majumdar, S. V. Mousavi, M. R. Mozaffari, and S. Sinha, "Strong quantum violation of the gravitational weak equivalence principle by a non-Gaussian wave packet", Classical and Quantum Gravity **29**, 025010 (2012) (cited on p. 4).

[37] D. M. Greenberger and A. W. Overhauser, "Coherence effects in neutron diffraction and gravity experiments", Reviews of Modern Physics **51**, 43 (1979) (cited on pp. 4, 83, 171).

[38] D. M. Greenberger, "The neutron interferometer as a device for illustrating the strange behavior of quantum systems", Reviews of Modern Physics **55**, 875 (1983) (cited on pp. 4, 83, 171).

[39] A. Herdegen and J. Wawrzycki, "Is Einstein's equivalence principle valid for a quantum particle?", Physical Review D **66**, 044007 (2002) (cited on p. 4).

[40] E. Okon and C. Callender, "Does quantum mechanics clash with the equivalence principle—and does it matter?", European Journal for Philosophy of Science **1**, 133 (2010) (cited on p. 4).

[41] E. Kajari, N. L. Harshman, E. M. Rasel, S. Stenholm, G. Süßmann, and W. P. Schleich, "Inertial and gravitational mass in quantum mechanics", Applied Physics B **100**, 43 (2010) (cited on pp. 4, 88, 90, 102, 172).

[42] R. Colella, A. W. Overhauser, and S. A. Werner, "Observation of gravitationally induced quantum interference", Physical Review Letters **34**, 1472 (1975) (cited on p. 4).

[43] M. Kasevich and S. Chu, "Atomic interferometry using stimulated Raman transitions", Physical Review Letters **67**, 181 (1991) (cited on p. 4).

[44] M. G. Tarallo, T. Mazzoni, N. Poli, D. V. Sutyrin, X. Zhang, and G. M. Tino, "Test of Einstein Equivalence Principle for 0-Spin and Half-Integer-Spin Atoms: Search for Spin-Gravity Coupling Effects", Physical Review Letters **113**, 023005 (2014) (cited on p. 4).

[45] B. Altschul et al., "Quantum tests of the Einstein Equivalence Principle with the STE–QUEST space mission", Advances in Space Research **55**, 501 (2015) (cited on p. 4).

[46] J. J. Berkhout, O. J. Luiten, I. D. Setija, T. W. Hijmans, T. Mizusaki, and J. T. M. Walraven, "Quantum reflection: Focusing of hydrogen atoms with a concave mirror", Physical Review Letters **63**, 1689 (1989) (cited on pp. 4, 7).

[47] M. A. Kasevich, D. S. Weiss, and S. Chu, "Normal-incidence reflection of slow atoms from an optical evanescent wave", Optics Letters **15**, 607 (1990) (cited on p. 4).

[48] H. Wallis, J. Dalibard, and C. Cohen-Tannoudji, "Trapping atoms in a gravitational cavity", Applied Physics B **54**, 407 (1992) (cited on p. 4).

[49] C. G. Aminoff, A. M. Steane, P. Bouyer, P. Desbiolles, J. Dalibard, and C. Cohen-Tannoudji, "Cesium atoms bouncing in a stable gravitational cavity", Physical Review Letters **71**, 3083 (1993) (cited on p. 4).

[50] P. W. Langhoff, "Schrödinger particle in a gravitational well", American Journal of Physics **39**, 954 (1971) (cited on p. 4).

[51] R. L. Gibbs, "The quantum bouncer", American Journal of Physics **43**, 25 (1975) (cited on p. 4).

[52] J. Gea-Banacloche, "A quantum bouncing ball", American Journal of Physics **67**, 776 (1999) (cited on pp. 4, 105).

[53] V. V. Nesvizhevsky et al., "Quantum states of neutrons in the Earth's gravitational field", Nature **415**, 297 (2002) (cited on pp. 4, 110, 176).

[54] V. V. Nesvizhevsky et al., "Measurement of quantum states of neutrons in the Earth's gravitational field", Physical Review D **67**, 102002 (2003) (cited on pp. 4, 110, 121, 176).

[55] V. V. Nesvizhevsky et al., "Study of the neutron quantum states in the gravity field", European Physical Journal C **40**, 479 (2005) (cited on pp. 4, 110, 121, 176).

[56] M. Kreuz et al., "A method to measure the resonance transitions between the gravitationally bound quantum states of neutrons in the GRANIT spectrometer", Nuclear Instruments and Methods in Physics Research Section A: Accelerators, Spectrometers, Detectors and Associated Equipment, Particle Physics with Slow Neutrons **611**, 326 (décembre 11, 2009) (cited on p. 4).

[57] T. Jenke, P. Geltenbort, H. Lemmel, and H. Abele, "Realization of a gravity-resonance-spectroscopy technique", Nature Physics **7**, 468 (2011) (cited on p. 4).

[58] S. Baeßler, M. Beau, M. Kreuz, V. N. Kurlov, V. V. Nesvizhevsky, G. Pignol, K. V. Protasov, F. Vezzu, and A. Y. Voronin, "The GRANIT spectrometer", Comptes Rendus Physique **12**, 707 (2011) (cited on p. 4).

[59] S. Baeßler, V. V. Nesvizhevsky, G. Pignol, K. V. Protasov, D. Rebreyend, E. A. Kupriyanova, and A. Y. Voronin, "Frequency shifts in gravitational resonance spectroscopy", Physical Review D **91**, 042006 (2015) (cited on p. 4).

[60] K.-T. Tang and J. P. Toennies, "Johannes Diderik van der Waals: A pioneer in the molecular sciences and Nobel prize winner in 1910", Angewandte Chemie (International Edition) **49**, 9539 (2010) (cited on p. 5).

[61] F. London, "The general theory of molecular forces", Transactions of the Faraday Society **33**, 8b (1937) (cited on pp. 5, 161).

[62] E. J. W. Verwey and J. T. G. Overbeek, "Long distance forces acting between colloidal particles", Transactions of the Faraday Society **42**, B117 (1946) (cited on p. 5).

[63] H. B. G. Casimir and D. Polder, "Influence of retardation on the London-van der Waals forces", Nature **158**, 787 (1946) (cited on pp. 5, 161).

[64] H. B. G. Casimir and D. Polder, "The Influence of Retardation on the London-van der Waals Forces", Physical Review **73**, 360 (1948) (cited on pp. 5, 47, 161, 165).

[65] H. B. G. Casimir, "Sur les forces van der Waals-London", in (1948) (cited on pp. 5, 162).

[66] H. B. G. Casimir, "On the attraction between two perfectly conducting plates", Proc. K. Ned. Akad. Wet **51**, 793 (1948) (cited on pp. 5, 162).

[67] S. K. Lamoreaux, "Demonstration of the Casimir force in the 0.6 to μm range", Physical Review Letters **78**, 5 (1997) (cited on pp. 5, 162).

[68] U. Mohideen and A. Roy, "Precision measurement of the Casimir force from 0.1 to 0.9 μm", Physical Review Letters **81**, 4549 (1998) (cited on pp. 5, 162).

[69] R. S. Decca, D. López, E. Fischbach, and D. E. Krause, "Measurement of the Casimir force between dissimilar metals", Physical Review Letters **91**, 050402 (2003) (cited on pp. 5, 162).

[70] K. A. Milton, "Resource Letter VWCPF-1: van der Waals and Casimir–Polder forces", American Journal of Physics **79**, 697 (2011) (cited on p. 5).

[71] G. Plunien, B. Müller, and W. Greiner, "The Casimir effect", Physics Reports **134**, 87 (1986) (cited on p. 6).

[72] J. Schwinger, "Casimir effect in source theory", Letters in Mathematical Physics **1**, 43 (1975) (cited on p. 6).

[73] J. Schwinger, L. L. DeRaad Jr., and K. A. Milton, "Casimir effect in dielectrics", Annals of Physics **115**, 1 (1978) (cited on p. 6).

[74] E. M. Lifshitz, "The theory of molecular attractive forces between solids", Soviet Physics JETP **2**, 73 (1956) (cited on p. 6).

[75] I. E. Dzyaloshinskii, E. M. Lifshitz, and L. P. Pitaevskii, "General theory of van der waals forces", Soviet Physics Uspekhi **4**, 153 (1961) (cited on p. 6).

[76] C. Genet, A. Lambrecht, and S. Reynaud, "Casimir force and the quantum theory of lossy optical cavities", Physical Review A **67**, 043811 (2003) (cited on pp. 6, 39, 40).

[77] A. Lambrecht, P. A. M. Neto, and S. Reynaud, "The Casimir effect within scattering theory", New Journal of Physics **8**, 243 (2006) (cited on pp. 6, 165).

[78] T. Emig, N. Graham, R. L. Jaffe, and M. Kardar, "Casimir forces between arbitrary compact objects", Physical Review Letters **99**, 170403 (2007) (cited on p. 6).

[79] K. A. Milton and J. Wagner, "Multiple scattering methods in Casimir calculations", Journal of Physics A: Mathematical and Theoretical **41**, 155402 (2008) (cited on pp. 6, 165).

[80] G. Feinberg and J. Sucher, "General theory of the van der Waals interaction: A model-independent approach", Physical Review A **2**, 2395 (1970) (cited on p. 6).

[81] D. Dalvit, P. Milonni, D. Roberts, and F. da Rosa, eds., *Casimir Physics*, Vol. 834, Lecture Notes in Physics (Springer Berlin Heidelberg, Berlin, Heidelberg, 2011) (cited on p. 6).

[82] M. DeKieviet, U. D. Jentschura, and G. Łach, "Modern Experiments on Atom-Surface Casimir Physics", in *Casimir Physics*, edited by D. Dalvit, P. Milonni, D. Roberts, and F. da Rosa, Lecture Notes in Physics 834 (Springer Berlin Heidelberg, 2011), pp. 393–418 (cited on p. 6).

[83] A. Landragin, J.-Y. Courtois, G. Labeyrie, N. Vansteenkiste, C. I. Westbrook, and A. Aspect, "Measurement of the van der Waals force in an atomic mirror", Physical Review Letters **77**, 1464 (août 19, 1996) (cited on p. 6).

[84] R. Côté, B. Segev, and M. G. Raizen, "Retardation effects on quantum reflection from an evanescent-wave atomic mirror", Physical Review A **58**, 3999 (1998) (cited on pp. 6, 7).

[85] H. Bender, P. W. Courteille, C. Marzok, C. Zimmermann, and S. Slama, "Direct measurement of intermediate-range Casimir-Polder potentials", Physical Review Letters **104**, 083201 (février 22, 2010) (cited on p. 6).

[86] A. K. Mohapatra and C. S. Unnikrishnan, "Measurement of the van der Waals force using reflection of cold atoms from magnetic thin-film atom mirrors", EPL (Europhysics Letters) **73**, 839 (2006) (cited on p. 6).

[87] L. Brekhovskikh, *Waves in layered media*, 2nd (Elsevier, 2012) (cited on p. 7).

[88] J. E. Lennard-Jones and A. F. Devonshire, "The interaction of atoms and molecules with solid surfaces. III. The Condensation and Evaporation of Atoms and Molecules", Proceedings of the Royal Society of London. Series A - Mathematical and Physical Sciences **156**, 6 (1936) (cited on p. 7).

[89] J. E. Lennard-Jones and A. F. Devonshire, "The interaction of atoms and molecules with solid surfaces. IV. The condensation and evaporation of atoms and molecules", Proceedings of the Royal Society of London. Series A - Mathematical and Physical Sciences **156**, 29 (1936) (cited on p. 7).

[90] F. O. Goodman, "Role of the attractive potential in gas-surface interaction theory", The Journal of Chemical Physics **55**, 5742 (1971) (cited on p. 7).

[91] P. M. Echenique and J. B. Pendry, "Reflectivity of liquid ^{4}He surfaces to ^{4}He atoms", Physical Review Letters **37**, 561 (août 30, 1976) (cited on p. 7).

[92] D. O. Edwards and P. P. Fatouros, "Theory of atomic scattering at the free surface of liquid ^{4}He", Physical Review B **17**, 2147 (1978) (cited on p. 7).

[93] C. Carraro and M. W. Cole, "Sticking coefficient at ultralow energy : Quantum reflection", Progress in Surface Science **57**, 61 (1998) (cited on p. 7).

[94] V. U. Nayak, D. O. Edwards, and N. Masuhara, "Scattering of ^{4}He Atoms Grazing the Liquid-^{4}He Surface", Physical Review Letters **50**, 990 (1983) (cited on p. 7).

[95] I. A. Yu, J. M. Doyle, J. C. Sandberg, C. L. Cesar, D. Kleppner, and T. J. Greytak, "Evidence for universal quantum reflection of hydrogen from liquid ^{4}He", Physical Review Letters **71**, 1589 (1993) (cited on p. 7).

[96] F. Shimizu, "Specular reflection of very slow metastable neon atoms from a solid surface", Physical review letters **86**, 987 (2001) (cited on pp. 7, 77, 79).

[97] V. Druzhinina and M. DeKieviet, "Experimental observation of quantum reflection far from threshold", Physical Review Letters **91**, 193202 (2003) (cited on pp. 7, 77, 81).

[98] T. A. Pasquini, Y. Shin, C. Sanner, M. Saba, A. Schirotzek, D. E. Pritchard, and W. Ketterle, "Quantum reflection from a solid surface at normal incidence", Physical Review Letters **93**, 223201 (2004) (cited on pp. 7, 77).

[99] F. Shimizu and J.-i. Fujita, "Reflection-type hologram for atoms", Physical Review Letters **88**, 123201 (2002) (cited on p. 7).

[100] F. Shimizu and J.-i. Fujita, "Giant quantum reflection of neon atoms from a ridged silicon surface", Journal of the Physical Society of Japan **71**, 5 (2002) (cited on p. 7).

[101] H. Oberst, D. Kouznetsov, K. Shimizu, J.-i. Fujita, and F. Shimizu, "Fresnel diffraction mirror for an atomic wave", Physical Review Letters **94**, 013203 (2005) (cited on p. 7).

[102] H. Oberst, Y. Tashiro, K. Shimizu, and F. Shimizu, "Quantum reflection of He^* on silicon", Physical Review A **71**, 052901 (2005) (cited on p. 7).

[103] T. A. Pasquini, M. Saba, G.-B. Jo, Y. Shin, W. Ketterle, D. E. Pritchard, T. A. Savas, and N. Mulders, "Low velocity quantum reflection of Bose-Einstein condensates", Physical Review Letters **97**, 093201 (2006) (cited on pp. 7, 69).

[104] B. S. Zhao, S. A. Schulz, S. A. Meek, G. Meijer, and W. Schöllkopf, "Quantum reflection of helium atom beams from a microstructured grating", Physical Review A **78**, 010902 (2008) (cited on p. 7).

[105] B. S. Zhao, H. C. Schewe, G. Meijer, and W. Schoellkopf, "Coherent reflection of He atom beams from rough surfaces at grazing incidence", Physical Review Letters **105**, 133203 (2010) (cited on p. 7).

[106] B. S. Zhao, W. Zhang, and W. Schöllkopf, "Non-destructive quantum reflection of helium dimers and trimers from a plane ruled grating", Molecular Physics **111**, 1772 (2013) (cited on pp. 7, 81).

[107] N. Fröman and P. O. Fröman, *JWKB approximation: contributions to the theory* (North-Holland Pub. Co., 1965) (cited on p. 7).

[108] H. Bremmer, "The W.K.B. approximation as the first term of a geometric-optical series", Communications on Pure and Applied Mathematics **4**, 105 (1951) (cited on pp. 7, 18).

[109] V. L. Pokrovskii, S. K. Savvinykh, and F. R. Ulinich, "Reflection from a barrier in the quasi-classical approximation", Soviet Physics JETP **7**, 879 (1958) (cited on pp. 7, 34).

[110] M. V. Berry and K. E. Mount, "Semiclassical approximations in wave mechanics", Reports on Progress in Physics **35**, 315 (1972) (cited on pp. 7, 17, 23, 29, 34, 134, 163).

[111] M. V. Berry, "Semiclassically weak reflections above analytic and non-analytic potential barriers", Journal of Physics A: Mathematical and General **15**, 3693 (1982) (cited on pp. 7, 34).

[112] N. T. Maitra and E. J. Heller, "Semiclassical perturbation approach to quantum reflection", Physical Review A **54**, 4763 (1996) (cited on pp. 7, 34).

[113] J. Böheim, W. Brenig, and J. Stutzki, "On the low energy limit of reflection and sticking coefficients in atom surface scattering", Zeitschrift für Physik B Condensed Matter **48**, 43 (1982) (cited on p. 7).

[114] G. F. Gribakin and V. V. Flambaum, "Calculation of the scattering length in atomic collisions using the semiclassical approximation", Physical Review A **48**, 546 (1993) (cited on pp. 7, 69).

[115] R. Côté, H. Friedrich, and J. Trost, "Reflection above potential steps", Physical Review A **56**, 1781 (1997) (cited on p. 7).

[116] C. Boisseau, E. Audouard, and J. Vigué, "Quantization of the highest levels in a molecular potential", EPL (Europhysics Letters) **41**, 349 (1998) (cited on p. 7).

[117] C. Eltschka, M. J. Moritz, and H. Friedrich, "Near-threshold quantization and scattering for deep potentials with attractive tails", Journal of Physics B: Atomic, Molecular and Optical Physics **33**, 4033 (2000) (cited on pp. 7, 69).

[118] A. Mody, M. Haggerty, J. M. Doyle, and E. J. Heller, "No-sticking effect and quantum reflection in ultracold collisions", Physical Review B **64**, 085418 (2001) (cited on p. 7).

[119] H. Friedrich, G. Jacoby, and C. G. Meister, "Quantum reflection by Casimir-van der Waals potential tails", Physical Review A **65**, 032902 (2002) (cited on pp. 7, 70, 140, 142).

[120] H. Friedrich and A. Jurisch, "Quantum reflection times for attractive potential tails", Physical Review Letters **92**, 103202 (2004) (cited on p. 7).

[121] A. Jurisch and H. Friedrich, "Realistic model for a quantum reflection trap", Physics Letters A **349**, 230 (2006) (cited on p. 7).

[122] J. Madroñero and H. Friedrich, "Influence of realistic atom wall potentials in quantum reflection traps", Physical Review A **75**, 022902 (2007) (cited on p. 7).

[123] A. Jurisch and J.-M. Rost, "Trapping cold atoms by quantum reflection", Physical Review A **77**, 043603 (2008) (cited on p. 7).

[124] A. Y. Voronin, P. Froelich, and B. Zygelman, "Interaction of ultracold antihydrogen with a conducting wall", Physical Review A **72**, 062903 (2005) (cited on pp. 7, 36, 70, 110, 112, 170).

[125] A. Y. Voronin and P. Froelich, "Quantum reflection of ultracold antihydrogen from a solid surface", Journal of Physics B: Atomic, Molecular and Optical Physics **38**, L301 (2005) (cited on pp. 7, 110, 112, 142, 170).

[126] A. Y. Voronin, P. Froelich, and V. V. Nesvizhevsky, "Gravitational quantum states of Antihydrogen", Physical Review A **83**, 032903 (2011) (cited on pp. 7, 110, 112, 127, 174, 177).

[127] A. Y. Voronin, V. V. Nesvizhevsky, and S. Reynaud, "Whispering-gallery states of antihydrogen near a curved surface", Physical Review A **85**, 014902 (2012) (cited on p. 7).

[128] A. Y. Voronin, V. V. Nesvizhevsky, and S. Reynaud, "Interference of the whispering gallery states of antihydrogen", Journal of Physics B-Atomic Molecular and Optical Physics **45**, 165007 (2012) (cited on p. 7).

[129] L. D. Landau and E. M. Lifshitz, *Quantum mechanics: non-relativistic theory*, trans. by J. B. Sykes and J. S. Bell (Oxford, Royaume-Uni, 1965) (cited on pp. 14, 35, 65, 111).

[130] C. Cohen-Tannoudji, B. Diu, and F. Laloe, *Quantum mechanics* (Wiley, 1991) (cited on pp. 16, 34, 42).

[131] J. Liouville, "Second mémoire sur le développement des fonctions ou parties de fonctions en séries dont les divers termes sont assujétis à satisfaire à une même équation différentielle du second ordre, contenant un paramètre variable", Journal de mathématiques pures et appliquées **2**, 16 (1837) (cited on pp. 17, 26).

[132] G. Green, "On the motion of waves in a variable canal of small depth and width", Transactions of the Cambridge Philosophical Society **Vol. 6**, 457 (1838) (cited on p. 17).

[133] G. Wentzel, "Eine Verallgemeinerung der Quantenbedingungen für die Zwecke der Wellenmechanik", Zeitschrift für Physik **38**, 518 (1926) (cited on pp. 17, 31).

[134] H. A. Kramers, "Wellenmechanik und halbzahlige Quantisierung", Zeitschrift für Physik **39**, 828 (1926) (cited on pp. 17, 31).

[135] L. Brillouin, "Remarques sur la mécanique ondulatoire", Journal de Physique et le Radium **7**, 353 (1926) (cited on pp. 17, 31).

[136] H. Jeffreys, "On certain approximate solutions of linear differential equations of the second order", Proceedings of the London Mathematical Society **s2-23**, 428 (1924) (cited on p. 17).

[137] E. R. Pike, "On the related-equation method of asymptotic approximation (WKB or A-A Method) I. A proposed new existence theorem", The Quarterly Journal of Mechanics and Applied Mathematics **17**, 105 (1964) (cited on p. 17).

[138] F. Olver, *Asymptotics and special functions* (Taylor & Francis, 1997) (cited on pp. 17, 25, 164).

[139] E. C. Kemble, "A Contribution to the Theory of the B. W. K. Method", Physical Review **48**, 549 (1935) (cited on pp. 23, 134).

[140] J. Liouville, "Mémoire sur le développement des fonctions ou parties de fonctions en séries dont les divers termes sont assujétis à satisfaire à une même équation différentielle du second ordre, contenant un paramètre variable", Journal de mathématiques pures et appliquées **1**, 253 (1836) (cited on p. 25).

[141] S. C. Miller and R. H. Good, "A WKB-type approximation to the Schrödinger equation", Physical Review **91**, 174 (1953) (cited on pp. 26, 29).

[142] H. Jeffreys, "On approximate solutions of linear differential equations", Mathematical Proceedings of the Cambridge Philosophical Society **49**, 601 (1953) (cited on p. 26).

[143] R. B. Dingle, "The method of comparison equations in the solution of linear second-order differential equations (generalized W.K.B. method)", Applied Scientific Research, Section A **5**, 345 (1956) (cited on pp. 26, 29).

[144] C. E. Hecht and J. E. Mayer, "Extension of the WKB Equation", Physical Review **106**, 1156 (1957) (cited on p. 26).

[145] P. Pechukas, "Analysis of the Miller–Good method for approximating bound states", The Journal of Chemical Physics **54**, 3864 (1971) (cited on p. 26).

[146] M. J. Richardson, "Approximate solutions to the one-dimensional Schrödinger equation by the method of comparison equations", Physical Review A **8**, 781 (1973) (cited on p. 26).

[147] J. Giraldo, R. G. Barrera, and G. A. Estévez, "An improvement to the comparison equation method for solving the Schrödinger equation", Chemical Physics Letters **113**, 37 (1985) (cited on p. 26).

[148] F. Robicheaux, U. Fano, M. Cavagnero, and D. A. Harmin, "Generalized WKB and Milne solutions to one-dimensional wave equations", Physical Review A **35**, 3619 (1987) (cited on p. 26).

[149] R. Milson, "Liouville transformation and exactly solvable schrodinger equations", International Journal of Theoretical Physics **37**, 1735 (1998) (cited on p. 26).

[150] J. Dereziński and M. Wrochna, "Exactly solvable Schrödinger operators", Annales Henri Poincaré **12**, 397 (2011) (cited on p. 26).

[151] P. Boonserm and M. Visser, "Transmission probabilities and the Miller–Good transformation", Journal of Physics A: Mathematical and Theoretical **42**, 045301 (2009) (cited on p. 26).

[152] G. Junker, "Remarks on the local time rescaling in path integration", Journal of Physics A: Mathematical and General **23**, L881 (1990) (cited on p. 26).

[153] H. Kleinert, *Path integrals in quantum mechanics, statistics, polymer physics, and financial markets* (World Scientific, 2009) (cited on p. 26).

[154] G. Dufour, R. Guérout, A. Lambrecht, and S. Reynaud, "Quantum reflection and Liouville transformations from wells to walls", EPL (Europhysics Letters) **110**, 30007 (2015) (cited on pp. 26, 38, 159, 168, 170).

[155] G. Dufour, R. Guérout, A. Lambrecht, and S. Reynaud, "Liouville transformations and quantum reflection", Journal of Physics B: Atomic, Molecular and Optical Physics **48**, 155002 (2015) (cited on pp. 26, 38, 159, 168, 170).

[156] R. E. Langer, "On the asymptotic solutions of ordinary differential equations, with an application to the Bessel functions of large order", Transactions of the American Mathematical Society **33**, 23 (1931) (cited on p. 31).

[157] R. E. Langer, "On the connection formulas and the solutions of the wave equation", Physical Review **51**, 669 (1937) (cited on pp. 31, 174).

[158] R. Bellman, "On a Liouville transformation for $u_{xx} + u_{yy} \pm a^2(x, y)u = 0$", Bollettino Unione Matematica Italiana **13**, 535 (1958) (cited on p. 32).

[159] P. Pechukas, "Semiclassical approximation of multidimensional bound states", The Journal of Chemical Physics **57**, 5577 (1972) (cited on p. 32).

[160] V. L. Pokrovskii, F. R. Ulinich, and S. K. Savvinykh, "Reflection from a barrier in the quasi-classical approximation 2.", Soviet Physics JETP **7**, 1119 (1958) (cited on p. 34).

[161] E. P. Wigner, "On the behavior of cross sections near thresholds", Physical Review **73**, 1002 (1948) (cited on p. 35).

[162] F. Dalfovo, S. Giorgini, L. P. Pitaevskii, and S. Stringari, "Theory of Bose-Einstein condensation in trapped gases", Reviews of Modern Physics **71**, 463 (1999) (cited on p. 35).

[163] J. Weiner, V. S. Bagnato, S. Zilio, and P. S. Julienne, "Experiments and theory in cold and ultracold collisions", Reviews of Modern Physics **71**, 1 (1999) (cited on p. 35).

[164] N. Balakrishnan, V. Kharchenko, R. C. Forrey, and A. Dalgarno, "Complex scattering lengths in multi-channel atom–molecule collisions", Chemical Physics Letters **280**, 5 (1997) (cited on p. 36).

[165] G. Dufour, A. Gérardin, R. Guérout, A. Lambrecht, V. V. Nesvizhevsky, S. Reynaud, and A. Y. Voronin, "Quantum reflection of antihydrogen from the Casimir potential above matter slabs", Physical Review A **87**, 012901 (2013) (cited on pp. 38, 159, 162).

[166] G. Dufour, R. Guérout, A. Lambrecht, V. V. Nesvizhevsky, S. Reynaud, and A. Y. Voronin, "Quantum reflection of antihydrogen from nanoporous media", Physical Review A **87**, 022506 (février 19, 2013) (cited on pp. 38, 159, 166, 168).

[167] S. Reynaud and A. Lambrecht, "Casimir forces", in Proceedings of the 101th Les Houches summer school on "Quantum Optics and Nanophotonics", August 2013 (2013) (cited on pp. 39, 40).

[168] A. Lambrecht, M.-T. Jaekel, and S. Reynaud, "The Casimir force for passive mirrors", Physics Letters A **225**, 188 (1997) (cited on p. 40).

[169] R. Guérout, A. Lambrecht, K. A. Milton, and S. Reynaud, "Derivation of the Lifshitz-Matsubara sum formula for the Casimir pressure between metallic plane mirrors", Physical Review E **90**, 042125 (2014) (cited on pp. 40, 45).

[170] R. Messina, D. A. R. Dalvit, P. A. M. Neto, A. Lambrecht, and S. Reynaud, "Dispersive interactions between atoms and nonplanar surfaces", Physical Review A **80**, 022119 (2009) (cited on pp. 42, 44, 165).

[171] A. Derevianko, S. G. Porsev, and J. F. Babb, "Electric dipole polarizabilities at imaginary frequencies for hydrogen, the alkali–metal, alkaline–earth, and noble gas atoms", Atomic Data and Nuclear Data Tables **96**, 323 (2010) (cited on p. 42).

[172] A. Lambrecht and S. Reynaud, "Casimir force between metallic mirrors", The European Physical Journal D - Atomic, Molecular and Optical Physics **8**, 309 (2000) (cited on p. 44).

[173] G. Bimonte, T. Emig, and M. Kardar, "Casimir-Polder interaction for gently curved surfaces", Physical Review D **90**, 081702 (2014) (cited on p. 44).

[174] L. D. Landau and E. M. Lifshitz, *Electrodynamics of continuous media*, Course of Theoretical Physics (Pergamon Press, 1960) (cited on pp. 44, 53).

[175] A. Lambrecht, I. Pirozhenko, L. Duraffourg, and P. Andreucci, "The Casimir effect for silicon and gold slabs", Europhysics Letters (EPL) **77**, 44006 (2007) (cited on p. 44).

[176] I. Pirozhenko and A. Lambrecht, "Influence of slab thickness on the Casimir force", Physical Review A **77**, 013811 (2008) (cited on p. 44).

[177] L. Bergström, "Hamaker constants of inorganic materials", Advances in Colloid and Interface Science **70**, 125 (1997) (cited on p. 45).

[178] E. D. Palik, *Handbook of Optical Constants of Solids* (Academic Press: New York, 1985) (cited on pp. 45, 46).

[179] C. Koughia, S. Kasap, and P. Capper, *Springer handbook of electronic and photonic materials*, Springer Handbook Of Series (Springer, 2006) (cited on p. 45).

[180] G. Ghosh, *Handbook of thermo-optic coefficients of optical materials with applications*, 1 vols. (Academic Press, San Diego, Etats-Unis, 1998) (cited on p. 46).

[181] M. J. Sparnaay, "On the additivity of London-van der Waals forces: An extension of London's oscillator model", Physica **25**, 217 (1959) (cited on p. 48).

[182] J. N. Israelachvili, *Intermolecular and surface forces* (Academic press, 2011) (cited on p. 48).

[183] A.-F. Bitbol, A. Canaguier-Durand, A. Lambrecht, and S. Reynaud, "Pairwise summation approximation for Casimir potentials and its limitations", Physical Review B **87**, 045413 (2013) (cited on p. 48).

[184] A. K. Geim and K. S. Novoselov, "The rise of graphene", Nature Materials **6**, 183 (2007) (cited on p. 50).

[185] M. Bordag, I. V. Fialkovsky, D. M. Gitman, and D. V. Vassilevich, "Casimir interaction between a perfect conductor and graphene described by the Dirac model", Physical Review B **80**, 245406 (2009) (cited on p. 50).

[186] M. Chaichian, G. L. Klimchitskaya, V. M. Mostepanenko, and A. Tureanu, "Thermal Casimir-Polder interaction of different atoms with graphene", Physical Review A **86**, 012515 (2012) (cited on p. 50).

[187] K. Sinko, "Influence of chemical conditions on the nanoporous structure of silicate aerogels", Materials **3**, 704 (2010) (cited on p. 52).

[188] P. Granitzer and K. Rumpf, "Porous silicon - A versatile host material", Materials **3**, 943 (2010) (cited on p. 52).

[189] O. Bisi, S. Ossicini, and L. Pavesi, "Porous silicon: a quantum sponge structure for silicon based optoelectronics", Surface Science Reports **38**, 1 (2000) (cited on p. 52).

[190] P. Decarli and J. Jamieson, "Formation of diamond by explosive shock", Science **133**, 1821 (1961) (cited on p. 52).

[191] V. Y. Dolmatov, "Detonation-synthesis nanodiamonds: synthesis, structure, properties and applications", Russian Chemical Reviews **76**, 339 (2007) (cited on p. 52).

[192] A. E. Aleksenskii, M. V. Baidakova, A. Y. Vul', and V. I. Siklitskii, "The structure of diamond nanoclusters", Physics of the Solid State **41**, 668 (1999) (cited on p. 52).

[193] V. V. Nesvizhevsky, E. V. Lychagin, A. Y. Muzychka, A. V. Strelkov, G. Pignol, and K. V. Protasov, "The reflection of very cold neutrons from diamond powder nanoparticles", Nuclear Instruments & Methods in Physics Research Section a-Accelerators Spectrometers Detectors and Associated Equipment **595**, 631 (2008) (cited on p. 52).

[194] V. Nesvizhevsky, R. Cubitt, E. Lychagin, A. Muzychka, G. Nekhaev, G. Pignol, K. Protasov, and A. Strelkov, "Application of diamond nanoparticles in low-energy neutron physics", Materials **3**, 1768 (2010) (cited on p. 52).

[195] V. V. Nesvizhevsky, A. Y. Voronin, A. Lambrecht, and S. Reynaud, "Study of levitating nanoparticles using ultracold neutrons", New Journal of Physics **14**, 093053 (2012) (cited on p. 52).

[196] V. B. Efimov, L. P. Mezhov-Deglin, C. D. Dewhurst, A. V. Lokhov, and V. V. Nesvizhevsky, "Neutron scattering on impurity nanoclusters in gel samples", Advances in High Energy Physics **2015**, 808212 (2015) (cited on p. 52).

[197] J. C. Maxwell Garnett, "Colours in metal Glasses and in metallic films", Philosophical Transactions of the Royal Society of London. Series A, Containing Papers of a Mathematical or Physical Character **203**, 385 (1904) (cited on p. 52).

[198] D. A. G. Bruggeman, "Berechnung verschiedener physikalischer Konstanten von heterogenen Substanzen. I. Dielektrizitätskonstanten und Leitfähigkeiten der Mischkörper aus isotropen Substanzen", Annalen der Physik **416**, 636 (1935) (cited on p. 52).

[199] R. Esquivel-Sirvent, "Reduction of the Casimir force using aerogels", Journal of Applied Physics **102**, 034307 (2007) (cited on p. 53).

[200] G. Bimonte, T. Emig, M. Krüger, and M. Kardar, "Dilution and resonance-enhanced repulsion in nonequilibrium fluctuation forces", Physical Review A **84**, 042503 (2011) (cited on p. 53).

[201] N. Cherroret, R. Guérout, A. Lambrecht, and S. Reynaud, "Fluctuations of the Casimir potential above a disordered medium", The European Physical Journal D **69**, 1 (2015) (cited on p. 54).

[202] N. Cherroret, R. Guérout, A. Lambrecht, and S. Reynaud, "Statistical approach to Casimir-Polder potentials in heterogeneous media", (2015) (cited on p. 54).

[203] G. Gamow, "Zur Quantentheorie des Atomkernes", Zeitschrift für Physik **51**, 204 (1928) (cited on p. 65).

[204] G.-R. Wang, T. Xie, Y. Huang, and S.-L. Cong, "Quantum reflection by the Casimir–Polder potential: a three-parameter model", Journal of Physics B: Atomic, Molecular and Optical Physics **46**, 185302 (2013) (cited on p. 69).

[205] W. Magnus, "On the exponential solution of differential equations for a linear operator", Communications on Pure and Applied Mathematics **7**, 649 (1954) (cited on p. 84).

[206] P. Storey and C. Cohen-Tannoudji, "The Feynman path integral approach to atomic interferometry: A tutorial", Journal de Physique II **4**, 29 (1994) (cited on pp. 88, 151).

[207] E. Wigner, "On the Quantum Correction For Thermodynamic Equilibrium", Physical Review **40**, 749 (1932) (cited on p. 88).

[208] W. B. Case, "Wigner functions and Weyl transforms for pedestrians", American Journal of Physics **76**, 937 (2008) (cited on pp. 88, 98).

[209] M. V. Berry, "Semi-classical mechanics in phase space: A study of Wigner's function", Philosophical Transactions of the Royal Society of London. Series A, Mathematical and Physical Sciences **287**, 237 (1977) (cited on p. 88).

[210] G. Nogues, A. Rauschenbeutel, S. Osnaghi, P. Bertet, M. Brune, J. M. Raimond, S. Haroche, L. G. Lutterbach, and L. Davidovich, "Measurement of a negative value for the Wigner function of radiation", Physical Review A **62**, 054101 (2000) (cited on p. 89).

[211] P. Bertet, A. Auffeves, P. Maioli, S. Osnaghi, T. Meunier, M. Brune, J. M. Raimond, and S. Haroche, "Direct Measurement of the Wigner Function of a One-Photon Fock State in a Cavity", Physical Review Letters **89**, 200402 (2002) (cited on p. 89).

[212] M. Wadati, "The free fall of quantum particles", Journal of the Physical Society of Japan **68**, 2543 (1999) (cited on p. 91).

[213] R. v. Eötvös, D. Pekár, and E. Fekete, Annalen der Physik (Leipzig) **68**, 11 (1922) (cited on p. 94).

[214] O. Vallée and M. Soares, *Airy functions and applications to physics* (Imperial College Press, 2004) (cited on pp. 100, 102, 106, 109, 147, 173).

[215] V. Nesvizhevsky and A. Voronin, *Surprising quantum bounces* (Imperial College Press, 2015) (cited on pp. 104, 105).

[216] G. Dufour, P. Debu, A. Lambrecht, V. V. Nesvizhevsky, S. Reynaud, and A. Y. Voronin, "Shaping the distribution of vertical velocities of antihydrogen in GBAR", European Physical Journal C **74**, 2731 (2014) (cited on pp. 104, 159, 175).

[217] G. Dufour, D. B. Cassidy, P. Crivelli, P. Debu, A. Lambrecht, V. V. Nesvizhevsky, S. Reynaud, A. Y. Voronin, and T. E. Wall, "Prospects for studies of the free fall and gravitational quantum states of antimatter", Advances in High Energy Physics **2015**, 379642 (2015) (cited on pp. 104, 160, 177).

[218] A. I. Frank, "Modern optics of long-wavelength neutrons", Soviet Physics Uspekhi **34**, 980 (1991) (cited on p. 105).

[219] G. Pignol, "Préparation de l'expérience GRANIT et recherche de nouvelles interactions avec les neutrons.", PhD Thesis (Université Joseph-Fourier - Grenoble I, 2009) (cited on p. 105).

[220] D. M. Goodmanson, "A recursion relation for matrix elements of the quantum bouncer. Comment on "A quantum bouncing ball," by Julio Gea-Banacloche [Am. J. Phys. 67 (9), 776–782 (1999)]", American Journal of Physics **68**, 866 (2000) (cited on p. 106).

[221] R. W. Robinett, "The Stark effect in linear potentials", European Journal of Physics **31**, 1 (2010) (cited on p. 106).

[222] A. Y. Voronin, H. Abele, S. Baeßler, V. V. Nesvizhevsky, A. K. Petukhov, K. V. Protasov, and A. Westphal, "Quantum motion of a neutron in a waveguide in the gravitational field", Physical Review D **73**, 044029 (février 23, 2006) (cited on p. 110).

[223] A. E. Meyerovich and V. V. Nesvizhevsky, "Gravitational quantum states of neutrons in a rough waveguide", Physical Review A **73**, 063616 (2006) (cited on p. 110).

[224] P. Debu, "GBAR", Hyperfine Interactions **212**, 51 (2012) (cited on p. 119).

[225] A. Walther, F. Ziesel, T. Ruster, S. T. Dawkins, K. Ott, M. Hettrich, K. Singer, F. Schmidt-Kaler, and U. Poschinger, "Controlling fast transport of cold trapped ions", Physical Review Letters **109**, 080501 (août 20, 2012) (cited on p. 120).

[226] V. V. Nesvizhevsky, "Interaction of neutrons with nanoparticles", Physics of Atomic Nuclei **65**, 400 (2002) (cited on p. 121).

[227] V. Nesvizhevsky, H. Börner, A. Gagarski, G. Petrov, A. Petukhov, H. Abele, S. Bäßler, T. Stöferle, and S. Soloviev, "Search for quantum states of the neutron in a gravitational field: gravitational levels", Nuclear Instruments and Methods in Physics Research Section A: Accelerators, Spectrometers, Detectors and Associated Equipment **440**, 754 (février 11, 2000) (cited on p. 121).

[228] P. Debu, *GBAR internal notes*, 2013 (cited on p. 127).

[229] A. Y. Voronin, V. V. Nesvizhevsky, G. Dufour, P. Debu, A. Lambrecht, S. Reynaud, O. D. Dalkarov, E. A. Kupriyanova, and P. Froelich, "A spectroscopy approach to measure the gravitational mass of antihydrogen", International Journal of Modern Physics: Conference Series **30**, 1460266 (2014) (cited on pp. 127, 159, 177).

[230] A. Y. Voronin, V. V. Nesvizhevsky, O. D. Dalkarov, E. A. Kupriyanova, and P. Froelich, "Resonance spectroscopy of gravitational states of antihydrogen", Hyperfine Interactions **228**, 133 (2014) (cited on p. 127).

[231] A. Y. Voronin, "Singular potentials and annihilation", Physical Review A **67**, 062706 (2003) (cited on p. 140).

[232] T. F. O'Malley, L. Spruch, and L. Rosenberg, "Modification of effective-range theory in the presence of a long-range r^{-4} potential", Journal of Mathematical Physics **2**, 491 (1961) (cited on p. 144).

[233] N. a. W. Holzwarth, "Mathieu function solutions to the radial Schrödinger equation for the $-f/r^4$ interaction", Journal of Mathematical Physics **14**, 191 (1973) (cited on pp. 144, 145).

[234] B. Gao, "Quantum-defect theory for $-1/r^4$ type interactions", Physical Review A **88**, 022701 (2013) (cited on p. 144).

[235] N. W. Mac Lachlan, *Theory and application of Mathieu functions* (At the Clarendon Press, Oxford, Royaume-Uni, 1951) (cited on p. 144).

[236] P. M. C. Morse and H. Feshbach, *Methods of theoretical physics*, International series in pure and applied physics (McGraw, 1953) (cited on p. 144).

[237] G. B. Airy, "On the intensity of light in the neighbourhood of a caustic", Transactions of the Cambridge Philosophical Society **6**, 379 (1838) (cited on p. 146).

[238] G. B. Airy, "Supplement to a paper "On the intensity of light in the neighbourhood of a caustic"", Transactions of the Cambridge Philosophical Society **8**, 595 (1849) (cited on p. 146).

[239] M. V. Berry and N. L. Balazs, "Nonspreading wave packets", American Journal of Physics **47**, 264 (1979) (cited on p. 149).

[240] K. Husimi, "Miscellanea in elementary quantum mechanics II", Progress of Theoretical Physics **9**, 381 (1953) (cited on p. 151).

[241] W. P. Schleich, *Quantum optics in phase space* (John Wiley & Sons, 2011) (cited on p. 153).

[242] L. Parker, "Quantized fields and particle creation in expanding universes. I", Physical Review **183**, 1057 (1969) (cited on p. 154).

[243] J. Audretsch, "Cosmological particle creation as above-barrier reflection: approximation method and applications", Journal of Physics A: Mathematical and General **12**, 1189 (1979) (cited on p. 154).

[244] L. H. Ford, "Quantum field theory in curved spacetime", in Proceedings of the 9th Jorge Andre Swieca Summer School (1997) (cited on p. 154).

[245] S. A. Fulling and P. C. W. Davies, "Radiation from a moving mirror in 2 dimensional space-time - conformal anomaly", Proceedings of the Royal Society of London. A. Mathematical and Physical Sciences **348**, 393 (1976) (cited on p. 154).

[246] W. R. Walker, "Particle and energy creation by moving mirrors", Physical Review D **31**, 767 (février 15, 1985) (cited on p. 154).

[247] A. Lambrecht, M.-T. Jaekel, and S. Reynaud, "Frequency up-converted radiation from a cavity moving in vacuum", European Physical Journal D **3**, 95 (1998) (cited on p. 154).

[248] A. Fabbri, J. Navarro-Salas, and G. J. Olmo, "Particles and energy fluxes from a conformal field theory perspective", Physical Review D **70**, 064022 (2004) (cited on p. 154).

[249] M. V. Berry, "Transitionless quantum driving", Journal of Physics A: Mathematical and Theoretical **42**, 365303 (2009) (cited on p. 158).

[250] J. G. Muga, X. Chen, S. Ibáñez, I. Lizuain, and A. Ruschhaupt, "Transitionless quantum drivings for the harmonic oscillator", Journal of Physics B: Atomic, Molecular and Optical Physics **43**, 085509 (2010) (cited on p. 158).

[251] A. del Campo, "Shortcuts to adiabaticity by counterdiabatic driving", Physical Review Letters **111**, 100502 (2013) (cited on p. 158).

[252] X. Chen, A. Ruschhaupt, S. Schmidt, A. del Campo, D. Guéry-Odelin, and J. G. Muga, "Fast optimal frictionless atom cooling in harmonic traps: Shortcut to adiabaticity", Physical Review Letters **104**, 063002 (février 11, 2010) (cited on p. 158).

[253] X. Chen, E. Torrontegui, and J. G. Muga, "Lewis-Riesenfeld invariants and transitionless quantum driving", Physical Review A **83**, 062116 (2011) (cited on p. 158).

[254] H. J. Lewis and W. B. Riesenfeld, "An exact quantum theory of the time-dependent harmonic oscillator and of a charged particle in a time-dependent electromagnetic field", Journal of Mathematical Physics **10**, 1458 (1969) (cited on p. 158).

[255] M. V. Berry and C. J. Howls, "Fake Airy functions and the asymptotics of reflectionlessness", Journal of Physics A: Mathematical and General **23**, L243 (1990) (cited on p. 158).

[256] I. Gjaja and A. Bhattacharjee, "Asymptotics of reflectionless potentials", Physical Review Letters **68**, 2413 (1992) (cited on p. 158).

[257] G. Dufour, R. Guérout, A. Lambrecht, V. Nesvizhevsky, S. Reynaud, and A. Voronin, "Quantum reflection of antihydrogen in the GBAR experiment", International Journal of Modern Physics: Conference Series **30**, 1460265 (2014) (cited on p. 159).

[258] P. Indelicato et al., "The GBAR project, or how does antimatter fall?", Hyperfine Interactions **228**, 141 (2014) (cited on p. 159).

[259] P. Pérez et al., "The GBAR antimatter gravity experiment", Hyperfine Interactions **233**, 21 (2015) (cited on p. 160).

Sujet : Réflexion quantique sur le potentiel de Casimir-Polder

Résumé : Les collisions entre atomes ultrafroids et surfaces matérielles sont caractérisées par la réflexion de l'onde de matière atomique sur le potentiel attractif de Casimir-Polder. Cette réflexion quantique est déterminante pour des expériences telles que GBAR, qui mesurera l'accélération d'un atome d'antihydrogène froid chutant vers une plaque de détection. Dans cette thèse, le potentiel de Casimir-Polder est calculé à partir des propriétés de diffusion électromagnétique de l'atome et de la surface. Il s'avère dépendre de la réponse diélectrique, de l'épaisseur et de la densité du milieu. Nous montrons que la réflexion sur ce potentiel est associée à une rupture de l'approximation semiclassique et qu'elle augmente pour des atomes lents et des potentiels faibles. Les transformations de Liouville relient des équations de Schrödinger avec des potentiels différents mais les mêmes amplitudes de diffusion. L'équivalence entre la réflexion quantique sur un puits de potentiel et l'effet tunnel à travers une barrière offre de nouvelles perspectives sur le problème. Nous discutons aussi des effets de la gravité sur le paquet d'onde atomique et de ses conséquences pour les expériences avec des atomes en chute libre. Associée à la réflexion quantique sur un miroir horizontal, la gravité permet de maintenir des particules dans des états à longue durée de vie aux applications prometteuses pour la métrologie. En particulier, nous proposons un système pour améliorer la précision de GBAR en réduisant la dispersion en vitesse des atomes d'antihydrogène.

Mots clés : Réflexion quantique, interaction de Casimir-Polder, antihydrogène, gravitation, équation de Schrödinger, transformation de Liouville.

Subject : Quantum reflection from the Casimir-Polder potential

Abstract : Collisions between ultracold atoms and material surfaces are characterized by the reflection of the atomic matter wave from the attractive Casimir-Polder potential. This quantum reflection is particularly relevant to experiments such as GBAR, which will determine the gravitational acceleration of a cold antihydrogen atom by timing its fall onto a detection plate. In this thesis, the Casimir-Polder potential is computed from the electromagnetic scattering properties of the atom and surface and it is found to depend notably on the dielectric response, thickness and density of the medium. We show that reflection on this potential is associated with a breakdown of the semiclassical approximation and that it is enhanced for slow atoms and weak potentials. Liouville transformations relate Schrödinger equations with different potential landscapes but identical scattering properties. We gain new insights on the problem of quantum reflection on a potential well by mapping it onto an equivalent problem of tunneling through a wall. We also discuss the effect of gravity on the atomic wavepacket and its implications for free fall experiments with atoms. When combined with quantum reflection from a horizontal mirror, gravity can be used to trap particles in long lived states with promising applications for metrology. In particular, we suggest a scheme to improve the precision of the GBAR experiment by reducing the velocity dispersion of the falling atoms.

Keywords : Quantum reflection, Casimir-Polder interaction, antihydrogen, gravity, Schrödinger equation, Liouville transformation.